Non-unique stage-discharge relations: Bayesian analysis of complex rating curves and their uncertainties

Valentin Mansanarez

Communauté
UNIVERSITÉ Grenoble Alpes

THÈSE

Pour obtenir le grade de

DOCTEUR DE LA COMMUNAUTÉ UNIVERSITÉ GRENOBLE ALPES

Spécialité : **Océan, Atmosphère, Hydrologie**

Arrêté ministériel : 7 août 2006

Présentée par

Valentin MANSANAREZ

Thèse dirigée par **Michel LANG**
et co-encadrée par **Jérôme LE COZ** et **Benjamin RENARD**

préparée au sein **de l'unité de recherche Hydrologie-Hydraulique (HHLY), à Irstea Lyon-Villeurbanne, France** en collaboration avec **la Compagnie Nationale du Rhône (CNR)**
et de l'École Doctorale **Terre, Univers, Environnement (TUE)**

Non-unique stage-discharge relations: Bayesian analysis of complex rating curves and their uncertainties

Thèse soutenue publiquement le **2 Novembre 2016**,
devant le jury composé de :

M. Jean-Luc Bertrand-Krajewski
Professeur, INSA, Lyon, France, Laboratory DEEP, Président
M. Giuliano Di Baldassarre
Professeur, Uppsala Universitet, Uppsala, Sweden, Rapporteur
M. Jan Seibert
Professeur, Universität Zürich (UZH), Zürich, Switzerland, Rapporteur
Mme Anne-Catherine Favre
Professeur, G-INP/ENSE3, Grenoble, France, LTHE, Examinatrice
M. Arnaud Belleville
Ingénieur spécialiste, EDF-DTG, Grenoble, France, Examinateur
M. Michel Lang
Chercheur IDTPE (HDR), Irstea Lyon-Villeurbanne, France, U.R. HHLY, Directeur de thèse
M. Jérôme Le Coz
Chercheur IPEF, Irstea Lyon-Villeurbanne, France, U.R. HHLY, Co-Encadrant de thèse
M. Benjamin Renard
Chargé de recherche, Irstea Lyon-Villeurbanne, France, U.R. HHLY, Co-Encadrant de thèse
M. Gilles Pierrefeu
Ingénieur spécialiste, CNR, Lyon, CACOH, Invité

Remerciements

Au fil de ces trois ans, tant de gens ont fait fleurir cette belle thèse qu'il m'est impossible de ne pas les remercier. Je m'excuse par avance à ceux que j'oublie injustement.

Je tiens tout d'abord à remercier à la fois les membres du jury et ceux des deux comités de pilotage pour leur apport indédiable. Leurs questions, critiques, suggestions et débats m'ont été d'une aide précieuse et ont grandement contribué à l'achèvement de ce manuscript.

Je remercie ensuite mon encadrement (quel encadrement !) en les personnes de Benjamin, Jérôme et Michel. Ce trio de choc m'a laissé assez d'autonomie pour que je fasse ce que je veux... tout en resserrant la vis lorsque j'en avais besoin. L'encadrement est même parfois allé au delà du cadre professionnel. Mention spéciale à souflette et .....-toutou.

Je remercie Benoît Camenen et Jean-Philippe Vidal pour leur aide, le premier sur l'hydraulique et les sédiments, le second sur l'esthétique et le perfectionnement graphique. Je remercie bien sûr aussi tous les autres collègues de HH qui ont suivi et même certaines fois subit mon baratin de thésard. Je remercie également Céline Berni, Guillaume Dramais, Claire Lauvernet, Sébastien Proust et Fabien Thollet qui ont toujours su répondre à mes questions et ce, même quand ils n'avaient pas le temps. Je remercie également les autres collègues de HHLY et de PolDif qui participent grandement au cadre si particulier et si exceptionnel qu'est le 1er étage d'Irstea Lyon.

Je tiens à remercier d'autres personnes, d'Irstea, passées par Irstea ou extérieur à Irstea, qui ont su dépasser le cadre de travail et avec qui j'ai passé d'agréables bons moments, à savoir Adrien, Alexis, Antoine C., Baptiste M., Camille B., Camille F., Chloé L., Claire F., Claire L., Clotaire, Elise, Emeline, Jean-ϕ, Lilly-Rose, Marina, Maxime M., Maxime T.,

Musaab, Pierre E., Ricardo, Romain VDB, Sarah, Sophie, Sheng, Tamas et Victor. Désolé pour les oubliés. Je remercie aussi toutes les personnes qui ont accepté de venir jouer à l'ultimate les soirs, notamment les ingé-stagiaires de la CNR et avec qui j'ai pu partager le plaisir du disque. Je remercie mes co-bureaux Pierre-Henri, Christine, Houleymatou et Alexandre de m'avoir supporté pendant ma thèse, cela n'a pas dû être facile. Mention spéciale à Christine qui m'a supporté la moitié de ma thèse.

Je remercie aussi l'empailleuse boxeuse Delphine qui en plus de te défoncer, te garantit une exposition digne des plus grand pharaons ; la lapinonaco maniaco Laurie qui m'a appris que les lapins ne vivent pas dans des clapiers, ne mange pas de carottes (pas que car Gandalf a quand même l'air d'aimer cela) et surtout que le lapin ne se mange pas (euh tjrs pas compris l'enseignement) ; l'informaticien geek (Lapalissade ?) Sylvain, qui te laisse Muscat et olives dans ton frigo et surtout, en forme, te délivre le packaging complet en soirée (du before à l'after en passant par le retour en politesse) et le verbeux défenseur de la langue française Tristan auquel je dédie toutes les fôtes dans ce manuscrit. Vos conversations plus que WTF recèlent quelques pépites qui ont certainement éclairé mes journées.

Je remercie la Coloc' pour leurs nombreuses invitations chez eux et les soirées inoubliables que j'ai pu partager. Et comme cette coloc' est intiment liée au Tchouk, je remercie en même temps toute les personnes que j'ai pu rencontrer lors de la pratique de ce sport en or méconnu. Je remercie particulièrement Anto, Colin, Flo, Marlène, Mika et Narcisse pour tous les moments que l'on a partagé. Je souhaite une bonne fin de saison aux anciens et nouveaux Tchoukeurs de Lyon et qui sait, on se reverra sans doute sur le terrain.

Je tiens à remercier le grimpeur émérite, maître Capello Grégoire et sa copine Fanny en leurs souhaitant un heureux début dans la vie familiale ; la sportive ("moi du sport ?... Jamais") Violaine et le compétiteur Olivier pour les chouettes moments qu'ils ont pu partager ; Thomas et Aurélia, agriculteur en devenir, man la tradition est morte avec ton départ ; la coureuse Lucie G., le grand chelem est aussi mort avec ton départ. Je remercie également Lucie L. pour son enthousiasme et sa bonne humeur le matin, je te souhaite un bon développement de ton activité rando ; Chloé LG, d'une compagnie et bonne humeur fort appréciable ; le grimpeur Xavier régulier de l'envers (merci à Baptiste

et Romain aussi). Je remercie la famille Le Coz-Branger en les personnes de Jérôme, Flora et Madeleine pour votre accueil en NZ, pour tous les bons moments que l'on a passé ensemble et pour la découverte d'une magnifique chanson. Je remercie également mon compatriote nantais Pierre pour tout ce que l'on a partagé. J'espère vous revoir tous un jour.

Je remercie aussi Laura pour ces soirées mémorables et pour m'avoir fait découvrir le Tchouk, bon chance pour la suite de ta thèse ; sa complice brato, maîtresse de la cuisine et du bon goût, qui ne se limite qu'aux extrêmes en cuisine, je te souhaite une bonne continuation dans ta vie ; le philosophe des soirées Ivan, thésard débutant, toujours le mot pour rire, merci pour tes nombreux accueils chez toi ; l'apitoyable Martin toujours à se plaindre mais d'une compagnie en or ; son jeune complice Eric, tu deviendras calif ! ; l'inimitable Anne-Lauuure, NZ road trip body et son frère jumeau Ben, vous voir vous chercher des noises, cela n'a pas de prix ! et merci pour tout ce que vous avez fait tous les deux. También quiero agradecer a Albert por todo lo que hacemos vivido juntos. Sus logros deportivos nunca dejan de sorprenderme. Je remercie le duo Raphtance en leurs souhaitant tout le bonheur du monde et une excitante nouvelle vie à Barcelona. Prévoyez de la place je débarquerai assez vite. Simplement merci à vous deux. Je remercie Dragana pour sa patience devant mes nombreuses fautes d'anglais et merci pour ton accueil en Serbie ! Je remercie François et Marko pour la complicité que l'on partage (et les nombreux calins !), hâte de vous avoir à Stockholm avec moi.

Je remercie mes vieux copains de Nantes pour les moments que l'on a et que l'on passera ensemble. Merci à 51, Céline, Charlotte, Clémence, Divad, Eloïse, Estelle, Fenec, Fro, Jejej, Jf, Kiki, Lod, Marie, Maxence, Max, Poiraud, Popo, Solène, Thomas, Tinss et Victor. Merci aux derniers du Clan, Naïs, Loan et Elsa ; Victor t'es le prochain à soutenir.

Je n'aurais jamais pu en arriver là sans le soutien précieux et inestimable de ma famille : je les remercie du fond du cœur. Je dédie cette thèse à mes parents, mes sœurs et mon frère : Catherine, Guy, Louise, Margaux et Paul.

Résumé

Les courbes de tarage complexes, qui prennent en entrée la hauteur d'eau et des variables supplémentaires, sont nécessaires pour établir les chroniques de débit des cours d'eau là où la relation hauteur-débit n'est pas univoque.

Dans le même cadre bayésien, des méthodes à base hydraulique sont proposées et testées pour construire les courbes de tarage complexes et estimer leurs incertitudes : des modèles hauteur-gradient-débit (SGD) pour résoudre l'hystérésis due aux écoulements transitoires, des modèles hauteur-dénivelée-pente (SFD) pour résoudre le remous variable aux stations à double échelle, le modèle hauteur-période-débit (SPD) pour résoudre les détarages nets dus aux évolutions du lit.

Chaque modèle a été appliqué à des stations hydrométriques variées et évalué grâce à des analyses de sensibilité. Pour chacune des trois sources de non-univocité de la relation hauteur-débit, les méthodes bayésiennes proposées fournissent non seulement une analyse d'incertitude quantitative mais aussi des solutions efficaces à des problèmes récurrents que posent les procédures traditionnelles pour les courbes de tarage complexes.

Mots clés : BaRatin, inférence bayésienne, contrôles hydrauliques, courbes de tarage complexes, Hydrométrie, hystérésis, MCMC, non univocité, détarages morphodynamiques, relations hauteur-débit, débit des cours d'eau, incertitudes, influence aval variable.

Abstract

Complex rating curves, with stage and additional variables as inputs are necessary to establish streamflow records at sites where the stage-discharge relation is non-unique.

Within the same Bayesian framework, hydraulically-based methods are introduced and tested to develop complex rating curves and estimate their uncertainties: stage-gradient-discharge (SGD) models to address hysteresis due to transient flow, stage-fall-discharge (SFD) models to address variable backwater at twin gauge stations, stage-period-discharge (SPD) model to address net rating changes due to bed evolution.

Each model was applied to contrasting hydrometric stations and evaluated through sensitivity analyses. For each of the three sources of non-uniqueness in the stage-discharge relation, the proposed Bayesian methods provide not only quantitative uncertainty analysis but also efficient solutions to recurrent problems with the traditional procedures for complex ratings.

Key words: BaRatin, Bayesian inference, controls, complex rating curves, Hydrometry, hysteresis, MCMC, non-uniqueness, rating changes, stage-discharge relation, streamflow, uncertainties, variable backwater influence.

Résumé étendu en français

1. Introduction

L'hydrologie possède la particularité qu'une de ses principales variables – le débit des cours d'eau – ne peut pas être mesurée en continu. Le plus souvent en effet, les chroniques de débit utilisées par les hydrologues résultent de la transformation de mesures continues de hauteur d'eau *via* un modèle hauteur-débit, appelé courbe de tarage (cf. manuel WMO No. 1044 [2010]). Cette courbe de tarage doit être estimée à chaque station hydrométrique, à partir de mesures hauteur-débit ponctuelles (appelées jaugeages) et de considérations sur les lois hydrauliques qui gouvernent la relation hauteur-débit. Les plus fortes incertitudes sur la courbe de tarage sont rencontrées en situation d'étiage, où la géométrie de la section d'écoulement s'avère souvent instable et peu sensible (faible variation de hauteur d'eau rapportée à une variation de débit) ; et en situation de crue, où le manque de jaugeages induit une incertitude accrue sur l'extrapolation du modèle hauteur-débit, et où des écoulements complexes peuvent intervenir, notamment en cas de débordement.

Etant donné le rôle central joué par la variable débit en hydrologie, la quantification des incertitudes associées à la courbe de tarage est une thématique centrale, que ce soit en hydrologie opérationnelle, par exemple pour statuer par exemple sur le respect d'un débit réservé ou positionner un débit de crue vis-à-vis de valeurs de référence (crue centennale), ou en hydrologie prospective pour évaluer le futur régime des eaux sous différents scénarios d'impacts anthropiques (émission de gaz à effet de serre ou occupation du sol).

Des travaux récents effectués au sein de l'unité de recherche Hydrologie-Hydraulique d'Irstea ont permis de mettre en place une méthode d'estimation de ces incertitudes, nom-

mée BaRatin (BAyesian RATINg curve estimation, Le Coz et al., 2014). BaRatin est basé sur une estimation bayésienne des paramètres de la courbe de tarage, prenant en compte les incertitudes associées à chaque jaugeage, et permettant d'inclure des connaissances a priori sur les contrôles hydrauliques de la relation hauteur-débit. Les résultats en sortie peuvent être également interprétés en termes hydrauliques pour en vérifier le réalisme.

Une hypothèse contraignante sur la transformation d'une chronique de hauteur d'eau via une courbe de tarage est de supposer que la relation hauteur-débit est univoque et qu'elle ne change pas au cours du temps, sinon sur l'ensemble de la période d'enregistrement, du moins par période stable. Le passage d'une période stable à une autre est souvent supposé être relatif à un changement brutal, suite par exemple à un changement de géométrie du lit de la rivière après une crue ou des travaux sur la rivière. En pratique, on observe également des phénomènes de détarage continu, avec un éloignement temporaire ou définitif de la relation hauteur-débit à la courbe de tarage en cours de validité. Ces phénomènes de détarage continu peuvent être saisonniers (par exemple, la végétation aquatique, cf. figure 1-c, la couverture de glace, cf. figure 1-d, la rugosité variable), épisodiques (hystérésis due au régime transitoire, cf. figure 1-g, influence aval variable, cf. figures 1-e et 1-f), ou progressifs (ajustement suite à un déséquilibre sédimentaire, cf. figure 1-b). Lorsque la relation hauteur-débit n'est pas univoque, il faut recourir à des courbes de tarage "complexes", c'est-à-dire des modèles prenant d'autres variables d'entrée en plus de la hauteur pour modéliser le débit.

L'objectif principal de la thèse est de développer et valider des méthodes statistiques utilisant la connaissance hydraulique pour estimer les courbes de tarage complexes et quantifier leurs incertitudes. Trois principales sources de non-univocité dans les relations hauteur-débit sont étudiées dans cette thèse :

- l'hystérésis due aux écoulements transitoires. Il s'agit d'un phénomène modifiant de façon épisodique la relation hauteur-débit pendant les crues ;
- la présence d'un remous variable dans le cas des stations hydrométriques à double échelle. Ce phénomène affecte continuellement la relation hauteur-débit ;

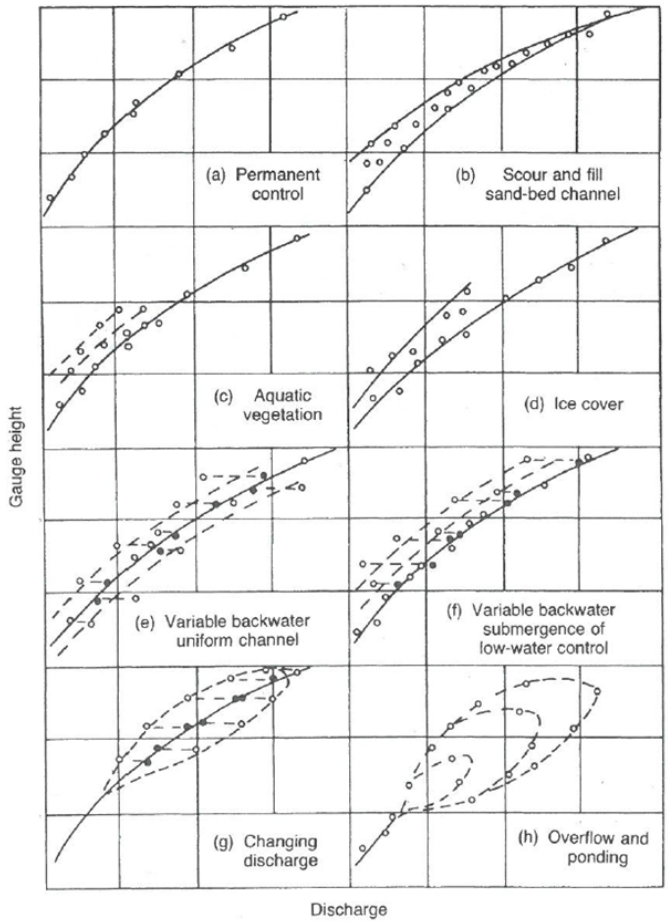

Figure 1 – Représentation de plusieurs courbes de tarage complexes avec leurs effets hydrauliques [figure tirée de Herschy, 1995].

- les détarages nets dus aux évolutions soudaines du lit de la rivière. Ces phénomènes modifient la relation hauteur-débit de façon soudaine et permanente, pendant une crue morphogène ou une intervention dans le lit.

Les principales questions de recherche sous-jacentes sont les suivantes :

- Est-il possible de construire un cadre statistique général prenant en compte les différentes sources possibles de non-univocité ou est-il préférable de developper des modèles spécifiques à chaque phénomène de non-univocité ? Un cadre statistique unifié peut être plus facile à mettre en œuvre alors que des modèles spécifiques peuvent être plus adaptés aux phénomènes qu'ils décrivent ;
- Est-il suffisant d'introduire des covariables rendant compte de la dynamique du phénomène causant la non-univocité ? Et si oui, quelles sont ces covariables ?

- Comment prendre en compte la connaissance *a priori* des processus physiques causant la non-univocité ? Notamment, quelle information *a priori* spécifique améliore l'estimation des courbes de tarage des stations peu jaugées ?

- D'un point de vue opérationnel, comment gère-t-on une station affectée par une relation hauteur-débit non univoque ? Les stratégies de jaugeage habituelles sont-elles toujours adaptées ou ont-elles besoin d'être modifiées afin d'améliorer l'estimation des courbes de tarage et la détection de la non-univocité dans la relation hauteur-débit ?

- Est-ce que les jaugeages anciens doivent être systématiquement écartés quand une nouvelle courbe est établie ? Ou peuvent-ils toujours être utilisés pour l'estimation des courbes de tarage et la quantification des incertitudes associées ?

2. Outils hydrauliques et statistiques

2.1. L'analyse hydraulique

Les stations hydrométriques sont de préférence positionnées de façon à bénéficier d'une relation univoque entre la hauteur d'eau h et le débit Q. Cette relation est déterminée par les caractéristiques physiques du chenal, appelées "contrôles hydrauliques" ou simplement "contrôles". Deux types de contrôles existent :

- le contrôle par section. La relation hauteur-débit est déterminée par la géométrie de la section de la rivière en laquelle l'écoulement passe en régime critique. Ce régime est matérialisé par une chute d'eau à l'aval de la section et une ligne d'eau quasi-horizontale à l'amont (cf. figure 2-a) ;
- le contrôle par chenal. La relation hauteur-débit est gouvernée par la géométrie et la résistance à l'écoulement du chenal sur l'ensemble du tronçon hydraulique homogène s'étendant à la fois en amont et en aval de la station (cf. figure 2-b).

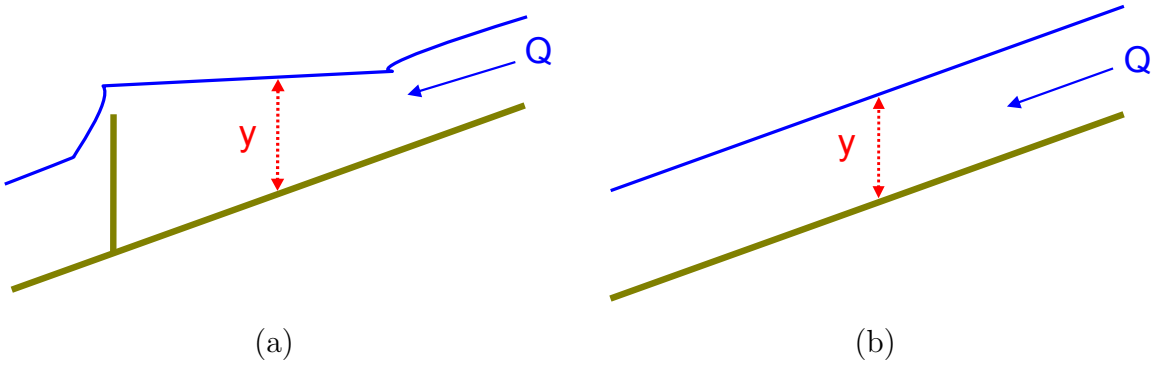

Figure 2 – Schémas : (a) d'un contrôle par section (le tirant d'eau y est sous l'inflence de la chute d'eau); (b) d'un contrôle par chenal (la ligne rouge représente la position de la station de jaugeage).

La plupart des contrôles hydrauliques peuvent être approchés par une fonction puissance entre le tirant d'eau et le débit. Les formules hydrauliques des contrôles par section et des contrôles par chenal ayant une section rectangulaire large s'expriment en effet sous

la forme suivante [Degoutte, 2006, WMO No. 1044, 2010, ISO 1100-2:2010, 2010] :

$$Q\left(h\right) = \begin{cases} 0 & \text{si } h \leq b \text{ ou } h \leq \kappa \\ a\left(h-b\right)^{c} & \text{si } h > b \text{ et } h > \kappa \end{cases} \tag{1}$$

où a est un coefficient lié aux propriétés physiques du contrôle hydraulique, b est l'offset du contrôle hydraulique, c est un exposant lié au type de contrôle hydraulique et κ est la hauteur d'activation du contrôle (ou hauteur de transition). Les deux hauteurs κ et b sont généralement différentes : par exemple dans le cas d'un contrôle par chenal qui succède à un contrôle par section, b correspond à la cote moyenne du fond du chenal alors que κ va correspondre à la hauteur d'ennoiement du contrôle par section, hauteur qui est physiquement différente de b.

Dans le cadre d'un contrôle par section de type seuil rectangulaire, c vaut 3/2 et $a = CB\sqrt{2g}$ où C $[-]$ est un coefficient de débit modélisant les pertes de charge entre la section de mesure (à l'amont) et la section critique du seuil (à l'aval), B [m] est la largeur déversante du seuil et g [m.s^{-2}] est l'accélération de la gravité.

Dans le cadre d'un contrôle par chenal, l'équation 1 est classiquement établie à partir de l'équation de Manning-Strickler appliquée à la géométrie du chenal. L'équation de Manning-Strickler s'écrit :

$$Q\left(h\right) = K_S A R_{\mathrm{h}}^{2/3} \sqrt{S_f} \tag{2}$$

où K_S [m$^{1/3}$.s^{-1}] est la résistance à l'écoulement moyenne du chenal (coefficient de Strickler) , A [m^2] est la surface mouillée, $R_{\mathrm{h}} = A/P$ [m] est le rayon hydraulique, P [m] est le périmètre mouillé, S_f $[-]$ est la pente de la ligne d'énergie qui est approchée par la pente moyenne du lit de la rivière lorsque l'écoulement est uniforme. Si la section du chenal est rectangulaire large ($h - b \ll B$) alors l'équation 2 peut se ramener à la forme de l'équation 1 avec $c = 5/3$ et $a = K_S B\sqrt{S_f}$ où B [m] est la largeur moyenne du chenal.

L'identification de tels contrôles et leur enchaînement dans la relation hauteur-débit permet de modéliser l'équation de la courbe de tarage. Cette identification permet ainsi de définir le nombre de contrôles hydrauliques, leur type (section ou chenal) et leur ordre d'apparition et de disparition. Elle permet aussi de définir l'information sur la

configuration hydraulique de chaque contrôle (géométrie, résistance à l'écoulement par exemple). Cette information est ensuite utilisée comme information *a priori* dans l'inférence bayésienne.

Un tel enchaînement de contrôles est représenté par la matrice des contrôles $\mathcal{M}$ qui est la clef de voûte du modèle hauteur-débit (SD) de BaRatin. En effet, l'équation de la courbe de tarage d'un tel modèle peut s'écrire sous la forme générale suivante:

$$Q(h) = \sum_{i=1}^{N_{\text{seg}}} \left(\mathbf{1}_{[\kappa_{i-1};\kappa_i[}(h) \sum_{j=1}^{N_{\text{c}}} \mathcal{M}\,(i,j)\, a_j\, (h - b_j)^{c_j} \right) \tag{3}$$

où :

- h [m] est la hauteur d'eau ;
- Q [$\text{m}^3.\text{s}^{-1}$] est le débit ;
- N_{seg} est le nombre de segments ;
- $\mathcal{M}\,(i,j)$ est la matrice des contrôles, valant 1 si le contrôle est actif, 0 sinon ;
- la fonction $\mathbf{1}_{[\kappa_{i-1};\kappa_i[}(h)$ est la fonction indicatrice de l'intervalle $[\kappa_{i-1};\kappa_i[$, égal à 1 si h appartient à l'intervalle et 0 sinon ;
- a_j, b_j et c_j sont les paramètres de l'équation de la courbe de tarage : ce sont respectivement le coefficient, l'offset et l'exposant du contrôle j.

2.2. L'inférence bayésienne

2.2.1. Paramétrage

Le vecteur $\boldsymbol{\theta} = (\boldsymbol{\theta}_{\mathbf{RC}}, \boldsymbol{\gamma})$ représente les paramètres de l'inférence bayésienne, $\boldsymbol{\theta}_{\mathbf{RC}}$ étant les paramètres de la courbe de tarage et $\boldsymbol{\gamma} = (\gamma_1, \gamma_2)$ les paramètres du modèle d'erreur structurelle. Celle-ci représente l'erreur d'approximation de la relation hauteur-débit réelle par l'équation de la courbe de tarage.

Les hauteurs de transition κ_i sont déduites des autres paramètres *via* une relation de continuité du débit en $h = \kappa_i$ entre les segments i et $(i+1)$. A noter que cette procédure, mieux adaptée à l'étude des détarages, est différente de celle utilisée dans la version opérationnelle de BaRatin. Ce sont alors les offsets b_i qui sont déduits par continuité et non les hauteurs de transition κ_i. Si le $(i+1)^{\text{ème}}$ contrôle hydraulique s'ajoute au contrôle hydraulique précédent ($i^{\text{ème}}$), la hauteur de transition κ_i est égale au paramètre b_{i+1} du $(i+1)^{\text{ème}}$ contrôle. En revanche, si le $(i+1)^{\text{ème}}$ contrôle hydraulique remplace le $i^{\text{ème}}$ contrôle hydraulique, la condition de continuité devient :

$$a_i \left(\kappa_i - b_i\right)^{c_i} - a_{i+1} \left(\kappa_i - b_{i+1}\right)^{c_{i+1}} = 0 \tag{4}$$

La hauteur de transition κ_i est alors calculée numériquement en résolvant l'équation 4 avec l'algorithme de Newton-Raphson.

2.2.2. La vraisemblance

Les jaugeages $\left(\widetilde{\boldsymbol{X}}_i, \widetilde{Q}_i\right)_{i\in[\![1;N]\!]}$ représentent les estimations (mesures) des N valeurs réelles $(X_i, Q_i)_{i\in[\![1;N]\!]}$ des données d'entrée $\boldsymbol{X}$ du modèle (courbe de tarage complexe) et du débit (donnée de sortie). Les modèles présentés dans ce manuscrit ont deux données d'entrée : la première donnée d'entrée est toujours la hauteur d'eau à la station de jaugeage, comme pour les courbes de tarage simples (modèle SD) tandis que la seconde est respectivement pour les modèles SGD, SFD ou SPD : le gradient limnimétrique $\dfrac{\partial h}{\partial t}$, la hauteur d'eau h_2 à une seconde station ou le numéro de la période. Dans ce manuscrit, on suppose que les erreurs de mesure des données d'entrée sont négligeables devant les erreurs de mesure du débit :

$$\begin{cases} \widetilde{X}_i = X_i \\ \widetilde{Q}_i = Q_i + \epsilon_{Q,i} \quad \text{avec} \quad \epsilon_{Q,i} \overset{\text{indép.}}{\sim} \mathcal{N}\left(0, u_{Q,i}\right) \end{cases} \tag{5}$$

où les écarts-types $u_{Q,i}$ (incertitudes-types sur les mesures du débit) sont supposés connus. Des valeurs d'incertitude peuvent être atribuées aux jaugeages selon la technique de mesure et la procédure terrain utilisées. Ces valeurs peuvent s'appuyer sur des résultats des

méthodes de propagation d'incertitude [cf. Despax et al., 2016] et/ou sur des résultats de comparaison interlaboratoires [cf. Le Coz et al., 2016a].

Le vrai débit s'écrit comme la somme du débit prédit par la courbe de tarage et d'une erreur structurelle :

$$Q_i = \underbrace{f\left(\boldsymbol{X}_i|\boldsymbol{\theta}_{\mathbf{RC}}\right)}_{\widehat{Q}_i} + \epsilon_{f,i} \quad \text{avec} \quad \epsilon_{f,i} \overset{\text{indép.}}{\sim} \mathcal{N}\left(0, \sigma_{f,i} = \gamma_1 + \gamma_2 \widehat{Q_i}\right) \tag{6}$$

où $\boldsymbol{\theta}_{\mathbf{RC}}$ sont les paramètres de la courbe de tarage, $\boldsymbol{\sigma_f} = (\sigma_{f,1}, \ldots, \sigma_{f,N})$ sont les écarts-types des erreurs structurelles $\boldsymbol{\epsilon_f} = (\epsilon_{f,1}, \ldots, \epsilon_{f,N})$ et $\widehat{\boldsymbol{Q}} = \left(\widehat{Q}_1, \ldots, \widehat{Q}_N\right)$ sont les estimations de débit issues des N jaugeages.

Les écarts-types $\sigma_{f,i}$ des erreurs structurelles sont modélisés par une fonction affine basée sur de nombreuses observations : on observe en effet de plus fortes incertitudes structurelles pour les forts débits. Les erreurs structurelles $(\epsilon_{f,1}, \ldots, \epsilon_{f,N})$ et les erreurs de jaugeages $(\epsilon_{Q,1}, \ldots, \epsilon_{Q,N})$ sont supposées indépendantes.

En combinant les équations 6 et 5 on obtient la relation suivante :

$$\widetilde{Q}_i = f\left(\widetilde{h}_i \middle| \boldsymbol{\theta}_{\mathbf{RC}}\right) + \epsilon_{Q,i} + \epsilon_{f,i} \quad \text{avec} \quad \epsilon_{Q,i} + \epsilon_{f,i} \overset{\text{indép.}}{\sim} \mathcal{N}\left(0, \sqrt{\sigma_{f,i}^2 + u_{Q,i}^2}\right) \tag{7}$$

La fonction de vraisemblance L des débits observés $\widetilde{\boldsymbol{Q}}$ prend la forme suivante :

$$L\left(\widetilde{\boldsymbol{Q}} \middle| \boldsymbol{\theta} = (\boldsymbol{\theta}_{\mathbf{RC}}, \boldsymbol{\gamma}), \tilde{\boldsymbol{h}}\right) = \prod_{i=1}^{N} p_{\text{norm}}\left[\widetilde{Q}_i \middle| f\left(\widetilde{X}_i \middle| \boldsymbol{\theta}_{\mathbf{RC}}\right), \sqrt{\sigma_{f,i}^2 + u_{Q,i}^2}\right] \tag{8}$$

où $\widetilde{\boldsymbol{Q}} = \left(\widetilde{Q}_1, \ldots, \widetilde{Q}_N\right)$ sont les N débits jaugés, $\tilde{\boldsymbol{h}} = \left(\widetilde{h}_1, \ldots, \widetilde{h}_N\right)$ sont les données d'entrée et $p_{\text{norm}}[z|m, s]$ est la densité de probabilité d'une distribution gaussienne de moyenne m et d'écart-type s, évaluée en z.

2.2.3. Distribution a priori

Les distributions *a priori* permettent d'utiliser l'information hydraulique dans l'estimation de la courbe de tarage. Dans ce manuscrit, on suppose les distributions *a priori* de chaque paramètre indépendantes entre elles. Ainsi, la distribution *a priori* jointe prend la forme

suivante :

$$p\left(\boldsymbol{\theta_{RC}}, \boldsymbol{\gamma}\right) = p\left(\gamma_1\right) p\left(\gamma_2\right) \prod_{i=1}^{m} p\left(\theta_i\right) \tag{9}$$

Pour chaque paramètre du veteur $\boldsymbol{\theta_{RC}}$ de la courbe de tarage, on utilise des distributions gaussiennes comme distributions *a priori*. Pour les paramètres d'erreur γ_1 and γ_2, les distributions *a priori* sont des distributions uniformes plates ($U\left(0, 10^6\right)$) : on veut en effet que ces paramètres soient inférés grâce aux jaugeages. D'autres types de distributions sont utilisables, si des informations ou hypothèses le justifient.

2.2.4. Distribution a posteriori

Le théorème de Bayes permet de combiner l'information des observations $(\widetilde{\boldsymbol{X}}, \widetilde{\boldsymbol{Q}})$ (grâce à la vraisemblance) avec l'information *a priori*. On obtient alors une distribution, dite *a posteriori*, de paramètres inconnus $\boldsymbol{\theta}$. La fonction de densité de probabilité de cette distribution *a posteriori*, notée $p\left(\boldsymbol{\theta}\middle|\widetilde{\boldsymbol{X}}, \widetilde{\boldsymbol{Q}}\right)$, est définie par :

$$p\left(\boldsymbol{\theta}\middle|\widetilde{\boldsymbol{h}}, \widetilde{\boldsymbol{Q}}\right) = \frac{\overbrace{p\left(\widetilde{\boldsymbol{Q}}\middle|\boldsymbol{\theta}, \widetilde{\boldsymbol{h}}\right)}^{\text{vraisemblance}} \overbrace{p\left(\boldsymbol{\theta}\right)}^{a\ priori}}{\underbrace{\int p\left(\widetilde{\boldsymbol{Q}}\middle|\boldsymbol{\theta}, \widetilde{\boldsymbol{h}}\right) p\left(\boldsymbol{\theta}\right) d\boldsymbol{\theta}}_{\text{constante de normalisation}}} \tag{10}$$

Le numérateur est simplement le produit de la vraisemblance et de la distribution *a priori*. Le dénominateur est plus complexe puisqu'il nécessite de calculer l'intégrale de ce produit par rapport aux paramètres $\boldsymbol{\theta}$. Ce dénominateur ne reste toutefois qu'une constante de normalisation : $(\widetilde{\boldsymbol{X}}, \widetilde{\boldsymbol{Q}})$ est connu et les paramètres $\boldsymbol{\theta}$ n'existent plus dans le dénominateur car ils sont intégrés. Le dénominateur assure donc que l'aire sous de la fonction de densité de probabilité de la distribution *a posteriori* est égale à 1. En pratique, il n'est en général pas nécessaire de calculer cette constante car les algorithmes MCMC utilisés pour échantillonner la distribution *a posteriori* ne requièrent que la connaissance de cette distribution *a posteriori* à une constante près. Le théorème de Bayes se simplifie alors ainsi :

$$p\left(\boldsymbol{\theta}\middle|\widetilde{\boldsymbol{h}}, \widetilde{\boldsymbol{Q}}\right) \propto p\left(\widetilde{\boldsymbol{Q}}\middle|\boldsymbol{\theta}, \widetilde{\boldsymbol{h}}\right) p\left(\boldsymbol{\theta}\right) \tag{11}$$

où le symbole "$\propto$" signifie "est proportionnel à".

L'équation 11 montre que le calcul de la fonction de densité de probabilité *a posteriori* (à une constante près) est simple : il s'agit du produit de la vraisemblance et de la distribution *a priori*. La distribution *a posteriori* résultante représente la connaissance des paramètres $\boldsymbol{\theta}$ étant données deux sources d'information : les jaugeages et la connaissance *a priori*.

2.2.5. Échantillonnage MCMC

Une manière facile d'utiliser en pratique la fonction de densité de probabilité *a posteriori* est de simuler de nombreuses réalisations grâce aux méthodes de Monte-Carlo par chaînes de Markov (MCMC). Ces échantillons MCMC peuvent être utilisés pour représenter graphiquement les distributions *a posteriori* (par exemple l'histogramme des échantillons d'un paramètre particulier peut représenter la densité marginale *a posteriori*). De plus, ces échantillons peuvent être propagés pour estimer n'importe quelle grandeur dérivée des paramètres : par exemple, la courbe de tarage en utilisant l'estimateur du maximum *a posteriori* (MAP) et les intervalles d'incertitude à différents niveaux de confiance/crédibilié (95% usuellement en hydrométrie, cf. HUG, ISO/TS 25377:2007, 2007).

Dans cette thèse, on utilise un échantillonneur MCMC combiné [Sun, 2013]. Cet algorithme est la combinaison de trois échantillonneurs MCMC :

- la première étape utilise un algorithme "one-at-a-time" adaptatif de Metropolis avec des distributions de saut unidimensionnelles pour estimer la matrice de covariance des sauts ;
- la seconde étape utilise un algorithme adaptatif de Metropolis pour estimer les facteurs d'échelle de la matrice de covariance ;
- La troisème et dernière étape utilise l'algorithme classique non adaptatif de Metropolis avec la matrice de covariance estimée pour estimer la distribution cible.

3. Trois cas de relations hauteur-débit non univoques

3.1. L'hystérésis due aux écoulements transitoires

3.1.1. Une relation hauteur-gradient-débit

L'effet d'hystérésis étudié dans cette thèse est un processus hydraulique associé à un écoulement transitoire dans un chenal relativement plat. Ce phénomène affecte la relation hauteur-débit d'une station hydrométrique en la rendant non univoque : à une hauteur d'eau donnée, le débit en crue est plus fort que celui en décrue (cf. figure 3-b). Ce phénomène est dû au fait que, lors de la propagation d'un écoulement transitoire, la célérité de l'onde de pression (niveau d'eau) est inférieure à la célérité de l'onde de vitesse, et donc inférieure à la célérité de l'onde de débit (cf. figure 3-a). Le maximum de débit $Q_{\max}$ est atteint avant le maximum de hauteur d'eau $h_{\max}$, ce qui entraîne une représentation de la courbe de tarage en forme de boucle (cf. figure 3-b).

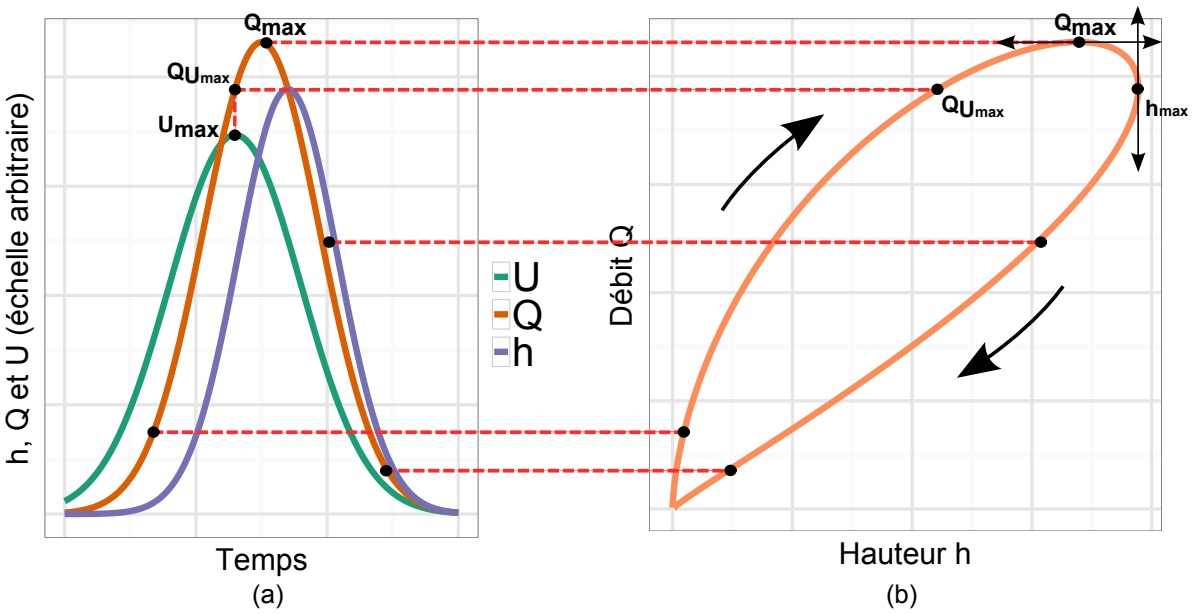

Figure 3 – Représentation graphique de l'hystérésis due aux écoulements transitoires : (a) courbes temporelles de la vitesse (U), du débit (Q) et de la hauteur d'eau (h) ; (b) représentation hauteur-débit associée.

Ne pas prendre en compte l'effet d'hystérésis lorqu'il existe peut entraîner des conséquences indésirables :

- des incertitudes plus grandes sur les débits estimés à cause de la dispersion des débits autour de la courbe de tarage simple (modèle hauteur-débit) ;
- une sous-estimation du pic de crue (débit max) ce qui est préjudiciable à l'établissement des mesures de sécurité. Cela peut potentiellement affecter le dimensionnement des déversoirs et digues de protection de crue ;
- un décalage temporel dans l'estimation des séries de débit, ce qui peut augmenter les incertitudes dans la prévision des crues.

3.1.2. Le modèle SGD (Stage-Gradient-Discharge)

La pratique usuelle en hydrométrie pour corriger l'effet d'hystérésis est de considérer la propagation de l'onde de crue dans l'estimation de la pente d'énergie S_f. Le modèle hauteur-gradient-débit (SGD) proposé dans ce manuscrit est basé sur la formule de Jones [Jones, 1915]. Celle-ci permet l'estimation de cette pente dans la formule de Manning-Strickler (cf. équation 2) en utilisant le gradient limnimétrique $\frac{\partial h}{\partial t}$ et la célérité c de propagation de l'onde de crue. Ainsi, pour un contrôle par chenal, le modèle SGD s'écrit :

$$Q = K_S A R_{\mathrm{h}}^{2/3} \sqrt{S_0 + \frac{1}{c}\frac{\partial h}{\partial t}} \tag{12}$$

où S_0 est la pente longitudinale moyenne du tronçon de contrôle autour de la station.

La célérité c peut être modélisée soit comme une constante, soit comme une fonction de la hauteur d'eau h sous hypothèse d'onde cinématique (cf. Chow, 1959, Henderson, 1966). Si le chenal est prismatique ou si les berges sont verticales sur la plage de variation de h, c'est-à-dire si $\partial A = B\partial h$, on a :

$$c = \frac{\partial Q}{\partial A} \simeq \frac{1}{B}\frac{\partial Q_0}{\partial h} \tag{13}$$

avec $Q_0 = K_S A R_{\mathrm{h}}^{2/3}\sqrt{S_0}$ le débit en régime permanent.

D'autres modèles SGD ont été testés dans la thèse : développements d'ordres 2 et 3 proposés par Fenton [1999]. Les résultats ne sont pas meilleurs, voire moins bons qu'avec le simple modèle de l'équation 12 (formule de Jones, 1915, ou développement d'ordre 1).

3.1.3. Exemples d'application

Le besoin de prendre en compte l'hystérésis lorsqu'elle existe dans l'estimation de la courbe de tarage est représenté par la figure 4. L'intervalle d'incertitude totale du modèle SD est jusqu'à plus de quatre fois plus large que celui du modèle SGD (figures 4-a et 4-b). Cela démontre les limites du modèle SD pour un tel écoulement transitoire. On peut aussi remarquer que l'intervalle d'incertitude paramétrique est plus large pour le modèle SD que pour le modèle SGD alors que l'information *a priori* est la même pour les deux modèles. Le décalage temporel des résultats du modèle SD et la sous-estimation du pic de crue n'existent plus lorsque l'on utilise un modèle SGD. En effet ce modèle représente bien la dynamique de la crue et la courbe de tarage reproduit la forme de boucle.

Deux stations affectées par l'effet d'hystérésis ont été étudiées : des chasses de barrage sur l'Èbre à Ascó en Espagne (figure 4) et une série de crues dans un canal jaugeur équipé d'un débitmètre continu Dopler. D'autres stations avec ou sans hystérésis ont aussi été analysées (cf. Annexe A). Ces cas d'étude illustrent l'importance de prendre en compte l'effet d'hystérésis quand il existe, et le bon comportement du modèle lorsque l'effet est négligeable.

Modéliser la célérité c de propagation de l'onde de crue comme une fonction de la hauteur d'eau entraîne moins d'incertitude dans l'estimation de la courbe de tarage que si cette célérité était supposée constante avec la hauteur d'eau. L'information *a priori* est importante pour le modèle SGD : en son absence, les paramètres de la courbe de tarage présentent de fortes interactions, ce qui peut entraîner des estimations non physiques de ces paramètres malgré de bons résultats graphiques. Ces problèmes d'interaction s'évitent facilement en spécifiant comme *a priori* au moins des ordres de grandeurs réalistes des paramètres. En l'absence d'autres détarages, le modèle SGD peut être calé sur un unique évènement pour ensuite estimer les courbes de tarage d'autres évènements. Ce calage peut aussi s'effectuer sur différents évènements de crue.

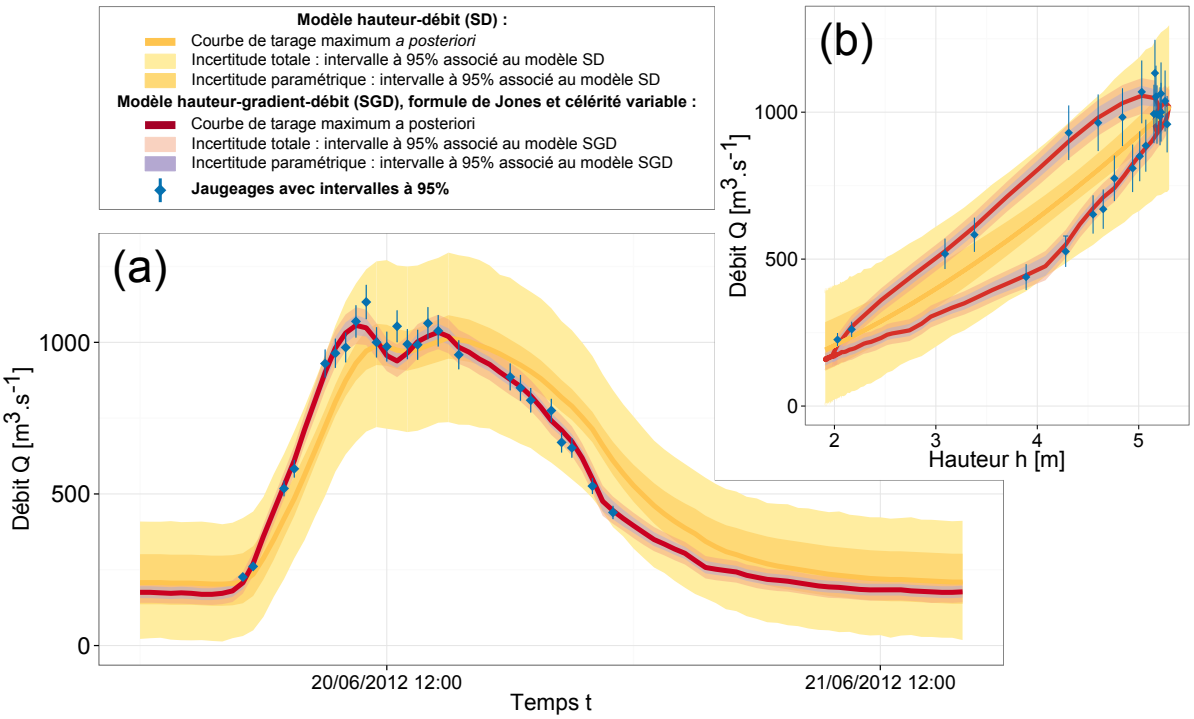

Figure 4 – L'Èbre à Ascó en Espagne, crue de juin 2012, comparaison entre le modèle hauteur-débit (SD) et le modèle hauteur-gradient-débit (SGD) utilisant la formule de Jones avec la célérité c de propagation de l'onde de crue modélisée comme fonction de la hauteur d'eau h : (a) représentation temporelle du débit ; (b) représentation hauteur-débit.

Une analyse des stratégies de jaugeage a été realisée. La stratégie usuelle consistant à jauger pendant la décrue juste après le pic de crue peut amener de plus fortes incertitudes en crue et une identification biaisée de l'importance de l'effet d'hystérésis. Une meilleure stratégie est de jauger près des points remarquables de l'évènement (minimum et maximum de hauteur, maximum de débit, minimum et maximum de gradient limnimétrique), et pendant la décrue (pour explorer proprement les gradients négatifs). Ces jaugeages peuvent être réalisés sur différents évènements.

3.2. Le remous variable et les stations hydrométriques à double échelle

3.2.1. Une relation hauteur-dénivelée-débit

Dans le cas où la pente de la ligne d'énergie d'un contrôle par chenal est variable, le modèle hauteur-débit (SD) n'est plus adapté pour l'estimation des débits. Cette variablilité est généralement due à une condition limite aval variable (cas typique: confluence, barrage, lac, marée, etc...) et peut parfois provenir d'écoulements transitoires.

La figure 5 schématise le cas typique d'un contrôle par chenal en amont d'un barrage mais peut illustrer n'importe quel autre cas équivalent d'influence aval variable. Suivant les conditions aux limites amont (débit) et aval (hauteur), l'échelle principale peut être sous un régime d'écoulement uniforme (cf. ligne d'eau (1)) ou sous un régime d'écoulement graduellement varié (cf. ligne d'eau (2)). Il est vraiment important de comprendre que les deux tronçons de contrôle ne sont pas les mêmes : le premier est centré autour de l'échelle principale alors que le second est situé entre les deux échelles. Cette différence essentielle implique que les offsets h'_0 et h_0 des deux chenaux ne sont pas les mêmes. Lorsque la charge dynamique est négligeable devant la charge statique ($V^2/2g \ll h$), la pente de la ligne d'énergie peut être approchée par la pente de la ligne d'eau calculée par $(h_1 - h_2)/L$, en considérant que la distance L est suffisamment courte pour avoir un profil de ligne d'eau linéaire entre les deux échelles (hypothèse de régime d'écoulement graduellement varié).

3.2.2. Le modèle SFD (Stage-Fall-Discharge)

Une pratique courante pour corriger un tel effet d'influence aval variable est de calculer la pente S_f dans la formule de Manning-Strickler en utilisant des relevés de hauteurs h_1 et h_2 à deux échelles disposées le long du tronçon de contrôle. Néanmoins, cette pratique peut être raffinée en effectuant une transition vers un contrôle par chenal non influencé lorsque la variabilité de la pente n'existe plus pour les débits plus importants. Le modèle

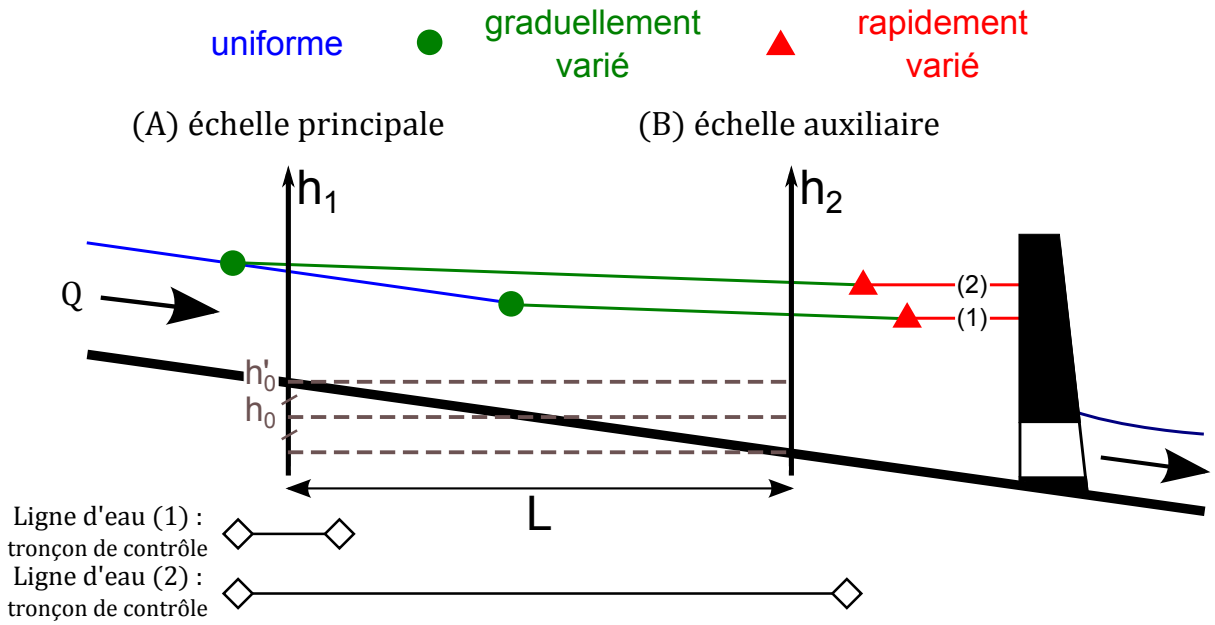

Figure 5 – Modèle hauteur-dénivelée-débit : transitions typiques entre un chenal non affecté par l'influence aval variable (ligne d'eau (1)) et un chenal affecté par l'influence aval variable (ligne d'eau (2)).

SFD s'écrit ainsi, dans le cadre d'un contrôle non influencé de type chenal :

$$Q\left(h_1,h_2\right)=\begin{cases} K_S B\left(h_1-h_0\right)^M\sqrt{\left(h_1-h_2-\delta_h\right)/L} & \text{si} \quad h_1<\kappa\left(h_2\right) \qquad \text{(pente variable)} \\ K'_S B'\left(h_1-h'_0\right)^{M'}\sqrt{S_0} & \text{si} \quad h_1\geq\kappa\left(h_2\right) \qquad \text{(contrôle par chenal)} \end{cases} \tag{14}$$

où h'_0 est la cote moyenne du fond du chenal autour de la station principale, h_0 est celle du contrôle entre les deux stations, δ_h est la différence de nivellement entre les échelles amont et aval, L la distance entre les deux échelles, et M et M' sont des exposants liés l'équation de friction et à la forme de la section du contrôle. M et M' sont égaux à 5/3 pour la formule de Manning-Strickler et un chenal de section rectangulaire large. La hauteur de transition $\kappa\left(h_2\right)$ entre les deux contrôles est calculée numériquement par continuité du débit avec l'algorithme de Newton-Raphson. D'autres configurations hydrauliques ont aussi été traitées dans la thèse comme par exemple lorsque le contrôle non influencé est de type section et lorsqu'il n'y a qu'un seul contrôle influencé (de type chenal) et que la rugosité est variable en fonction de la hauteur d'eau h_1.

Le modèle est original car il permet la transition d'un contrôle influencé à un contrôle non influencé par une simple continuité sur le débit de transition et car la différence δ_h

de nivellement entre les deux échelles est un paramètre du modèle (et donc se cale sur les jaugeages et l'information *a priori*).

3.2.3. Exemples d'application

Le modèle SFD a été appliqué à plusieurs stations à double échelle, dont le Rhône à Valence en France (figure 6). Toutes les courbes de tarage du maximum *a posteriori* s'accordent bien avec les jaugeages et possèdent de faibles incertitudes : l'incertitude totale est inférieure à ±10% pour des débits supérieurs à 2000 $m^3.s^{-1}$ (cf. figure 6). La représentation hauteur-débit des figures 6-a et b est caractéristique d'une courbe de tarage d'une relation hauteur-débit affectées par l'influence aval variable d'un barrage qui s'efface en crue. En effet, pour des valeurs de h_2 données, la courbe de tarage augmente jusqu'à coïncider avec celle du chenal non influencé.

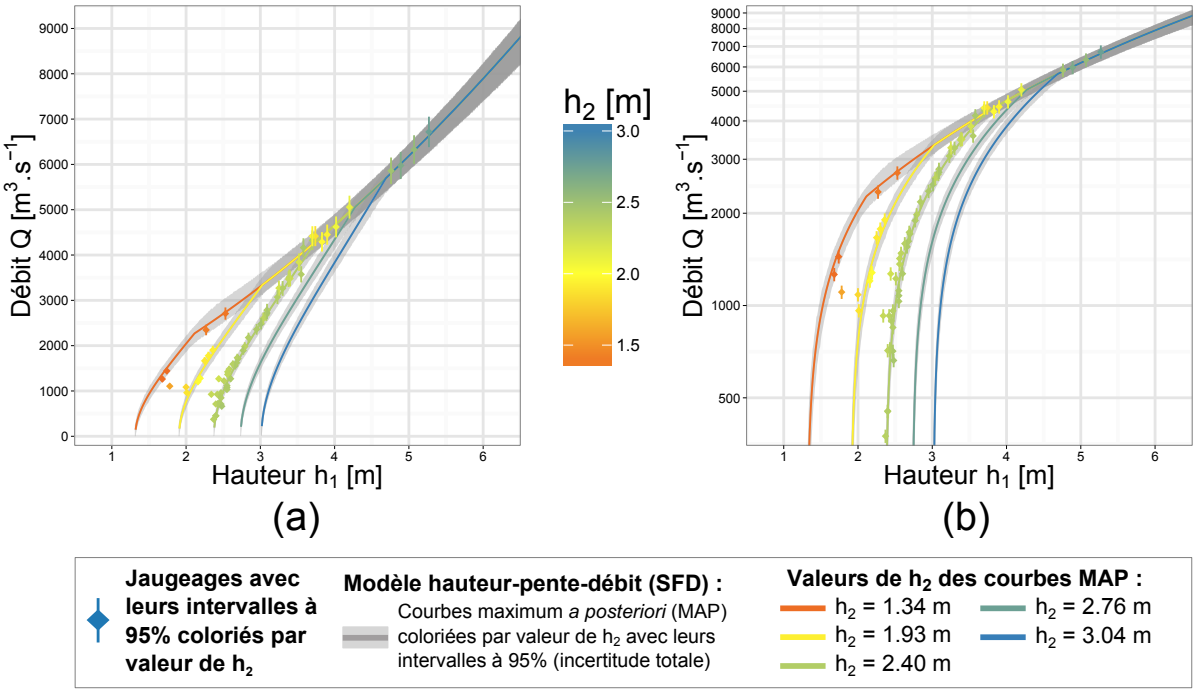

Figure 6 – Le Rhône à Valence en France sous l'influence variable de l'aménagement de Beauchastel : représentation hauteur-débit du modèle hauteur-dénivelée-débit (SFD) avec le débit en (a) échelle logarithmique et en (b) échelle normale.

La robustesse du modèle a été étudiée au travers de l'analyse de sensibilité à l'information *a priori* et aux jaugeages. Quand la relation hauteur-dénivelée-débit est bien documentée par des jaugeages, la performance du nouveau modèle est acceptable pour les applica-

tions hydrométriques. La transition entre les deux contrôles influencé et non influencé est en particulier bien estimée, les estimations de débit concordent bien avec les jaugeages et leurs incertitudes sont très acceptables comme pour l'exemple du Rhône à Valence. Lorsque la relation est moins bien documentée, les résultats demeurent acceptables mais plus incertains (cf. la rivière Guthusbekken à la station 0003·0033 en Norvège). Le cas d'étude plus complexe du Madeira à la station de Fazenda Vista Alegre au Brésil montre les limites du modèle SFD lorsque la résistance à l'écoulement varie aussi en fonction de la hauteur d'eau h_1 à cause de la présence de dunes de sable au fond du lit de la rivière, en plus de la pente variable due à l'influence aval variable de l'Amazone. Ce dernier cas d'étude montre aussi tout l'intérêt d'estimer la différence de nivellement δ_h dans la courbe de tarage car ce paramètre peut être mal connu, difficile à mesurer, et alors amener des incertitudes non négligeables.

La méthode SFD pour l'influence aval variable a fait l'objet d'un article scientifique [Mansanarez et al., 2016b] et a été opérationnellement déployée par la Compagnie Nationale du Rhône (CNR) sur ses stations à double échelle.

3.3. Les détarages nets dus aux évolutions du lit de la rivière

3.3.1. Une relation hauteur-période-débit

Différents types de détarage morphodynamique existent. Les détarages étudiés dans cette thèse correspondent aux changements nets dans la relation hauteur-débit suite à une évolution du lit de la rivière. Ces détarages peuvent affecter à la fois les contrôles par chenal et par section. Une modification globale du lit mineur (contrôle par chenal) va aussi affecter les contrôles par section du lit mineur (cf. figure 7), contrôles qui peuvent être en plus modifiés localement (cf. figure 7). Ces notions de changements locaux et globaux sont prises en compte dans le modèle SPD en reparamétrisant l'information *a priori* fournie par l'utilisateur. L'information *a priori* sur les changements peut aussi différer selon l'information disponible sur les changements de la station (changement incrémentiel entre deux périodes successives ou changement cumulé par rapport à une période de référence).

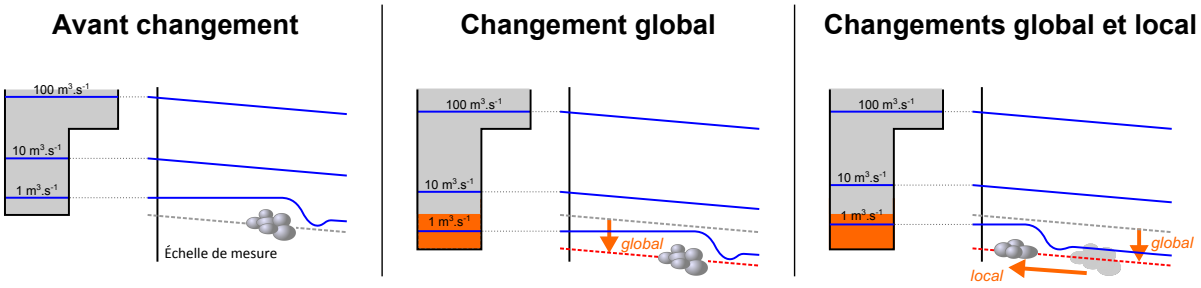

Figure 7 – Illustration des changements locaux et globaux dans le lit de la rivière. Le profil en travers est pris à la station de jaugeage.

3.3.2. Le modèle SPD (Stage-Period-Discharge)

Le modèle hauteur-période-débit (SPD) proposé dans cette thèse prend en compte à la fois les changements locaux et globaux et les changements cumulés ou incrémentiels. Il se base sur une segmentation du temps en périodes "stables" délimitées par les dates des détarages : on suppose dans ce modèle que les dates de détarage sont connues (dates fournis par l'utilisateur). En plus de l'information demandées par le modèle SD, le modèle SPD nécessite l'information sur les paramètres de la courbe de tarage susceptibles de changer entre les périodes (quels paramètres et de combien).

Dès lors l'équation 3 peut se réécrire de la façon suivante pour la période k :

$$Q^{(k)}(h) = \sum_{i=1}^{N_{\text{seg}}} \left(\mathbf{1}_{\left[\kappa_{i-1}^{(k)};\kappa_i^{(k)}\right[}(h) \sum_{j=1}^{N_c} \mathcal{M}(i,j)\, a_j^{(k)} \left(h - b_j^{(k)}\right)^{c_j} \right) \tag{15}$$

où:

- h est la hauteur d'eau;
- $Q^{(k)}$ est le débit pour la période k ;
- N_{seg} est le nombre de segments. Cela implique $N_{\text{seg}} + 1$ hauteurs de transition $\kappa_i^{(k)}$, $i \in [\![0, N_{\text{seg}}]\!]$, avec $\kappa_0^{(k)} = b_1^{(k)}$ pour la période k ;
- $\mathcal{M}(i,j)$ est la matrice des contrôles. Par hypothèse, le modèle SPD ne prend pas en compte l'ajout ou la suppression des contrôles : cette matrice $\mathcal{M}$ ne change pas entre les périodes;

- la fonction $\mathbf{1}_{\left[\kappa_{i-1}^{(k)};\kappa_i^{(k)}\right[}(h)$ est la fonction indicatrice de l'intervalle $\left[\kappa_{i-1}^{(k)};\kappa_i^{(k)}\right[$, égal à 1 si h appartient à l'intervalle et 0 sinon ;
- $a_j^{(k)}$, $b_j^{(k)}$ et c_j sont les paramètres de l'équation de la courbe de tarage : ce sont respectivement le coefficient, l'offset et l'exposant du contrôle j de la période k.

3.3.3. Exemples d'application

La figure 8 est la représentation hauteur-débit des résultats de l'application du modèle SPD sur l'Ardèche à la station de Meyras en France. Cette figure représente les courbes de tarage estimées avec leurs intervalles d'incertitude totale à 95% pour les cinq périodes stables entre 2001 et 2014, identifiées par les gestionnaires de la station. Les résultats sont acceptables : les courbes de tarage passent précisément par les jaugeages pour toutes les périodes stables.

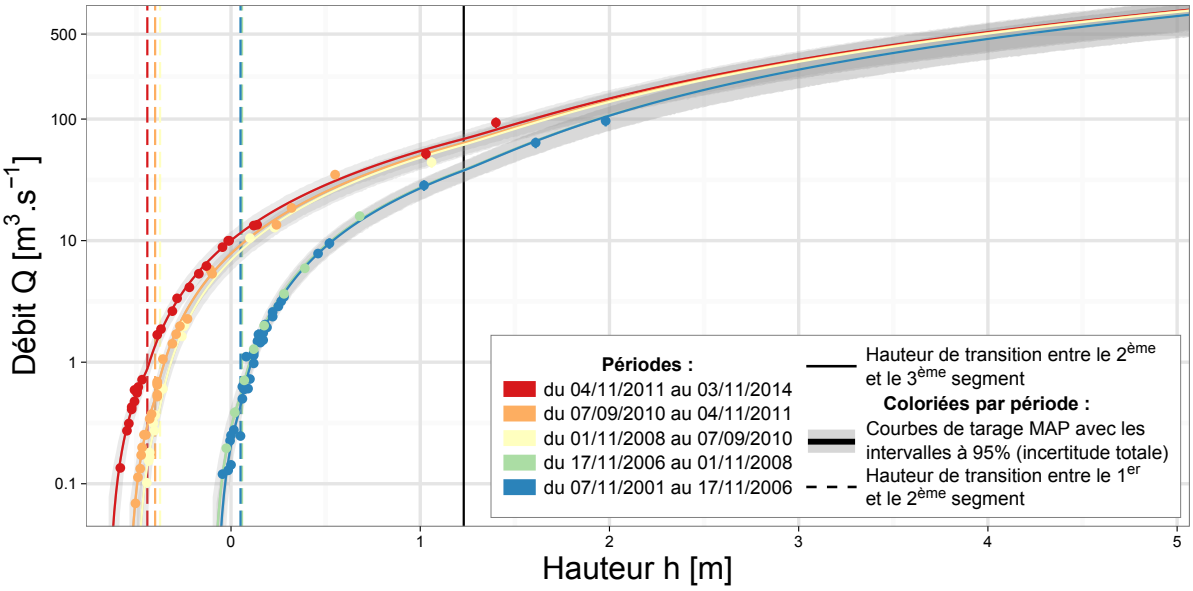

Figure 8 – L'Ardèche à Meyras en France : représentation hauteur-débit du modèle hauteur-période-débit (SPD) avec le débit en échelle logarithmique.

Contrairement à d'autres méthodes [Jalbert et al., 2011, Morlot et al., 2014], le modèle SPD ne suppose pas que les jaugeages vieillissent avec le temps. Ce modèle ne duplique pas non plus les jaugeages pour pouvoir les utiliser sur plusieurs périodes. Chaque jaugeage est assigné à la période même pendant laquelle il a été réalisé sans que son incertitude de mesure ne change. Ce sont les paramètres de la courbe de tarage qui peuvent ne pas

changer entre les périodes lorsque le changement de paramètre n'est pas jugé pertinent par l'utilisateur. Dès lors, les paramètres de la courbe de tarage peuvent être identifiés même si la période ou le segment est peu ou pas jaugé dès que de l'information sur ces paramètres se retrouve sur une autre période et/ou un autre segment. Le modèle SPD transfère en effet de l'information entre les périodes et entre les contrôles.

Le modèle SPD a montré des résultats acceptables sur des stations bien jaugées sujettes au changement d'offset uniquement (l'Ardèche à Meyras en France) en améliorant l'estimation des paramètres stables de la courbes de tarage. Les changements entre paramètres sont bien identifiés entre les périodes et entre les contrôles. Lorsque la station dispose de moins de jaugeages en moyenne par période stable (la Wairau à Barnett's Bank en Nouvelle-Zélande), les résultats demeurent acceptables mais sont plus incertains. Les paramètres stables sont toujours bien identifiés mais les estimations des paramètres variables sont moins précises. Les estimations des hauteurs de transition sont du coup aussi plus incertaines mais elles concordent toujours avec la configuration hydraulique de la station.

Contrairement à la pratique naïve qui consisterait à estimer séparément les courbes de tarage de chaque période stable, le modèle SPD montre de meilleurs résultats sur des stations peu jaugées grâce au transfert d'information entre les périodes et entre les contrôles.

4. Conclusions et perspectives

Dans cette thèse, trois modèles d'estimation de courbes de tarage complexes ont été proposés. Ces modèles diffèrent du modèle SD par les données d'entrée et leur paramétrisation bien que le cadre bayésien et l'analyse hydraulique restent les mêmes. La prise en compte de l'information *a priori* permet d'obtenir des résultats d'estimation des courbes de tarage acceptables même lorsque les segments sont peu jaugés et/ou lorsque les stations sont peu documentées.

D'autres relations hauteur-débit non univoques restent à étudier comme par exemple les détarages liés à la végétation aquatique ou l'influence du couvert de glace. Certaines des relations étudiées dans cette thèse pourrait être combinées comme les détarages nets et l'hystéresis. Les modèles d'erreur peuvent faire l'objet d'une étude plus spécifique comme par exemple les erreurs systématiques sur les jaugeages, sur les mesures de hauteur et dans le modèle d'erreur structurelle. Les modèles développés dans cette thèse sont rétrospectifs mais pourraient être adaptés au temps réel. L'étude de l'impact des incertitudes de la courbe de tarage sur le calage des modèles hydrologiques apporterait aussi beaucoup à la compréhension de tels modèles. Malgré un travail de déploiement opérationnel déjà commencé, il reste encore un important travail de transfert méthodologique, en premier lieu l'interfaçage des modèles SGD, SFD et SPD dans l'environnement de travail BaRatinAGE, et leur documentation pour l'utilisateur.

Contents

List of Figures

List of Tables

Chapter 1

Introduction

Contents

1.1. General background

In Hydrology, one of the main variables – river discharge – cannot be measured continuously. Most often, the discharge time series used by hydrologists result from the transformation of continuous measurements of water level via a stage-discharge relation, called the rating curve [e.g., Rantz, 1982a, Schmidt, 2002]. The rating curve must be estimated at each gauging station, from direct stage-discharge measurements (called gaugings) and some hydraulics considerations on the stage-discharge relation.

To measure low flows, the main difficulty is due to the geometry of the section. Unless some specific hydraulic structure has been built, the section is generally unstable and has a low sensitivity (wide section with low water level): the uncertainty in stage measurement propagates to discharge and dominates the uncertainty in the estimated discharge. The instability of the section may be due to morphologic adjustments such as sand deposits, to the seasonal growth of aquatic vegetation or to river debris. In addition, the discharge measurement at low flows is also affected by a very large relative uncertainty.

Gaugings during high flows are rare because of operational constraints during flood events. Moreover, measured discharges are affected by larger uncertainties than during medium flow conditions, yielding standard errors well above the typical 5-10% obtained during medium flows. These uncertainties affect the estimation of the rating curve, especially since it is frequently extrapolated far beyond the gauged domain. Lastly, complex hydraulic phenomena may further complicate the estimation of flood discharge during some events (overflows, hydraulic hysteresis, debris blocking, hydraulic vortices, damaged or broken hydraulic structure, etc.).

As a consequence of these difficulties, the uncertainty affecting the discharge estimated with the rating curve may exceed 100% during very low or very high flows. Moreover, an additional and poorly understood source of uncertainty is related to the fact that the stage-discharge relation may drift away from the established rating curve, temporarily or permanently. This might be caused by various phenomena, notably a change in the geometry of the section after a flood event, or the seasonal growth of aquatic vegetation. Figure 1.1 taken from Herschy [1995] illustrates some examples of rating curves drifting away due to a range of hydraulic effects (the list is not exhaustive):

(a) the permanent (or 'steady') rating curve is illustrated for comparison purposes and represents the stage-discharge relation without any drifting effect;

(b) the scour and fill of a sand bed channel. During flood events, a mobile riverbed can be subject to rating changes depending on the severity of the event. The flood may change the bottom of the river which creates a shift in the stage-discharge rating curve. This is a particular example of rating changes due to bed evolution;

(c) rating changes due to aquatic vegetation. The aquatic vegetation in the riverbed can grow during some parts of the year and can decay during others, according to various factors such as the climate, the water temperature or the dissolved oxygen in the river. This is a cyclical rating change which implies that different values of discharges may correspond to a same stage;

(d) the ice cover at the river surface. This is a complex process governed by two main factors: the temperature and the size of the river. This effect can be temporary as ice can be sporadically present in the river. It can also be cyclical: some stations are affected by ice cover every year, only during winter or permanently when ice no longer melt in warmer seasons. It affects the average roughness and the cross-sectional geometry of the river.

(e-f) the variable backwater influence of the station due to unsteady downstream boundary conditions. It can be caused by the stage fluctuations of a reservoir, a lake, a tidal outlet (sea, river), or even debris/ice jams or dike break for instance. The variable backwater influence can occur: (e) at low and medium flows in a channel; (f) after the flooding of a downstream section control;

(g) the changing discharge during the flood event. Rising limb and falling limb have distinct discharge values for the same stage. These discharge differences can reach 100% and more in natural rivers. This phenomenon can result from hysteresis due to transient flow.

(h) Overflow and ponding: for example, when the stage exceeds the riverbank height and the flow starts transiting through the floodplain. Then, the stage-discharge relation may be affected by the storage and release of water in the floodplain.

Given the key role of the variable 'discharge' in hydrology, quantifying the rating curve uncertainty is a topic of primary importance. This uncertainty, when ignored, challenges the validity of any hydrologic study, including flood or low-flow frequency analysis [Lang et al., 2010] or the calibration of hydrologic models [Moyeed and Clarke, 2005]. Despite this, the estimation of rating curves and their uncertainties is still based on complex and non-standardised procedures, where expertise is central but hydraulic analysis and modelling are rarely used.

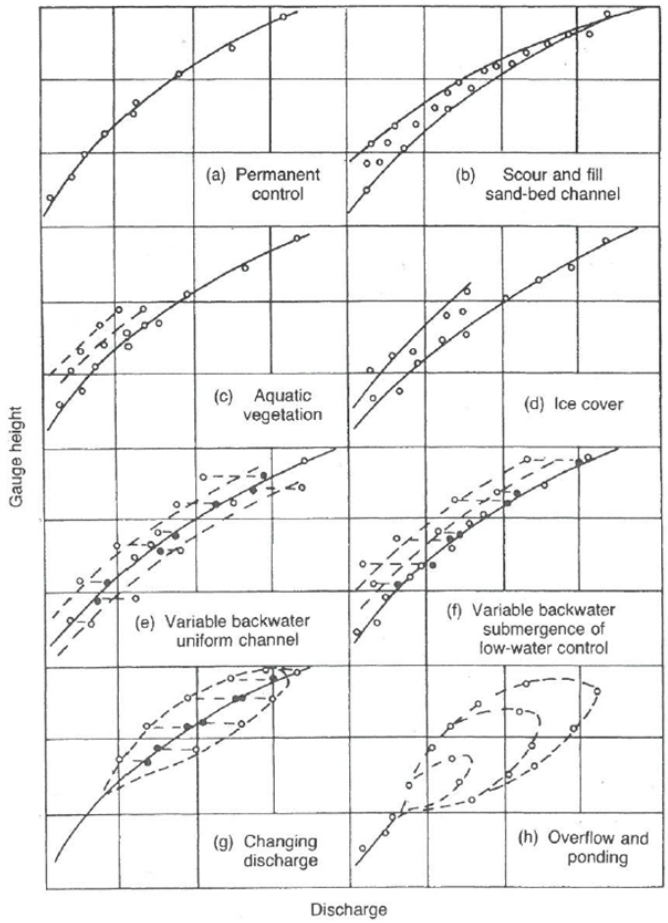

Figure 1.1 – Representation of several non-unique rating curves with their hydraulic effects [from Herschy, 1995].

It is therefore of prime importance to develop robust methods for these tasks, making the best of existing measurements (gaugings) and hydraulic knowledge, realistically accounting for operating conditions, and based as much as possible on verifiable physical constraints. The main objective of this thesis is to develop such a method in the context of non-unique rating curves, i.e. rating curves that may drift away from the permanent state as illustrated in figure 1.1.

1.2. State of the art

Hydrometric stations are preferably located at sites that ensure a unique (one-to-one) relation between water depth y and discharge Q. This can be achieved in two ways: (i) locating the station upstream of a control weir which cancels downstream effects; (ii) selecting a long and homogeneous reach where frictional forces induce a permanent uniform regime. The general form of the stage-discharge relation for a given hydraulic control is a power equation:

$$Q = ay^c \tag{1.1}$$

where the exponent c is for example equal to 3/2 for a rectangular weir (section control) and 5/3 for a simplified Manning-Strickler relation (wide rectangular channel control).

In practice flows can be much more complex than suggested by this simple power equation. During floods for instance, hysteresis effects (figure 1.1-g) or singular frictions in the main channel and the floodplain may affect the flow properties. Moreover actual flows may not be comparable with the 'reference flow conditions' for which the rating curve is valid. This may be due to a perturbation of the hydraulic control (e.g., backwater effects, figures 1.1-e and 1.1-f) or a change in the geometry of the section (e.g., siltation or vegetation during low flows, figure 1.1-c, erosion during floods).

The standard approach is to identify a set of stable periods, each of which is associated with a unique stage-discharge rating curve. When the reference regime is permanently modified, a new rating curve replaces the existing one. Temporary modifications of the hydraulic regime (e.g., due to vegetation) suggest using time-varying rating curves, but in usual operational practice the rating curve is preserved and instead, the stage measurement is sometimes artificially corrected. This operational approach (method CORTH used by the French hydrometric services) allows correcting the estimated discharge but is problematic when the vegetation is temporary washed away by a flood, for instance.

In general, rating curve uncertainties are either ignored or estimated based on a purely statistical procedure. Venetis [1970] proposed the first statistical approach to rating curve uncertainty estimation, based on least-square regression. Dymond and Christian [1982] proposed a method to account for rating curve uncertainty, stage measurement errors, and the effect of ignoring relevant physical processes in the rating curve formulation. Herschy [1999], Clarke [1999], Clarke et al. [2000] combined residual uncertainty with the estimation uncertainty affecting the parameters

of the rating curve. Petersen-Øverleir [2004] proposed a model suitable for heteroscedastic rating curve residuals, a phenomenon frequently observed and ignored in the previous approaches. The same author also investigated more complex stage-discharge relations, including piecewise-power relations [Petersen-Øverleir and Reitan, 2005], hysteresis-accounting models [Petersen-Øverleir, 2006] and floodplain overflows [Petersen-Øverleir, 2008].

These purely statistical approaches do not take advantage of hydraulic knowledge. As a consequence, they sometimes yield to physically unrealistic results (e.g. exponent c of the power relation larger than 3 or 4). Hydraulics-based approaches to rating curve estimation [Schmidt, 2002] are still insufficiently used, but are of interest to explicitly account for the underlying physics governing the flows and to assist the extrapolation of the rating curve for complex flow conditions where gaugings are often unavailable. Sensitivity analysis of a hydraulic model is hence a first step to obtain an order of magnitude of possible errors [Di Baldassarre and Montanari, 2009, Lang et al., 2010, Neppel et al., 2010]. However, translating such orders of magnitude into a distribution that enables a probabilistic quantification of the rating curve uncertainty is a challenging and yet unsolved issue.

A third approach is to verify the rating-curve estimated discharges using exogenous information. For instance, hydraulic consistency can be checked by verifying that the water level simulated by a hydraulic model along a stream is consistent with levels observed at some points of the stream. Hydrologic consistency can also be assessed by comparing the estimated discharges along the river network, or by simple water balance computations (e.g. based on the runoff coefficient). Such information that is not related to the hydrometric station where the rating curve is established may further restrict the range of estimated discharges.

Bayesian analysis is an attractive framework for rating curve uncertainty estimation, since it allows accounting for various sources of errors. Indeed, in addition to any source of uncertainty that can be managed by purely statistical procedures (stage/discharge gauging errors, estimation errors), the Bayesian framework allows accounting for hydraulic knowledge through the specification of the prior distributions of the rating curve parameters. Such knowledge can be expertise or can stem from hydraulic modelling or hydrologic consistency considerations. To our knowledge, Moyeed and Clarke [2005] published the first Bayesian analysis of a rating curve, based on a power relation and a Box-Cox transformation. Moreover, the individual uncertainty of each gauging can be incorporated into the likelihood function (yielding models similar to that of Petersen-Øverleir [2004]). The information content of gaugings (through the likelihood function) and from hydraulic knowledge (through the priors) can hence be combined into the

posterior distribution. This distribution quantifies the uncertainty of the stage-discharge relation, and can easily be processed to obtain uncertainty intervals. Recent work within the HHLY research unit (Irstea) yielded a Bayesian method unique stage-dischargefor rating curve estimation, named BaRatin (BAyesian RATINg curve estimation, Le Coz et al., 2014). This method is implemented as an operational software named BaRatinAGE.

In France, the processing of non-unique stage-discharge rating curves remains quite unsatisfying to date. From 2000 onward, Electricité de France (EDF, the main French electricity producer) started using a new approach to define an optimal number of rating curves based on the reanalysis of past gaugings (Moryciel software). Switching to a new rating curve has to be justified by significant deviations from the current rating curve, given existing uncertainties. However, this approach still relies on the assumption of unique stage-discharge relations for each defined sub-period. Alternative approaches have been proposed for cyclical changes in the rating curve (e.g. seasonal vegetation growth), by artificially correcting measured stages without modifying the base rating curve (CORTH method in the BAREME software used by French hydrometric services). Methodological developments are also in progress at EDF-DTG based on the variographic approach of Jalbert et al. [2011] and the PhD research by T. Morlot on dynamic rating curves (Morlot et al. [2014], Morlot [2014]). The Bayesian approaches proposed in this PhD complement these existing studies by proposing statistical and hydraulic frameworks to estimate specific non-unique stage-discharge rating curves along with their uncertainties.

In the international research literature, many approaches have been proposed to tackle specific causes of non-uniqueness in rating curves. These approaches will be thoroughly reviewed in each specific chapter of this manuscript, and are therefore not detailed in this introduction. Obviously, the developments made during this PhD build on these previous research works.

1.3. Objectives

The overall objective of the thesis is to develop and validate statistical methods using hydraulic knowledge to estimate non-unique stage-discharge rating curves and quantify their uncertainties. Three typical causes of non-uniqueness in stage-discharge relations are investigated:

- the hysteresis due to transient flow, which is an episodic change of the stage-discharge relation during floods;
- the influence of variable backwater due to unsteady downstream boundary conditions, which affect continuously the stage-discharge relation. Indeed, when a control is backwater-affected, variability in the stage-discharge rating curve is observed;
- 'net' rating changes due to bed evolution which is a sudden and permanent change of the stage-discharge relation.

The thesis primarily focuses on stage-discharge relations established at hydrometric stations affected by such effects.

The main research questions underlying this PhD work are the following:

- Is it possible to derive a unique statistical framework to account for the various possible causes of non-uniqueness, or is it preferable to develop case-specific models? A unique statistical model could be easier to implement whereas a case-specific model may be more adapted for the related effect as it underlines the physical process of the tackled effect;
- Is it possible and sufficient to introduce covariates reflecting the dynamics of the processes causing the non-uniqueness of the relation?
- How to include prior knowledge on the physical processes causing the non-uniqueness? In particular, what type of prior information can be specified to improve the rating curves at poorly-gauged stations?
- In an operational perspective, how should a station affected by a non-unique stage-discharge relation be managed? Are traditional gauging strategies still valid or do they need to be changed to enhance the rating curve uncertainty assessment and the detection of non-uniqueness in the stage-discharge relation?

- Should the old gaugings be systematically discarded when a new curve is established? Can these gaugings still be used for rating curve assessment and uncertainty quantification? How to account for the 'age' of gaugings ?

1.4. Outline

This thesis presents the study of three types of non-unique stage-discharge relations: the hysteresis due to transient flow, the variable backwater due to unsteady downstream conditions and net rating changes due to bed evolution. The same methodology is used across all chapters: a specific hydraulically-based model is proposed, and the Bayesian framework used to estimate its parameters is derived. Each model is then applied to two or more hydrometric stations and sensitivity analyses are performed to evaluate the proposed model.

The three models developed in this thesis differ by their inputs and by the rating curve equation itself, but they rely on the same methodology: the analysis of the controls for formulating the rating curve and specifying prior information on its parameters, the rating curve assessment itself using Bayesian inference and MCMC sampling, and the validation of posterior rating curve results by comparing rating curve and uncertainties with observations, and by verifying that rating curve parameter estimates are physically consistent or meaningful.

This PhD dissertation is composed of 6 chapters. It is organised as follows:

- chapter 2 introduces the hydraulic and statistical principles used in the whole PhD manuscript. Some specific vocabulary is first established. A short review of the hydraulic assumptions and notions related to rating curve is then included. Gauging uncertainties are briefly mentioned to introduce the overall statistical framework: the Bayesian inference and the MCMC sampling. An example of the application of a unique stage-discharge rating curve model is presented for the Ardèche River at the hydrometric station of Meyras, France;

- chapter 3 deals with the hysteresis effect due to transient flow. Stage-gradient-discharge (SGD) models using various hydraulic formulas along with stage and stage gradient measurements as inputs are compared. Typical gauging strategies for hysteretic flood events are also compared. Two stations are studied: two dam flushes in the Ebro River at Ascó, Spain, and a gauging flume 'A1' near Plymouth, USA;

- chapter 4 analyses stage-fall-discharge (SFD) rating curves at twin-gauge stations affected by variable backwater due to unsteady downstream conditions. This chapter corresponds to a paper from Mansanarez et al. [2016b] to be published soon in Water Resources Research. The proposed SFD model uses the stage records at two gauges for the computation of the energy slope. The Rhône River at Valence, France, and the Guthusbekken stream at station 0003·0033, Norway, are studied. A challenging case is also studied: the Madeira

River at Fazenda-Vista-Alegre, Brazil, for which the variable backwater influence of the Amazon River is combined with variable roughness due to the presence of sand dunes in the riverbed;

- chapter 5 presents a stage-period-discharge (SPD) model for treating net rating changes due to bed evolution. Stable periods between successive changes are assumed to be known which allows computing stage-discharge rating curves for each period. Information on the parameters and their changes is transferred between periods and between controls, e.g., when section controls can be affected by global bed changes which also affect channel controls. The Ardèche River at Meyras, France, and the Wairau River at Barnett's Bank, New Zealand, provide study cases to investigate the SPD model;
- chapter 6 ends the main document with a conclusion on this PhD work and perspectives of future research.

Two annexes are added to the main document:

- the study of the hysteresis effect at two additional stations: the Ohio River at Wheeling, USA, and the Ardèche River at Sauze, France;
- the derivation of specific formulas needed for the SPD model.

Chapter 2

Hydraulic and statistical tools

Contents

2.1. Vocabulary and conventional notations

This section is devoted to the establishment of the general vocabulary used in the manuscript. This vocabulary is inspired from Rantz [1982a,b], ISO/TS 25377:2007 [2007], WMO No. 1044 [2010], ISO 772:2011 [2011], and WMO No. 385 [2012].

The **stage-discharge relation** refers to the physical relation between the water level (stage) and the streamflow (discharge) at a given cross-section of a river. A stage-discharge (SD) relation is called 'unique' or 'steady' when the variable 'stage' is sufficient to determine the discharge. Conversely, as soon as other variables in addition to the stage are needed to determine the discharge, the stage-discharge relation is qualified as non-unique.

A **rating curve** is a p-parameterised $(\theta_1, \ldots, \theta_p)$ function which estimates a variable Q (called 'output' or 'response variable') from measurable variables $X_1, \ldots, X_n$ (called 'input variables' or 'forcings'). Typically, Q represents the discharge and X_1 represents the stage. The rating curve is the model which allows estimating discharge time series (hydrographs) when the inputs variables are continuously measured (e.g., stage records for the water level).

$$Q = f\left(X_1, \ldots, X_n | \theta_1, \ldots, \theta_p\right)$$

A rating curve is said 'assumed' or 'hypothesized' when parameters $\theta_1, \ldots, \theta_p$ are unknown. As soon as one or several measures of the input/output variables allow estimating these parameters, the rating curve is 'estimated'. $\widehat{\theta_1}, \ldots, \widehat{\theta_p}$ denote the estimations of these parameters.

A rating curve is called 'simple' when the stage is sufficient to determine the discharge. Conversely, it is called 'complex' as soon as other variables in addition to the stage are needed to determine the discharge.

In Hydrology, the rating curve refers to the function which approximates the stage-discharge relation. The estimated rating curve is graphically represented by plotting the discharge Q (in ordinate) against the stage (in abscissa). In case of a non-unique stage-discharge relation, this representation is the projection of the discharge on the stage variable. Therefore, it may graphically not correspond to a function, since one abscissa can be associated with several ordinates.

In other fields related to Hydrology, other rating curves can be found, such as turbidity-concentration rating curves which represents the concentration of suspended material in function of the turbidity at a turbidimetric station, or more generally environmental sensor rating curves. Also, sedimentary rating curves are used to model the suspended material concentration as a power function of the discharge.

A **stream gauging** or **gauging** is a one-off simultaneous measurement of all the inputs and the output of the assumed rating curve. These measurement are made in order to estimate the rating curve. A gauging is not just a discharge measurement, but must also include a gauge reading of the stage, and a measure of all other input variables e.g., the stage gradient, the stage at auxiliary station, the slope, the index velocity, etc. A discharge measurement which is not used to calibrate a rating curve is not a gauging (e.g., a continuous flowmeter) but can become one if it is used for that purpose. Therefore, a surface velocity measurement or a discharge estimate from a post event survey can become gaugings. Gaugings are frequently based on average values from several discharge measurements in order to reduce their uncertainties (e.g., ADCP measurements).

A **control** relates to the physical properties of a natural or artificial channel which determine the stage-discharge relation at a given location in the channel [WMO No. 385, 2012]. It can be linked to:

- A control is said to be a section control when the stage-discharge relation is determined by a cross-section located downstream of the gauge where the flow is critical;
- A control is said to be a channel control when the stage-discharge relation is determined by friction head losses along a reach extending downstream and upstream of the gauge.

Classification of non-unique stage-discharge relations: A non-unique relation can be physically linked with flow conditions modifying either the energy slope, or the roughness, or the cross-sectional geometry. Table 2.1 indicates which variable of the Manning-Strickler relation $Q = K_S \sqrt{J} A \ R_{\mathrm{h}}^{2/3}$ is influenced by the physcial process in case of a channel control.

Physical phenomenon	Strickler K_S (roughness)	Cross-sectional geometry R_h and A	Energy slope J	General comment
Hysteresis due to transient flow	-	-	×	Temporary phenomenon during flood wave propagation
Variable backwater influence (sea, river, hydraulic structure)	-	-	×	Downstream influence modifying the energy slope
Wind-related shear stress	-	-	×	External influence on the flow: direction of the wind impacts discharges
Log jams or ice jams	-	-	×	External influence for ice jams or influence due to a flow for log jams
Rating change due to bed evolution	(possibly)	×	-	Changes on offset or on discharge coefficient due to a scour and a fill of the reach with modification of the width of the river. The roughness of the bottom of the riverbed may also possibly change
Rating change due to vegetation	×	×	-	Cyclical phenomenon linked to the climate and the type of vegetation
Ice cover	×	×	-	-

Table 2.1 – Classification of various physical phenomenon for channel control with non-unique stage-discharge relation.

2.2. Hydraulics for rating curves

2.2.1. Hydraulic controls

In the river section where the hydrometric station is located, the relation between the water depth and the discharge is determined by the physical characteristics of the channel called 'hydraulic controls' or 'controls'. A more detail definition is given in section 2.1.

Two types of control exist:

1) The section control for which the stage-discharge relation is determined almost solely by the geometry of the controlling cross-section, where the flow becomes critical, which is materialised by a fall and an almost horizontal water line upstream (see figure 2.1-a). A rectangular weir or sill, a triangular weir and a pressurised orifice are some typical example of section controls;

2) The channel control for which the flow is assumed to be uniform. No fall will control the water level y. It is then governed by the geometry and the flow resistance (or roughness) of the channel over the entire homogeneous section (called controlling reach) which extends not only downstream, but also upstream of the gauge (see figure 2.1-b). The main channel, floodways and the floodplain are typical examples of channel controls.

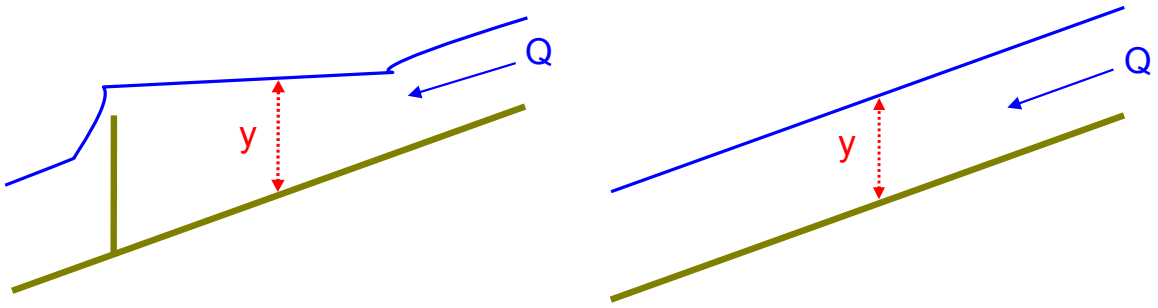

(a) (b)

Figure 2.1 – Diagrams of: (a) a section control (water depth y is under the influence of the fall); (b) a channel control (the red line represents the gauge site).

Standard controls are specific hydraulic controls which have been extensively studied and for which there are stage-discharge formulas [Degoutte, 2006, WMO No. 1044, 2010]. The rectangular weir and the wide rectangular channel control are the two most commonly used standard controls.

For most standard controls used in the rating curves, the stage-discharge relation can be described by a power function which is active above a given stage. In particular, hydraulics formulas for section controls and for channel controls with wide rectangular cross-section can be expressed as follows [Degoutte, 2006, WMO No. 1044, 2010, ISO 1100-2:2010, 2010]:

$$Q(h) = \begin{cases} 0 & \text{if } h \leq b \text{ or } h \leq \kappa \\ a(h-b)^c & \text{if } h > b \text{ and } h > \kappa \end{cases} \tag{2.1}$$

where Q is the discharge, h is the stage, κ is the activation stage (or 'transition' stage) below which the control becomes inactive, a is a coefficient related to the properties of the controlling section or channel, b is the offset (sometimes written h_0) below which the flow becomes zero, and c is an exponent related to the type of hydraulic control and the cross-sectional shape of the control for channel controls [e.g., Le Coz et al., 2014]. The water depth y is equal to $h - b$.

Note that the offset is generally different from the activation stage κ. For example, for a channel control that follows a weir control, the parameter b represents the average elevation of the bottom of the bed, but the control will only be active for a water level above which the weir is flooded, which is physically different from b.

For section controls, i.e. when the stage-discharge relation is determined by a cross-section where the flow is critical, equation (2.1) is established from the critical flow condition (when the Froude number is equal to 1). It gives the following relation:

$$Q(h) = CA\sqrt{gD_{\mathrm{h}}} \tag{2.2}$$

where C [−] is a discharge coefficient accounting for the head losses between the measurement cross-section (upstream) and the critical cross-section (downstream), A [m^2] is the wetted area, g [m.s^{-2}] is the gravity acceleration, $D_{\mathrm{h}} = A/B$ [m] is the hydraulic depth and B [m] is the width of the section control.

Using equation (2.2), the stage-discharge equation of a rectangular weir is given by:

$$Q(h) = CB\sqrt{2g}\,(h-b)^{3/2} \tag{2.3}$$

For channel controls, i.e. when the stage-discharge relation is determined by friction, equation (2.1) is established from the Manning-Strickler equation applied to the given geometry of

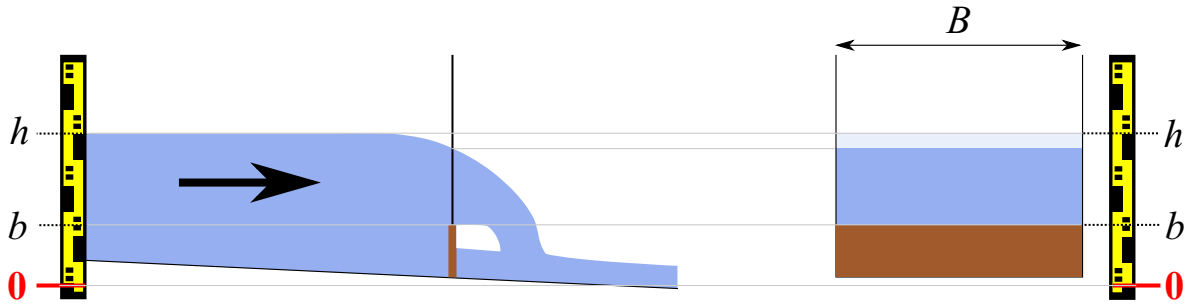

Figure 2.2 – Rectangular weir: longitudinal view (left) and front view of control cross-section (right).

the channel. The Manning-Strickler equation is:

$$Q(h) = K_S A R_{\mathrm{h}}^{2/3} \sqrt{S_f} \tag{2.4}$$

where K_S [$\mathrm{m}^{1/3}.\mathrm{s}^{-1}$] is the flow resistance coefficient, A [m^2] is the wetted area, $R_{\mathrm{h}} = A/P$ [m] is the hydraulic radius, P [m] is the wetted perimeter, S_f is the is head line slope (or friction slope), approximated by the longitudinal slope S_0 of the bed or of the water profile for steady uniform flows. This last variable is sometimes expressed as a percentage: in this manuscript we will express any slope as a ratio in the international units: [−] or [$\mathrm{m}.\mathrm{m}^{-1}$].

Using equation (2.4), the stage-discharge equation of a wide rectangular channel is given by:

$$Q(h) = K_S B \sqrt{S_0} (h - b)^{5/3} \tag{2.5}$$

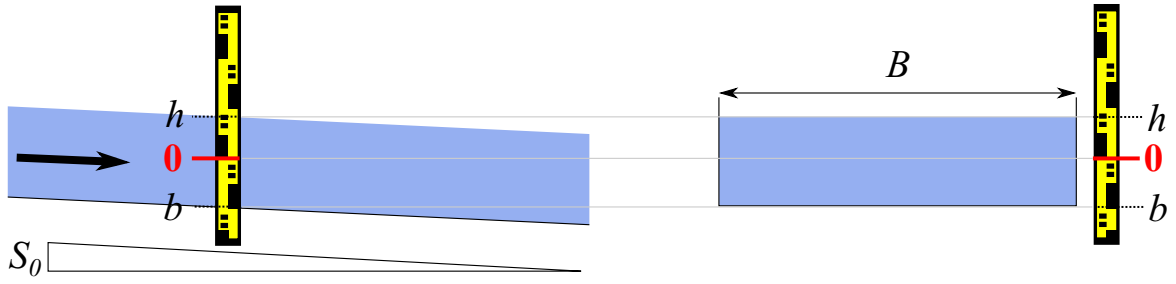

Figure 2.3 – Wide rectangular channel: longitudinal view (left) and cross-section at the staff gauge (right).

For both section and channel controls, similar formulas can be derived for other geometries of the controlling section and the channel (e.g. triangle, trapeze, parabola, see e.g., Degoutte [2006], Le Coz et al. [2014] and section 3.2.3).

2.2.2. Hydraulic analysis

In a hydraulic analysis at a hydrometric station, identification of controls allows the modelling of the rating curve equation. Each control has to be classified as either a section control or a channel control. This identification is part of the expertise of the station and is of particular importance as it determine the rating curve equation and provides information on the hydraulic configuration, which can be used to introduce prior knowledge, as will be described in section 2.4.1.3. Moreover it can also help detecting hydraulic effects which can cause non-unique stage-discharge relations. Each identified control should be compared to a standard control, or broken down into a combination of standard controls, according to a compound channel (or 'divided channel') approach. Note that the assimilation of a real control to a standard control is obviously an approximation. Nevertheless, the practice shows that it is often acceptable, in the sense that it properly matches the gaugings while maintaining a physical meaning.

When discharge and stage increase, active controls may follow on another or be added to each other, as shown by the simple but typical example in figure 2.4.

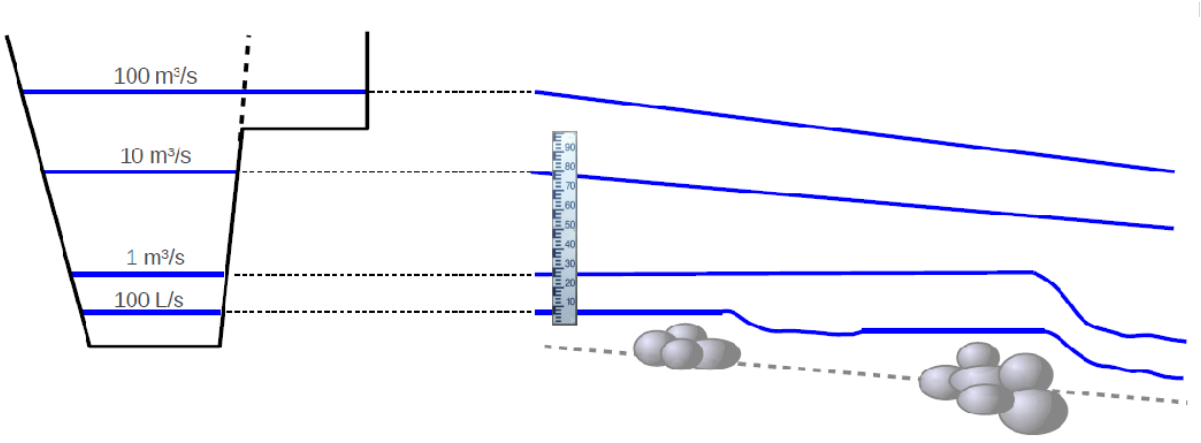

Figure 2.4 – Simplified illustration of controls at a typical gauging station: right, longitudinal profile of the bottom and water lines for different discharge values; left, water levels are shown at the cross-section of the staff gauge.

The hydraulic analysis usually begins with the study of lower flows and gradually extends to increasingly higher flows. To find out if an element of the site is a hydraulic control, it is helpful to imagine the effect on the water level of a significant change to this element (e.g., bed

scour or aggradation, widening or narrowing of the section, changing the width of a riffle, the bed roughness, etc.). If the water level would likely be influenced by the supposed change, then the studied site element is a hydraulic control or at least one of its components. For example, the hydraulic analysis at the dummy station in figure 2.4 is the following:

- for very low flows:
  - the water level is controlled by a small natural riffle;
  - this control can be approximated with a rectangular weir control;
- for low flows:
  - the first smaller riffle is flooded. The water level is then visibly controlled by a second natural riffle further downstream and displaying a greater fall.
  - the second control can be approximated with a rectangular weir control.
- for moderate to high flows, before overbank flows:
  - this second riffle is in turn flooded and there is no longer any fall controlling the water level. The water level is then controlled by the main river channel.
  - this control can be approximated with a standard uniform channel control, with a wide rectangular cross-section.
- for high flow rates, beyond overbank flow:
  - when the overbank flow occurs, a control by the floodplain is added to the main channel control. The water level is then under the simultaneous and added influence of both controls. The hydraulic interaction between the two flows is ignored.
  - the floodplain control is still treated as a standard uniform channel control, with a wide rectangular cross-section.

Note that although optional for a BaRatin analysis, hydraulic modelling can be useful for the hydraulic analysis: it helps identifying the sequence of controls, including their range of influence relative to stage and their association within complex channels. It can provide estimates of the riverbed slope. Note however gaugings should not be used in the hydraulic modelling (see section 2.4.1.4).

2.2.3. Equivalent geometry

Downstream and near the hydrometric station, the water flows through one or more controls. In a hydraulic analysis, we seek to ensure that we adequately addressed all the water 'paths', so as to not miss any control. The objective is to combine simple geometries of standard controls to best represent the possibly complex geometry of real controls.

To represent a real channel control, we typically combine as many rectangular channel standard controls as needed to represent the actual geometry. Figure 2.5 shows how the uneven riverbed is represented by an equivalent rectangular channel width B, and how the floodplain is represented by an equivalent rectangular channel width B'. Keep in mind that the vertical and horizontal scales of graphics are generally very distorted. Controls are often very flat, therefore neglecting the vertical edges in the calculation of the wetted perimeter is acceptable. The vertical water boundary between the two channels is especially very small compared to the horizontal extent of the riverbed.

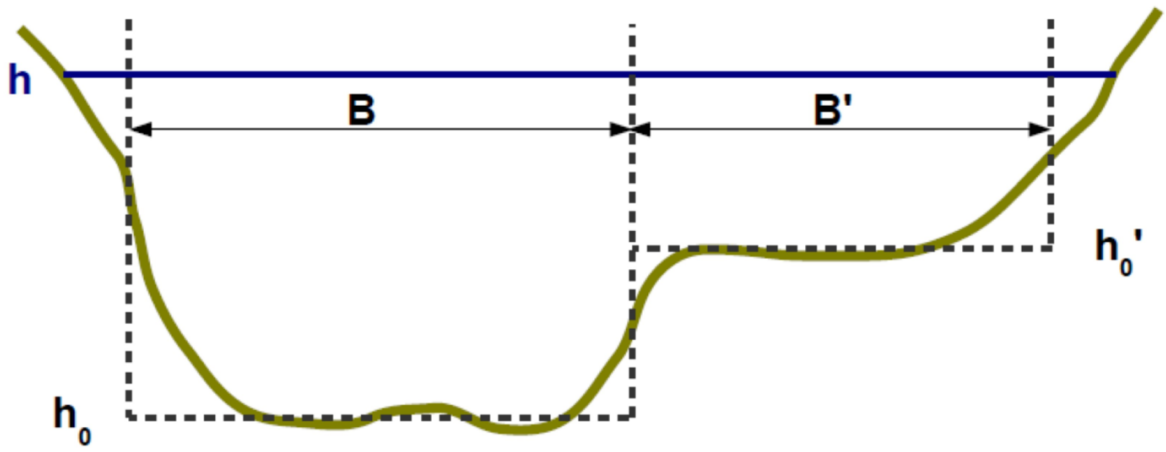

Figure 2.5 – Approximation of the main channel and the floodplain by equivalent rectangular channels.

Figure 2.6 shows the representative cross-section of a site where at very low discharge, the flow is concentrated in a kind of 'notch' which is the first control. This can be modelled by a rectangular weir standard control of width B'. For a slightly higher discharge, the flow takes the full width of the riverbed. For the second segment of the rating curve, the situation will be modelled using a single rectangular weir standard control of width B whose geometry encompasses that of the notch. For this segment, the first control is no longer considered active since it is integrated in the second control.

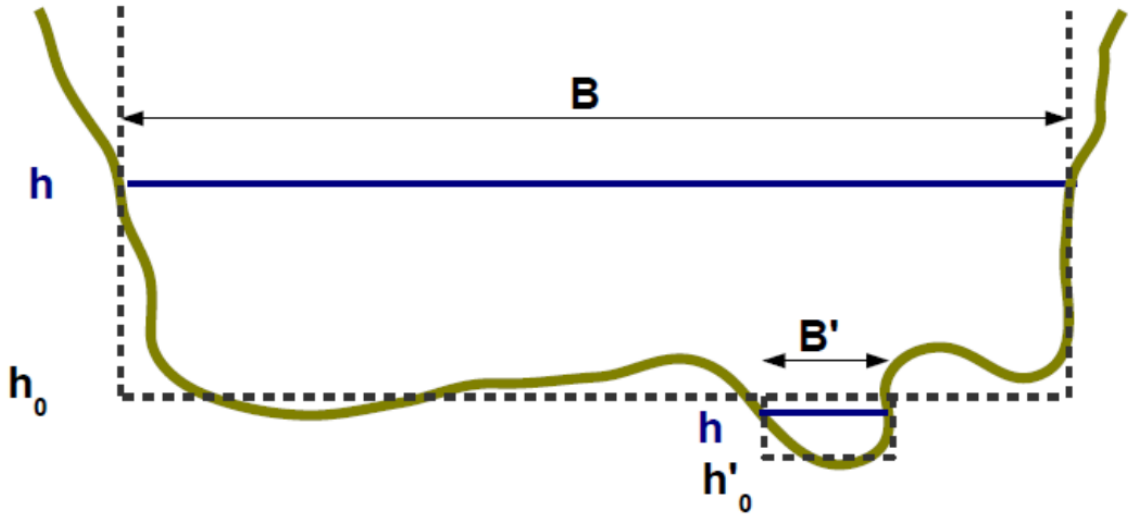

Figure 2.6 – Approximation of two successive riffles by equivalent rectangular weirs.

2.2.4. The matrix of controls $\mathcal{M}$

The hydraulic analysis can therefore be summarised as a matrix of controls. It comes in the form presented in figure 2.7.

$$\mathcal{M} = \begin{pmatrix} 1 & 0 & 0 & 0 \\ 0 & 1 & 0 & 0 \\ 0 & 0 & 1 & 0 \\ 0 & 0 & 1 & 1 \end{pmatrix}$$

(a)

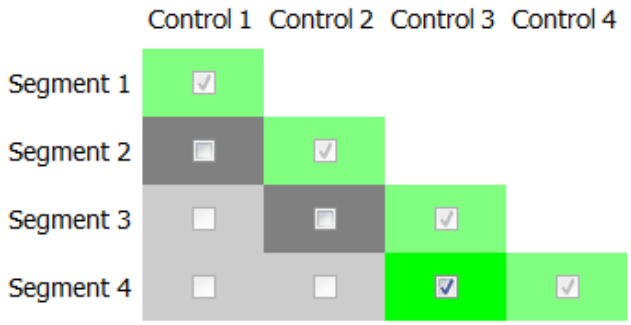

(b)

Figure 2.7 – Matrix of controls for the fictitious station presented in figure 2.4: (a) actual matrix; (b) representation in the BaRatinAGE software.

Segments are stage segments for which the number of controls affecting the water level does not change. For example if from a certain stage, a new control becomes active, then the previous segment ends and a new segment begins. There are therefore as many segments as identified controls. The segments are numbered in increasing stage. Thus segment #1, and therefore control #1 always correspond to the lowest considered flows. On the row of a stage segment, a value of 1 (green cell) means that the corresponding control affects the stage of the segment. On the same row / segment, several controls can influence the water level.

When a control is no longer active on a segment, it will no longer be active on a later segment. For instance, a weir flooded at a given stage cannot be unflooded at a greater stage. Getting back to the example of the fictitious station (figure 2.4) presented in section 2.2.2, we counted four controls, so 4 segments of stage:

- Segment #1: First natural riffle - rectangular weir (control #1)
- Segment #2: Second natural riffle - rectangular weir (control #2)
- Segment #3: Main channel (control #3)
- Segment #4: Main channel (control #3) + Floodplain (Control #4)

The matrix of control is of primary importance in the understanding of the SD model of this chapter. Indeed, accounting just for this matrix, the stage-discharge rating curve takes the following general form for any matrix $\mathcal{M}$, and hence at any steady station:

$$Q(h) = \sum_{i=1}^{N_{\text{seg}}} \left(\mathbf{1}_{[\kappa_{i-1};\kappa_i[}(h) \sum_{j=1}^{N_c} \mathcal{M}(i,j)\, a_j\, (h - b_j)^{c_j} \right) \tag{2.6}$$

where:

- h is the stage;
- Q is the discharge;
- N_{seg} is the number of segments;
- $\mathcal{M}(i,j)$ is the matrix of controls, taking 1 if the control is active, 0 otherwise;
- the function $\mathbf{1}_{[\kappa_{i-1};\kappa_i[}(h)$ is the indicator function of the interval $[\kappa_{i-1};\kappa_i[$ equal to 1 if h belongs to this interval and 0 otherwise. It gives the range of stage of the segment i;
- a_j, b_j and c_j are the parameters of the rating curve equation. a_j is the coefficient related to the properties of the control j, b_j is the offset and c_j is the exponent related to the type of control.

With some practice, identifying the controls of a hydrometric station is not difficult. This does not require extensive expertise in hydraulics but mostly common sense in observing the essential elements on the site and the flows for various discharges. It is obviously always useful to collect the knowledge of field hydrologists that operated the station and all of the station's record. We

stress that normally gaugings should not be used for hydraulic analysis (see section 2.4.1.4). However, if some gaugings are still considered essential to this analysis, they must be removed from the set of gaugings used for the rating curve calibration. Valuable information on the nature, geometry and operation of controls can generally be deduced from photos of the flows, topographic maps, GIS such as Google Earth or national GIS portals, surveys of cross-sections and bridges, an last but not least... field visits! The following diagram summarises the steps of such hydraulic analysis:

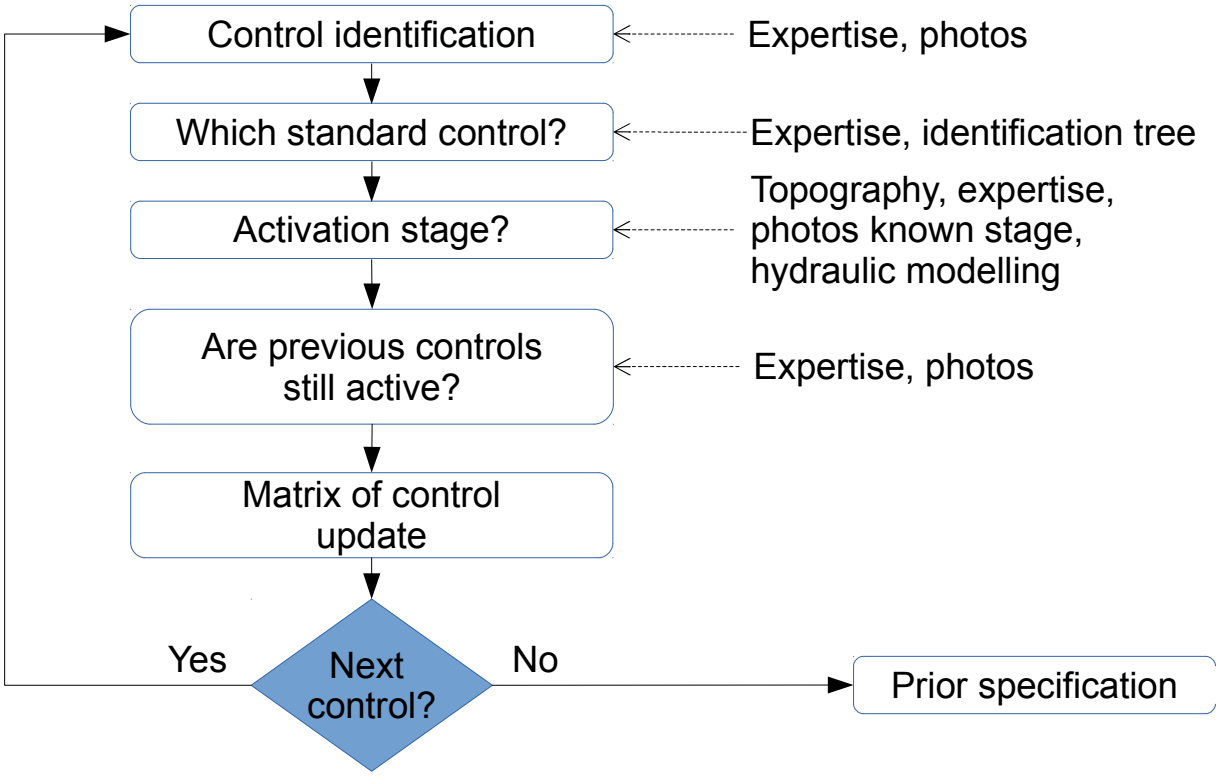

Figure 2.8 – General diagram of a hydraulic analysis.

2.3. Gauging uncertainties

2.3.1. Uncertain gaugings as calibration data

For estimating a rating curve through a Bayesian analysis, a set of gaugings representative of the stage-discharge relation (or other non-unique relations) is needed. The validity of these gaugings must be checked (quality assurance) beforehand in order to avoid outliers, to ensure the continuity of their stage with respect to the staff gauge of the station, and to control and document measurement errors. It is especially important to consider:

- the measurement technique and gauging procedure;
- the date and hydraulic conditions at the time of the measurement, including: vegetation, flood, rating changes, etc.;
- the datum of the gauged stage, particularly when the staff gauge of reference has undergone changes or displacement, or if multiple staff gauges were used simultaneously;
- other relevant measurements if needed in the rating curve model.

All Bayesian analyses of this manuscript allow consideration of uncertainties on the gauged discharges that are potentially different for each measurement. It is an interesting advantage when using more uncertain gaugings (e.g. surface velocity gaugings, historic gaugings that are poorly documented) or discharge estimates (e.g. post-flood survey and slope-area method) in stage ranges with few or no gaugings, because their contribution is weighted by their information content. It is important to specify realistic gauging uncertainty values, neither overestimated nor underestimated, as they impact both the fit of the curve and the width of its uncertainty envelope.

A (strong) assumption of these Bayesian analyses is that the measurement errors are independent between gaugings to another gauging. This assumption is clearly violated if some gaugings are performed under repeatability conditions, typically with the same instrument at the same place on the same day in the same hydraulic conditions, etc. This may be the case when the gauging teams decide to gauge, performing many gaugings the day under these typical repeatability conditions. This can lead to an underestimation of the uncertainty of the rating curve. We must therefore avoid including repeated gaugings (e.g. successive ADCP gaugings of a constant discharge at constant water level), but either sub-sample them or average them together. Indeed,

these repeated gaugings can be also smartly averaged, accordingly to standard [HUG, ISO/TS 25377:2007, 2007], to reduce their discharge uncertainty.

2.3.2. Uncertainties of gauged discharges

Uncertainty of the gauged discharge can be estimated from the available information on discharge measurements or calculated by methods of propagation of uncertainty. For velocity-area gaugings, uncertainty calculations can be done with the methods of ISO 748:2007 [2007], ISO 1088:2007 [2007] standards, or alternative methods: IVE (USGS), Q+ (French national hydrological services) or FLAURE (Électricité De France, EDF) methods. All of these methods have limitations [e.g., Despax et al., 2016]. According to the technique used and the measurement conditions, the individual gauging uncertainty can be evaluated simply by means of simplified calculations. Inter-laboratory comparisons are also used to determine empirically the uncertainty of gauging technologies deployed in the measurement conditions of the experiments [e.g., Le Coz et al., 2016a]. This uncertainty is typically taken to be ±7% for streamflows gauged using a current meter with at least a dozen verticals correctly sampling the flow field, and ±5% for a gauging by ADCP achieved in good conditions (±10% in bad conditions). When uncertainties on discharges measurement are unknown by the practitioner, table 2.2 provides typical discharge uncertainty values (expanded to 95% level) for the main gauging techniques. These typical uncertainty values are provided only as examples. Uncertainty analysis of discharge measurements in each case, at least by categories, is highly recommended.

Uncertainties of gauged stages or other inputs are considered negligible compared to discharge uncertainties, and are hence neglected in this manuscript.

Conditions	Volumetry	Velocity-area methods				Tracer dilution	Hydraulic formulas
		ADCP	Current meter	Floats	Radar, LSPIV		
Optimal	±5%	±5%	±7%	±10%	±10%	±3%	±5%
Poor	±10%	±10%	±15%	±50%	±20%	±10%	±40%

Table 2.2 – Typical discharge uncertainty values (expanded to 95% level) for the main gauging techniques.

2.4. Statistics

2.4.1. Bayesian inference

2.4.1.1. Parameterisation

Let $\boldsymbol{\theta} = (\boldsymbol{\theta}_{\mathbf{RC}}, \boldsymbol{\gamma})$ denote the inferred parameters where parameters $\boldsymbol{\theta}_{\mathbf{RC}}$ are the m parameters of the SD rating curve parameters and parameters $\boldsymbol{\gamma} = (\gamma_1, \gamma_2)$ are the parameters of the structural error model (described in the following section). Parameter $\boldsymbol{\theta}_{\mathbf{RC}}$ correspond to hydraulic parameters a, b and c.

Transition stages κ_i in equation (2.6) can be deduced from other parameters using a discharge continuity condition for $h = \kappa_i$ between the i-th control and the $(i+1)$-th control. If the $(i+1)$-th control adds to the i-th control, the transition stage κ_i is equal to the offset b_i of the $(i+1)$-th control. Conversely, if the $(i+1)$-th control replaces the i-th control, the discharge continuity condition leads to:

$$a\left(\kappa_i - b_i\right)^{c_i} - a_{i+1}\left(\kappa_i - b_{i+1}\right)^{c_{i+1}} = 0. \tag{2.7}$$

The Newton-Raphson algorithm is used to solve numerically equation (2.7) and find the transition stage κ_i.

In the associated operational software BaRatinAGE, and contrarily what is done in this manuscript: the transition stages are inferred and the offsets are deduced by continuity. We adopt a different convention because it turns out to be more convenient for the models developed in this thesis as will be explained in the following chapters.

2.4.1.2. Likelihood computation

Gaugings $\left(\widetilde{h}_i, \widetilde{Q}_i\right)_{i\in[\![1;N]\!]}$ are seen as the N estimates of the N real values $(h_i, Q_i)_{i\in[\![1;N]\!]}$ of stages and associated discharges. In this manuscript, we further assume that stage errors are negligible compared to discharge errors:

$$\begin{cases} \widetilde{h}_i = h_i \\ \widetilde{Q}_i = Q_i + \epsilon_{Q,i} \quad \text{with} \quad \epsilon_{Q,i} \overset{\text{indep.}}{\sim} \mathcal{N}\left(0, u_{Q,i}\right) \end{cases} \tag{2.8}$$

where the discharge errors $\boldsymbol{\epsilon_Q} = (\epsilon_{Q,1}, \ldots, \epsilon_{Q,N})$ are assumed independent (indep.) and the standard deviations $u_{Q,i}$ (uncertainties of discharge measurements) are assumed to be known.

Depending on their measurement technique and field procedure, uncertainty values can be assigned to gaugings based on the typical results of available propagation methods [e.g., Despax et al., 2016] and in-situ intercomparisons [e.g., Le Coz et al., 2016a] (see table 2.2).

The true discharge is then written as the discharge predicted by the rating curve plus a structural error:

$$Q_i = \underbrace{f\left(h_i|\boldsymbol{\theta}_{\mathbf{RC}}\right)}_{\widehat{Q}_i} + \epsilon_{f,i} \quad \text{with} \quad \epsilon_{f,i} \overset{\text{indep.}}{\sim} \mathcal{N}\left(0, \sigma_{f,i} = \gamma_1 + \gamma_2 \widehat{Q_i}\right) \tag{2.9}$$

where $\boldsymbol{\theta}_{\mathbf{RC}}$ are the rating curve parameters, $\boldsymbol{\epsilon_f} = (\epsilon_{f,1}, \ldots, \epsilon_{f,N})$ are the structural errors, $(\sigma_{f,1}, \ldots, \sigma_{f,N})$ are the standard deviations of the structural errors $(\epsilon_{f,1}, \ldots, \epsilon_{f,N})$ and $\widehat{\boldsymbol{Q}} = \left(\widehat{Q}_1, \ldots, \widehat{Q}_N\right)$ are the discharge estimations related to the N gaugings (see section 2.4.1).

The linear function used for modelling the standard deviation $\sigma_{f,i}$ is based on repeat practise: indeed, we often observe higher structural uncertainty for higher flows, which can be reproduced by this linearly-varying standard deviation. We also assume that the structural errors $(\epsilon_{f,1}, \ldots, \epsilon_{f,N})$ and the discharge errors $(\epsilon_{Q,1}, \ldots, \epsilon_{Q,N})$ are independent.

Combining equations (2.8) and (2.9) yields the following stage-discharge relation between observed values:

$$\widetilde{Q}_i = f\left(\widetilde{h}_i \middle| \boldsymbol{\theta}_{\mathbf{RC}}\right) + \epsilon_{Q,i} + \epsilon_{f,i} \quad \text{with} \quad \epsilon_{Q,i} + \epsilon_{f,i} \sim \mathcal{N}\left(0, \sqrt{\sigma_{f,i}^2 + u_{Q,i}^2}\right) \tag{2.10}$$

The likelihood L of observed discharge values $\widetilde{\boldsymbol{Q}}$:

$$L\left(\widetilde{\boldsymbol{Q}} \middle| \boldsymbol{\theta} = (\boldsymbol{\theta}_{\mathbf{RC}}, \boldsymbol{\gamma}), \tilde{\boldsymbol{h}}\right) = \prod_{i=1}^{N} p_{\text{norm}}\left[\widetilde{Q}_i \middle| f\left(\widetilde{h}_i \middle| \boldsymbol{\theta}_{\mathbf{RC}}\right), \sqrt{\sigma_{f,i}^2 + u_{Q,i}^2}\right] \tag{2.11}$$

where $\widetilde{\boldsymbol{Q}} = \left(\widetilde{Q}_1, \ldots, \widetilde{Q}_N\right)$ are the N gauged discharge, $\widetilde{\boldsymbol{h}} = \left(\widetilde{h}_1, \ldots, \widetilde{h}_N\right)$ are the N observed stage values and $p_{\text{norm}}[z|m, s]$ denote the probability density function (pdf) of a Gaussian distribution with mean m and standard deviation s, evaluated at some value z.

2.4.1.3. Prior specification

Bayesian inference does not only use the information brought by the data, but allows including any knowledge on $\boldsymbol{\theta}$ that would be available even before acquiring the data. This prior information is encoded as a distribution, whose pdf is noted $p(\boldsymbol{\theta})$. As suggested by this notation, the prior distribution does not depend on the calibration data . It is actually a golden rule: a

data should never be used to specify the prior distribution, unless this observation is removed from the dataset used in the likelihood computation. Moreover, although using the calibration data to specify the prior distribution is strictly forbidden, it is not forbidden to use other data, such as the bathymetry realised during an ADCP measurement (not related to the flow condition but to the hydraulic configuration of the river).

The prior distribution offers the opportunity to include hydraulic knowledge. In this manuscript, we use independent prior distributions for each inferred parameter, leading to the joint prior distribution:

$$p\left(\boldsymbol{\theta_{RC}}, \boldsymbol{\gamma}\right) = p\left(\gamma_1\right) p\left(\gamma_2\right) \prod_{i=1}^{m} p\left(\theta_i\right) \tag{2.12}$$

In this thesis, for each hydraulic parameter, we use Gaussian prior distributions. Prior distributions of error parameters γ_1 and γ_2 are flat uniform distributions ($U\left(0, 10^6\right)$) as we want these parameters to be inferred from the gaugings.

For each control modelled as a rectangular weir, priors must be assigned from hydraulic analysis of the station for the following parameters (see equation (2.3)):

- b [m] is the weir crest elevation;
- B [m] is the spillway width, i.e. the transverse length of the weir, normal to the flow direction;

Default priors can be specified for the other parameters but remain to be verified with the available knowledge at the station:

- C is set by default to 0.4 ± 0.1 [Le Coz et al., 2011]. This prior can be criticized as the value is sometimes lower than 0.4 due to the degradation of the weir for example. In this manuscript, unless explicitly mentioned otherwise we use this specific prior;
- g is set by default to 9.81 m.s^{-2} $\pm$ 0.01 m.s^{-2};
- c is set by default to 1.5 ± 0.05 unless explicitly mentioned;

Prior for $a = CB\sqrt{2g}$ (equation (2.3)) can be obtained by propagation as recommended by the GUM [JCGM 100:2008, 2008].

For each control modelled as a wide rectangular channel control, priors must be assigned for the following parameters (see equation (2.5)):

- b [m] is the mean bed elevation at the gauge;

- B [m] is the average width of the controlling reach;
- S_0 [−] is the longitudinal slope of the river channel;
- K_S [$m^{1/3}.s^{-1}$] is the Strickler coefficient modelling the flow resistance. Corresponding value of Manning coefficient $n = 1/K_S$ can be found in Chow [1959].

Default priors can be specified for the other parameters but remain to be verified with the available knowledge at the station:

- c is set by default to 1.667 $\pm$ 0.05 unless explicitly mentioned;

Priors for $a = K_S B\sqrt{S_0}$ (equation (2.5)) can be obtained by propagation as recommended by the GUM [JCGM 100:2008, 2008]. Prior on $K_S B$ (used in non-unique relations) is also obtained by propagation.

2.4.1.4. Posterior distribution

Bayes' theorem allows combining the information brought by the data $(\widetilde{\boldsymbol{h}}, \widetilde{\boldsymbol{Q}})$ (through the likelihood) with prior information into a distribution for the unknown parameter $\boldsymbol{\theta}$, termed the posterior distribution. The pdf of the posterior distribution, noted $p\left(\boldsymbol{\theta}\middle|\widetilde{\boldsymbol{h}}, \widetilde{\boldsymbol{Q}}\right)$, is defined by:

$$p\left(\boldsymbol{\theta}\middle|\widetilde{\boldsymbol{h}}, \widetilde{\boldsymbol{Q}}\right) = \frac{\overbrace{p\left(\widetilde{\boldsymbol{Q}}\middle|\boldsymbol{\theta}, \widetilde{\boldsymbol{h}}\right)}^{\text{likelihood}} \overbrace{p\left(\boldsymbol{\theta}\right)}^{\text{prior}}}{\underbrace{\int p\left(\widetilde{\boldsymbol{Q}}\middle|\boldsymbol{\theta}, \widetilde{\boldsymbol{h}}\right) p\left(\boldsymbol{\theta}\right) d\boldsymbol{\theta}}_{\text{normalizing constant}}} \tag{2.13}$$

The numerator is simply the product of the likelihood and the prior pdf. The denominator looks more complex, since it requires integrating this product with respect to parameter $\boldsymbol{\theta}$. However, this denominator is in fact just a constant: the data $(\widetilde{\boldsymbol{h}}, \widetilde{\boldsymbol{Q}})$ are given and fixed, and parameter $\boldsymbol{\theta}$ disappear from the denominator since it is the integration variable. Consequently, the denominator only serves as a normalizing constant: it ensures that the area below the posterior pdf is equal to 1 (which is required for any pdf). In practice, it is actually not even necessary to compute this constant in general, because MCMC algorithms used to sample the posterior distribution (see section 2.4.2) only require the posterior to be known up to a constant of proportionality. This allows simplifying Bayes theorem as follows:

$$p\left(\boldsymbol{\theta}\middle|\widetilde{\boldsymbol{h}}, \widetilde{\boldsymbol{Q}}\right) \propto p\left(\widetilde{\boldsymbol{Q}}\middle|\boldsymbol{\theta}, \widetilde{\boldsymbol{h}}\right) p\left(\boldsymbol{\theta}\right) \tag{2.14}$$

where the symbol '$\propto$' stands for 'is proportional to'.

Equation (2.14) shows that the derivation of the posterior pdf (up to a constant of proportionality) is simple: it is just the product of the likelihood and the prior pdf. The resulting posterior pdf quantifies the knowledge on parameter $\boldsymbol{\theta}$ given two sources of information: the data and prior knowledge.

It is worth noting that the raw result of Bayesian estimation is a distribution, as opposed to a value (as in other estimation methods such as moments, maximum likelihood, etc.). This remark calls for further comments:

- the raw result of Bayesian inference directly provides a quantification of uncertainty;
- this does not mean that quantifying uncertainty is impossible with other estimation methods: in fact, most estimation methods come with a solid and well-developed theory for uncertainty quantification. But this quantification only comes in a second step, after having estimated a particular value;
- conversely, this does not mean that estimating a value is impossible with Bayesian estimation: typically, the maximum of the posterior pdf is a standard choice[1];

2.4.2. MCMC sampling

In general, the posterior probability density function (pdf) is a multi-dimensional pdf which cannot be easily represented graphically. Moreover, the posterior pdf is not the final stage of a rating curve estimation process. Indeed, the posterior pdf of parameters $\boldsymbol{\theta}_{\mathbf{RC}}$ needs to be further processed to derive the rating curve and its uncertainties.

A convenient way to use the posterior pdf in practice is to simulate many realisations from it which can be achieved with Markov Chain Monte Carlo (MCMC) sampling. These MCMC simulations can be used to represent the posterior distribution graphically (e.g., a histogram of samples for one particular parameter represents its marginal posterior distribution). Moreover, they can be propagated to any quantity derived from the parameters (typically, the rating curve).

In this thesis, we use a combined MCMC sampler [Sun, 2013]. This algorithm is a combination of three MCMC samplers:

- The first step uses an adaptive 'one-at-a-time' Metropolis algorithm with one-dimensional jump distribution to estimate the jump covariance matrix;

[1]This can be considered as the Bayesian version of the maximum likelihood estimate, and it is often abbreviated as the Maxpost estimate (or alternatively the MAP estimate for Maximum A Posteriori)

- The second step uses a adaptive Metropolis algorithm and adapts the scale factor of the covariance matrix;
- The third and last step uses the classical non-adaptive Metropolis sampler with the estimated covariance matrix to approximate the target distribution.

For each MCMC sampling, 4 MCMC chains are drawn in the third step to evaluate the algorithm convergence with the Gelmann-Rubin criterion [Gelman and Rubin, 1992]. Unless explicitly mentioned otherwise, by default, a chain is composed by $10,000$ simulations for the two first step and by $100,000$ simulation for each of the 4 chains. A burn factor of 0.5 is used, i.e. for each chain, the $50,000$ first simulations are discarded. Moreover, the simulations are slimmed by a factor of 50before further use. This is made to reduce computing time and storage issues, and does not result in a noticeable loss of information because the raw MCMC are strongly autocorrelated.

2.5. Application: the Ardèche River at Barutel, Meyras, France

This section illustrates briefly the hydraulic analysis to be done before the rating curve calibration with Bayesian analysis.

2.5.1. Data and models

The Ardèche River at the downstream station of Sauze has a mean interannual discharge of 65 $m^3.s^{-1}$ for a catchment area of 2388 km^2. It flows along 125 km from the Massif Central, down into the Rhône River. The Ardèche basin experiences severe flash floods in autumn. These floods can be very important (maximum instantaneous flow recorded of 4500 $m^3.s^{-1}$ at the outlet of Saint-Martin-d'Ardèche, historical floods possibly exceeding 8000 $m^3.s^{-1}$ [Naulet et al., 2005]). These flash floods, called *coups de l'Ardèche*, have been thoroughly studied by the FloodScale project, contribution to the HyMeX (Hydrological Cycle in the Mediterranean Experiment) international program [Braud et al., 2014, Adamovic et al., 2015, e.g.,], and by many other projects [e.g., Lang et al., 2002, Naulet et al., 2005].

At Meyras (Barutel locality) the Ardèche River drains a catchment area of 120 km^2 (figure 2.9). The gauge is located just under a bridge (figure 2.10-a, GPS locations: 4°16′11.2″E, 44°40′12.3″N). The bed of the station changes regularly due to the intensity of the flash floods. In this section, we only focus on a period without rating changes: the 2011-2014 period (04/11/2011 to 18/09/2014).

Located approximately 50 m downstream of the bridge, a natural gravel riffle controls the low-flow (figure 2.10-a). The riffle is approximated by a rectangular section control. A main channel (wide rectangular channel control) replaces this riffle as the flow increases and then two floodways (on each bank) are added to the main channel at high flows (figure 2.10-b). The two floodways are combined as an equivalent wide rectangular channel control since they become active for approximately the same stage. Therefore, the rating curve equation can be written as

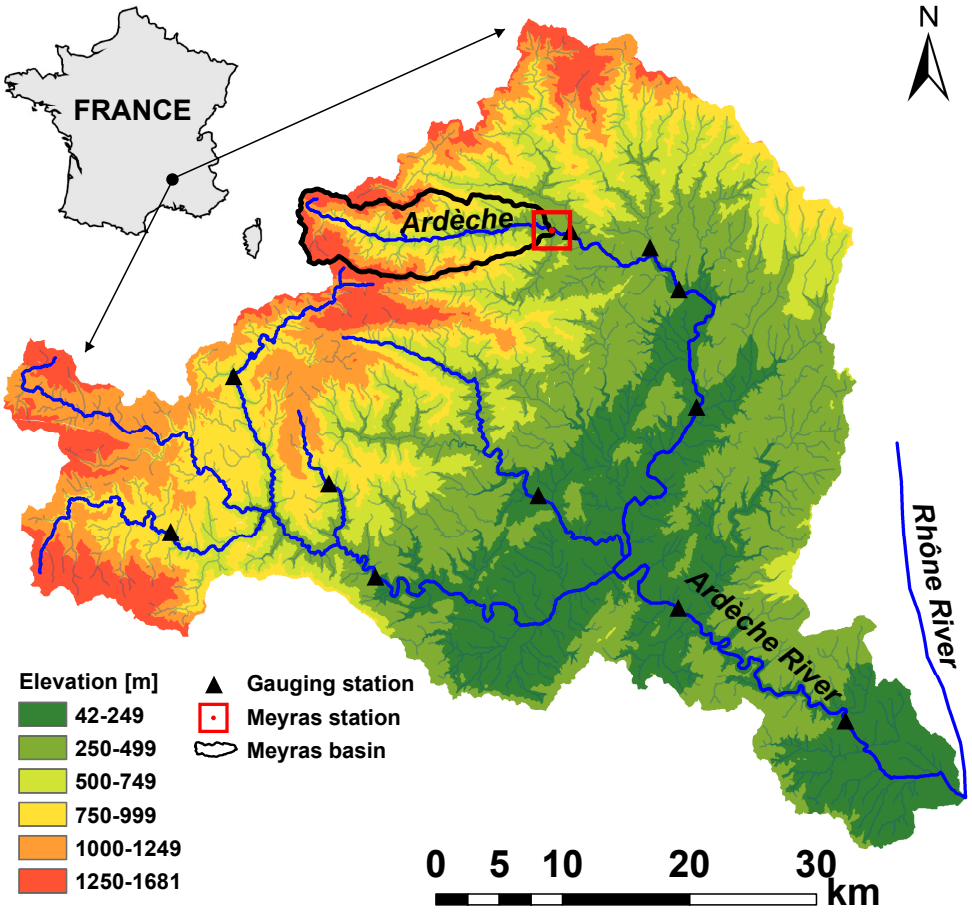

Figure 2.9 – The Ardèche River basin, south-central France with Meyras subcatchment delineated, taken from Adamovic et al. [2015].

follows:

$$Q(h) = \begin{cases} a_1 (h - b_1)^{c_1} & \text{if } h < \kappa \quad \text{(riffle)} \\ a_2 (h - b_2)^{c_2} & \text{if } \kappa \leq h < b_3 \quad \text{(main channel)} \\ a_2 (h - b_2)^{c_2} + a_3 (h - b_3)^{c_3} & \text{if } h \geq b_3 \quad \text{(main channel and floodways)} \end{cases} \tag{2.15}$$

where a_1, a_2 and a_3 are coefficients related to the characteristics of the controls (section or channel), b_1, b_2 and b_3 are the offsets and c_1, c_2 and c_3 are exponents related to the type of hydraulic control. The transition stage κ between the section control and the channel control is numerically computed.

25 gaugings were performed at the Meyras station during this period. They are distributed from 0.14 $m^3.s^{-1}$ to 93.5 $m^3.s^{-1}$. The mean annual discharge is 3.64 $m^3.s^{-1}$ and the 2-year flood corresponds to 150 $m^3.s^{-1}$.

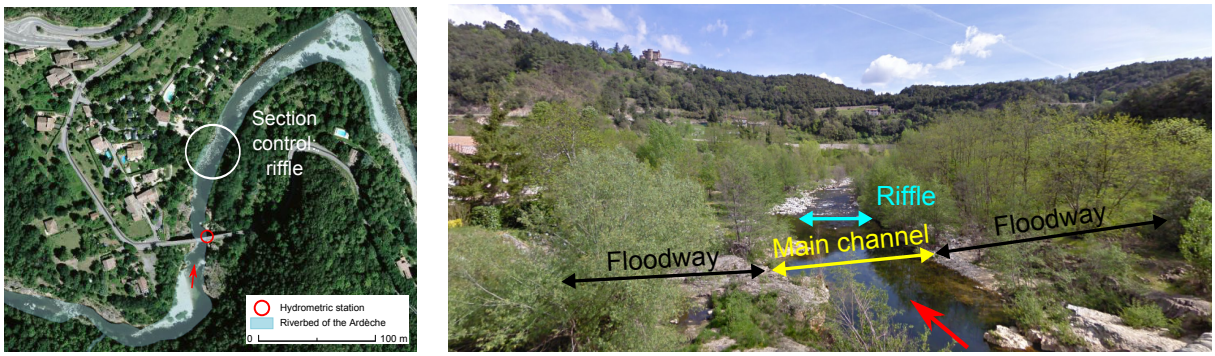

(a) (b)

Figure 2.10 – Views of the hydraulic controls of the Ardèche River at Meyras: (a) from above, Géoportail database; (b) downstream of the bridge from the left bank, Google Earth view.

2.5.2. Prior specification

The width of the riffle is set to 8 m ± 4 m. The widths of the main channel and the combined floodway are set to 15 m ± 5 m and 30 m ± 10 m respectively. Both offsets of the section control (natural riffle) and the channel control (main channel), b_1 and b_2, are set to -0.6 m ± 1 m, which corresponds to the minimum stage recorded during the 2011-2014 period. The overflow stage b_3 between both channel controls is set to 1.2 m ± 0.4 m. It represents the mean bed elevation of the combined floodway. This floodway is vegetated (trees). From existing hydraulic models, the Strickler coefficients of the main channel and the combined floodway are set to 25 $m^{\frac{1}{3}}.s^{-1}$ ± 5 $m^{\frac{1}{3}}.s^{-1}$ and 15 $m^{\frac{1}{3}}.s^{-1}$ ± 5 $m^{\frac{1}{3}}.s^{-1}$ respectively. Slopes of the riverbed of the main channel and the floodway are set to 0.005 ± 0.005. Corresponding priors are summarised in table 2.3.

Inferred parameters	Physical parameters	Units	Prior distributions	SD posterior results: MAP $[Q_{2.5}; Q_{97.5}]$
θ_1	a_1	$[\mathrm{m}^{\frac{3}{2}}.\mathrm{s}^{-1}]$	$\mathcal{N}(14.174; 5.01)$	10.86 [8.84; 14.27]
θ_2	b_1	[m]	$\mathcal{N}(-0.6; 0.5)$	-0.638 [-0.657;-0.619]
θ_3	$c_1 = 3/2$	[−]	$\mathcal{N}(1.5; 0.025)$	1.498 [1.453; 1.550]
θ_4	a_2	$[\mathrm{m}^{\frac{4}{3}}.\mathrm{s}^{-1}]$	$\mathcal{N}(26.52; 8.4)$	24.00 [22.51; 25.94]
θ_5	b_2	[m]	$\mathcal{N}(-0.6; 0.5)$	-0.585 [-0.604;-0.566]
θ_6	$c_2 = 5/3$	[−]	$\mathcal{N}(1.6667; 0.025)$	1.662 [1.626; 1.722]
θ_7	a_3	$[\mathrm{m}^{\frac{4}{3}}.\mathrm{s}^{-1}]$	$\mathcal{N}(31.82; 10.93)$	35.70 [17.31; 57.75]
θ_8	b_3	[m]	$\mathcal{N}(1.2; 0.2)$	0.965 [0.762; 1.372]
θ_9	$c_3 = 5/3$	[−]	$\mathcal{N}(1.6667; 0.025)$	1.669 [1.618; 1.717]
γ_1	-	$[\mathrm{m}^3.\mathrm{s}^{-1}]$	$\mathcal{U}(0; 10^6)$	0.0012 [0.0005; 0.0472]
γ_2	-	[−]	$\mathcal{U}(0; 10^6)$	0.0398 [0.0211; 0.0745]

Table 2.3 – The Ardèche River at Meyras, 2011-2014 period: parameters, prior distributions and posterior results of the stage-discharge (SD) model.

2.5.3. Results

Figure 2.11 shows the parameters simulated by the MCMC sampler after burning and slimming (see section 2.4.2). The kernel densities of the simulated values (figure 2.12) represents the marginal posterior pdf of each parameter which can be compared with the prior pdf to evaluate the information brought by the gaugings. The simulated values shown in figure 2.11 can be propagated through the rating curve equation.

Figure 2.13 shows the estimated rating curve as stage-discharge representation with 95% uncertainty envelopes. The SD model yields an accurate rating curve that agree well with gaugings. Moreover, this rating curve is precise, due to the high number of gaugings (25) for the studied period. Transition stage between the section control and the main channel (first two controls) is precisely identified as the number of gaugings (23) on these two controls is high. The overflow stage remains vaguely estimated as well as the parameter a_3 (see table 2.3): they are not identified in the gaugings as there is not enough high-flows gaugings.

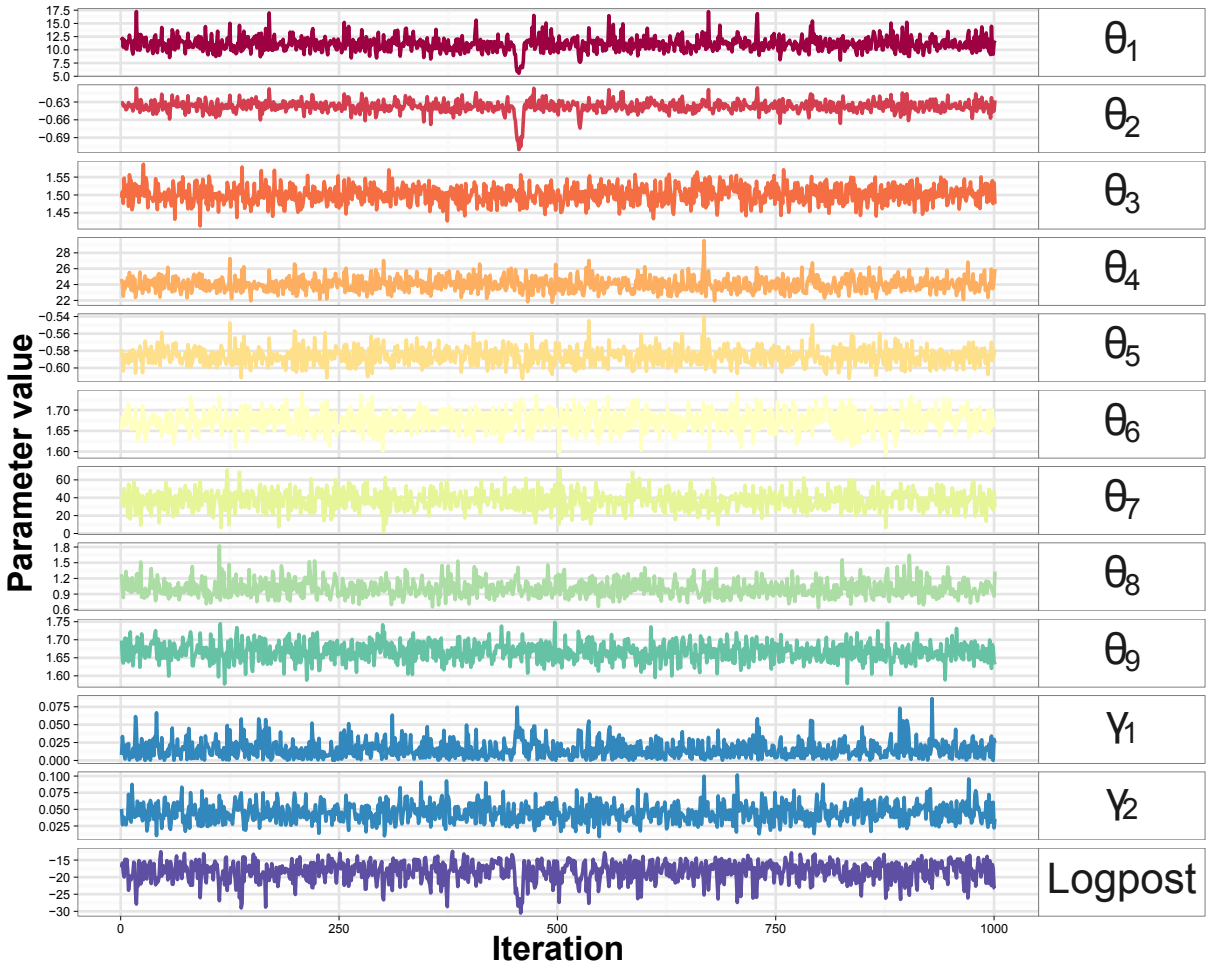

Figure 2.11 – The Ardèche River at Meyras: representation of the MCMC samples of the stage-discharge (SD) model.

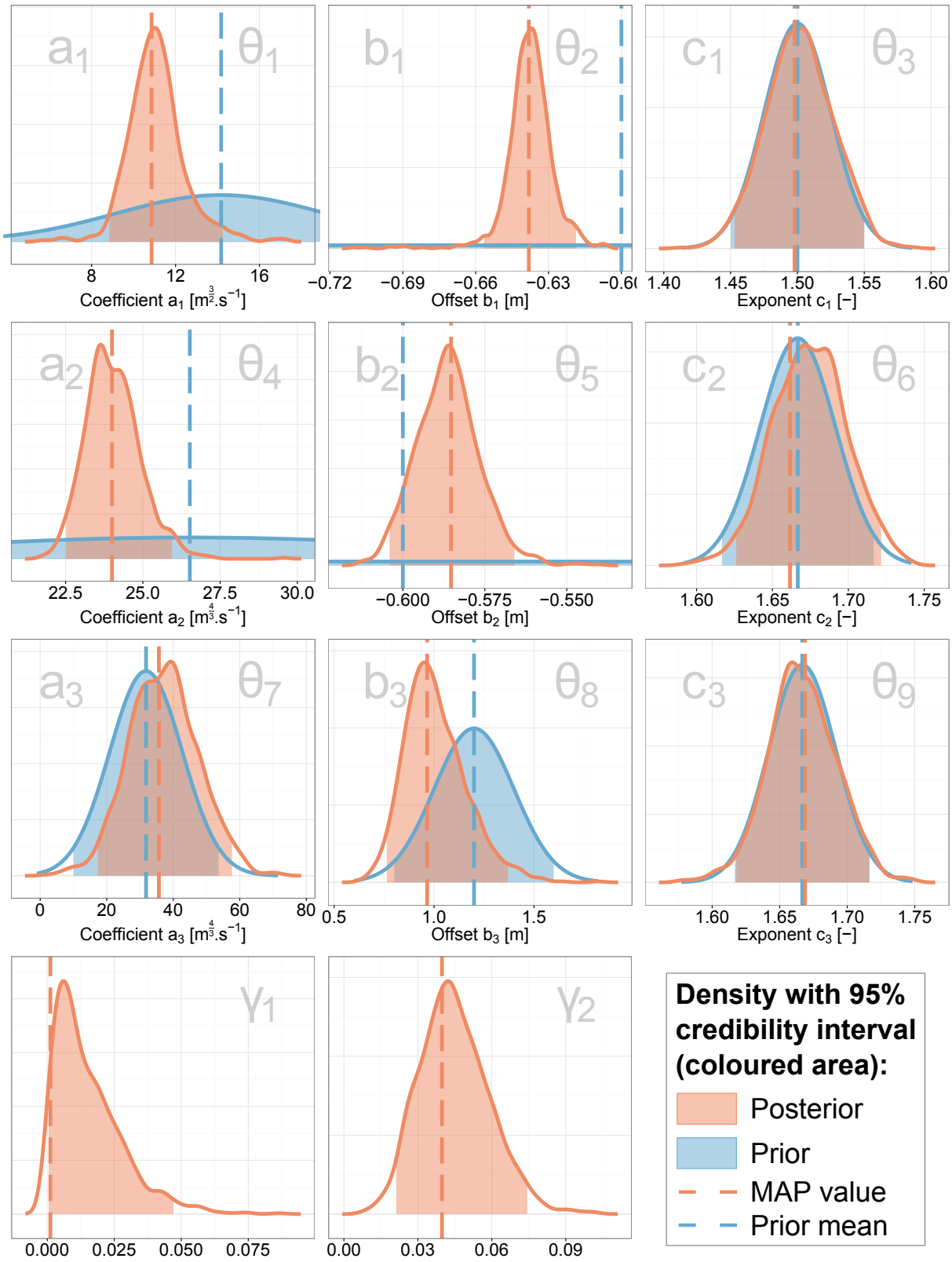

Figure 2.12 – The Ardèche River at Meyras: posterior and prior densities of rating curve parameters of the stage-discharge (SD) model.

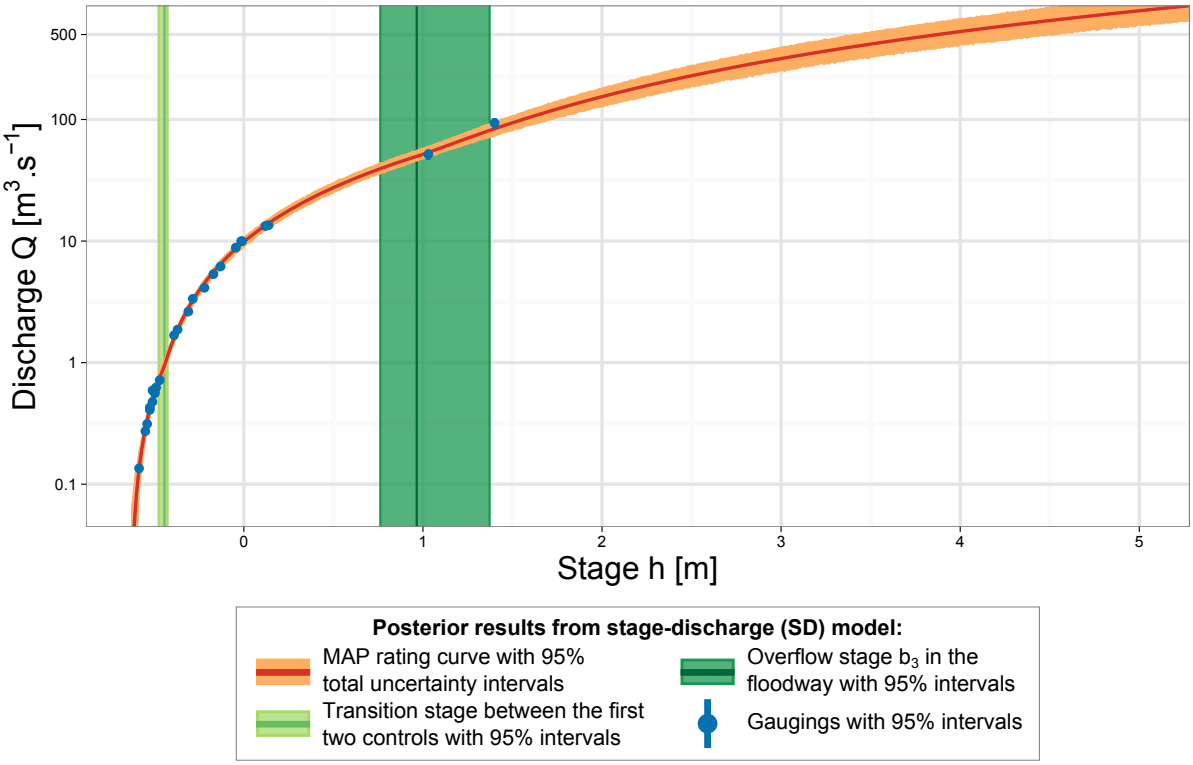

Figure 2.13 – The Ardèche River at Meyras: stage-discharge representation of the stage-discharge (SD) model with discharges in logarithm scale.

Chapter 3

Stage-discharge hysteresis due to transient flow

This chapter is planned to be published soon. Hysteresis due to transient flow has also been presented at the *European Geosciences Union General Assembly 2015* (Oral communication, Mansanarez et al., 2015).

Contents

3.1. Introduction

3.1.1. Stage-discharge hysteresis

The hysteresis effect studied in this chapter is a hydraulic process associated with a transient flow in a relatively flat channel. This phenomenon changes the stage-discharge relation at a hydrometric station from a unique into a non unique relation. At a given stage, discharge is greater for the rising limb than for the falling limb. This effect can be quickly explained by the fact that during the propagation of a transient flow the celerity of the pressure (stage) wave is smaller than the celerity of the velocity wave, therefore smaller than the celerity of the discharge wave [Lee, 2013], as illustrated in figure 3.1-a. The maximum discharge Q_{max} occurs before the maximum stage h_{max}. This can be represented by a loop in the stage-discharge relation (see figure 3.1-b). Two discharge values are associated with a given stage : the larger one for the rising limb and the smaller one for the falling limb. However, looped curves are not necessarily associated with this kind of hysteresis. Other rating change processes, like variable backwater and variable roughness, may yield similar (or opposite) looped curves (see the Madeira River at Fazenda, figure 4.12 in chapter 4).

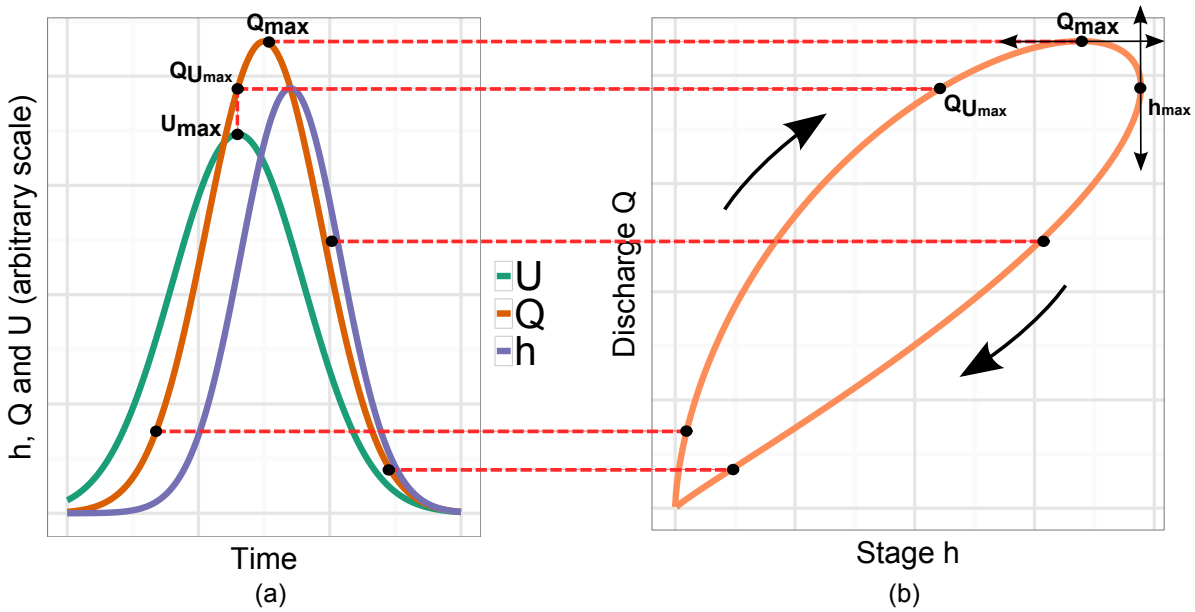

Figure 3.1 – Graphical representations of hysteresis due to transient flow: (a) velocity (U), discharge (Q) and stage (h) temporal curves; (b) the associated stage-discharge representation.

3.1.2. Gauging hysteretic events

Currently, the common gauging strategy is to gauge during the falling limb, as soon as possible after the peak discharge. This gauging strategy aims to secure the operator from fast discharge and stage evolutions. However, this strategy may not be suitable for hysteretic events. Indeed, a standard stage-discharge rating curve may fit well these gaugings for such a strategy but this might be misleading: if hysteresis exists, discharge will be underestimated for the rising limb.

More generally, ignoring hysteresis when it is in fact present may have several undesired consequences:

- higher uncertainties of the discharge estimations due to the dispersion of the gaugings along the rating curve;
- an underestimation of the peak flow event, which may have consequences for safety measures [e.g., Muste et al., 2011, Holmes, 2016]. For example, it can potentially affect the design of spillways and flood-protection dikes.;
- a biased reconstruction of flood hydrographs with a time lag. It may bring a high level of uncertainties in e.g. flood forecasting.

3.1.3. Hysteresis formulas

In case the hysteresis effect is not simply ignored, the most common practice is to make a correction of the steady flow rating curve (i.e. the standard stage-discharge relation) by using the Jones' formula [Jones, 1915]. This correction is based on the fact that the energy slope is not equal to the riverbed slope for unsteady flows: consequently, the riverbed slope is adjusted depending on the flood wave celerity and the stage gradients (this will be detailed in section 3.2).

Many other physical methods were developed in the literature, based on the same principle of correcting the steady flow rating curve. These methods have been reviewed and compared by Schmidt [2002], Dottori et al. [2009], Lee [2013]. They differ in their assumptions and approximations. In particular, some of them use a single stage record $h(t)$ and its gradient dh/dt as input variables, while others require using multiple stage records which are rarely available at hydrometric stations. They also differ in their complexity: some provide an explicit discharge formula, while for others the discharge formula is implicit and therefore needs to be solved with numerical methods. Table 3.1 lists the main hysteresis formulas that use a single stage record

and its gradient. In particular it describes the type of formula (explicit vs. implicit) and the approximation made to describe flood routing.

3.1.4. Estimation of hysteretic rating curves

All formulas discussed in the previous section use several physical variables (e.g., roughness, geometry of the control reach, dynamics of the flood wave). These variables may be measured in controlled experimental conditions. However, they are not all available at typical hydrometric stations controlling natural rivers. Consequently, the formulas of the previous section contain in practice unknown parameters that need to be estimated.

Boyer [1937] and Lewis [1939] proposed a graphical analysis for estimating the correction of the steady flow rating curve in the Jones' formula.

Other methods based on the Artificial Neural Network (ANN) theory neglect the physical principles to focus on the observed stage and/or discharge. First introduced by Tawfik et al. [1997] and pursued by Jain and Chalisgaonkar [2000], Sudheer and Jain [2003] and Bhattacharya and Solomatine [2005], these methods are able to model hysteresis events but can be criticised as lacking hydraulic basis and being difficulty to apply by end-users. Moreover, they do not encompass an uncertainty quantification step.

Petersen-Øverleir [2006] highlights the limits of these approaches and proposes an innovative step for the uncertainty analysis of hysteresis effect. His method is based on the Jones' formula. He also uses non linear regression and maximum likelihood estimation to model hysteresis and provide the uncertainties of the discharge estimates. The method has solid hydraulic and statistic justifications, however it does not take into account the uncertainties of each gauging. Furthermore, as recognised by the author, in the first application the method provides unrealistic and very unstable values without physical justifications.

Method	Type of formula	Flood routing
Jones [1915]	Explicit	Kinematic approximation
Wiggins [1925]	Explicit	Kinematic approximation
Henderson [1966]	Explicit	Parabolic approximation
Fenton [1999]	Explicit	Long wave approximation (Higher order advection diffusion approximation)
Di Silvio [1969]	Implicit (num)	Triangular approximation
Fread [1975]	Implicit (num)	Parabolic approximation
Marchi [1976]	Implicit (ODE)	Kinematic approximation
Faye and Cherry [1980]	Implicit (ODE)	Kinematic approximation
Lamberti and Pilati [1990]	Implicit (ODE)	Kinematic or quasikinematic approximation
Perumal et al. [2004]	Implicit (num)	Advection diffusion approximation

Table 3.1 – Hysteresis formulas based on a single stage record, modified from Lee [2013]. 'num' means that a numerical method is required to solve the equation, 'ODE' means that the equation takes the form of an Ordinary Differential Equation.

The latter issue could be addressed by using priors to constrain physical parameters. However, as far as we are aware of, hysteresis due to transient flow was never treated through Bayesian analysis in the literature.

3.1.5. Objectives

The method proposed in this chapter is a Bayesian analysis based on the Jones' formula and kinematic approximations made by Lighthill and Whitham [1955] and Chow [1959]. This Bayesian method incorporates information from hydraulic knowledge (equations of channel controls based on geometry and roughness estimates) and stage-gradient-discharge observations (gauging data). The obtained total uncertainty combines parametric uncertainty (estimation

of the rating curve parameters) and structural uncertainty (imperfection of the rating curve model). This method provides a direct estimation of the physical inputs of the rating curve model (roughness, bed slope, kinematic wave celerity and cross-sectional geometry).

The application of the proposed method is illustrated with two case studies:

(a) two dam flushing operations in the Ebro river, Spain. These events are extremely violent events in a large river. There are well documented with gaugings especially in the rising limb;

(b) a year of discharge measurements in a calibrated cross-section equipped with a continuous Doppler velocimeter, near Plymouth, North Carolina, USA. This equipment captures many hysteresis events.

Further exploration of the hysteretic rating curve estimation process is presented :

- the comparison between a steady stage-discharge model and the stage-gradient-discharge hysteresis model;
- the comparison between the simple formula of Jones and the high-order approximation of Fenton formula [Fenton, 1999];
- the impact of the prior knowledge;
- the impact of the gauging strategy.

3.2. Stage-gradient-discharge (SGD) models

Usually, stage-discharge (SD) models for channel controls are based on the assumption of steady uniform flow: $S_f \approx S_0$, where S_f is the friction slope and S_0 is the bed slope. They also use the Manning-Strickler formula:

$$Q = K_S A \, R_{\mathrm{h}}^{\frac{2}{3}} \sqrt{S_f} \tag{3.1}$$

where K_S [$\mathrm{m}^{1/3}.\mathrm{s}^{-1}$] is the Strickler coefficient, A [m^2] the wetted area of the cross-section and R_{h} [m] the hydraulic radius.

The common practice for a hysteretic event is to reflect the flood wave propagation effects in the estimation of the friction slope S_f. This approach leads to excellent empirical results which have validated this correction [Degoutte, 2006].

The correction is made by using the one dimensional Barré de Saint Venant equation which is commonly used to model transient flows in open channels :

$$S_f = S_0 - \frac{1}{g}\left(\frac{\partial U}{\partial t} + U\frac{\partial U}{\partial x}\right) - \frac{\partial h}{\partial x} \tag{3.2}$$

where g [$\mathrm{m.s}^{-2}$] is the gravitational acceleration, U [$\mathrm{m.s}^{-1}$] the cross-sectional average water velocity, x [m] the abscissa along the channel and h [m] the stage. Equation (3.2) provides an instantaneous value of the flow surface of the wave profile [Chow, 1959].

Combining equations (3.1) and (3.2) leads to:

$$Q = K_S A R_{\mathrm{h}}^{2/3} \sqrt{S_0 - \frac{1}{g}\left(\frac{\partial V}{\partial t} + V\frac{\partial V}{\partial x}\right) - \frac{\partial h}{\partial x}} \tag{3.3}$$

The terms $\frac{\partial V}{\partial t}$, $V\frac{\partial V}{\partial x}$ and $\frac{\partial h}{\partial x}$ in equations (3.2) and (3.3) are respectively the local acceleration, the convective acceleration and the longitudinal gradient terms. The two first terms represent the inertia terms of the one-dimensional Barré De Saint-Venant equation.

The diffusion wave assumption, a common simplification of the one-dimensional Saint-Venant equation, states that the inertia term in this equation $\frac{1}{g}\left(\frac{\partial V}{\partial t} + V\frac{\partial V}{\partial x}\right)$ is negligible compared to the pressure term $\frac{\partial h}{\partial x}$ and the slope S_0 [Ferrick et al., 1984]. This approximation of Barré

de Saint-Venant equation, has also been explained in other references [Chow, 1959, Henderson, 1966, Weinmann and Laurenson, 1979].

Therefore, by using the latter assumption in the equation 3.3, the Manning-Strickler formula for a prismatic channel can be expressed as:

$$Q = K_S A R_{\mathrm{h}}^{2/3} \sqrt{S_0 - \frac{\partial h}{\partial x}} \tag{3.4}$$

Equation (3.4) based on the diffusion wave assumption only holds if the permanent flow regime is a steady flow and under a uniformly progressive wave. We can therefore rewrite this equation as follows:

$$Q = Q_0 \sqrt{1 - \frac{1}{S_0}\frac{\partial h}{\partial x}} \tag{3.5}$$

where $Q_0 = K_S A R_{\mathrm{h}}^{2/3} \sqrt{S_0}$ is the discharge at steady flow.

3.2.1. Standard approximation: the Jones' formula

The longitudinal gradient term $\frac{\partial h}{\partial x}$ is rarely measured, except for twin-gauge stations (see chapter 4), and hence equations (3.4) and (3.5) cannot be applied to every hydrometric station. A strong hypothesis named the kinematic wave hypothesis [Lighthill and Whitham, 1955] can be made to overpass this difficulty. It assumes that the flood wave propagates with no attenuation along the channel.

By definition:

$$c = \frac{\partial Q}{\partial A} = \frac{\partial x}{\partial t} \tag{3.6}$$

where c [m.s^{-1}] is the kinematic wave celerity also called flood wave celerity. In other words [Chow et al., 1988], if an observer moves at the velocity c with the flow, he sees a constant discharge.

For a steady flow, the continuity equation, described below, is also verified:

$$\frac{\partial Q}{\partial x} + \frac{\partial A}{\partial t} = 0 \tag{3.7}$$

Then, equation (3.7) can be reduced by using the definition of the kinematic wave celerity (equation (3.6)):

$$\frac{\partial Q}{\partial h}\frac{\partial h}{\partial x} + \frac{\partial A}{\partial Q}\frac{\partial Q}{\partial h}\frac{\partial h}{\partial t} = 0$$

$$\frac{\partial h}{\partial x} + \frac{1}{\frac{\partial Q}{\partial A}} \frac{\partial h}{\partial t} = 0$$
$$\frac{\partial h}{\partial x} + \frac{1}{c} \frac{\partial h}{\partial t} = 0 \tag{3.8}$$

Therefore, equation (3.4) can be rewritten by substituting equation (3.8) for the $\frac{\partial h}{\partial x}$ term:

$$Q = K_S A R_{\mathrm{h}}^{2/3} \sqrt{S_0 + \frac{1}{c} \frac{\partial h}{\partial t}} \tag{3.9}$$

Although old, the Jones' formula is still used today. Indeed, it only needs one staff gauge, the slope S_0 of the riverbed and an estimation of the kinematic wave celerity c to correct the rating curve for steady flow.

When the assumption of a constant celerity is not deemed reasonable, Chow [1959] and Henderson [1966] explained that the kinematic wave celerity c can be computed (see equation (3.10)) from the width B of the river, the discharge Q_0 at steady flow and the stage h. This relation only applies if the cross-section shape of the channel is assumed prismatic ($\partial A = B \partial h$) or if the banks are vertical in the range of variation of h and $Q \approx Q_0$.

$$c = \frac{\partial Q}{\partial A} \simeq \frac{1}{B} \frac{\partial Q_0}{\partial h} \tag{3.10}$$

Thus, equation (3.9) becomes:

$$Q = K_S A R_{\mathrm{h}}^{2/3} \sqrt{S_0 + \frac{1}{\frac{1}{B} \frac{\partial Q_0}{\partial h}} \frac{\partial h}{\partial t}} \tag{3.11}$$

Therefore, in this chapter, equations (3.9) and (3.11) are used as a basis for modelling hysteresis due to transient flow. These two equations differ by the fact that the wave celerity c is modelled as a constant (3.9) or as a function of the stage (3.11).

3.2.2. High-order approximations: the Fenton formulas

Fenton [1999] proposed a method (described in detail in [Fenton and Keller, 2001]) which can be seen as an extension of the Jones' formula (equation (3.9)). With the same assumptions he used the full long wave equations and he reduced them by the polynomial Taylor series expansion. Two equations result from those approximations corresponding to the second and third order

Taylor developments:

$$Q = \underbrace{\underbrace{\underbrace{\underbrace{K_S A R_{\mathrm{h}}^{2/3}}_{Q_0}\left(S_0 + \frac{1}{c}\frac{\partial h}{\partial t}}_{\text{Jones}} - \frac{D}{c^3}\frac{\partial^2 h}{\partial t^2}}_{\text{Fenton second order}} - \frac{G}{c^5}\frac{\partial^3 h}{\partial t^3}\right)^{1/2}}_{\text{Fenton third order}} \tag{3.12}$$

where $D = Q_0/(2BS_0)$ [m^2.s^{-1}] is the diffusion term coefficient using the approximation of equation (3.10) and the advection-diffusion theory [Fenton, 2001], G [m^4.s^{-2}] is given by $G = -D\left(gA/B + \beta V(c-V)\right)/\left(gAS_0/Q_0\right)$, g [m.s^{-2}] is the gravity constant, $V = c - Q_0/A$ [m.s^{-1}] and β [−] is the Boussinesq momentum coefficient. Jones' formula and formulas of Fenton second and third order are stage-gradient-discharge (SGD) models whereas Q_0 is computed using a stage-discharge (SD) model.

As the Jones' formula described in section 3.2.1, the kinematic wave celerity c can be seen as function of a stage, by replacing c by $\frac{1}{B}\frac{\partial Q_0}{\partial h}$ in equation (3.12).

3.2.3. Formulas for simple cross-sectional geometries

Let y denote the water depth in the river. By definition, y is equal to $h - h_0$ where h is the stage at the staff gauge and h_0 the vertical coordinate of the bottom of the riverbed with respect to the zero of the staff gauge.

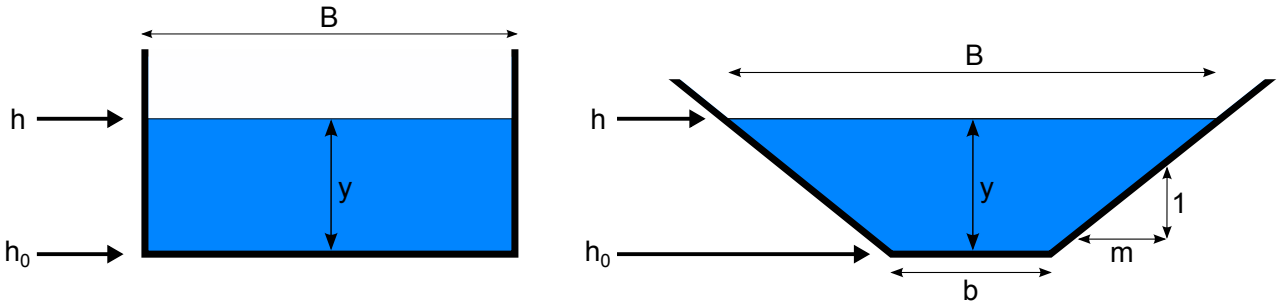

Figure 3.2 – Diagram of the geometry of both the rectangular and trapezoidal cross-sections.

We remind the hydraulic geometry for a wide rectangular cross-section ($B \gg h$) and a trapezoidal cross-section (figure 3.2). This latter one is a general formula including the rectangular cross-section. Indeed, for a batter m of the bank equal to $m = 0$, the trapezoidal cross-section corresponds to a rectangular cross-section (see figure 3.2). Moreover, for each hydraulic variable all the equations in table 3.2 match for the two cases, when $m = 0$.

Hydraulic variables	Wide rectangular cross-section	Trapezoidal cross-section
Width B	B	$b + 2my$
Wetted area A	By	$(b + my)\, y$
Wetted perimeter P	$B + 2y \sim B$	$b + 2y\sqrt{1 + m^2}$
Hydraulic radius R_h	$\dfrac{By}{B + 2y} \sim y$	$\dfrac{(b + my)\, y}{b + 2y\sqrt{1 + m^2}}$
Steady flow Q_0	$K_S\sqrt{S_0}B\ y^{5/3}$	$K_S\sqrt{S_0}A\ R_\mathrm{h}^{2/3}$
Flood wave celerity c	$5/3\ K_S\sqrt{S_0}y^{2/3}$	$\left(5 - 4\sqrt{1 + m^2}\dfrac{R_\mathrm{h}}{B}\right)\dfrac{Q_0}{3A}$
Diffusion term coefficient D	$K_S(2\sqrt{S_0})^{-1}y^{5/3}$	$K_S(2B\sqrt{S_0})^{-1}A\ R_\mathrm{h}^{2/3}$
Coefficient G	$-\dfrac{K_S^2 y^{10/3}}{2gS_0}\left(g + \dfrac{2}{3}\beta K_S^2 S_0\ y^{1/3}\right)$	$-\dfrac{Q_0^2}{2gABS_0^2}\left[g\dfrac{A}{B} - \beta V^2 + \beta V c\right]$

Table 3.2 – Hydraulic geometry for the wide rectangular cross-section and the trapezoidal cross-section assuming $D = Q_0/(2BS_0)$.

The wide rectangular cross-section is often used in practice. Chow [1959] states that a cross-section can be considered as wide when the width B of the river is more than 10 times bigger than the stage h (5 times in Graf [1998]). This assumption allows simplifying the Manning-Strickler equation into a power law. Indeed, the hydraulic radius $R_\mathrm{h} = (by)/(b + 2y)$ can be simplified to $R_\mathrm{h} = y$, where $y = h - h_0$.

We denote by M the exponent in the steady flow Q_0 equation (see table 3.2). For a wide rectangular cross-sectional shape, M equals 5/3 whereas for a trapezoidal cross-sectional shape, it equals 2/3.

Equation (3.12) can be rewritten according to the expressions of B, A, R_h, Q_0, c, D and G in table 3.2. Thus we can derive 12 models depending on the order of expansion (Jones, Fenton

second order and Fenton third order), the cross-sectional geometry (wide rectangle or trapezoid) and the celerity models (constant or variable with stage).

3.3. Bayesian inference

3.3.1. Parameterisation

Let $\boldsymbol{\theta} = (\boldsymbol{\theta_{RC}}, \boldsymbol{\gamma})$ denote the inferred parameters where parameters $\boldsymbol{\theta_{RC}}$ are the SGD rating curve parameters and parameters $\boldsymbol{\gamma} = (\gamma_1, \gamma_2)$ are the parameters of the error model. The hydraulic interpretation of the parameter $\boldsymbol{\theta_{RC}}$ is summarizes in table 3.3. For example, in case of a wide rectangular cross-section, the SGD model using the Jones' formula with variable celerity uses the following parameterisation:

$$\begin{aligned} Q(h) &= K_S B (h-h_0)^M \sqrt{S_0 + \frac{1}{M K_S \sqrt{S_0}\,(h-h_0)^{M-1}} \frac{\partial h}{\partial t}} \\ Q(h) &= \theta_1 \theta_4 (h-\theta_2)^{\theta_3} \sqrt{\theta_5 + \frac{1}{\theta_3 \theta_1 \sqrt{\theta_5}\,(h-\theta_2)^{\theta_3 - 1}} \frac{\partial h}{\partial t}} \end{aligned} \tag{3.13}$$

This parameterisation allows having a direct physical interpretation of the hydraulic variables. The 11 other formulas (Fenton second/third order, wide rectangle/trapeze, constant/variable celerity) can be obtained in a similar way from equation (3.12), by using the adequate terms in table 3.2 and the parameterisation in table 3.3.

3.3.2. Likelihood computation

In this section, we denote the stage gradient $\partial h/\partial t$ by the notation ∂h. As described in section 2.4.1, gaugings $\left(\widetilde{h}_i, \widetilde{\partial h}_i, \widetilde{Q}_i\right)_{i \in [\![1;N]\!]}$ are seen as estimates of the real values $(h_i, \partial h_i, Q_i)_{i \in [\![1;N]\!]}$ of stages, stage gradients and associated discharges. We also further assume that stage errors and stage gradient errors are negligible compared to discharge errors:

$$\begin{cases} \widetilde{h}_i = h_i \\ \widetilde{\partial h}_i = \partial h_i \\ \widetilde{Q}_i = Q_i + \epsilon_{Q,i} \quad \text{with} \quad \epsilon_{Q,i} \overset{\text{indep.}}{\sim} \mathcal{N}(0, u_{Q,i}) \end{cases} \tag{3.14}$$

Parameters	**Wide, rectangular cross-section**					
	Jones		**Fenton 2nd order**		**Fenton 3rd order**	
	constant c	$c\,(h)$	**constant** c	$c\,(h)$	**constant** c	$c\,(h)$
θ_1	$K_S B$	K_S				
θ_2	h_0					
θ_3	exponent $M \simeq 5/3$					
θ_4	S_0	B				
θ_5	c	S_0				
θ_6	-	-	c	-	c	β
θ_7	-	-	-	-	β	V
θ_8	-	-	-	-	V	-

Parameters	**Trapezoidal cross-section**					
	Jones		**Fenton 2nd order**		**Fenton 3rd order**	
	constant c	$c\,(h)$	**constant** c	$c\,(h)$	**constant** c	$c\,(h)$
θ_1	K_S					
θ_2	h_0					
θ_3	exponent $M \simeq 2/3$					
θ_4	b					
θ_5	m					
θ_6	S_0					
θ_7	c	-	c	-	c	β
θ_8	-	-	-	-	β	V
θ_9	-	-	-	-	V	-

Table 3.3 – Hydraulic interpretation of the parameters for the Jones and second and third order Fenton models, whether or not the kinematic wave celerity c $\left[m.s^{-1}\right]$ depends on the stage. K_S $\left[m^{1/3}.s^{-1}\right]$ is the Strickler coefficient, B $[m]$ the top width of the river, b $[m]$ the width of the bed, h_0 $[m]$ the elevation of the bottom, m $[m]$ is the batter, β $[-]$ the Boussinesq coefficient and V $\left[m.s^{-1}\right]$ the cross-sectional average water velocity

where the standard deviations $u_{Q,i}$ (uncertainties of discharge measurements) are assumed to be known (see section 2.3).

The true discharge is then written as the discharge predicted by the rating curve plus a structural error:

$$Q_i = \underbrace{f\left(h_i, \partial h_i | \boldsymbol{\theta}_{\mathbf{RC}}\right)}_{\widehat{Q}_i} + \epsilon_{f,i} \quad \text{with} \quad \epsilon_{f,i} \overset{\text{indep.}}{\sim} \mathcal{N}\left(0, \sigma_{f,i} = \gamma_1 + \gamma_2 \widehat{Q_i}\right) \tag{3.15}$$

where $\boldsymbol{\theta}_{\mathbf{RC}}$ are the rating curve parameters, $\boldsymbol{\epsilon_f} = (\epsilon_{f,1}, \ldots, \epsilon_{f,N})$ are the structural errors, $(\sigma_{f,1}, \ldots, \sigma_{f,N})$ are the standard deviations of the structural errors $(\epsilon_{f,1}, \ldots, \epsilon_{f,N})$ and $\widehat{\boldsymbol{Q}} = \left(\widehat{Q}_1, \ldots, \widehat{Q}_N\right)$ are the discharge estimations related to the N gaugings (see section 2.4.1).

The linear function used for modelling the standard deviation $\sigma_{f,i}$ is the same as that described in section 2.4.1. We also assume that the structural errors $(\epsilon_{f,1}, \ldots, \epsilon_{f,N})$ and the discharge errors $(\epsilon_{Q,1}, \ldots, \epsilon_{Q,N})$ are independent.

Combining equations (3.14) and (3.15) yields the following stage-gradient-discharge relation between observed values:

$$\widetilde{Q}_i = f\left(\widetilde{h}_i, \widetilde{\partial h}_i \middle| \boldsymbol{\theta}_{\mathbf{RC}}\right) + \epsilon_{Q,i} + \epsilon_{f,i} \quad \text{with} \quad \epsilon_{Q,i} + \epsilon_{f,i} \sim \mathcal{N}\left(0, \sqrt{\sigma_{f,i}^2 + u_{Q,i}^2}\right) \tag{3.16}$$

The likelihood L of observed discharge values $\widetilde{\boldsymbol{Q}}$ for the stage-gradient-discharge (SGD) model is given by:

$$L\left(\widetilde{\boldsymbol{Q}} \middle| \boldsymbol{\theta} = (\boldsymbol{\theta}_{\mathbf{RC}}, \boldsymbol{\gamma}), \tilde{\boldsymbol{h}}, \widetilde{\boldsymbol{\partial h}}\right) = \prod_{i=1}^{N} p_{\text{norm}}\left[\widetilde{Q}_i \middle| f\left(\widetilde{h}_i, \widetilde{\partial h}_i \middle| \boldsymbol{\theta}_{\mathbf{RC}}\right), \sqrt{\sigma_{f,i}^2 + u_{Q,i}^2}\right] \tag{3.17}$$

where $\widetilde{\boldsymbol{Q}} = \left(\widetilde{Q}_1, \ldots, \widetilde{Q}_N\right)$ are the N gauged discharges, $\widetilde{\boldsymbol{h}} = \left(\widetilde{h}_1, \ldots, \widetilde{h}_N\right)$ are the N related observed stage values, $\widetilde{\boldsymbol{\partial h}} = \left(\widetilde{\partial h}_1, \ldots, \widetilde{\partial h}_N\right)$ are the N related observed stage gradient values and $p_{\text{norm}}[z|m, s]$ denote the probability density function (pdf) of a Gaussian distribution with mean m and standard deviation s, evaluated at some value z.

3.3.3. Prior specification

Bayesian inference requires specifying a prior distribution for the vector of parameters $\boldsymbol{\theta}$ as described in section 3.3.2. The prior information of the SGD models therefore needs to be entered by the practitioner depending on the information available at the gauging station: this is completely site-specific, and will therefore be described for each case study.

3.4. Application to distinct cases

3.4.1. Dam flushes in the Ebro River at Ascó, Spain

The first case study focuses on two flood events in the river Ebro at Ascó, Spain. These flood events are remarkable by the strength of the hysteresis effect and the availability of many gaugings during the events. Such cases are extremely rare among hysteresis events: they are scheduled dam flushes on a large river with successive gaugings on two flood events. Moreover, these events are recent and well-documented.

Sanchez et al. [2013] present the Ascó station and these two flood events with a simple use of the Jones' formula (equation (3.12)) as a correction of the steady rating curve. Lee [2013] also studied these events with a Fread's formula [Fread, 1975].

3.4.1.1. Data and models

The Ebro River is a medium-sized river in terms of length (928 km), catchment area (85, 550 km^2) and floods (up to 4000 $m^3.s^{-1}$). The hydrometric station (GPS locations: $0°34'11.5''$E, $41°11'0.76''$N) is located upstream of the delta of the Ebro river between Zaragoza (upstream) and Tortósa (downstream) about 100 km from the Mediterranean sea.

Many reservoirs and dams are established along the river. Upstream of the station, a system of large reservoirs (Mequinenza-Ribarroja-Flix) controls the floods and regulates the lower Ebro River. Due to this regulation, the stage-discharge relation is not well known for large discharges (above 1000 $m^3.s^{-1}$). For low discharges, the proliferation of aquatic vegetation affects the hydraulic behaviour. The vegetation is problematic for navigation and operation of a nuclear power plant. In order to remove vegetation, two artificial floods are produced every year through dam flushing [Sanchez et al., 2013]. Thanks to a close collaboration between the Hydrology department of the *Confederación Hidográfica del Ebro* and the researchers of the RIUS group of the University of Lleida, several series of discharge measurements have been conducted during these flood events.

The discharge measurements for the events of November 2010 and June 2012 were performed with an ADCP (RiverSurveyor-M9, from SonTek). Only one river crossing was performed for each discharge measurement: we decide to associate an uncertainty of 10% with these gaugings.

Figure 3.3 shows the stage-discharge measurements for both events. 18 gaugings are available for the first event, 25 for the second one. For both November 2010 and June 2012 events,

30-50% discharge differences are observed between the rising limb and the falling limb. An important shift of the stage-discharge relation can also be seen between the two events: despite the controlled dam flushing, the vegetation has increased [Sanchez et al., 2013], which has led to this rating change. The available discharge measurements since 1978 are also represented in figure 3.3. The rating change phenomenon between the events of November 2010 and June 2012 does not seem extraordinary: the discharge measurements are scattered and different stage-discharge relations can be observed. As an example, the discharge measurements after the June 2012 event are differentiated: two different stage-discharge relations exist. These rating changes will not be treated in this manuscript.

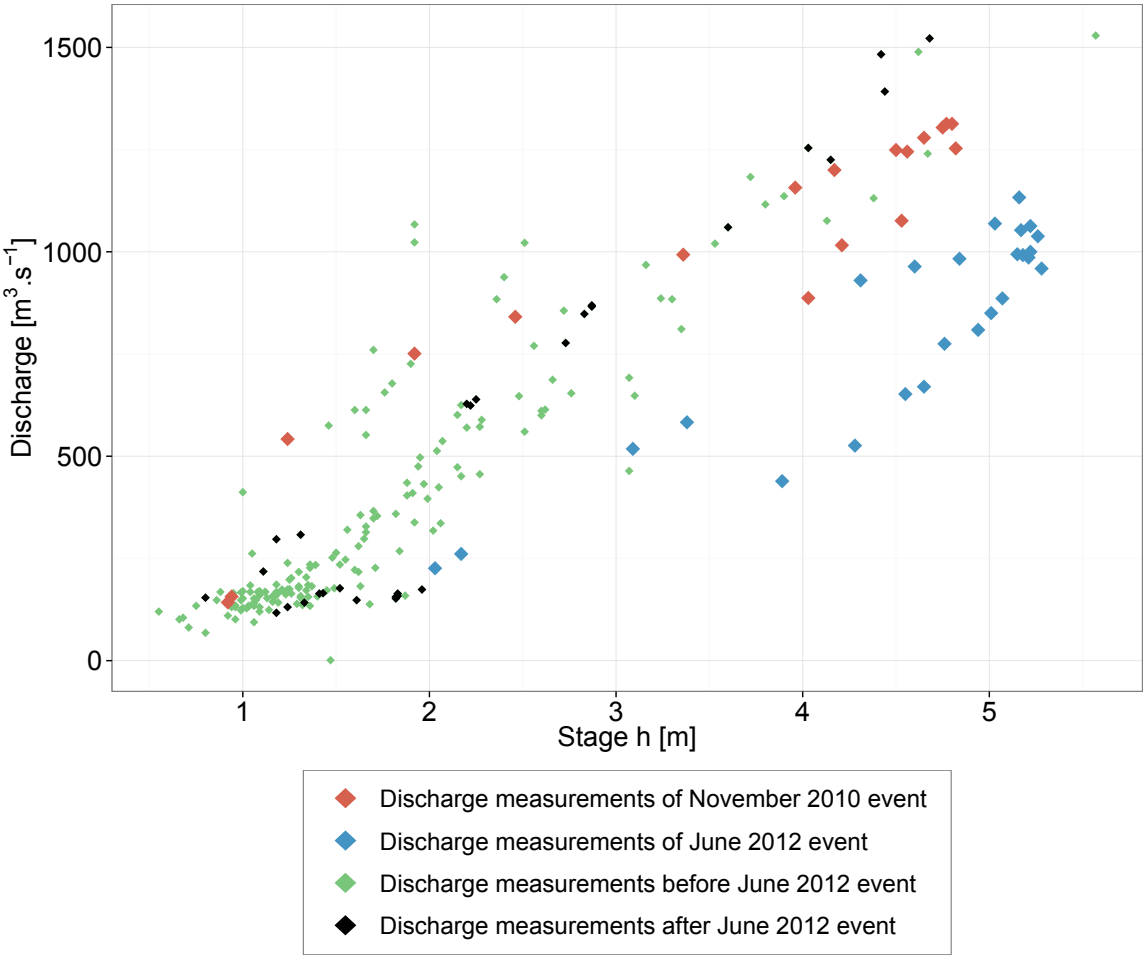

Figure 3.3 – Discharge measurements made on the Ebro River at Ascó since 1978.

3.4.1.2. Prior specification

The banks upstream and downstream the station are partially vegetated along the channel (see figure 3.4-a) and there is some aquatic vegetation in the main channel. According to Chow [1959], the Manning-Strickler coefficient K_S is set to 30 $m^{1/3}.s^{-1}$ with an uncertainty of ± 10 $m^{1/3}.s^{-1}$.

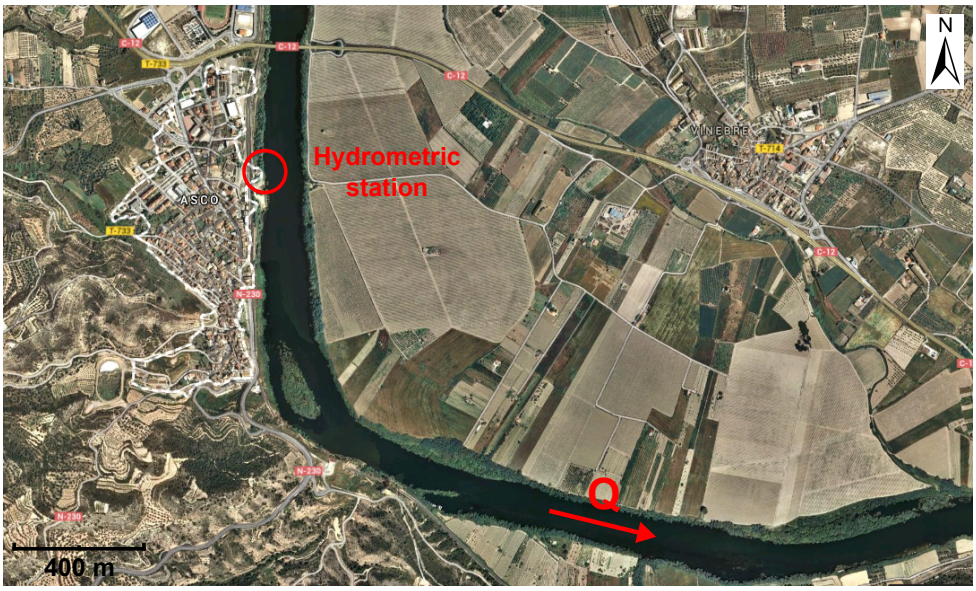

(a)

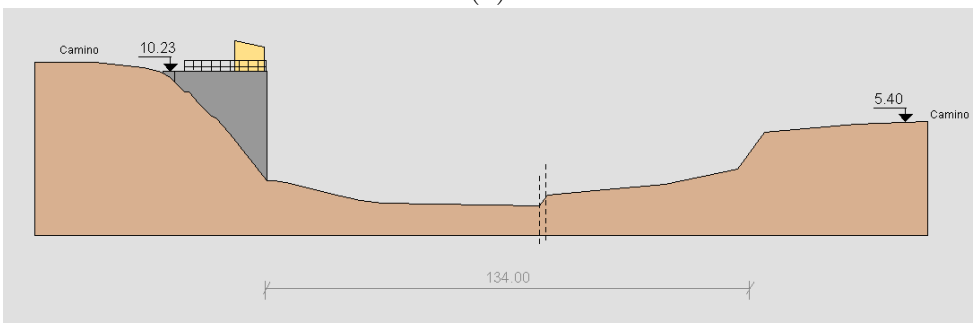

(b)

Figure 3.4 – The Ebro River at Ascó: (a) view from above (Google Earth view); (b) cross-section of the gauging station (SAIH Ebro, the Automatic Hydrologic Information System of the Ebro river basin). All lengths are in meters. The dashed vertical lines indicates where the cross-section is not represented.

Just around the station, the channel is fairly uniform (figure 3.4-a) with an average width estimated at 130 m $\pm$20 m. The width is therefore much larger than the depth (up to 5.3 m): the cross section is hence approximated by a wide, rectangular cross-section. It matches well with the cross-section of the gauging station (see figure 3.4-b). Overflows in the floodplain are neglected as stage values of the two events do not exceed the overflow stage (5.4 m). Vegetation

effects during both events do not allow us to precisely determine the coordinates h_0 of the bottom of the bed: h_0 is vaguely set to 0 m $\pm$ 2 m. Moreover, there were no stage measurements made near the station to directly estimate the slope surface at steady flow. From old hydraulic studies [Sanchez et al., 2013], the bed slope is directly estimated to $S_0 = 0.001$ m/m. As explained by Sanchez et al. [2013], this estimation is uncertain, we therefore set a large standard deviation of 0.001 m/m (i.e. S_0 is set to 0.001 m/m $\pm$ 0.002 m/m). The average value of the kinematic wave celerity c is also given by a simple estimate: the distance between the gauging station and the downstream Tortosa station is divided by the time it took for the peak flood to get from one station to the other. This average celerity is estimated to 1.4 m.s^{-1} and we also set a large standard deviation of 1 m.s^{-1}, i.e. c is set to 1 m.s^{-1} $\pm$ 2 m.s^{-1}. In accordance with these possible values of the flood wave celerity c, V is also set to 1 m.s^{-1} $\pm$ 2 m.s^{-1}. The Boussinesq coefficient β is vaguely set to 1 $\pm$ 0.3 according to Chow [1959]. Flat uniform distributions are used for both parameters γ_1 and γ_2 of the structural error model: we let these parameters be inferred from the gaugings. Corresponding priors are summarised in table 3.4.

Physical parameters	Units	Prior distributions
$K_S B\sqrt{S_0}$	$[\text{m}^{\frac{4}{3}}.\text{s}^{-1}]$	$\mathcal{N}(123.3; 66)$
$K_S B$	$[\text{m}^{\frac{4}{3}}.\text{s}^{-1}]$	$\mathcal{N}(3900; 716)$
K_S	$[\text{m}^{\frac{1}{3}}.\text{s}^{-1}]$	$\mathcal{N}(30; 5)$
h_0	[m]	$\mathcal{N}(0; 1)$
M	[−]	$\mathcal{N}(1.6667; 0.01)$
B	[m]	$\mathcal{N}(130; 10)$
S_0	[−]	$\mathcal{N}(0.001; 0.001)$
c	$[\text{m.s}^{-1}]$	$\mathcal{N}(1.4; 1)$
β	[−]	$\mathcal{N}(1; 0.15)$
V	$[\text{m.s}^{-1}]$	$\mathcal{N}(1; 1)$
γ_1	$[\text{m}^3.\text{s}^{-1}]$	$\mathcal{U}\left(0; 10^6\right)$
γ_2	[−]	$\mathcal{U}\left(0; 10^6\right)$

Table 3.4 – Prior distributions of the hydraulic variables for the Ebro events. The symbol $\mathcal{N}(\mu; \sigma)$ corresponds to the normal distribution with mean μ and standard deviation σ. The symbol $\mathcal{U}(a; b)$ corresponds to the uniform distribution on the interval $[a, b]$.

3.4.1.3. Results

Figure 3.5 shows the need to use a stage-gradient-discharge (SGD) model instead of a stage-discharge (SD) model when a flood event is affected by a hysteresis effect. The total uncertainty

interval of the SD model is more than four times larger than the total uncertainty interval of the Jones model with variable celerity (figures 3.5-a and 3.5-b). This highlights the limits of the SD model to account for such complex flows. We can also notice that the parametric uncertainty interval is a bit larger for the SD model than for the SGD model whereas the prior distributions are the same. Moreover, as explained in the introduction, we observe a time lag between the SD results and the discharge measurements, and an underestimation of the peak flow. By contrast, the SGD model adequately reproduces the timing of the flood event and the hysteresis loop in the stage-discharge representation.

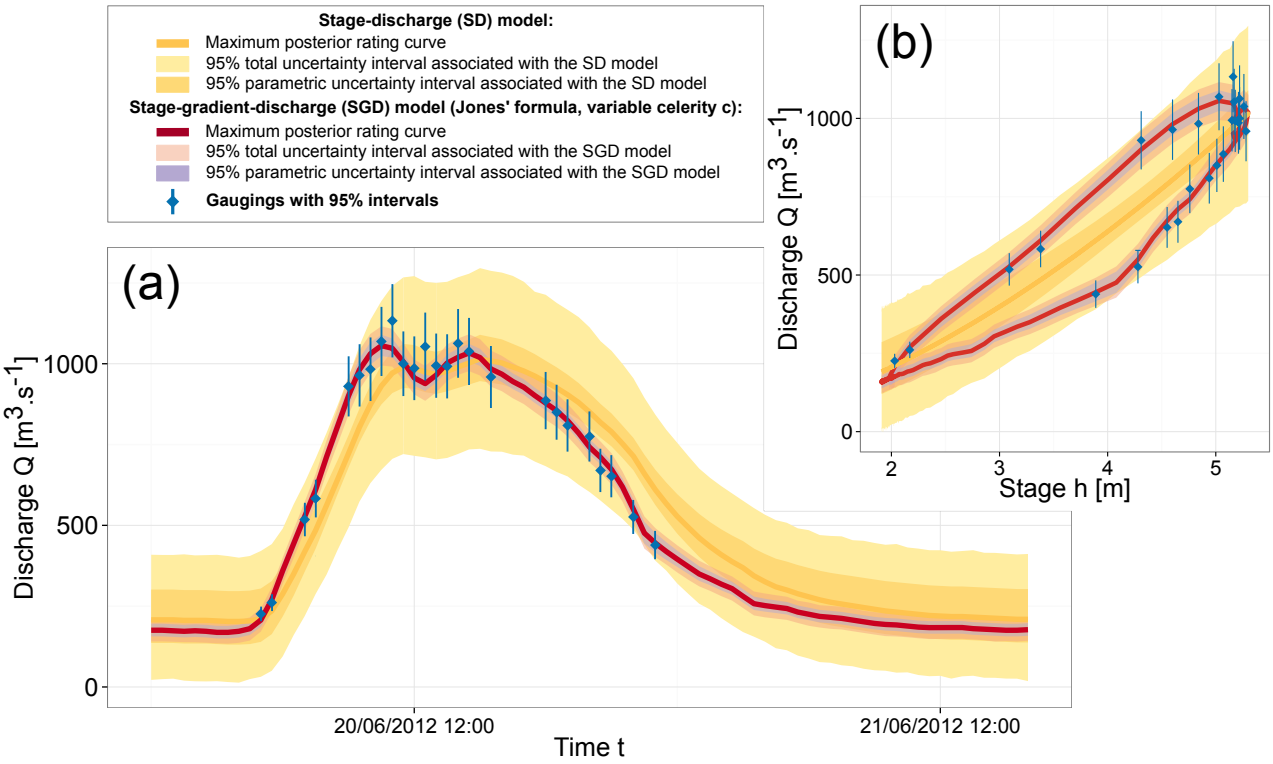

Figure 3.5 – The Ebro River at Ascó, event of June 2012, comparison between a stage-discharge (SD) model and the stage-gradient-discharge (SGD) model using the Jones' formula with the flood wave celerity c modelled as a function of stage: (a) time-discharge representation; (b) stage-discharge representation.

We now seek to establish which of the 6 distinct SGD models (see sections 3.2.2 and 3.2.3) for a wide rectangular cross-section brings the best results. For each model and each event the prior distributions of table 3.4 are used.

Figures 3.6 and 3.7 show results for both events of November 2010 and June 2012. All models detect a hysteresis effect: all the rating curves present the looped shape and fit well with discharge measurements.

However, both SGD models using the Jones' formula follow the discharge measurements more closely. Moreover these two models have smaller total uncertainties than the others. Thus, the Jones' formula shows an acceptable goodness-of-fit, irrespective of the assumption made on the celerity c (constant or variable).

Looking carefully at the parametric uncertainties of each model, the SGD model using the Jones' formula with variable celerity c seems to have smaller uncertainties than the SGD model using the Jones' formula with constant celerity. Furthermore, these specific parametric uncertainty intervals become smaller for the June 2012 event than for the November 2010 event (which has less gaugings). This is not surprising, since the parametric uncertainty is directly linked to the number of gaugings used to calibrate the rating curve.

Therefore, from this first graphical analysis, the two SGD models using the Jones' formula, with celerity as a function of stage or as a constant, seem to be, in this order, the best two models in terms of uncertainty intervals (parametric and total) and in terms of goodness-of-fit.

Figure 3.8 shows the evolution of the flood wave celerity c with respect to the stage h for both Ebro events. For each of the November 2010 and June 2012 events, the constant celerity option leads to similar results in terms of maximum posterior celerity values (respectively 1.46 $m.s^{-1}$ and 1.60 $m.s^{-1}$). These values match with the average prior celerity of 1.4 $m.s^{-1}$ (see section 3.4.1.2). The associated parametric uncertainty intervals are large: the width of these intervals are 168% and 129% respectively. In contrast, results for the variable celerity option differ between the two events. This arises because the variable celerity is directly linked to the slope of the rating curve (see equation (3.10)) and there is a shift between the two events. However for both events the width of the parametric uncertainty intervals is smaller than for the constant celerity (less than 30%). Thus, the celerity estimation is more precise for the variable celerity option than for the constant celerity option and values are still physically consistent.

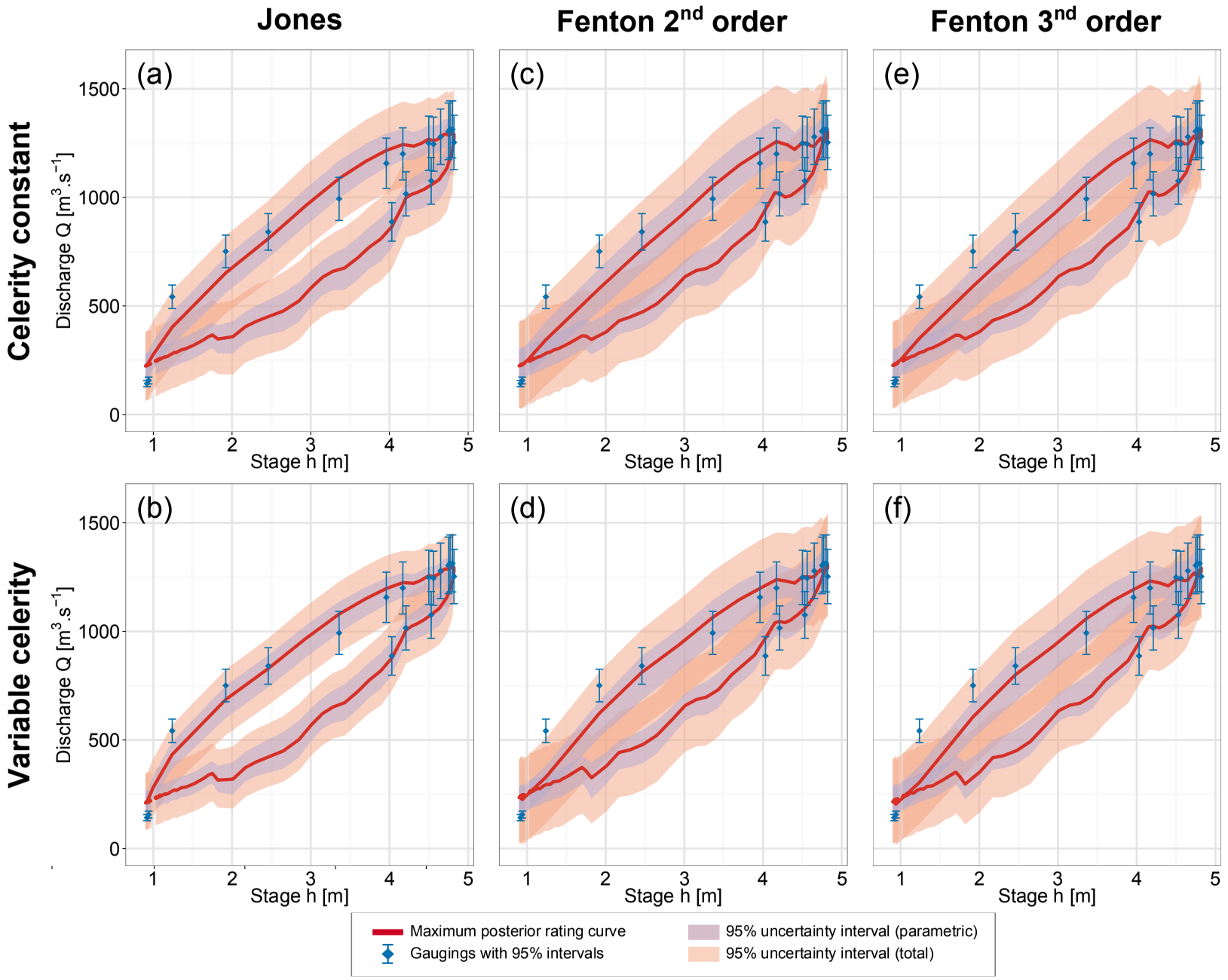

Figure 3.6 – The Ebro River at Ascó, **event of November 2010**: SGD rating curves using the Jones' formula (a and b), using the Fenton formula of second order (c and d) and using the Fenton formula of third order (e and f). For each formula, the flood wave celerity c is either constant or variable.

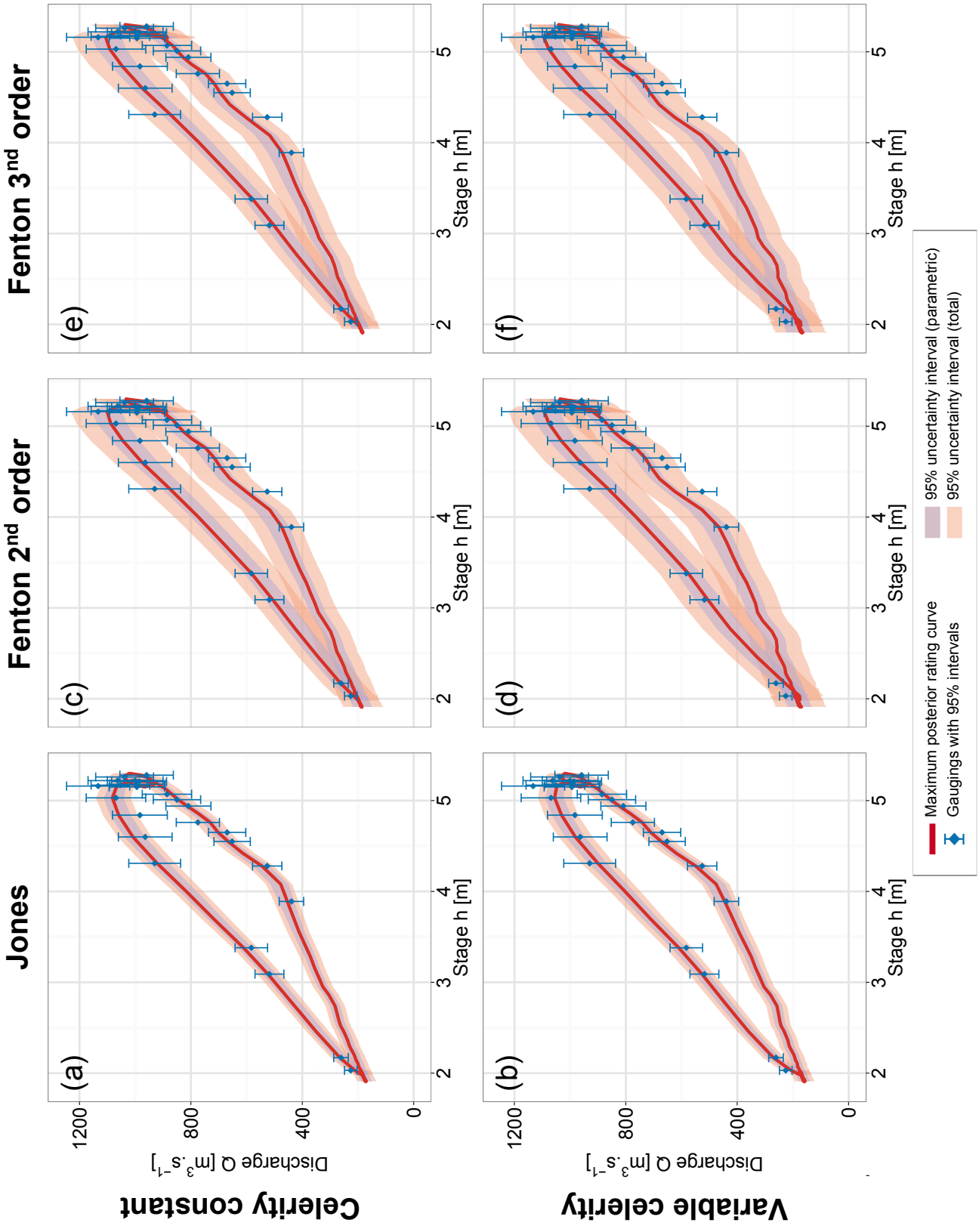

Figure 3.7 – The Ebro River at Ascó, **event of June 2012**: same legend as figure 3.6.

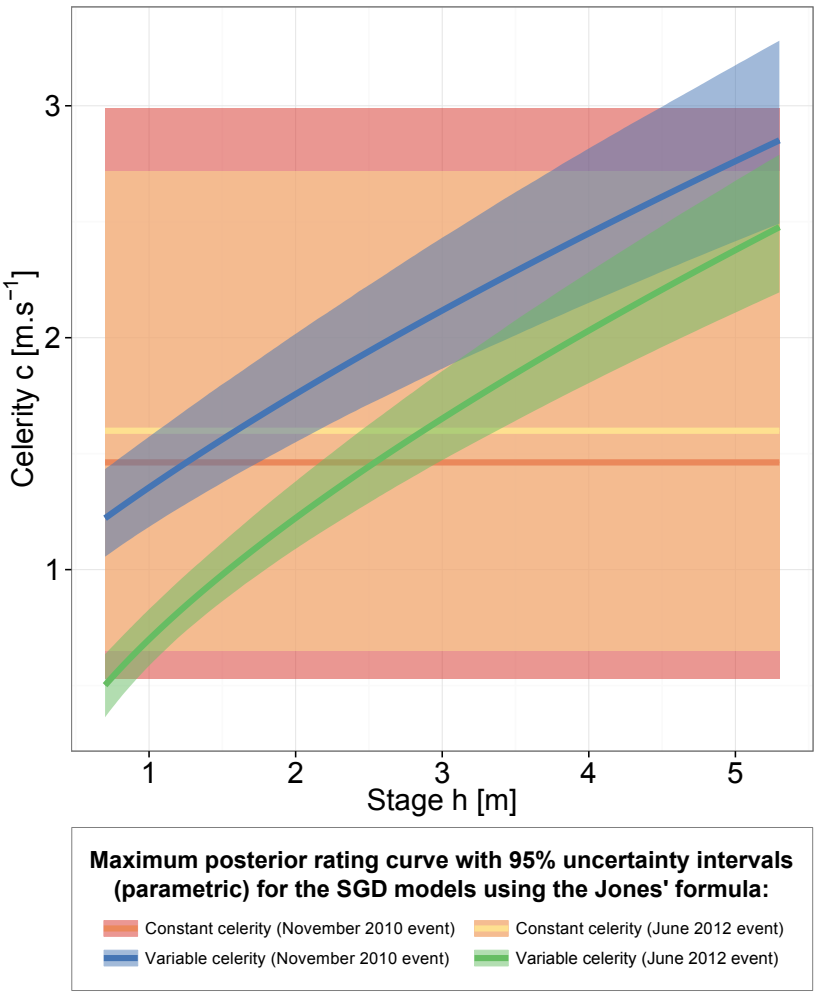

Figure 3.8 – The Ebro River at Ascó, events of November 2010 and June 2012: stage-celerity representations for the SGD models using the Jones' formula with constant celerity or variable celerity. The shift between the variable celerity curves is due to the observed rating changes between these two events

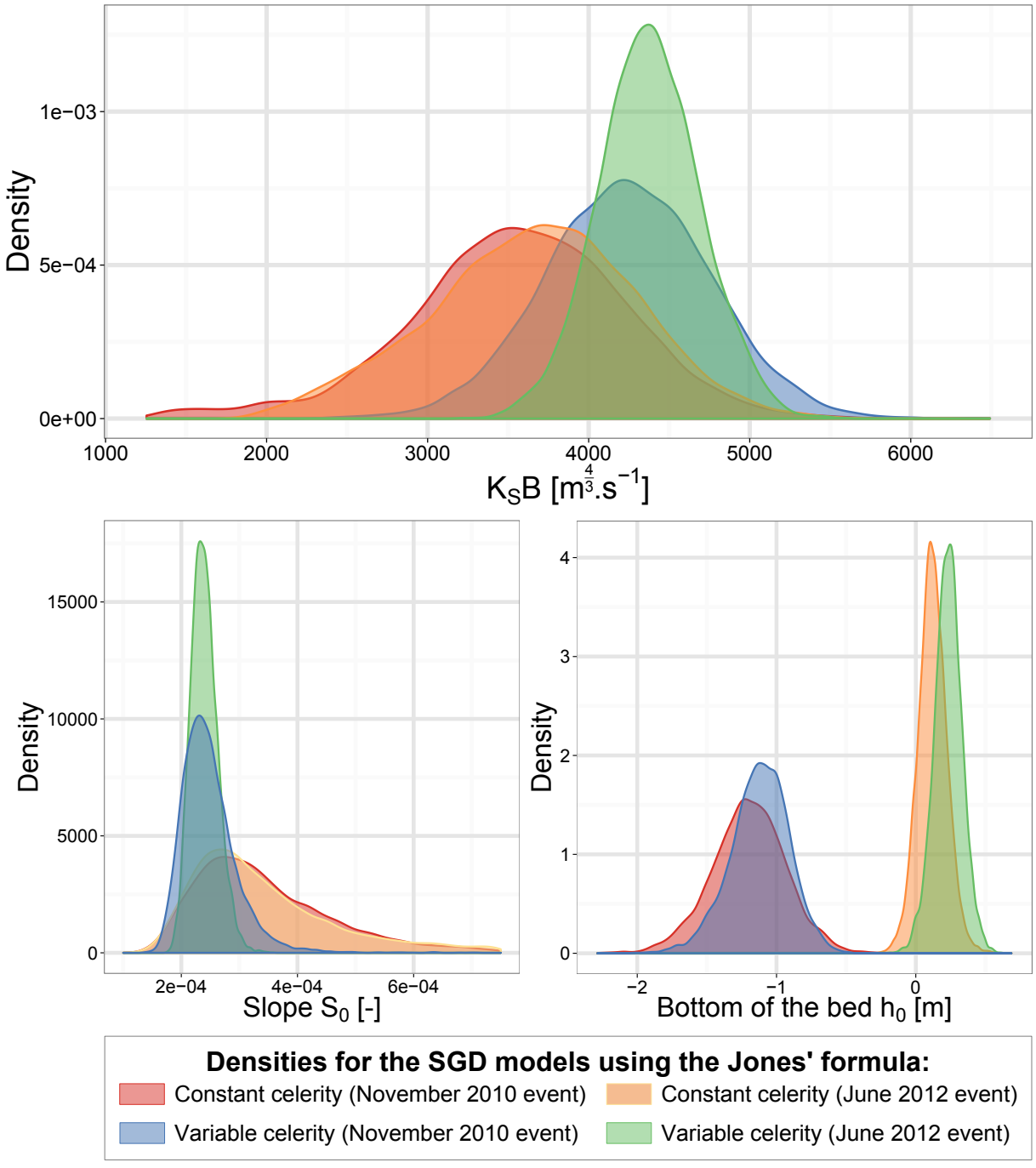

Figure 3.9 – The Ebro River at Ascó, events of November 2010 and June 2012: posterior densities of the product KB, the slope S_0 and h_0 for the SGD models using the Jones' formula with constant celerity or variable celerity.

For each event, the posterior densities of $K_S B$ and S_0 are more precise for the variable celerity option (see figure 3.9) and hence lead to less uncertainties on these parameters than for the constant celerity option. For h_0, a rating shift of approximately 1.5 meters between the two events can be observed.

Max. post. values		SGD model												SD model	
		Fenton third order				Fenton second order				Jones					
	Celerity option	Constant		Variable		Constant		Variable		Constant		Variable			
	Event	Nov.	June	Nov.	June	Nov.	June	Nov.	June	Nov.	June	Nov.	June	Nov.	June
Parameter	$K_S B\sqrt{S_0}$ [$m^{4/3}.s^{-1}$]	47.7	58.8	62.8	60.9	61.8	59.2	63.5	62.4	64.1	65.2	64.9	67.2	57.1	61.8
	$K_S B$ [$m^{4/3}.s^{-1}$]	3575	4336	3228	3404	3509	4391	3394	3497	3395	3768	4277	4355	Not identifiable	
	K_S [$m^{1/3}.s^{-1}$]	26.8	31.4	25.6	27.1	27.1	31.1	26.6	27.8	Not identifiable		32.4	32.4		
	h_0 [m]	-1.34	-0.094	-1.33	0.01	-1.27	-0.09	-1.24	0.061	-1.21	0.11	-1.10	0.23	-1.75	-0.06
	exponent M [−]	1.669	1.666	1.666	1.666	1.666	1.665	1.666	1.666	1.666	1.665	1.668	1.671	1.671	1.667
	B [m]	133.4	138.1	126.1	125.6	129.5	141.1	127.6	125.8	Not identifiable		134.1	134.4	Not identifiable	
	S_0 [‰]	0.178	0.185	0.378	0.32	0.31	0.182	0.35	0.318	0.359	0.299	0.233	0.238		
	c [$m.s^{-1}$]	2.72	3.27	Not identifiable		2.45	3.38	Not identifiable		1.46	1.60	Not identifiable			
	β [−]	0.97	0.96	0.98	0.98	Not identifiable									
	V [$m.s^{-1}$]	0.95	0.50	1.31	1.24										
	Error γ_1 [$m^3.s^{-1}$]	74.9	3.40	80.2	31.7	83.7	1.97	69.7	34.5	59.9	0.62	50.9	2.8	122	99.6
	Error γ_2 [−]	2.4 e-04	3.9e-02	5.8 e-04	8.3e-03	1.6 e-04	3.0e-02	9.4 e-04	2.1e-03	7.9 e-04	2.5e-03	1.2 e-04	8.7e-05	3.7 e-05	2.1e-03

Table 3.5 – The Ebro River at Ascó, events of November 2010 and June 2012: values of the maximum posterior estimator for each SGD model. Grey values are computed from other values.

The maximum posterior estimates of all models are hydraulically consistent (see table 3.5). For example, all the slopes S_0 have an order of magnitude of 10^{-4}. The rating shift between the two events is also observed with an overall difference of $1.30 - 1.40$m between h_0 values for a same model. The K_S, B and S_0 maximum posterior values are more stable between events for models with the variable celerity option than for models with constant celerity option. As an aside, for both events and both celerity options, posterior results of the Boussinesq coefficient β for the SGD models using Fenton formula of the third order are close to 1 which matches with the assumption of a uniform channel.

To conclude, SGD models using the Jones' formula lead to lower total and parametric uncertainties, and a better goodness-of-fit than higher order approximation using the Fenton formulas. All parameter estimates make physical sense. The two celerity options yield similar discharge estimates. However, the variable celerity option provides estimation of hydraulic parameters with lower uncertainties.

3.4.2. The gauging flume of Plymouth, North Carolina, USA

3.4.2.1. Data and models

The second case study uses a year of continuous discharge measurements in a calibrated cross-section equipped with a continuous Doppler velocimeter, near Plymouth, North Carolina, USA. This station captures many hysteresis events with very high temporal resolution (10 min) which can never be reached with conventional gaugings [Birgand et al., 2013].

The geometry of the station was forced into a trapezoidal flume with wooden boards. Figure 3.10-a illustrates the configuration of the station. A continous Doppler velocimeter is placed at the bottom of the flume.

The velocity index (ration between the cross-sectional average velocity and the velocity measured by the velocimeter) was precisely established using velocity-area gaugings (linear regression with $R^2 = 0.995$). Figure 3.10-b is a view from upstream of the station. In the absence of additional information, uncertainties of discharge measurements are estimated to be $\pm$ 10%.

This data set includes many flood events between August 1998 and July 1999. The first six flood events of 1999 (during January and February) exhibit hysteresis without rating shifts (figure 3.11). The fifth event of January 1999 presents a discontinuity in the stage-discharge

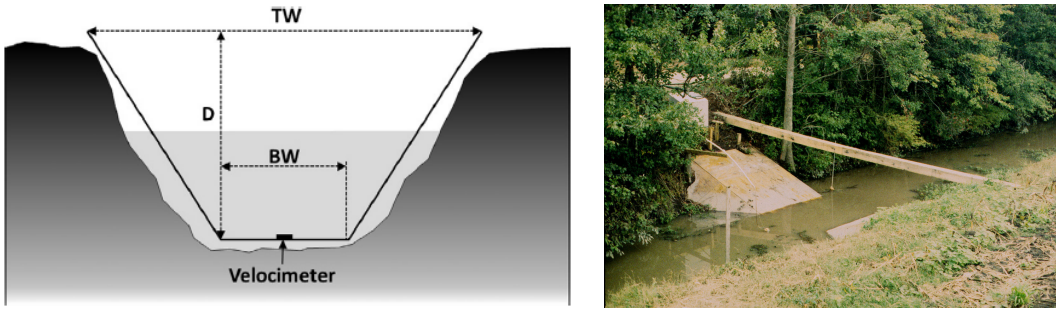

(a) (b)

Figure 3.10 – The A1 station, gauging flume near Plymouth: (a) configuration (TW: top width; D: depth; BW: bottom width) [taken from Birgand et al., 2013]; (b) photo of the hydrometric station (source François Birgand).

relation (see pink curve in figure 3.11, around $h \approx 0.8$ m). This discontinuity may be due to a farmer modifying the farmer intake to his field just upstream the station.

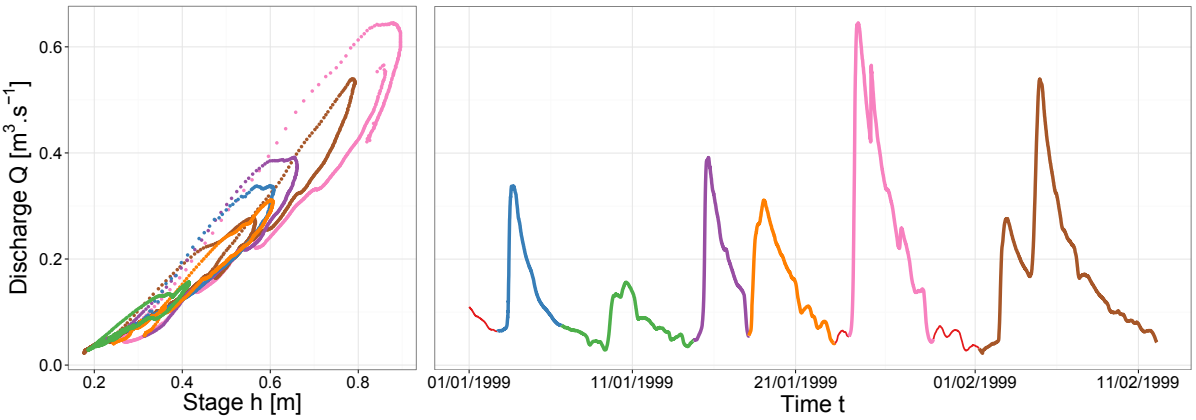

Figure 3.11 – Discharge records in the A1 gauging flume during 6 flood events in January and February 1999: stage-discharge and stage-time representations.

Figure 3.12-b shows that the stage gradient is affected by small fluctuations due to stage measurements errors. These fluctuations are a problem for establishing the SGD rating curve and the associated uncertainties because they are not related to the flood wave propagation and have a significant impact on posterior results (see figure 3.12-c). In order to fix this problem, a simple third order central moving average is used to smooth the stage gradient. For this case study, such pre-processing proved to be efficient to reduce the fluctuations of the rating curve and its uncertainty (see figures 3.12-c and 3.12-d). Other pre-processings can be used to smooth the stage gradient, e.g. spline regression [Petersen-Øverleir, 2006].

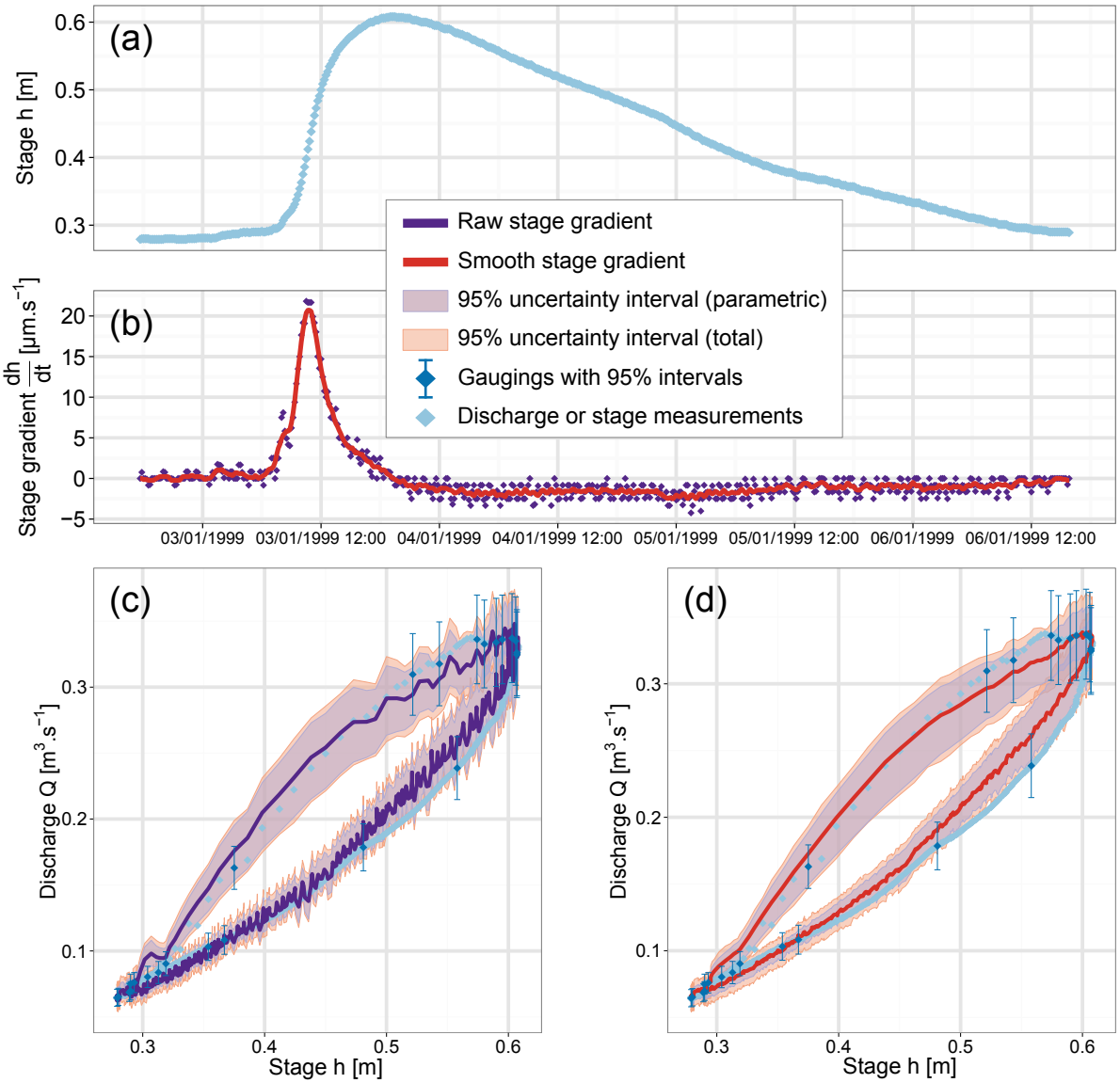

Figure 3.12 – First hysteresis event of January 1999 at the A1 station near Plymouth, impact of the stage gradient on rating curve uncertainty assessment: (a) stage records; (b) stage gradient records; posterior results (stage-discharge representation) of the SGD model using the Jones' formula with variable celerity for: (c) a raw stage gradient; (d) a smooth stage-gradient.

3.4.2.2. Prior specification

As the cross-section of the flume is trapezoidal, a trapezoidal cross-section is considered for this case study. Considering values in Chow [1959] for the Strickler coefficient K_S for old wooden boards, we set up a mean value of 62.5 $m^{1/3}.s^{-1}$ and a standard deviation of 10 $m^{1/3}.s^{-1}$.

Birgand et al. [2013] listed all the geometric variables m and b of the trapezoidal flume. Accordingly, prior distributions on the batter m of the bank and the width b of the riverbed are

precisely set to 2.6603 $\pm$ 0.02 and 0.55 m $\pm$ 0.02 m respectively. The slope S_0 is also supplied in this article but without information about its uncertainty, hence a large standard deviation. The slope S_0 is set to 0.0001 $\pm$ 0.001.

The prior distribution of the offset h_0 is also vague due to lake of information about its uncertainty. Prior distributions of the flood wave celerity c and the parameter V of SGD models using the Fenton formulas are vaguely set to 1 m.s^{-1} $\pm$ 1 m.s^{-1}. The prior distribution of the Boussinesq coefficient β is set to 1 $\pm$ 0.3 according to Chow [1959]. Two error parameters γ_1 and γ_2 are let to be identified by the gaugings, hence the flat uniform distribution. Corresponding priors are summarised in table 3.6.

Physical parameters	Units	Prior distributions
$K_S\sqrt{S_0}$	$[\mathrm{m}^{\frac{1}{3}}.\mathrm{s}^{-1}]$	$\mathcal{N}(0.625; 3.127)$
K_S	$[\mathrm{m}^{\frac{1}{3}}.\mathrm{s}^{-1}]$	$\mathcal{N}(62.5; 10)$
h_0	[m]	$\mathcal{N}(-0.05; 0.2)$
exponent M	$[-]$	$\mathcal{N}(0.6667; 0.01)$
b	[m]	$\mathcal{N}(0.55; 0.01)$
m	[m]	$\mathcal{N}(2.6603; 0.01)$
S_0	$[-]$	$\mathcal{N}(0.0001; 0.001)$
c	[m.s^{-1}]	$\mathcal{N}(1; 1)$
β	$[-]$	$\mathcal{N}(1; 0.15)$
V	[m.s^{-1}]	$\mathcal{N}(1; 1)$
Error γ_1	[m^3.s^{-1}]	$\mathcal{U}\left(0; 10^6\right)$
Error γ_2	$[-]$	$\mathcal{U}\left(0; 10^6\right)$

Table 3.6 – Prior distribution of the hydraulic variables for the A1 events. The symbol $\mathcal{N}(\mu; \sigma)$ corresponds to the normal distribution with mean μ and standard deviation σ. The symbol $\mathcal{U}(a; b)$ corresponds to the uniform distribution on the interval $[a, b]$.

3.4.2.3. Results

As the previous case study, the conventional SD model produces a time lag of around 40 minutes with respect to the discharge measurements (figure 3.13). Moreover the uncertainties are more than 3 times larger than with a SGD model. The SD model also overestimates the maximum discharge (4.4%) and the recession flow (by 8% on average). The rising limb is underestimated (by 4% on average).

As for the Ebro case study we compare the six stage-gradient-discharge (SGD) models. These comparisons are made using 24 gaugings from the first flood event of January 1999. These gaugings are sampled from the continuous (every 10 min) discharge measurements of the Doppler

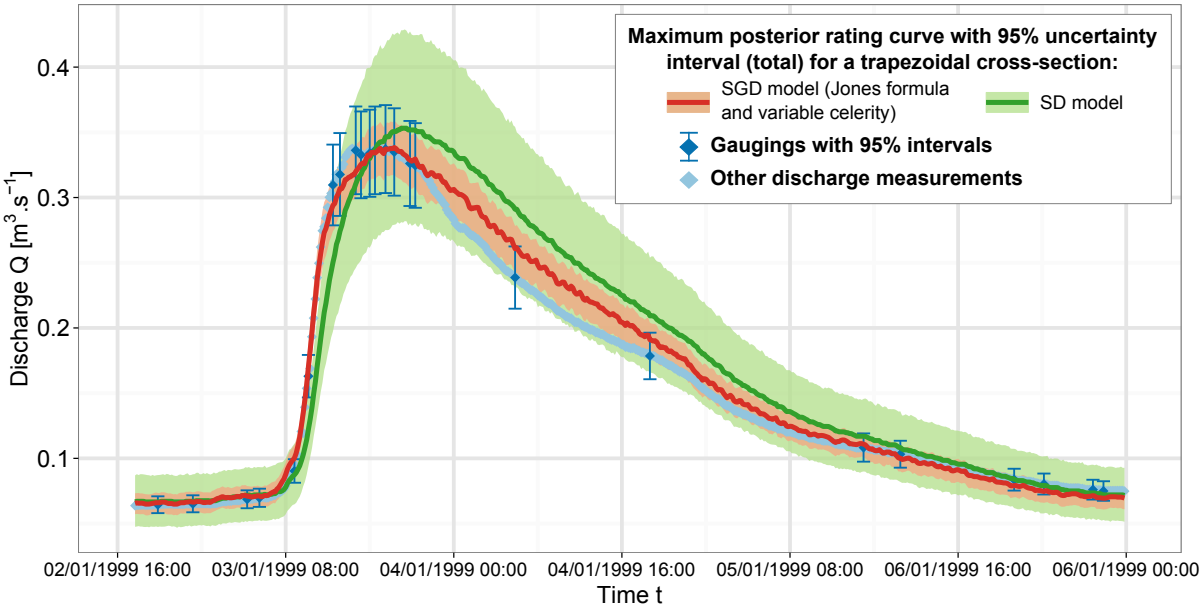

Figure 3.13 – Hydrograph of the first event of January 1999 at the A1 gauging flume near Plymouth: comparison between a stage-discharge (SD) model and the stage-gradient-discharge model using Jones' formula with variable celerity. For both models, a trapezoidal cross-section shape is used.

velocimeter. These measurements are split into 6 classes: both rising and falling limbs are equally divided in three intervals according to discharge values. On each class, 4 gaugings are sampled randomly. This sampling of discharge measurements is made to kept the dynamic of the flood (see gaugings in figure 3.13). Others discharge measurements are not used for calibration but for validation of the results.

Again, all the models detect the hysteresis effect correctly (figure 3.14). Indeed the rating curves are looped and follow the discharge observations; there is no time lag at the peak flow and deviations from discharge measurements are less than 15%. Moreover, there is not much difference between the total and parametric uncertainty intervals: the structural uncertainty is very small, which suggests that the models are suitable for modelling hysteresis. The uncertainties of the SGD models using the Fenton formulas are larger than the uncertainties of the two Jones models in the rising limb.

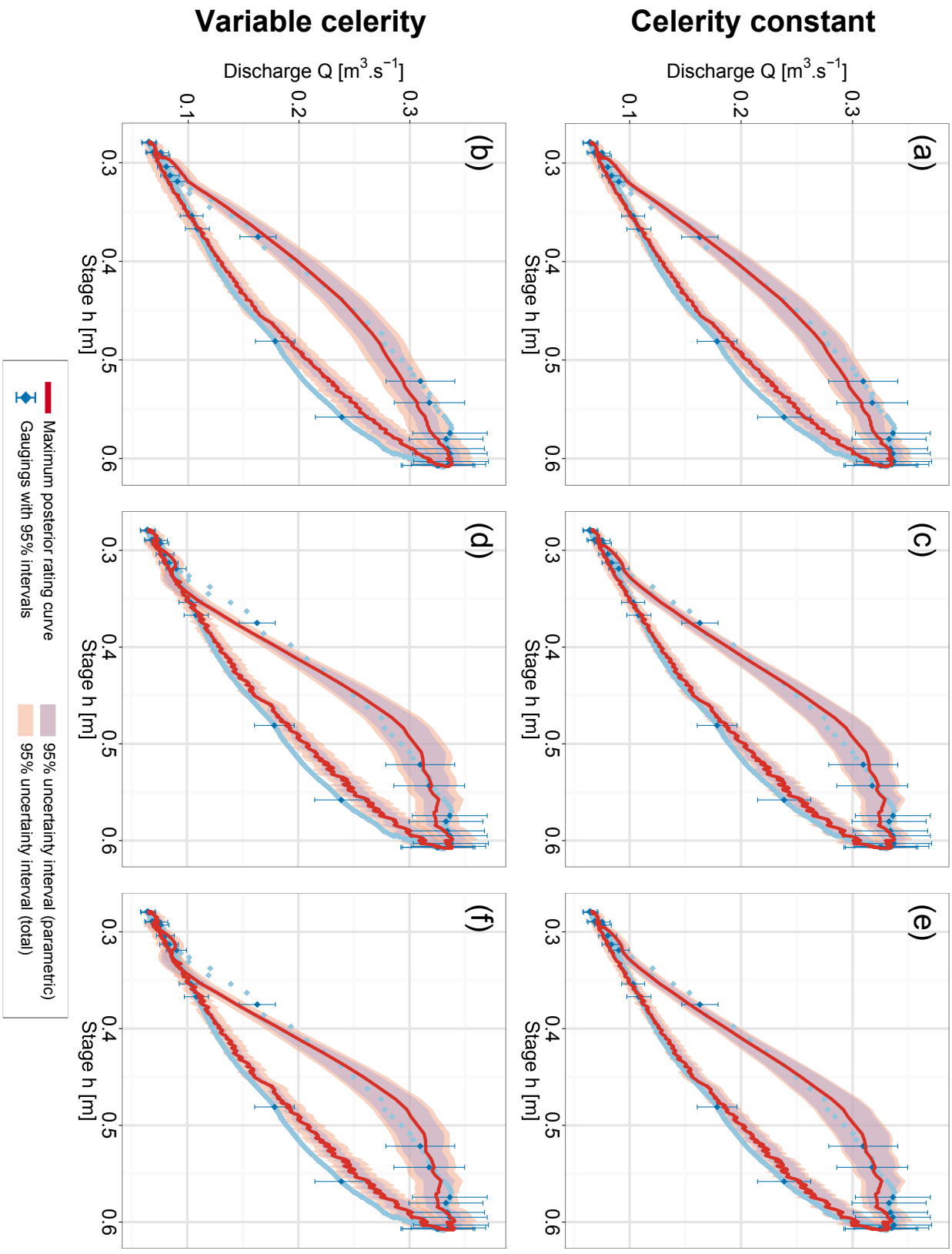

Figure 3.14 – The A1 gauging flume near Plymouth, **first hysteresis event of January 1999**: SGD rating curves using the Jones' formula (a and b), using the Fenton formula of second order (c and d) and using the Fenton formula of third order (e and f). For each formula, the flood wave celerity c is either constant or variable.

For SGD models using Jones' formula, posterior distributions are more precise when the celerity c is variable with stage h regardless of the stage value (see figure 3.15). Similarly, the posterior distribution of the parameters K_S and S_0 (figure 3.15) are more precise and parameters have less correlation between them. Moreover, when the celerity is constant, parameter K_S cannot be identified from the gaugings: its posterior distribution is the same than the prior distribution. This is due to the high correlations with parameters S_0 and c (correlation values of -0.91 and 0.86 respectively).

Therefore, we focus on the SGD model using the Jones' formula with variable flood wave celerity c for further evaluation of the SGD model.

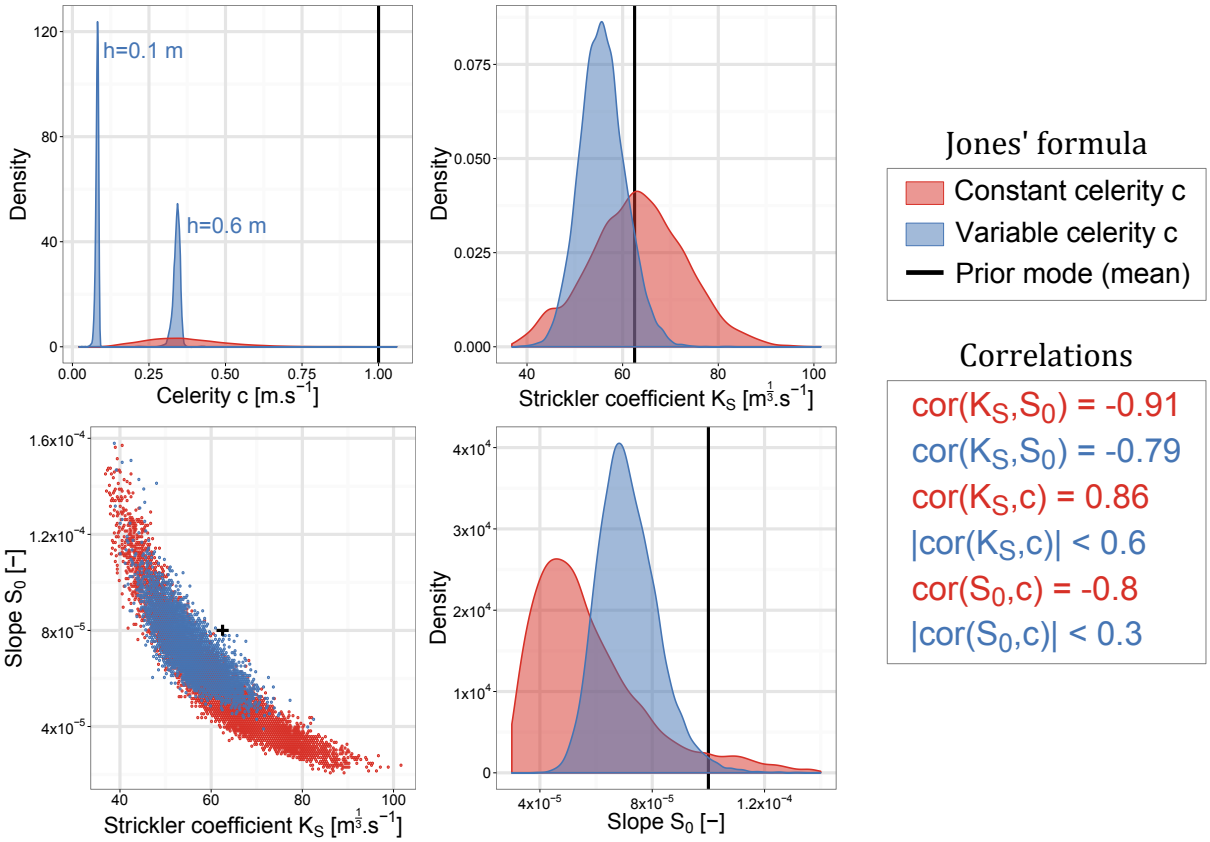

Figure 3.15 – Station A1 near Plymouth: first hysteresis event of January 1999, posterior densities of K_S and S_0 for the two SGD models using the Jones' formula with constant or variable celerity c, and scatterplot of K_S/S_0 posterior samples.

3.5. Evaluation of the stage-gradient-discharge (SGD) model

3.5.1. Importance of prior information

The event of June 2012 of the Ebro case is used to highlight the importance of prior information in the SGD rating curve estimation. We calibrate the SGD model (Jones' formula with variable celerity) using two distinct sets of priors: informative priors described in section 3.4.1.2 are compared with non-informative priors. Non-informative prior distributions of positive parameters K_S, B and S_0 is a wide positive uniform distribution $\mathcal{U}\left(0; 10^6\right)$. Prior distribution of the offset h_0 are wide uniform distributions $\mathcal{U}\left(-10^6; 10^6\right)$. Only the prior of the exponent parameter M is kept informative (see table 3.5) because this parameter is bound to the cross-sectional shape. Note that the use of non informative priors means that the estimation of rating curve parameters other than M is only based on the gaugings.

Figure 3.16 shows that more precise information on the hydraulic variables and hence on prior distributions brings better results on the rating curve estimation. Posterior rating curve results show the same goodness-of-fit for both sets of priors whereas the convergence of the MCMC algorithm is not satisfied for non-informative priors. In fact, with non-informative priors, the posterior distributions of K_S, S_0 and B are wide and these parameters show higher correlations to each other than if with informative priors. Moreover, with non-informative priors, rating curve estimations lead to physically inconsistent results. Indeed, parameter B (modelling the width) can be equal up to 400 m for Strickler coefficient of 8 $\mathrm{m}^{\frac{1}{3}}.\mathrm{s}^{-1}$ which does not match with the hydraulic configuration of the station ($B \approx 130$ m and $K_S \approx 30$ $\mathrm{m}^{\frac{1}{3}}.\mathrm{s}^{-1}$).

Therefore, informative priors appear to be necessary to estimate the parameters of the SGD model. In their absence, several parameters are not identifiable due to the strong interactions, leading to physically unrealistic values and poorly-behaved MCMC sampling.

3.5.2. Cross-validation between events

The A1 station case study allows cross-validation between several successive hysteretic flood events. We calibrate the SGD model using the Jones' formula with variable celerity c on the first event. Then we use the calibrated SGD model to predict other validation events. Thus we obtain event-specific rating curves with their associated uncertainties (figure 3.17). Relative

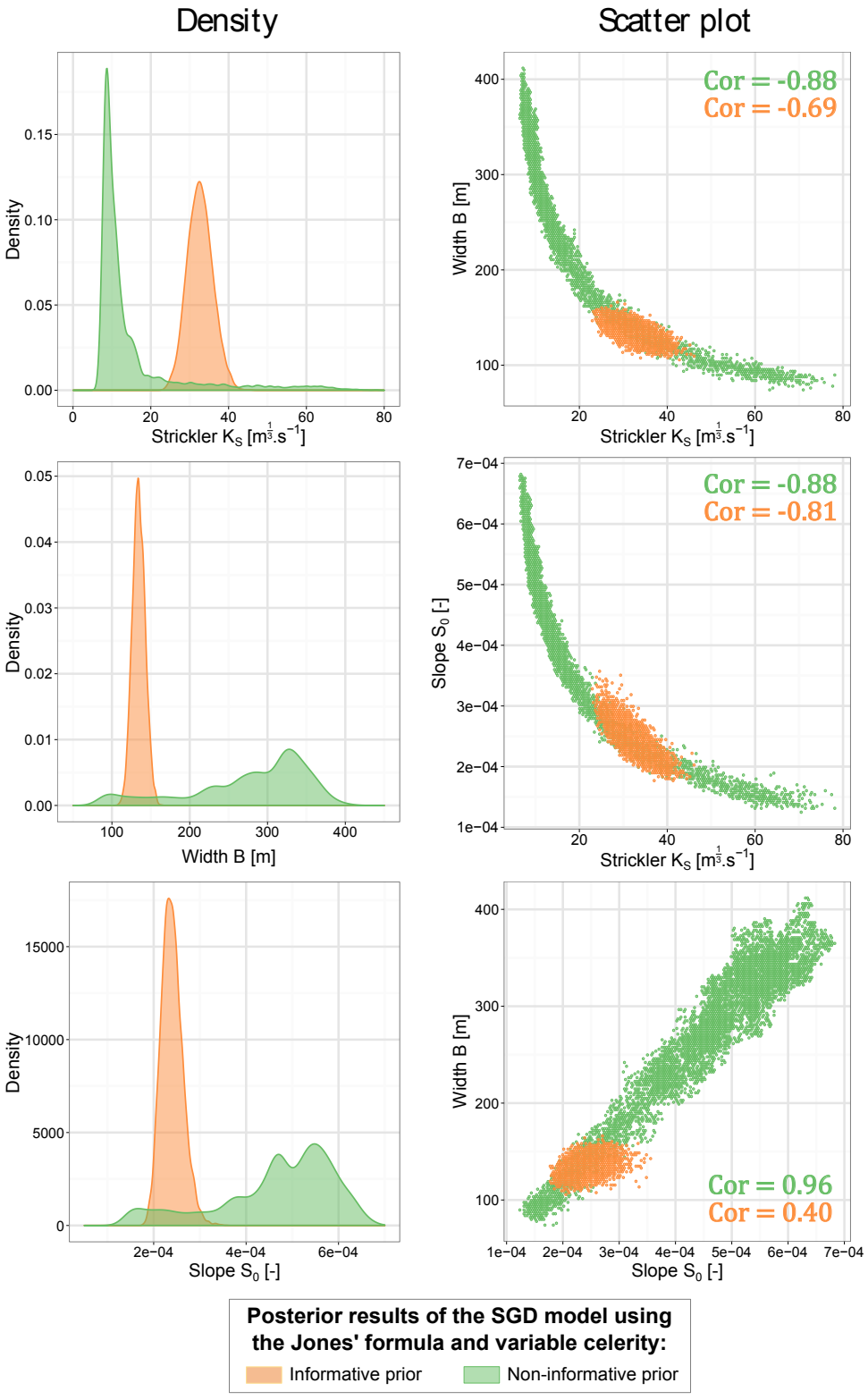

Figure 3.16 – The Ebro River at Ascó, event of June 2012: effect of the prior knowledge in the rating curve estimation, posterior densities and scatterplot of parameters K_S, S_0 and B from the SGD model using the Jones' formula with variable celerity.

errors between discharge observations and maximum posterior rating curves are always less than ± 10% except for the second event during the rising limb (underestimation of discharges by 15%). Moreover, for this second event, most validation points are outside of the total uncertainty interval during the rising limb. It is unclear at this stage whether this is due to an underestimation of the uncertainty in the SGD model, or the uncertainty in the validation points themselves, or both. Note that this second event is the smallest in terms of both stage and stage gradient.

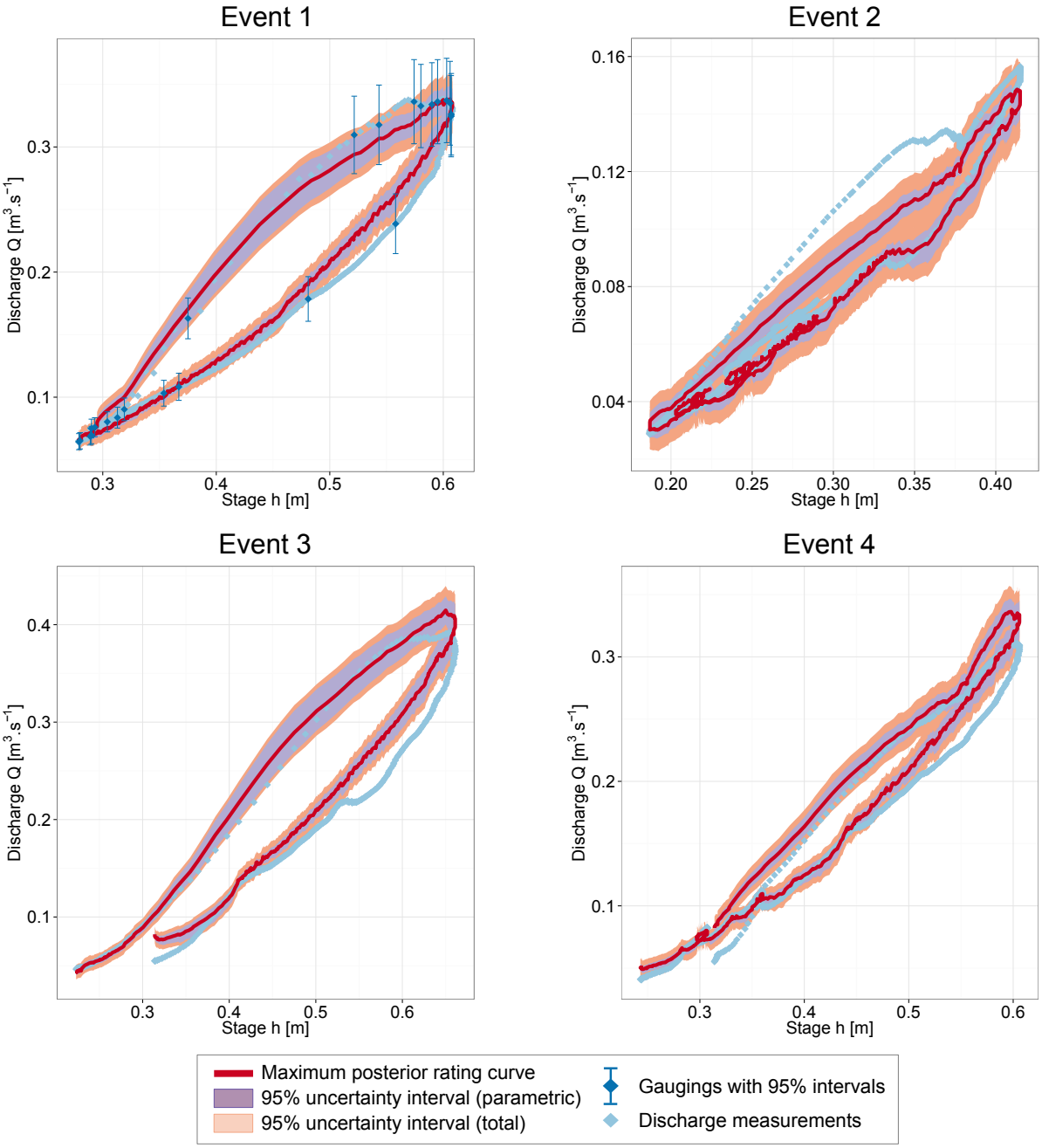

Figure 3.17 – Station A1 near Plymouth: rating curves of the first four hysteretic events of January 1999. The SGD model using the Jones' formula with variable celerity is calibrated on the first event only.

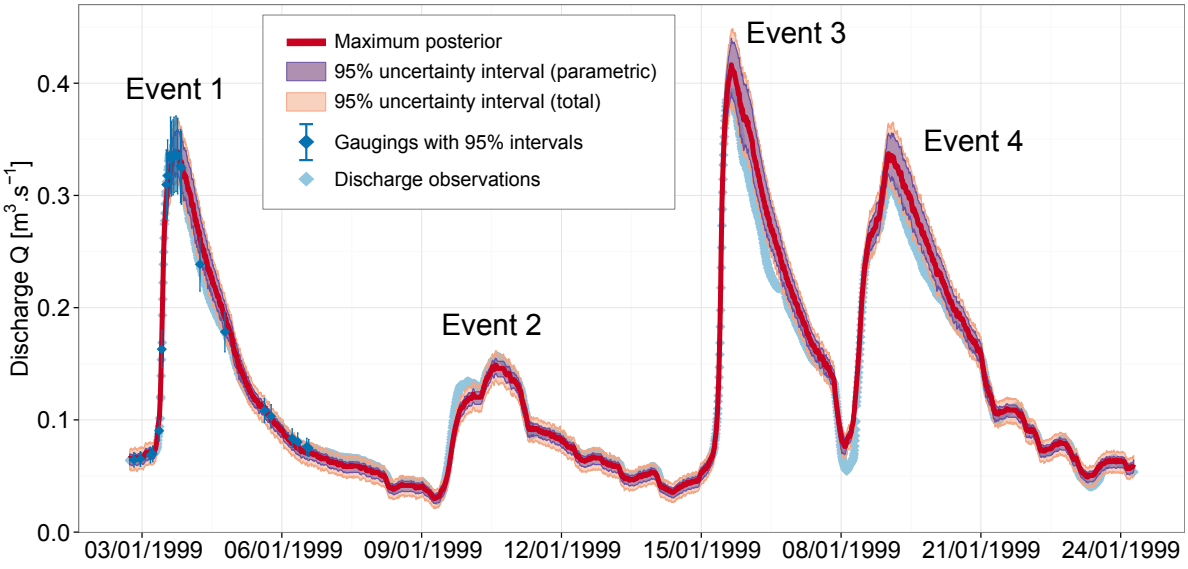

Figure 3.18 – Station A1 near Plymouth: hydrographs of the first four hysteresis event of January 1999. Use of the SGD model using the Jones' formula with variable flood wave celerity c calibrated with the first event.

The time-discharge representation (figure 3.18) illustrates the overall goodness-of-fit of the cross-validation on the first four events of January 1999. The maximum posterior estimator follows discharge observations acceptably and the associated uncertainties are small.

The cross-validation results of the fifth and sixth events (figure 3.19) are acceptable for low-flow discharges, and the dynamics of floods is well reproduced (no timing error). However, notable overestimations (over 30%) arise for peak flows. These two events are the largest and in particular, they are almost twice larger than the calibration event in terms of discharge. The discrepancy we observe is therefore probably an extrapolation problem. We made attempts at solving this problem by modifying the SGD model. In particular, we tested a model with a variable roughness to account for the fact that the properties of the controlling reach change for very high stages. Unfortunately, this modification did not solve the problem. Further investigations, including more precise topographic data and hydraulic modelling, are therefore needed to identify the cause of this over-estimation.

3.5.3. Comparison of gauging strategies

The common practice for gauging flood events is to measure during the recession, after the peak, to get less variable flows and safer operating conditions. It is also due to the difficulty to forecast the flood and the time needed to mobilise a gauging team and reach the station.

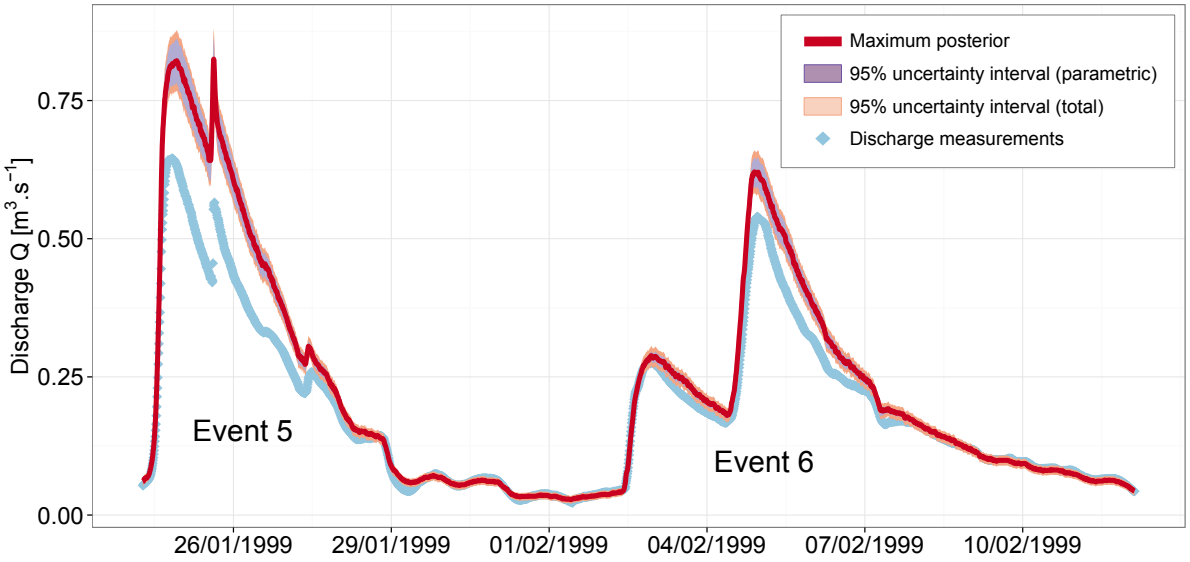

Figure 3.19 – Station A1 near Plymouth: hydrographs of the fifth and sixth hysteresis event of 1999. Use of the SGD model using the Jones' formula with variable flood wave celerity c calibrated on the first event.

The development of non-intrusive gauging techniques (e.g., hand held radars and image velocimetry) have recently made measurements during flood rise easier [e.g., Muste et al., 2011, Dramais et al., 2011, Westerberg et al., 2011]. Gauging during flood recessions only may have hindered stage-discharge hysteresis at some sites and may have given excessive confidence in steady stage-discharge rating curves.

In this section, we compare several possible gauging strategies, i.e. to gauge:

1) around a few remarkable points around the hysteresis loop (see below);

2) at the flood peak (between the maximum discharge and the maximum stage);

3) during the rising limb only;

4) during the falling limb only;

5) during the rising limb for high stages (just before the peak flow);

6) during the falling limb for high stages (just after the peak flow). It is the most common strategy;

7) at some remarkable points of the rising limb with low-flow gaugings.

The first six gauging strategies are shown in figure 3.20. The remarkable points characterize the loop of the rating curve and span over the whole range of stage and stage gradient. These

five remarkable points are defined as (A) the minimum of stage h, (B) the maximum of stage gradient $\frac{\partial h}{\partial t}$, (C) the maximum of discharge Q, (D) the maximum of stage and (E) the minimum of stage gradient (see figure 3.20).

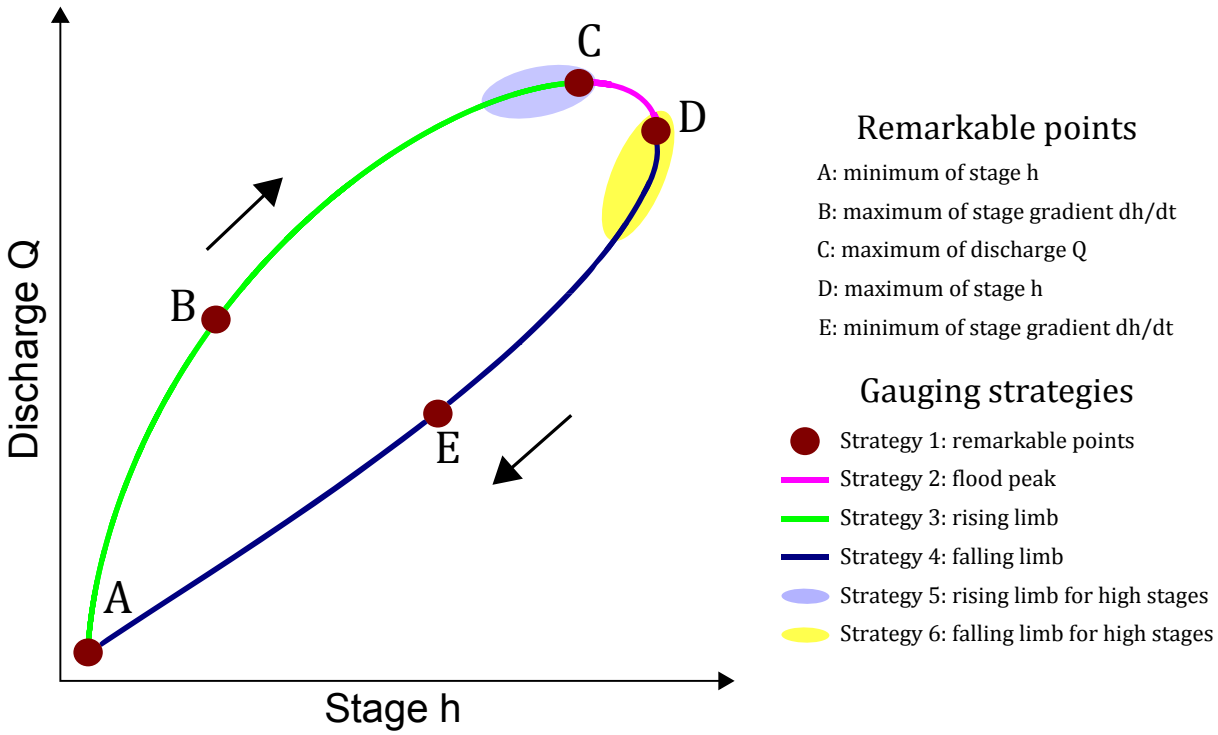

Figure 3.20 – Definition of the 5 remarkable points of the stage-discharge hysteresis loop and of 6 gauging strategies.

In order to match with usual operational constraints, the comparison is made under some realistic assumptions. Cross-validation is performed for each strategy using only 15 gaugings spread over the first four events of 1999 to calibrate the most successful SGD model, i.e. the SGD model using the Jones' formula with variable celerity c. As an illustration, figure 3.21 shows the calibration gaugings for strategies 1 and 7.

Results show that several gaugings strategies are not mathematically and/or physically suitable for modelling hysteresis events with the SGD model.

A strategy is not mathematically suitable when the term under the square root (see equation (3.9)) modelling the energy slope is negative, which may occur for negative stage gradients. The problem arises when the whole range of the stage gradient is not covered during the rating curve calibration. Then the possible variations of the stage gradient may be underestimated and, out of the range of calibrated stage gradients, the cross-validation may no longer be possible. For example, with only small positive stage gradients, as provided by the second and fifth gauging strategies, cross-validation for high negative values of the stage gradient (around the

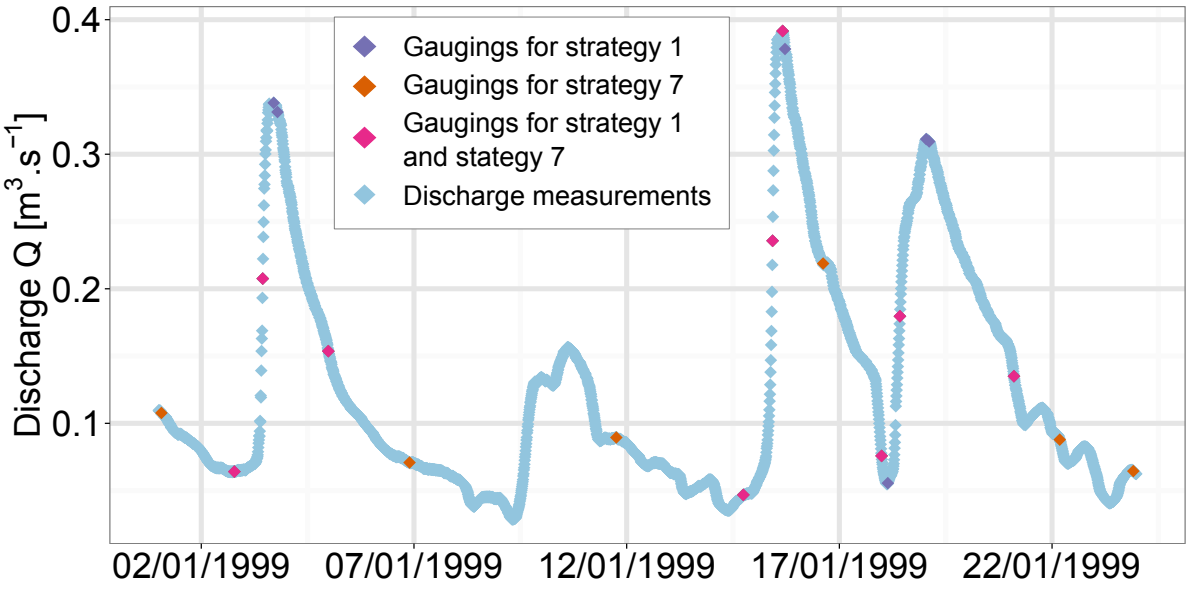

Figure 3.21 – Station A1 near Plymouth, Januray 1999: time-discharge representation. Gaugings used for the first and seventh gauging strategies are represented.

fifth remarkable point) may be impossible. The sixth gauging strategy provides negative stage gradients but no high absolute values: the cross-validation does not work for high negative stage gradients.

A strategy is not physically suitable when hysteresis is not detected: the loop is not wide enough or not open at all. The third gauging strategy, i.e. gauging during the rising limb only, yields flat loops with huge uncertainties.

Figure 3.22 shows the performances of the best three gauging strategies in terms of uncertainties (total and parametric in percentage) at the remarkable points during a single event. Only the first event of January is shown but results from other events are similar. For each strategy, the rating curve is displayed.

We can first notice that all gauging strategies allows cross-validation on those events. Moreover all rating curves are wide open: hysteresis is detected.

The first gauging strategy has the largest uncertainties for low discharges. The structural uncertainty dominates in the total uncertainty. Although the calibration of rating curves is made on the extremes of the input data (stage and stage gradient), the uncertainty is not reduced efficiently between these extremes.

The fourth gauging strategy has very small uncertainties during the falling limb but in the rising limb the parametric uncertainty values are more than twice larger than for the other two gauging strategies. With this gauging strategy, all the stage gradients of the gaugings are

negative: the slope S_0 is calibrated with these high negative values, whereas in the rising limb, the stage gradients are positive and higher in absolute value (up to four times larger). Moreover, the rating curve parameters are poorly estimated.

The seventh gauging strategy yields the best results. Total uncertainties are small, especially the structural uncertainty for both rising and falling limbs. The parametric uncertainties are constant in percentage during the whole event: the parameters are well-calibrated all over the flood. It seems that combining gaugings at remarkable points with gaugings from the falling limb and/or low flows provides the best information

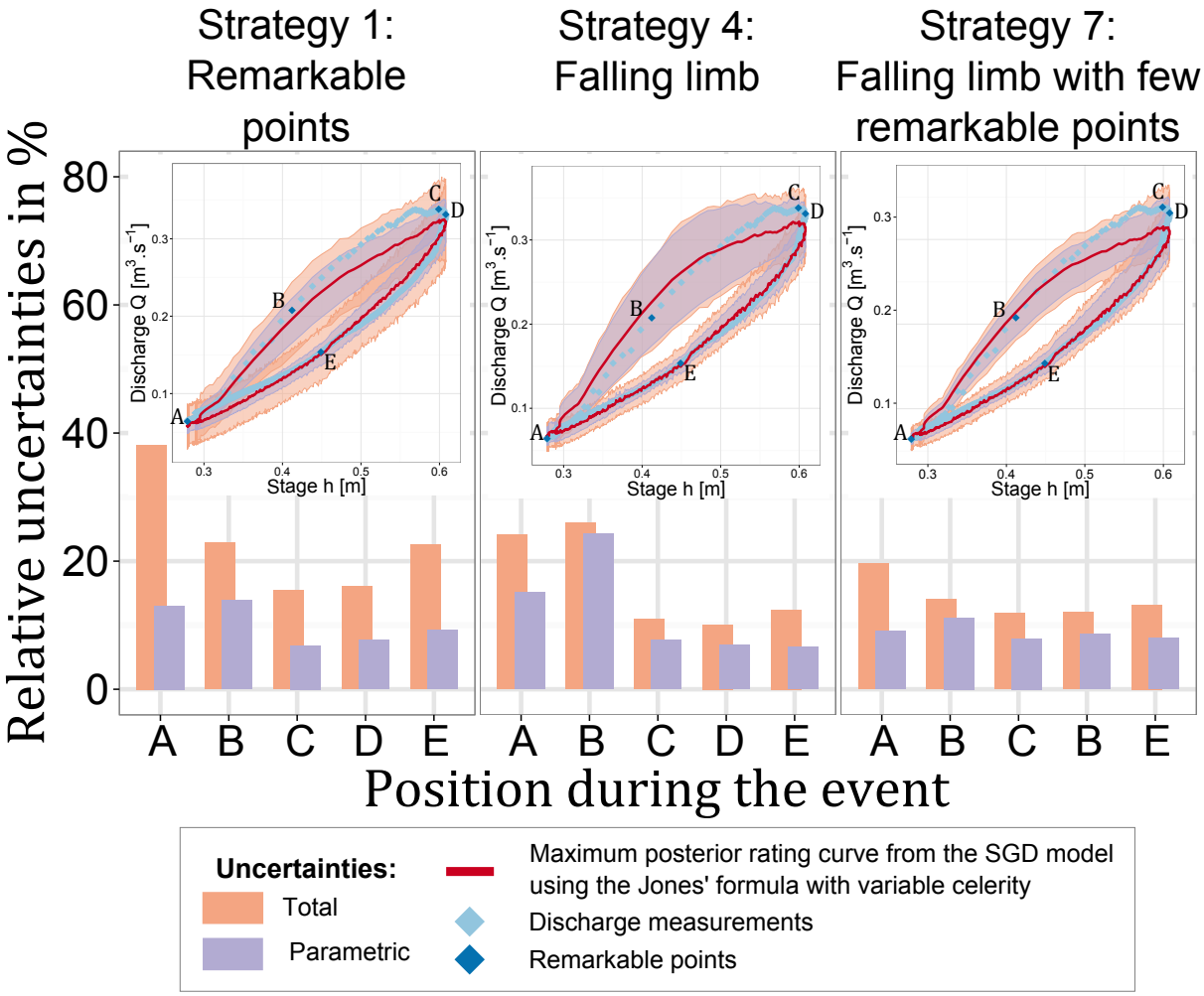

Figure 3.22 – Station A1 near Plymouth: relative uncertainty results of gauging strategies 1, 4 and 7 with associated stage-discharge representations.

3.6. Conclusions and perspectives

3.6.1. Summary

This chapter proposes a stage-gradient-discharge (SGD) model to describe hysteretic rating curves, based on several hysteresis formulas of the literature. The SGD model needs two variables as inputs: the stage and the stage gradient. The second input can be computed from the first when a stage time series is provided but can show strong fluctuations that are not related to flood wave propagation but rather to stage measurement errors, which requires smoothing the stage gradient.

The proposed method uses Bayesian analysis. An expertise of the hydrometric station is needed to set up prior distributions on hydraulic variables. As results, it provides a rating curve with a total uncertainty envelope. This total uncertainty can be split into parametric uncertainty (uncertainty on the rating curve parameters) and structural uncertainty (linked to the imperfection of the rating curve model). This method also provides a direct estimation of the physical parameters of the rating curve: results can therefore be criticised based on their physical meaning.

Two sites with hysteretic stage-discharge relations were presented: dam flushes in a natural lowland stream (the Ebro River) and a series of floods in a gauging flume equipped with a continuous Dopler flowmeter. Other sites with and without hysteresis were also tested (see appendix A). These case studies highlight the importance of taking into account the hysteresis effect when it occurs. Contrary to a conventional stage-discharge model, the time lag between estimated discharges and discharge measurements no longer exists with a stage-gradient-discharge (SGD) model and the maximum of discharge is no longer underestimated. The SGD model also reduces uncertainties on discharge estimations; these uncertainties differ on the rising limb and on the falling limb.

Many hydraulic formulas for modelling stage-discharge hysteresis exist in the literature. The simple Jones' formula, a correction of the riverbed slope based on kinematic wave assumption, is the oldest and most well-known formula. Our results suggest that it provides a remarkable goodness-of-fit with discharge observations and small uncertainties. It leads to as good results as the more complex Fenton formulas. Moreover, modelling the flood wave celerity as a function of stage rather than a constant yields less uncertain estimations on the rating curve parameters.

Prior information is of particular importance for SGD models: in its absence, several parameters show very strong interactions, which may lead to physically unrealistic parameter values (despite a perfectly acceptable goodness-of-fit of the rating curve). Specifying realistic orders of magnitudes for such parameters prior to the inference is sufficient to strongly restrict these interactions.

In the absence of rating changes, the SGD model calibrated during a specific event can be applied to subsequent events with acceptable accuracy as long as extrapolation remains limited. We encountered some problems for highly extrapolated values (see section 3.5.2) whose cause could not be identified precisely.

Finally, an analysis of the best gauging strategy demonstrates that for a hysteretic flow event, the most common gauging strategy, i.e. to gauge during the falling limb after the peak flow, yields high uncertainties in the rising limb and a biased identification of the hysteresis magnitude. The best gauging strategy is to gauge near a few remarkable points of the flood wave (minimum and maximum of the stage, maximum of discharge, minimum and maximum of the stage gradient), and during the falling limb (to properly explore negative stage gradients). These gaugings can be spread over conducted during distinct flood events.

3.6.2. Discussion

3.6.2.1. Hysteresis formulas

Several assumptions have been made for deriving the SGD models. Some of them are conventional assumptions of the literature but other are more disputable.

The kinematic wave hypothesis (equation (3.6)) allows avoiding some constraints linked to the pressure term $\frac{\partial h}{\partial x}$. Combined with the continuity equation (equation (3.7)), this variable is no longer used: it is replaced with the stage gradient and the celerity c. A possible future work is to ensure the validity of this assumption by comparing SGD rating curve results with rating curve results from stage-fall-discharge (SFD) models. For that purpose, several stage measurements along the river are necessary to measure the fall. The challenge is therefore to find twin-gauge stations affected by hysteresis. This work would also allow verifying the relevance of the diffusion wave assumption by estimating the inertia term and comparing it to the pressure term and the slope of the bed S_0. Application of a one-dimensional hydraulic model would also be useful to verify these assumptions.

The variable G in the third order Fenton formula (equation (3.12)) uses the velocity V. This variable was modelled as a constant but this modelling is controversial and can be questioned: as the stage increases, this velocity, directly linked to the wetted area and thus to the stage, should increase. Therefore, the results for this method are probably influenced by this assumption. The use of a varying velocity $V = c - \frac{Q_0}{A}$ should be tested.

The assumption $D = Q_0/(2BS_0)$ from the advection-diffusion theory (see equation (3.12)) should also be verified by using the complete formula of D described by Fenton [1999]:

$$D = \frac{Q_0}{2gAS_0}\left[g\frac{A}{B} - \beta V^2 + (\beta - 1)c^2\right]$$

For steady flow, with the Manning-Strickler equation, the flood wave celerity c is linked to the cross-sectional average water velocity U by a constant coefficient $k_c = 5/3$, in case of a wide rectangular cross-sectional shape:

$$c = k_c U$$

Lighthill and Whitham [1955] already pointed out that this kinematic wave celerity c cannot be directly associated with the average velocity U by using a constant coefficient k_c when the energy slope J differs from the slope S_0 of the bed. The coefficient can have the same variation than the energy slope J: larger in the rising limb than in the falling limb. A model allowing this coefficient k_c to vary with stage may bring a better understanding of the link between celerity c and average velocity U for these events. Therefore, this modelling could be compared with the variable celerity c option.

With continuous discharge measurements, like in the station A1 near Plymouth, the computation of the celerity c is directly possible from the definition $c = \frac{\partial Q}{\partial A}$ without using equation (3.10). This computation could be compared with the variable celerity option.

Studied events in the Ebro river are dam flushes. These flushes are made to remove vegetation in the river. Thus, modelling a constant roughness during the event is disputable: discharges at the beginning of the rising limb can be higher than rating curve estimations (see event of November 2010, figure 3.6) due to the change of the average roughness of the river. Modelling a variable roughness, from the vegetation roughness to the natural roughness of the bed without vegetation, could be trialled. A variable roughness model was also tested with the station A1 near Plymouth where the cross-section is calibrated with wooden boards. For very high stages, the boards are not long enough to cover the whole controlling reach. However this variable roughness model did not substantially improve the performance of the SGD model.

3.6.2.2. SGD rating curve estimation

All models are parameterised in order to provide a physical meaning for each parameter: this parameterisation is not always optimised, i.e. the number of parameters can be reduced. For example, the SGD model using the Jones' formula with variable celerity can have only 4 parameters instead of 5 (current configuration) using the following parameterisation:

$$\text{Current parameterisation} \begin{cases} Q(h) = K_S B (h-h_0)^M \sqrt{S_0 + \dfrac{1}{M K_S \sqrt{S_0}\,(h-h_0)^{M-1}} \dfrac{\partial h}{\partial t}} \\ Q(h) = \theta_1 \theta_4 (h-\theta_2)^{\theta_3} \sqrt{\theta_5 + \dfrac{1}{\theta_3 \theta_1 \sqrt{\theta_5}\,(h-\theta_2)^{\theta_3-1}} \dfrac{\partial h}{\partial t}} \end{cases}$$

$$\text{Alternative parameterisation} \begin{cases} Q(h) = K_S B \sqrt{S_0} (h-h_0)^M \sqrt{1 + \dfrac{1}{M K_S S_0^{3/2}\,(h-h_0)^{M-1}} \dfrac{\partial h}{\partial t}} \\ Q(h) = \theta_1 (h-\theta_2)^{\theta_3} \sqrt{1 + \dfrac{1}{\theta_3 \theta_4\,(h-\theta_2)^{\theta_3-1}} \dfrac{\partial h}{\partial t}} \end{cases}$$

The current parameterisation of this chapter has the advantage of linking each parameter θ to a unique hydraulic parameter, which makes interpretations easier. The alternative parameterisation saves one parameter, but is more difficult to interpret: for instance, θ_1 represents $K_S B \sqrt{S_0}$ and θ_4 represents $K_S S_0^{3/2}$. A comparison between 'natural' parameterisations and 'optimal' (in terms of parameter number) parameterisations would be valuable.

A future work would be to analyse the effect of input data uncertainty (stage and stage gradient) on the rating curve calibration. Indeed, stage measurement uncertainties are ignored as well as uncertainties of stage gradients. However, both types of uncertainties may have a strong effect on the quality of the rating curve and the related uncertainty intervals. The stage gradient is directly derived from the stage time series in which uncertainties exist. These uncertainties may impact stage gradient values and may degrade the rating curve estimation.

3.6.2.3. Operational perspectives

We observed that when there is no hysteresis effect, the SGD model using the Jones' formula with variable celerity does not detect it (see the Ardèche River at Sauze in appendix A). An

interesting application would be to apply the method to a station for which flood events are not always affected by hysteresis. This would allow carrying out the following experiments:

- a calibration of the rating curve on hysteretic events and a cross-validation on other events, whether or not they are hysteretic events. If hysteresis is only detected for hysteretic events, it would demonstrate the versatility of the model;
- a calibration of the rating curve on steady events and also a cross-validation on others. If hysteresis is detected only for hysteretic events, it would suggest the SGD model using the Jones' formula with variable celerity can be applied for all events;
- a comparison of input data between steady events and hysteretic events. It would allow identifying possible signatures and criteria on these signatures for detecting hysteresis effect from input records and assessing the significance of this hysteresis effect.

In an operational context, hydrometric stations being potentially affected by hysteresis could be identified. This analysis could be done at a national scale (France for example). Indeed, when hysteresis effect is present, the stage-gradient-discharge relation can be seen as a correction of the stage-discharge relation (see Sauze station in appendix A). The corrective term only depends on the slope S_0 of the riverbed, the average width B of the river at the station, the stage gradient $\frac{\partial h}{\partial t}$ and the gradient $\frac{\partial Q_0}{\partial h}$ of the steady rating curve. A rough estimate of this terms can be obtained at most hydrometric stations. If the corresponding correction strongly differs from 1, it would suggest that the station has the potential to be affected by hysteresis.

Chapter 4

Variable backwater and twin-gauge stations

This chapter has been published in *Water Resources Research* [Mansanarez et al., 2016b]. Variable backwater and twin gauge station has also been presented at the *European Geosciences Union General Assembly 2016* (PICO communication, Mansanarez et al., 2016a) and at the RiverFlow 2016 Conference [Le Coz et al., 2016b].

Contents

4.1. Introduction

Most of the streamflow records are established at water level monitoring stations using stage-discharge functions. Actually, such simple 'rating curves' are valid if the stage-discharge relation is governed by either a section control (upstream of a critical flow section) or a channel control with constant energy slope. Under those assumptions, hydraulics formulas for section controls and for channel controls with wide rectangular cross-section can be expressed as simple power functions as follows [WMO No. 1044, 2010, ISO 1100-2:2010, 2010]:

$$Q(h) = a\,(h-b)^c \tag{4.1}$$

where Q is the discharge, h is the stage, a is a coefficient related to the characteristics of the controlling section or channel, b is an offset, and c is an exponent related to the type of hydraulic control [e.g., Le Coz et al., 2014].

The ideal situation of a channel control is that of a uniform flow when the energy slope is parallel to the water surface slope and to the bed slope. In some cases the energy slope varies over time, generally due to a variable downstream boundary condition (or 'variable backwater'), or sometimes due to transient flow conditions ('varying discharge'). Comprehensive reviews can be found in Schmidt [2002] and Petersen-Øverleir and Reitan [2009a].

The importance of managing hydrometric stations affected by a variable slope has been recognised in hydrometry guidance and standards for long [e.g., Hall et al., 1914, Réméniéras, 1949, Rantz, 1982b, ISO 9123:2001, 2001, WMO No. 1044, 2010]. When energy slope is affected by transient flow effects, the resulting stage-discharge hysteresis can be approximated by single-gauge methods [e.g., Jones, 1915, Fenton and Keller, 2001]. Index velocity systems [e.g., Le Coz et al., 2008, Nihei and Kimizu, 2008, Hoitink et al., 2009, Hidayat et al., 2011, Levesque and Oberg, 2012] have been developed and increasingly used for streams affected by variable backwater. However the traditional stage-fall-discharge (SFD) method remains commonly used in such situations. The SFD method requires to measure the fall, hence the water surface slope between the main gauge and an auxiliary gauge usually located further downstream along the same river reach. As long as the flow depth variation along the reach remains limited, the flow is said to be 'gradually varied' and usual friction formulas (Darcy-Weisbach, Manning-Strickler, Chézy) designed for uniform flows can still be applied. According to these friction formulas, discharge is proportional to the square root of the energy slope. Therefore, the real discharge Q

can be derived from the fall ratio to a power N, close to 1/2, as:

$$Q = Q_r \left(\frac{F}{F_r} \right)^N \tag{4.2}$$

with Q_r the discharge computed from stage-discharge rating curve established for reference conditions, F the measured fall and F_r the fall established for reference conditions. The reference conditions are the usual flow regime not affected by variable backwater.

Though this method is not fully hydraulically accurate [Schmidt, 2002], it proved to be convenient and often produced acceptable discharge estimates at hydrometric stations with variable slope [ISO 9123:2001, 2001]. Valuable streamflow records are based on this technique in canals and rivers affected by the water level of lakes, seas, dams or main stems located further downstream [e.g., Callède et al., 2001]. Nevertheless, it is still needed to develop practical and rigorous methods for establishing such stage-fall-discharge models and for conducting the uncertainty analysis of the resulting discharge records.

To bring new solutions to this problem, this work builds on the avenue opened by Petersen-Øverleir and Reitan [2009a]. The Bayesian approach they introduced appears to be a promising way to analyse stage-fall-discharge relations and the related uncertainties. Like other Bayesian methods applied to stage-discharge relations [e.g., Moyeed and Clarke, 2005, Reitan and Petersen-Øverleir, 2008, Sikorska et al., 2013, Juston et al., 2014, Le Coz et al., 2014] it provides a flexible framework for incorporating prior information on control segmentation and hydraulic extrapolation beyond the largest gauged flows. Other non-Bayesian statistical methods have also been applied to stage-discharge relations [e.g., Shrestha et al., 2007, McMillan et al., 2010, Westerberg et al., 2011, Morlot et al., 2014, Coxon et al., 2015, McMillan and Westerberg, 2015], and might be adapted to the case of SFD relations.

Compared to the original work of Petersen-Øverleir and Reitan [2009a], we propose a different stage-fall-discharge model. Petersen-Øverleir and Reitan [2009a] considered the frequent situation when a gauging station is not permanently affected by variable backwater, which requires a two-segment rating curve and a discharge continuity condition:

$$Q\left(h_1, h_2\right) = \begin{cases} C_1 (h_1 - h_0)^{b_1} & \text{if } \; h_2 \leq h_0 \quad \text{backwater unaffected} \\ C_1 (h_1 - h_2)^{\eta} (h_1 - h_0)^{b_1 - \eta} & \text{if } \; h_2 > h_0 \quad \text{backwater affected} \end{cases} \tag{4.3}$$

where η is a parameter and C_1 and b_1 are hydraulic quantities according to Petersen-Øverleir and Reitan [2009a] model. Some assumptions of this model are disputable. The first concern is the

assumption that the 'cease-to-flow' stage, or offset h_0, would be the same for the two controls. A second concern is the statement that the transition to backwater-affected regime occurs when the downstream stage h_2 is greater than h_0. In this paper, both assumptions will be shown to be disputable from a hydraulic point of view, and models based on different assumptions will be introduced. Moreover, considering the common case of wide and rectangular channel controls, the Manning-Strickler friction formula leads to:

$$Q\left(h_1, h_2\right) = \begin{cases} BK_S\sqrt{S_0}\ \left(h_1 - h_0\right)^{5/3} & \text{backwater unaffected} \\ BK_S\sqrt{(h_1 - h_2)/L}\ \left(h_1 - h_0\right)^{5/3} & \text{backwater affected} \end{cases} \tag{4.4}$$

where B is the channel width, K_S is the Strickler flow resistance coefficient, S_0 is the river bed slope and L the distance between the twin gauges. Matching equations (4.3) and (4.4) yields:

$$\begin{cases} C_1 = BK_S\sqrt{S_0} & [\mathrm{m}^{4/3}.\mathrm{s}^{-1}] \text{ and } b_1 = 5/3 & \text{backwater unaffected} \\ C_1 = BK_SL^{-1/2} & [\mathrm{m}^{5/6}.\mathrm{s}^{-1}],\ \eta = 1/2 \text{ and } b_1 = 13/6 & \text{backwater affected} \end{cases} \tag{4.5}$$

with non-consistent values of C_1 and b_1 parameters on the two components of the rating curve model.

In the case where the backwater-unaffected control is no longer a wide rectangular channel but a critical cross-section represented as a horizontal crested weir, equation (4.4) becomes:

$$Q\left(h_1, h_2\right) = \begin{cases} CB'\sqrt{2g}\ \left(h_1 - h_0\right)^{3/2} & \text{backwater unaffected} \\ BK_S\sqrt{(h_1 - h_2)/L}\ \left(h_1 - h_0\right)^{5/3} & \text{backwater affected} \end{cases} \tag{4.6}$$

where C is the discharge coefficient, B' the width of the weir and g the gravity acceleration. Matching equations (4.3) and (4.6) yields:

$$\begin{cases} C_1 = CB'\sqrt{2g} & [\mathrm{m}^{3/2}.\mathrm{s}^{-1}] \text{ and } b_1 = 3/2 & \text{backwater unaffected} \\ C_1 = BK_SL^{-1/2} & [\mathrm{m}^{5/6}.\mathrm{s}^{-1}],\ \eta = 1/2 \text{ and } b_1 = 13/6 & \text{backwater affected} \end{cases} \tag{4.7}$$

with again non-consistent values of C_1 and b_1 parameters on the two components of the rating curve model.

Probably due to this rating-curve model, the application cases reported by Petersen-Øverleir and Reitan [2009a] led to unrealistic estimates of some hydraulic exponents and coefficients. Typically, the resulting median values for hydraulic exponents b_1 and $b_1 - \eta$ of the two segments (e.g. Table III: $b_1 = 2.4$ and $b_1 - \eta = 1.99$) were generally found to be inconsistent with the

assumed controls, such as a wide, rectangular control channel (1.67) or a horizontal critical section (1.5).

The original contribution of this paper to the Bayesian analysis of stage-fall-discharge rating curves is to introduce a model accounting for gradually varied flows in wide open-channels (section 4.2). We also establish the segmentation of the rating curve based on continuity constraints between segments governed by a backwater-affected channel control and a backwater-unaffected control, the latter being either a channel control or a section control. The operational applicability is demonstrated using two real situations typical of channel-controlled and section-controlled sites: the Rhône at Valence, France, and the Guthusbekken at station 0003·0033, Norway [Petersen-Øverleir and Reitan, 2009a], respectively (section 4.3). The performance of the new method is tested through sensitivity analyses to priors and observations (section 4.4) using a channel-controlled site that has been comprehensively documented with gaugings (the Rhône at Valence, France). Last, the limitations of stage-fall-discharge rating curves are investigated using a challenging case in a mega-river with variable roughness due to bedforms: the Madeira at Fazenda Vista Alegre, Brazil, affected by the variable backwater of the Amazon River (section 4.5).

4.2. Stage-fall-discharge (SFD) models

4.2.1. Stage-discharge controls in gradually varied flows

The variable backwater due to unsteady downstream boundary condition can be caused by the stage fluctuations of a reservoir, a lake, a tidal outlet, or even debris/ice jams or dike break for instance. As in the idealised examples of figure 4.1, a station is not always affected by variable backwater, so a transition (assumed to be instantaneous) to at least one unaffected control must be considered. Necessarily, the backwater-affected control is a channel control since a section control does not depend on the energy slope, nor on the flow conditions downstream of the critical cross-section. Assuming that both the main and auxiliary gauges are located within a gradually varied flow, we apply the conventional Manning-Strickler friction formula, assumed to be valid for this kind of slightly non uniform flows. When the flow is rapidly varied or heavily impounded, like in a lake or a reservoir, friction formulas like the Manning-Strickler equation do not apply any longer.

The backwater-unaffected control can be either a section control (flow choked upstream of a critical section) or a channel control (friction dominated flow). We will introduce two different SFD models for the section control (SFD-s) and the channel control (SFD-c) situations. Considering two controls may not be enough, especially at stations where an unaffected channel control or a variable slope channel control can both take over a low-flow section control. Obviously, other perturbations of the controls may not be captured by measuring the variable slope, especially variable roughness (due to weeds, ice cover, bedforms, etc.), additional head losses in compound channel flows and rating shifts due to morphodynamical evolution of the channel [e.g. Westerberg et al., 2011, Morlot et al., 2014]. Only the issue of variable roughness will be addressed in this paper, as an example of the limitations of stage-fall-discharge rating curves (see section 4.5).

Figure 4.1-a shows a typical channel control situation upstream of a dam but would equivalently apply to any type of variable downstream boundary condition. Depending on upstream (discharge) and downstream (stage) boundary conditions, the primary gauge may be located within a fairly uniform flow (cf. water profile (1)) or within a gradually varied flow (cf. water profile (2)). It is very important to realise that the two controlling channels are not the same, the former being centred around the primary gauge, whereas the latter is mainly located in between the two gauges. A critical implication is that offsets h'_0 (mean bottom level at the main

gauge) and h_0 (mean bottom level between both gauges) cannot be considered to be the same, as assumed by Petersen-Øverleir and Reitan [2009a]. Moreover, it clearly appears that their transition condition when the auxiliary stage h_2 is equal to h_0 does not apply since h_2 is likely to always remain greater than h_0 in such a deep, flat channel configuration. When velocity head is negligible ($V^2/2g \ll h$), the friction slope can be approximated by the water surface slope, estimated by $(h_1 - h_2)/L$ considering that the distance L is short enough to have a linear water profile between the twin gauges (gradually varied flow assumption).

Figure 4.1-b shows a typical section control that may be drowned or not, according to discharge and water level at a lake located downstream (again, any type of variable downstream boundary condition may apply). The submersion of the weir does not necessarily imply a non-unique rating curve: the channel control that takes over may be affected or not by variable backwater from the lake. Again, the assumption that both section control (cf. water profile (1)) and channel control (cf. water profile (2)) have equal offsets h_0 (offset of the channel control) and h'_0 (weir crest elevation) appears to be inadequate. Moreover, such a transition is usually predicted to occur when the stage downstream of the weir h_{ds} exceeds the weir crest elevation h_0 (as used by Petersen-Øverleir and Reitan [2009a]) or when $(h_{\mathrm{ds}} - h_0) < \lambda(h_1 - h_0)$ with $\lambda \approx 2/3$. Actually such weir submergence conditions cannot be applied since usually the auxiliary gauge is not located in the flow re-establishment section downstream of the control, rather much further downstream. As a consequence, measured h_2 is substantially lower than h_{ds} and the relation between both stages is not straightforward since it depends on the hydraulic conditions along the long reach between the weir and the auxiliary gauge.

4.2.2. Stage-fall-discharge rating curve models

4.2.2.1. SFD-c model: channel controls with constant and variable slope

A channel control is modelled using a three-parameter power-law, after simplification of the Manning-Strickler equation for a wide, rectangular cross-section: wetted area $A \approx B(h_1 - h_0)$ and hydraulic radius $R_h \approx h_1 - h_0$, with B the mean channel width and h_0 the average bottom level at primary gauge. The backwater-unaffected control is assumed to have a constant friction slope S_0, whereas the variable slope of the backwater-affected control is approximated by $(h_1 - h_2)/L$ where L is the longitudinal distance between the two gauges.

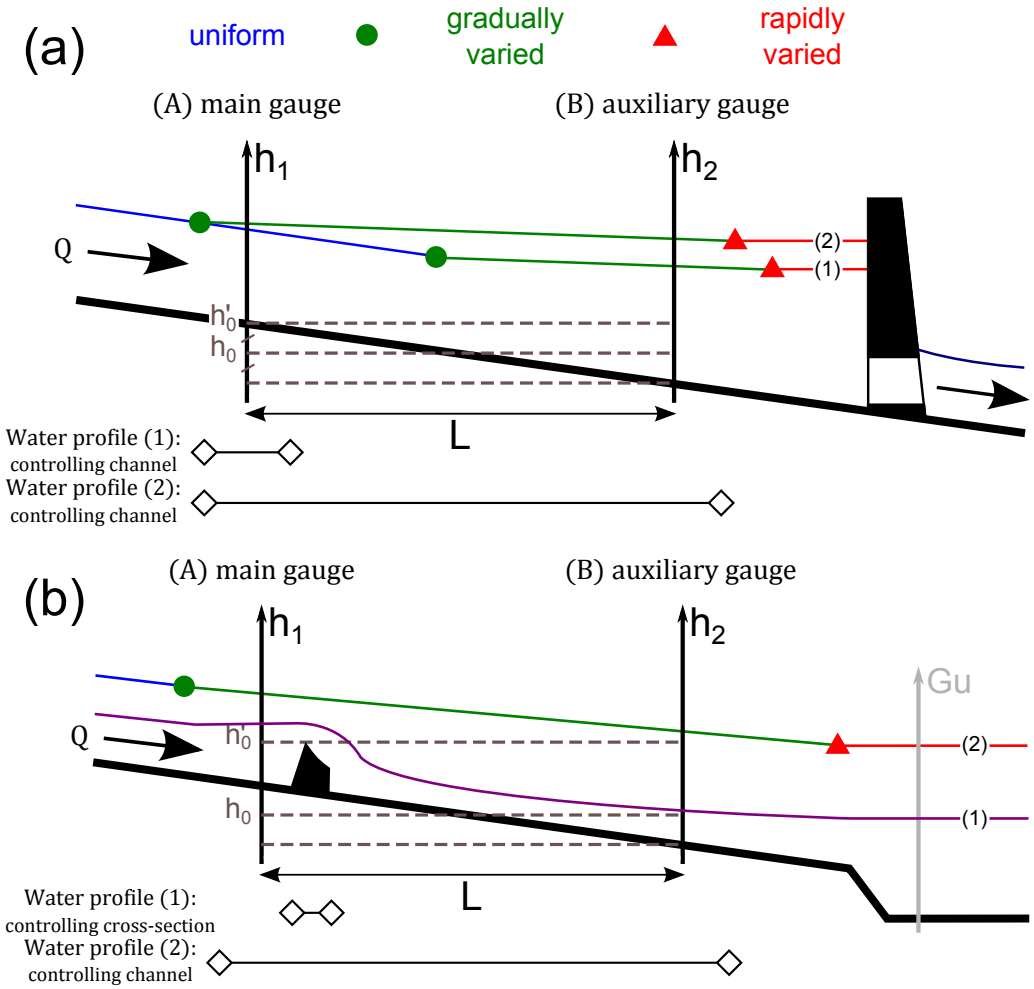

Figure 4.1 – Typical transitions for stage-fall-discharge model: (a) from non affected channel control (water profile (1)) to a variable slope channel control (water profile (2)) upstream of a dam; (b) from non affected section control (water profile (1)) to variable slope channel control (water profile (2)) upstream of a rivers' confluence or a lake. For the Guthusbekken case, the downstream station h_2 is located in the lake (Gu). Red triangles correspond to the transition between gradually varied flow and rapidly varied flow whereas green circle to the transition between uniform flow and gradually varied flow.

Therefore, equation (4.4) can be rewritten as follow:

$$Q\left(h_1,h_2\right)=\begin{cases} K_S B\left(h_1-h_0\right)^M\sqrt{\left(h_1-h_2-\delta_h\right)/L} & \text{if } \; h_1<\kappa\left(h_2\right) \quad \text{(variable slope)} \\ K'_S B'\left(h_1-h'_0\right)^{M'}\sqrt{S_0} & \text{if } \; h_1\geq\kappa\left(h_2\right) \quad \text{(channel control)} \end{cases} \tag{4.8}$$

where δ_h is the difference in datum reference levels between the auxiliary gauge and the main gauge, and M an exponent related to the assumed friction equation and the cross-sectional shape. M is equal to 5/3 for Manning-Strickler equation in a wide rectangular channel. Unlike

existing stage-fall-discharge approaches, we deem it important to estimate the parameter δ_h as it may be affected by significant uncertainties.

Compared with Petersen-Øverleir and Reitan [2009a] we use two separate h_0 and h_0' parameters for the two channel controls to avoid hydraulic conflicts. Moreover we assume the flow resistance coefficients K_S and K_S' and the widths B and B' are different. In many cases, the controlling channels are similar for both backwater-affected and backwater-unaffected conditions. In such cases, equation (4.8) can be rewritten with $K_S' = K_S$ and $B' = B$.

Another important difference with the SFD model proposed by Petersen-Øverleir and Reitan [2009a] is that the transition condition comes as a discharge continuity condition for $h_1 = \kappa(h_2)$ in equation (4.8), which leads to:

$$K_S B \left(\kappa(h_2) - h_0\right)^M \sqrt{\left(\kappa(h_2) - h_2 - \delta_h\right)/L} - K_S' B' \left(\kappa(h_2) - h_0'\right)^{M'} \sqrt{S_0} = 0 \tag{4.9}$$

The Newton-Raphson algorithm is used to solve equation (4.9) and find the transition stage $\kappa(h_2)$.

4.2.2.2. SFD-s model: a section control and a variable slope channel control

If the backwater-unaffected control is a section control, it can be modelled as an equivalent weir. Therefore, considering the most common situation, i.e. a natural or artificial control that can be approximated as a horizontal-crested weir, equation (4.6) can be rewritten as:

$$Q(h_1, h_2) = \begin{cases} CB' \sqrt{2g} \left(h_1 - h_0'\right)^{M'} & \text{if } h_2 < \kappa'(h_1) \quad \text{(section control)} \\ K_S B \left(h_1 - h_0\right)^M \sqrt{(h_1 - h_2 - \delta_h)/L} & \text{if } h_2 \geq \kappa'(h_1) \quad \text{(variable slope)} \end{cases} \tag{4.10}$$

where the width B' of the weir often differs from the channel width B, the discharge coefficient C is approximatively equal to 0.4, the exponent M' is close to 3/2 and the gravity acceleration g is given equal to 9.81 m.s^{-2}.

Following Petersen-Øverleir and Reitan [2009a], we do not consider the possible occurrence of a third control, i.e. a constant-slope channel control, and we assume therefore that variable backwater occurs as soon as the section control is submerged. Again, the transition between the backwater affected and unaffected controls is computed through a discharge continuity condition

for $h_2 = \kappa'(h_1)$, which can now be solved explicitly:

$$\kappa'(h_1) = h_1 - \delta_h - L\left(\frac{CB'\sqrt{2g}}{K_S B}\right)^2 \frac{\left(h_1 - h_0'\right)^{2M'}}{\left(h_1 - h_0\right)^{2M}} \tag{4.11}$$

Unlike the case of channel controls, the transition condition is governed by the stage at the auxiliary gauge: the weir is submerged and backwater affected channel control takes over when stage h_2 exceeds $\kappa'(h_1)$.

4.2.3. Inference/Parameter estimation

The proposed method is an extension of the Bayesian framework associated with the BaRatin method [Le Coz et al., 2014]. The main updates and extensions made for this study are described hereafter. The reader is referred to Le Coz et al. [2014] for a comprehensive description of the existing BaRatin framework and an overview of its principles.

Gaugings $(\tilde{h}_{1,i}, \tilde{h}_{2,i}, \tilde{Q}_i)_{i=1,N}$ are seen as estimates of the real values $(h_{1,i}, h_{2,i}, Q_i)_{i=1,N}$ of stages and associated discharges. We further assume that stage errors are negligible compared to discharge errors:

$$\begin{cases} \tilde{h}_{1,i} = h_{1,i} \\ \tilde{h}_{2,i} = h_{2,i} \\ \tilde{Q}_i = Q_i + \epsilon_{Q_i} \quad \text{with} \quad \epsilon_{Q_i} \overset{\text{indep.}}{\sim} \mathcal{N}(0, u_{Q_i}) \end{cases} \tag{4.12}$$

where the standard deviations u_{Q_i} are assumed to be known. Depending on their measurement technique and field procedure, uncertainty values were assigned to gaugings based on the typical results of available propagation methods [e.g., Despax et al., 2016] and in-situ intercomparisons [e.g., Le Coz et al., 2016a].

The stage-discharge relationship is given by:

$$Q_i = f(h_{1,i}, h_{2,i}|\boldsymbol{\theta}) + \epsilon_{f,i} \text{ with } \epsilon_{f,i} \overset{\text{indep.}}{\sim} \mathcal{N}\left(0, \sigma_{f,i} = \gamma_1 + \gamma_2 \hat{Q}_i\right) \tag{4.13}$$

where $\boldsymbol{\theta} = (\theta_1, \ldots, \theta_{N_{par}})$ are the rating curve parameters, $\boldsymbol{\epsilon_f} = (\epsilon_{f,1}, \ldots, \epsilon_{f,N})$ are the structural errors and $(\sigma_{f,1}, \ldots, \sigma_{f,N})$ are the standard deviations of the structural errors $(\epsilon_{f,1}, \ldots, \epsilon_{f,N})$.

As discussed by Le Coz et al. [2014], an affine function for modelling the standard deviation $\sigma_{f,i}$ is used. This affine model assumes that this standard deviation is dominated at low flows by a constant term γ_1 whereas at high flows the error is proportional to the discharge estimation $\hat{Q}$.

Wide uniform distributions (between 0 and 10^6) are used as non-informative priors for both γ_1 and γ_2 parameters. We also assume that the structural errors $(\epsilon_{f,1}, \ldots, \epsilon_{f,N})$ are independent. This assumption may be acceptable when the gaugings are separated by a duration of several weeks or months. However, it is more problematic in terms of uncertainty propagation, because independent structural errors will be generated to produce uncertain hydrographs, even for consecutive time steps separated by a few minutes or hours. This is a difficult issue that has no complete solution as far as we know, and we refer the reader to the in-depth discussion in Le Coz et al. [2014] for more details on this topic.

Combining equations (4.12) and (4.13) yields the following stage-fall-discharge relation between observed values, assuming independence between ϵ_{Q_i} and $\epsilon_{f,i}$:

$$\tilde{Q}_i = f(\tilde{h}_{1,i}, \tilde{h}_{2,i}|\boldsymbol{\theta}) + \epsilon_{Q_i} + \epsilon_{f,i} \text{ with } \epsilon_{Q_i} + \epsilon_{f,i} \sim \mathcal{N}\left(0, \sqrt{\sigma_{f,i}^2 + u_{Q_i}^2}\right) \tag{4.14}$$

Unknown quantities that have to be estimated are the parameters $\boldsymbol{\theta}$ of the rating curve and the parameters $\boldsymbol{\gamma} = (\gamma_1, \gamma_2)$ of the structural error model. Equation (4.14) allows computing the likelihood function as described in Le Coz et al. [2014]. Combined with prior distributions for $\boldsymbol{\theta}$ and $\boldsymbol{\gamma}$, this yields a posterior distribution that can be explored by MCMC sampling [Renard et al., 2006]. In the following sections, uncertainty bounds are computed from the MCMC samples with a probability level of 95% (i.e. 2.5% and 97.5% percentiles), as usually done in hydrometric applications [ISO/TS 25377:2007, 2007]. The maximum *a posteriori* (MAP) estimator is used to estimate the rating curve. This estimator is the mode of the posterior density.

4.3. Application to typical cases with channel and section controls

4.3.1. Channel-control case: The Rhône River at Valence

The Rhône River has a mean interannual discharge of 1690 $m^3.s^{-1}$ at its outlet (Beaucaire station, catchment area of 95590 km^2). It flows along 812 km from a glacier in Switzerland, through Lake Geneva down to the Mediterranean Sea.

At Valence station the Rhône drains a catchment area of 66450 km^2 (68% of the whole catchment area). The primary gauge is located just upstream of a motorway bridge (Longitudinal position: Kilometric Point 109.7 km, GPS locations: 4°53′03.7″E, 44°55′54.3″N). The streamwise distance L between the two stations is known to be 3900 m ± 200 m. The friction slope S_0 at the highest flows is not accurately measured but is estimated to be roughly 0.001 $m.m^{-1}$ ± 0.001 $m.m^{-1}$.

Figure 4.2 shows different cross-sectional profiles all along the section between the twin gauges. Over approximately 2 km (down to the Kilometric Point 111.5 km) downstream of the primary gauge, the channel is fairly uniform and rectangular with a mean width $B = 180$ m ± 20 m; then the channel gradually expands on its left side up to the auxiliary station (Longitudinal position: Kilometric Point 113.6 km, GPS locations: 4°51′32.2″E, 44°54′04.1″N). The mean width between the two gauges differs from that around the primary gauge and is set to 200 m ± 100 m.

Both channel control offsets, h_0 and $h_0^{'}$, are set to -3 m ± 2 m. From existing hydraulic models, both Strickler flow resistance coefficients K_S and $K_S^{'}$ are set to 30 $m^{\frac{1}{3}}.s^{-1}$ ± 5 $m^{\frac{1}{3}}.s^{-1}$. The datum difference δ_h between the two staff gauges is accurately levelled by the Compagnie Nationale du Rhône (CNR) and is set to 0 m ± 0.05 m. Corresponding priors are summarised in table 4.1.

68 gaugings were performed at the Valence station. Those gaugings are densely distributed from 375 $m^3.s^{-1}$ to 6717 $m^3.s^{-1}$, which roughly corresponds to the 50-year flood. The mean annual discharge is 1400 $m^3.s^{-1}$. Figure 4.3 shows the estimated rating curves as $h_1 - Q$ plots with the 95% total uncertainty envelopes. The SFD rating curves are plotted for 5 h_2 values which correspond to 4 available gaugings ($h_2 = 1.34$, 1.93, 2.40 and 2.76 m) and to the maximum h_2 value (3.04 m) recorded over the last 40 years. As expected from the hydraulic analysis,

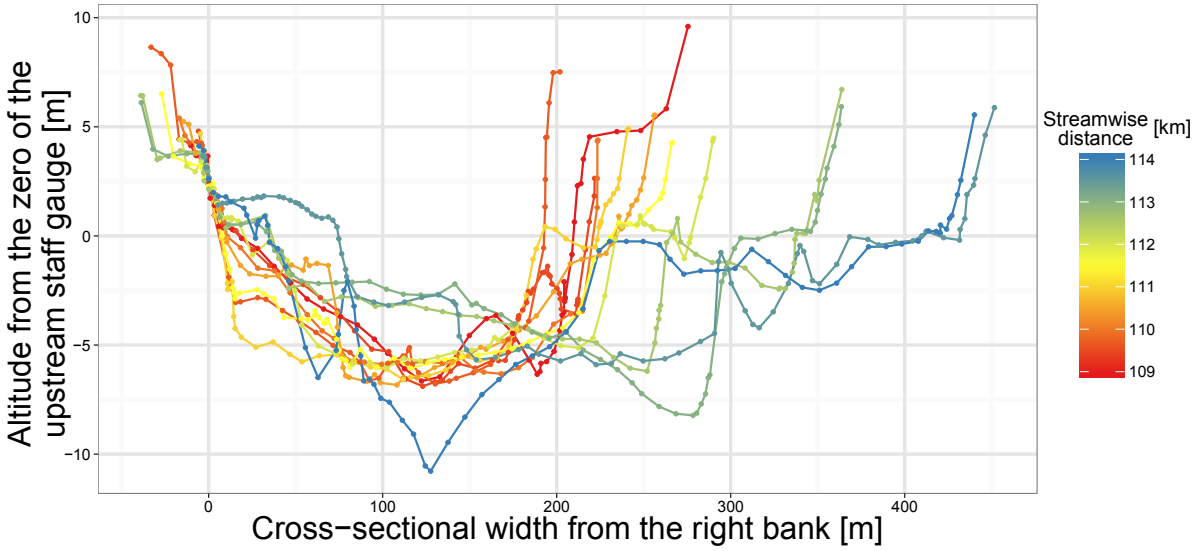

Figure 4.2 – The Rhône River at Valence: cross-sectional profiles between the main and auxiliary stations.

BaRatin parameter	Physical parameter	Units	Prior distribution	SFD-c results: MAP $[Q_{2.5}; Q_{97.5}]$
θ_1	$K_S B$	$[\mathrm{m}^{\frac{4}{3}}.\mathrm{s}^{-1}]$	$\mathcal{N}(6000, 1582)$	6712 [5641; 8578]
θ_2	h_0	[m]	$\mathcal{N}(-3, 1)$	-4.51 [-5.29; -3.69]
θ_3	$M \simeq 5/3$	[−]	$\mathcal{N}(1.6667, 0.025)$	1.67 [1.62; 1.71]
θ_4	L	[m]	$\mathcal{N}(3900, 100)$	3898 [3697; 4091]
θ_5	h'_0	[m]	$\mathcal{N}(-3, 1)$	-1.43 [-2.16; -1.15]
θ_6	$K'_S B' \sqrt{S_0}$	$[\mathrm{m}^{\frac{4}{3}}.\mathrm{s}^{-1}]$	$\mathcal{N}(171, 46)$	269 [216; 304]
θ_7	δ_h	[m]	$\mathcal{N}(0, 0.025)$	-0.025 [-0.035; -0.018]
θ_8	$M' \simeq 5/3$	[−]	$\mathcal{N}(1.6667, 0.025)$	1.68 [1.64; 1.73]
γ_1	error	$[\mathrm{m}^3.\mathrm{s}^{-1}]$	$\mathcal{U}(0, 10^6)$	69 [45; 91]
γ_2	error	[−]	$\mathcal{U}(0, 10^6)$	0.0009 [0.0002; 0.022]

Table 4.1 – Parameters, prior distributions and results of the Bayesian analysis of the stage-fall-discharge rating curve of the Rhône River at Valence. The symbol $\mathcal{N}(\mu, \sigma)$ corresponds to the normal distribution with mean μ and standard deviation σ. The symbol $\mathcal{U}(a, b)$ corresponds to the uniform distribution on the interval $[a, b]$.

individual rating curves for distinct h_2 values merge with the unaffected channel control curve when h_1 exceeds the transition threshold $\kappa(h_2)$.

For the sake of comparison, results from the standard stage-discharge (SD) model is also computed with a single constant-slope channel control, using the same prior information as for the SFD model. The SD model is clearly not adequate for capturing the variable backwater effect. Despite the MAP rating curve of this model agreeing with the highest gaugings (i.e.

the unaffected channel control), it obviously fails to describe the scattered low-flow gaugings (cf. figure 4.3). The associated total uncertainties are extremely high at both low and high flows. On the opposite, all the MAP rating curves estimated by the SFD model agree with gaugings and have much smaller uncertainties: total uncertainty is lower than ±10% for discharges above 2000 $m^3.s^{-1}$ (cf. figure 4.4). Relative errors of MAP predictions compared to observations are also small and decrease with discharge. The lower agreement at very low flows may be explained by the lack of low-flow gaugings available for calibrating the model (only 3 gaugings at $Q < 500$ $m^3.s^{-1}$).

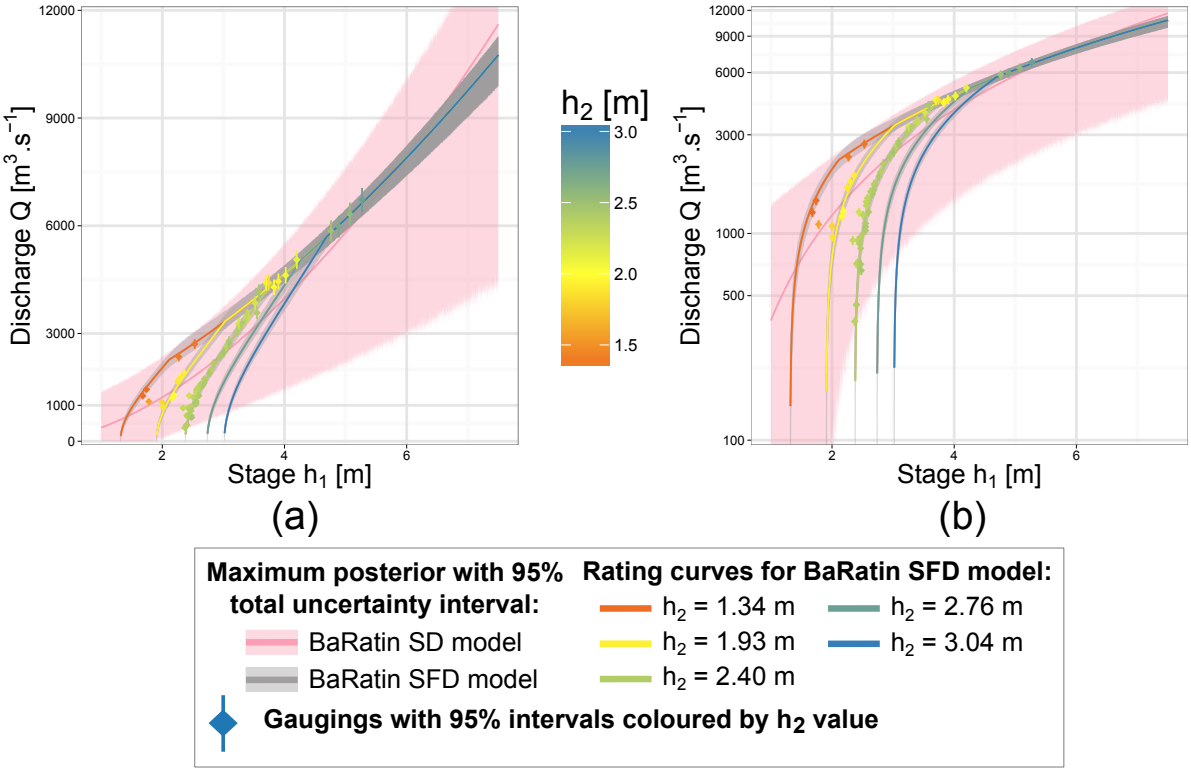

Figure 4.3 – The Rhône River at Valence: stage-discharge representation of the stage-fall-discharge (SFD) and stage-discharge (SD) models, with discharges in (a) natural scale and in (b) logarithm scale. The SFD rating curves are plotted for 5 values of h_2 corresponding to available gaugings (h_2 = 1.34, 1.93, 2.40 and 2.76 m) and to the maximum recorded value (3.04 m) over the last 40 years.

The SD and SFD rating curves can be used to propagate stage time series into discharge time series (in this paper we always estimate instantaneous discharges). Only rating curve errors are taken into account in such a propagation (i.e. stage errors are ignored). Figure 4.5 illustrates the resulting uncertain hydrographs for the September-November 1993 period, which covers the highest flood ever measured at the Valence station. Again, total uncertainties computed by a standard stage-discharge rating curve (SD model) are extremely large: more than ±70%

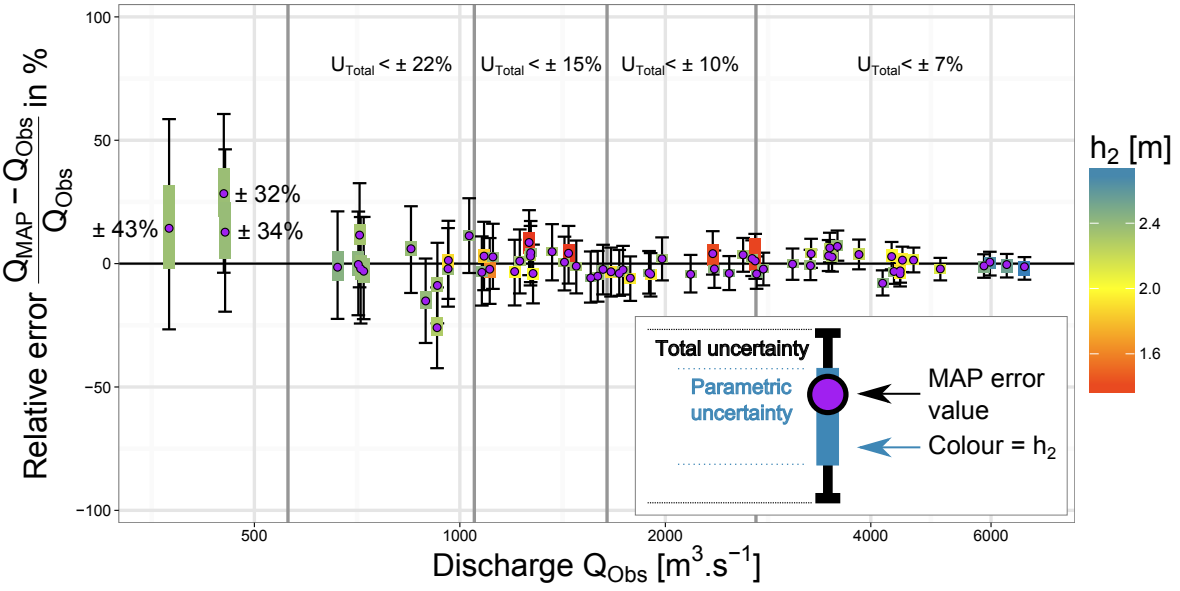

Figure 4.4 – Application of the stage-fall-discharge (SFD) model to the Rhône River at Valence: relative errors between the maximum *a posteriori* discharges (Q_{MAP}) and the gaugings (Q_{Obs}). Error bars represent the parametric and total 95% uncertainty bounds of the discharge estimates, with h_2 values colour-coded.

for low flows and between ±40% and ±60% for high flows. Moreover the SD model seems to underestimate high flows. This assement is clear on the first and fourth gaugings on figure 4.5. When the discharge is higher than the discharge associated with stage transition, both SFD and SD model have the same formulation (channel control part in equation (4.8)) but their parameters differ ($K'_S B' \sqrt{S_0}$ and h'_0) because there are no longer estimated on only high flows but also on low flows for the SD model. The BaRatin SFD model shows much better performance. High flow measurements are accurately estimated by the MAP rating curve and the related uncertainties do not exceed ±10% for discharges above 2000 $\mathrm{m}^3.\mathrm{s}^{-1}$. The model clearly makes the transition from backwater affected to backwater unaffected channel control, when discharge Q exceeds the discharge threshold for $h_1 = \kappa(h_2)$. That discharge threshold, plotted in green with its uncertainties in figure 4.5, is found to decrease during the flood due to a concurrent decrease in h_2.

4.3.2. Section-control case: Guthusbekken at station 0003·0033

For an application of the proposed SFD-s model, we use the study of the Guthusbekken stream at station 0003·0033 in Norway fully described in Petersen-Øverleir and Reitan [2009a]

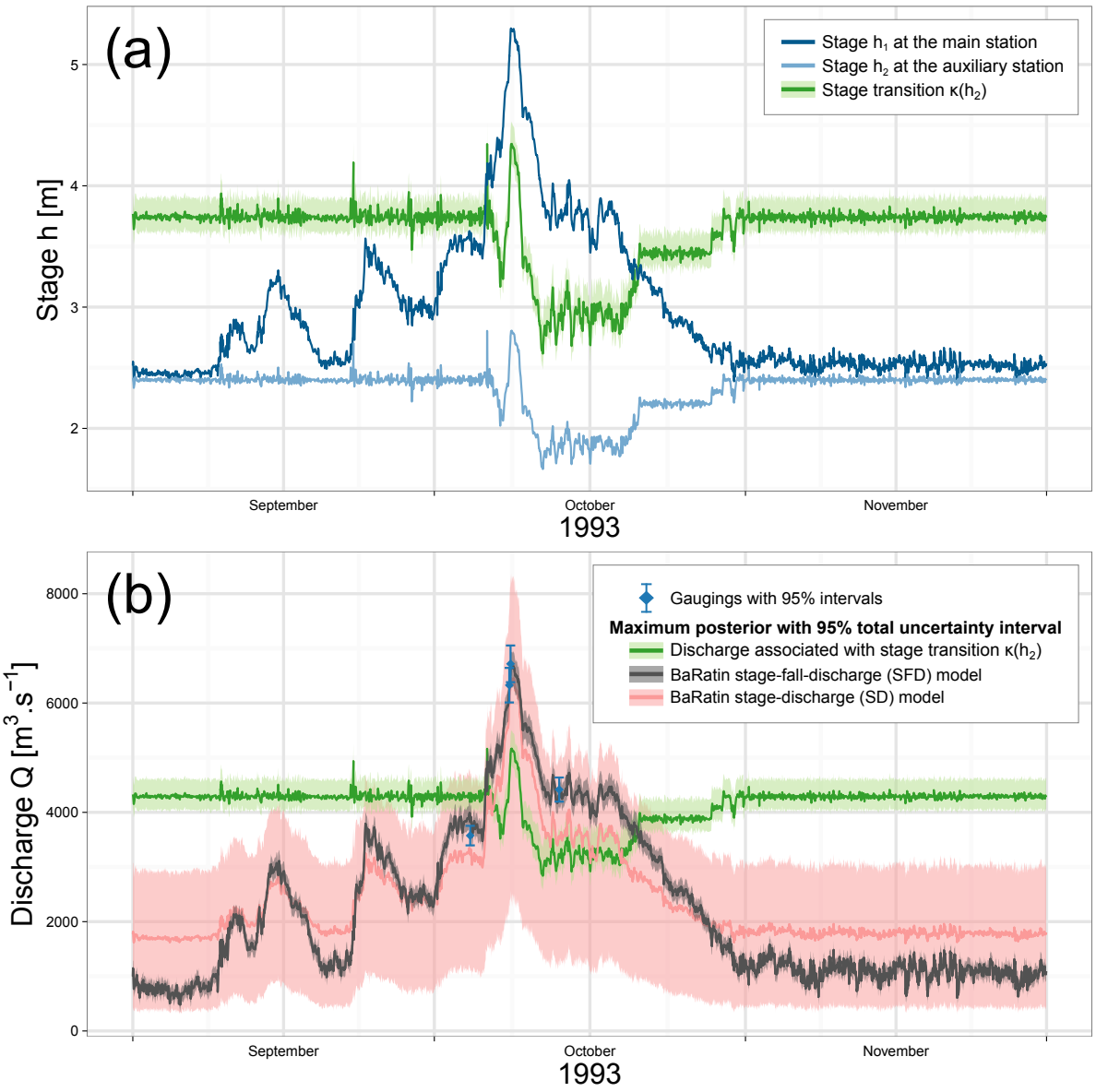

Figure 4.5 – The Rhône River at Valence, flood of October 1993: (a) stage records h_1 and h_2 at respectively the main and auxiliary stations with the estimated stage transition $\kappa(h_2)$ of the stage-fall-discharge (SFD) model; (b) instantaneous discharge estimated by the SFD and stage-discharge (SD) models.

who shared the data. It is a small, 2-metre wide stream contracted to 1.5 m as the flow goes through a canyon and a natural sill of 0.2 m fall before widening up to 4 m as it enters into the lake Vansjø. The critical section is periodically drowned due to variable backwater effects from the lake when level gets high. The main gauge is located 7 m upstream of the sill whereas the auxiliary gauge is actually located in the lake itself (cf. figure 4.1-b, mark Gu), at a distance of about 1400 m from the main gauge. This situation is not ideal, since the measured fall divided

by the constant distance between gauges may then be not representative of the actual water slope in the gradually varied flow section.

27 gaugings were performed at the Guthusbekken station and 8 among them are reported to be the only ones affected by variable backwater. Those 8 measurements are actually four ADCP transects repeated twice, and 14 out of the backwater-unaffected 19 gaugings are also replicates. As a consequence, only 16 independent gaugings could be derived from the whole dataset. Despite the limitations of this case study, it is the best documented at hand, and equation (4.10) was applied to model the unaffected section control and the variable slope channel control.

From the description of the stream bed within a canyon, the Strickler flow resistance coefficient K_S of the stream is guessed to be equal to 20 $\mathrm{m}^{\frac{1}{3}}.\mathrm{s}^{-1} \pm 10$ $\mathrm{m}^{\frac{1}{3}}.\mathrm{s}^{-1}$. As described above, the mean width B between the two gauges is set to 4 m $\pm$ 2 m and the width $B^{'}$ of the sill is set to 1.5 m $\pm$ 0.3 m. The distance between the two gauges is set to 1400 m $\pm$ 100 m. Ignoring the contraction effects, the sill can be approximated by a horizontal weir with discharge coefficient $C = 0.40 \pm 0.05$. The crest elevation, $h_0^{'}$, is precisely assessed as 25.32 m ($\pm$ 0.02 m) whereas the channel offset, h_0, is left imprecise around 25.32 m ($\pm$ 4 m). The datum difference δ_h is set up to 0 m $\pm$ 0.2 m. Both exponents M and $M^{'}$ related to the nature and shape of the controls (wide rectangular channel and horizontal weir) are precisely specified respectively to 1.667 $\pm$ 0.05 and 1.5 $\pm$ 0.05, based on hydraulic formulas. These priors are summarised in table 4.2. The BaRatin stage-discharge (SD) model with a single section control is also applied, using the same prior information as for the SFD model.

Table 4.2 – Parameters, prior distributions and results of the Bayesian analysis of the stage-fall-discharge rating curve of Guthusbekken.

BaRatin parameter	Physical parameter	Units	Prior distribution	SFD-s results: MAP $[Q_{2.5}; Q_{97.5}]$
θ_1	$K_S B$	$[\mathrm{m}^{\frac{4}{3}}.\mathrm{s}^{-1}]$	$\mathcal{N}(80, 28.3)$	44.0 [34.2; 51.3]
θ_2	h_0	[m]	$\mathcal{N}(25.32, 2)$	25.12 [25.02; 25.18]
θ_2	$M = 5/3$	[−]	$\mathcal{N}(1.6667, 0.025)$	1.672 [1.615; 1.715]
θ_4	L	[m]	$\mathcal{N}(1400, 50)$	1417 [1304; 1498]
θ_5	h_0'	[m]	$\mathcal{N}(25.32, 0.01)$	25.331 [25.324; 25.337]
θ_6	$CB^{'}\sqrt{2g}$	$[\mathrm{m}^{\frac{3}{2}}.\mathrm{s}^{-1}]$	$\mathcal{N}(2.7, 0.3)$	1.12 [1.05; 1.19]
θ_7	δ_h	[m]	$\mathcal{N}(0, 0.1)$	0.0138 [0.0061; 0.0191]
θ_8	$M^{'} = 3/2$	[−]	$\mathcal{N}(1.5, 0.025)$	1.507 [1.465; 1.552]
γ_1	-	$[\mathrm{m}^3.\mathrm{s}^{-1}]$	$\mathcal{U}(0, 10^6)$	9.3×10^{-4} $[2.0 \times 10^{-4}; 4.5 \times 10^{-3}]$
γ_2	-	[−]	$\mathcal{U}(0, 10^6)$	0.031 [0.0029; 0.078]

Figure 4.6 shows the results of the application of the BaRatin SFD-s model for section controls, as $h_1 - Q$ representations with the 95% total uncertainty intervals. The SFD rating curves are plotted for 5 h_2-values corresponding to one section control gauging ($h_2 = 25.21$ m) and to four gaugings affected by variable backwater ($h_2 = 25.55$, 25.64, 25.72 and 26.03 m). The stage-discharge rating curve computed for the backwater-unaffected section control is plotted as a black dotted line. MAP values and 95% credibility intervals of each parameter of the SFD-s model are summarised in table 4.2. Gaugings corresponding to the unaffected section control are well seen on those representations (cf. figure 4.6) as they follow the weir law curve irrespective of the h_2-values. Gaugings affected by variable backwater are also well identified by the model, in accordance with statements by Petersen-Øverleir and Reitan [2009a] on the hydraulic situation of these gaugings.

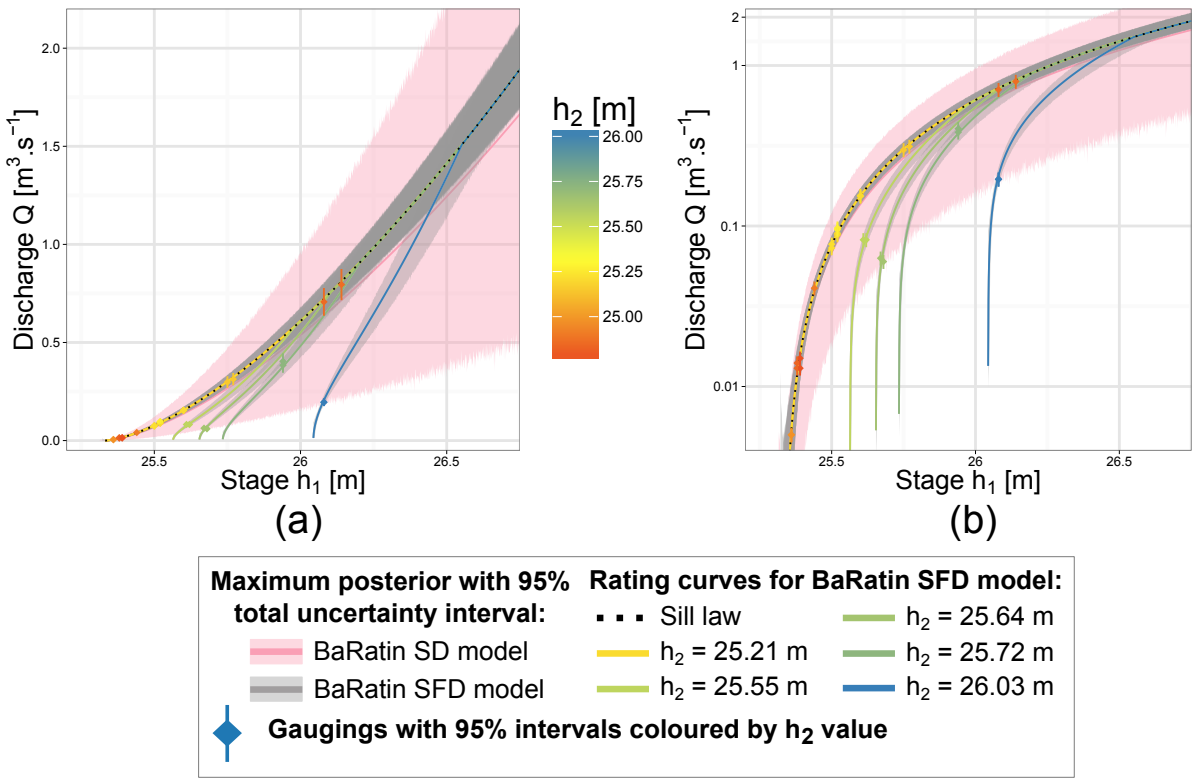

Figure 4.6 – The Guthusbekken stream at station 0003 · 0033, Norway: stage-discharge representation of the stage-fall-discharge (SFD) and stage-discharge (SD) models, with discharges in (a) natural scale and in (b) in logarithm scale. The SFD rating curves are plotted for 5 h_2-values corresponding to available gaugings (25.21, 25.55, 25.64, 25.72 and 26.03 m). The sill law computed by the SFD model is added in dark dotted line.

Figure 4.7 shows the agreement between predicted and gauged discharges as relative errors. MAP rating curves estimated by the SFD-s model agree well with gaugings: error values are

low. Total uncertainty envelopes are acceptable (less than ± 20% at high flows) and have the same width at high flows irrespective of the h_2 value. Uncertainty envelopes are large at low flow (up to ± 100% for the total uncertainty).

The relative contribution of the parametric uncertainty to the total uncertainty decreases when discharge decreases (cf. figure 4.7). Parameter $\theta_6 = CB'\sqrt{2g}$ of the weir equation takes posterior values more than twice smaller than prior values (cf. table 4.2). Prior information on this parameter appears to be in disagreement with the information found in the gaugings: a single horizontal weir may not represent well the complexity of this natural control. This cannot be explained without further investigation of the site conditions, especially the geometry of the canyon and its contracted section, and the possible transition to backwater-unaffected channel control for highest stages.

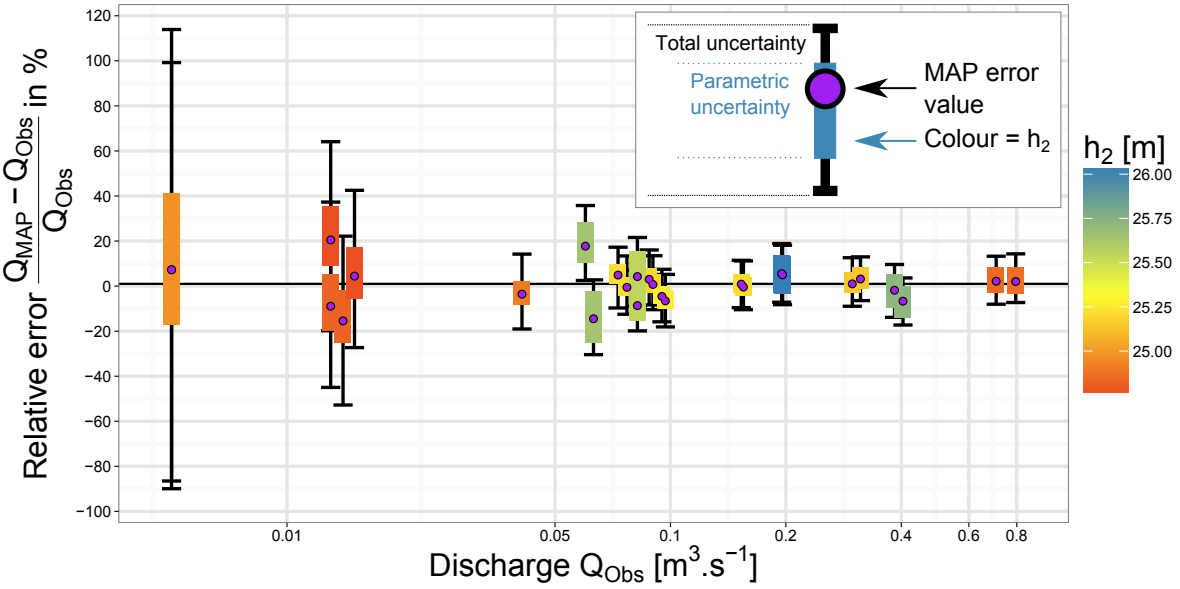

Figure 4.7 – Application of the stage-fall-discharge (SFD) model to the Guthusbekken stream at station 0003 · 0033 in Norway: relative errors in percentage between the maximum *a posteriori* discharges (Q_{MAP}) and the discharge observations (Q_{Obs}). Error bars represent the parametric and total 95% uncertainty bounds of the discharge estimates, with h_2 values colour-coded.

To sum up, the BaRatin SFD-s model for section control produces acceptable discharge estimates for the Guthusbekken station: the agreement of predicted (MAP) versus gauged discharges is good (less than ± 20 % for $Q > 0.03$ m^3.s^{-1}). However those results yield hydraulically questionable rating curves. The hydraulic configuration of this station may be more complex than assumed: channel within a complex canyon, auxiliary gauge located in the lake, transition to backwater-affected control possibly not well defined, and transition to channel control at high

flow possibly overlooked. The scarcity of independent measurements, especially for backwater-affected situations, also challenges the application of the model to that case. Consequently, additional investigations in the directions described above may lead to a more adequate SFD model, which may help in further reducing uncertainty.

4.4. Sensitivity to available information

The SFD-c model (cf. equation (4.8)) is used to perform sensitivity analyses on the Rhône River at the Valence station.

4.4.1. Sensitivity to prior information

Several sets of priors are used to determine which parameters require informative priors and which ones are easily inferred from the data. The first set of priors includes all the available prior information (see prior distributions in table 4.1). This set is named 'fully informative priors'. In the other eight sets of priors, named 'non informative priors', the precise prior distribution of one of the 8 parameters has been replaced by a wide uniform, non informative distribution.

Results from this prior sensitivity analysis are shown in figure 4.8, which represents for each parameter the prior density (in black), the posterior density associated with the fully informative prior (in pink) and posterior densities associated with the 8 non informative prior sets.

The longitudinal distance L requires prior information to be identified, otherwise its posterior density is very vague and encompasses physically unrealistic values. When the prior of this parameter is more precise, its posterior density matches with prior density. This illustrates that this parameter cannot be inferred from the gauging data only and instead requires prior information. Similarly, parameters M and M' also require precise informative priors.

Offsets h_0 and h'_0 can easily be inferred from the information contained in the gaugings: posterior densities are more precise than prior densities. Informative priors on those parameters are not absolutely necessary. However, they can reduce correlation effects with other parameters. Indeed parameters M', h'_0 and $a = K'_S B' \sqrt{S_0}$ appear to be correlated and any lack of prior information on one of them can propagate to the two other ones (figure 4.8, last row). Figure 4.8 shows that if a non informative prior on M' is assumed, the posterior density of $a = K'_S B' \sqrt{S_0}$ keeps close to the prior distribution and the posterior density of offset h'_0 differs from other prior sets.

The datum difference δ_h can be inferred from the data and seems to have no direct connection with other parameters. The $K_S B$ product can be identified from the data as well. However, strong correlations between parameters $K_S B$, h_0 and M impose to have precise prior information on at least two of them.

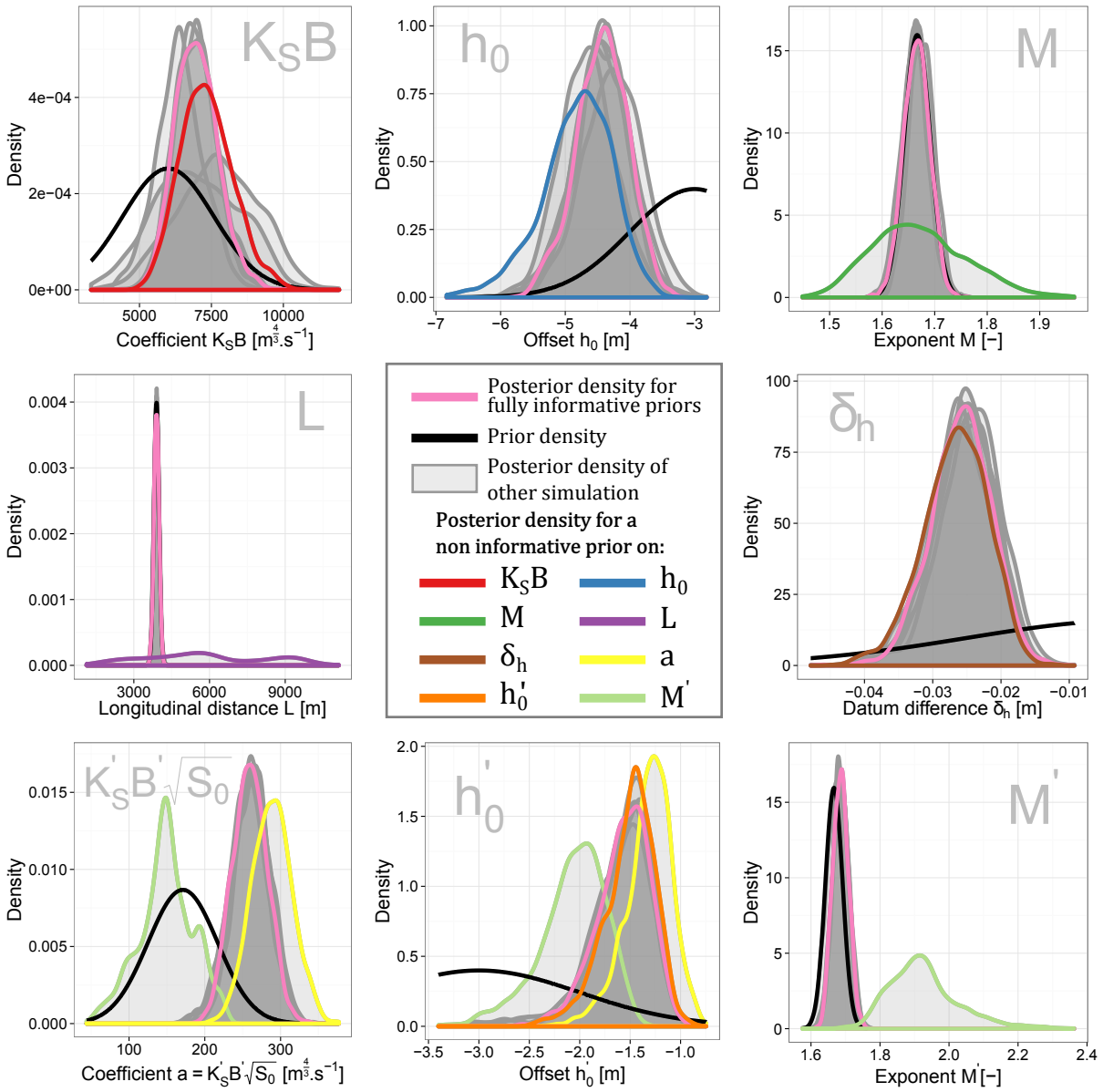

Figure 4.8 – Prior sensitivity analysis applied to the Rhône River at Valence: posterior and prior densities of rating curve parameters for fully or partially informative priors.

4.4.2. Sensitivity to observations (gaugings dataset)

An important issue for the management of stations affected by backwater influence is to establish a gauging strategy in order to optimise rating curve estimations and uncertainty assessment. In this section the sensitivity of the stage-fall-discharge model to the gauging dataset is investigated still using the Valence case. Several gauging subsamples are used: (1) gaugings covering the whole range, (2) high-flow gaugings only, (3) low-flow gaugings only, (4) gaugings with $h_2 < 2$ m, (5) gaugings with $h_2 = 2.4$ m $\pm\, 0.01$ m. For each of the 5 subsamples only 16

gaugings are used to calibrate the stage-fall-discharge model and cross-validation is performed on other gaugings.

The results of this analysis are summarised in figure 4.9. As expected, using only high-flow gaugings (2) for calibrating the model yields larger uncertainties on low flows, and brings MAP errors as large as ± 50%. It may even happen that very low discharges cannot be estimated: the MAP value of the h_0 parameter may indeed be higher than the h_1 value of the lowest gaugings. This is because the $K_S B$ and h_0 parameters of the SFD model for low flows (cf. variable slope part in equation (4.8)) have uncertain priors and are poorly identified from the data.

On the other hand, using only low-flow gaugings (3) reduces parametric uncertainties at low flows but the model does not precisely identify high flow parameters from the data. Results for $K_S^{'} B^{'} \sqrt{S_0}$ and $h_0^{'}$ remain close to their wide priors. High flow estimates are therefore affected by large uncertainties.

Using only gaugings with low values of h_2 (subsample (4)) seems to be an acceptable strategy. Similar to the whole panel (1), MAP error values are centred around zero and the uncertainties are small. Nevertheless, this strategy holds only if all the discharge range is represented. In fact, it may even be problematic at very low flows: for this order of discharge, h_2 values are always quite high. In figure 4.9-(4), parametric uncertainties on low discharges are larger than those for the whole range.

Finally, using gaugings with a nearly constant h_2 value (2.4 m, subsample (5)) leads to increased uncertainties of discharge estimates compared with the 'whole range', even if all the discharge range is sampled: parametric uncertainties are higher, which shows the difficulty of the model to estimate 'backwater' parameters when the covariate h_2 is not variable enough.

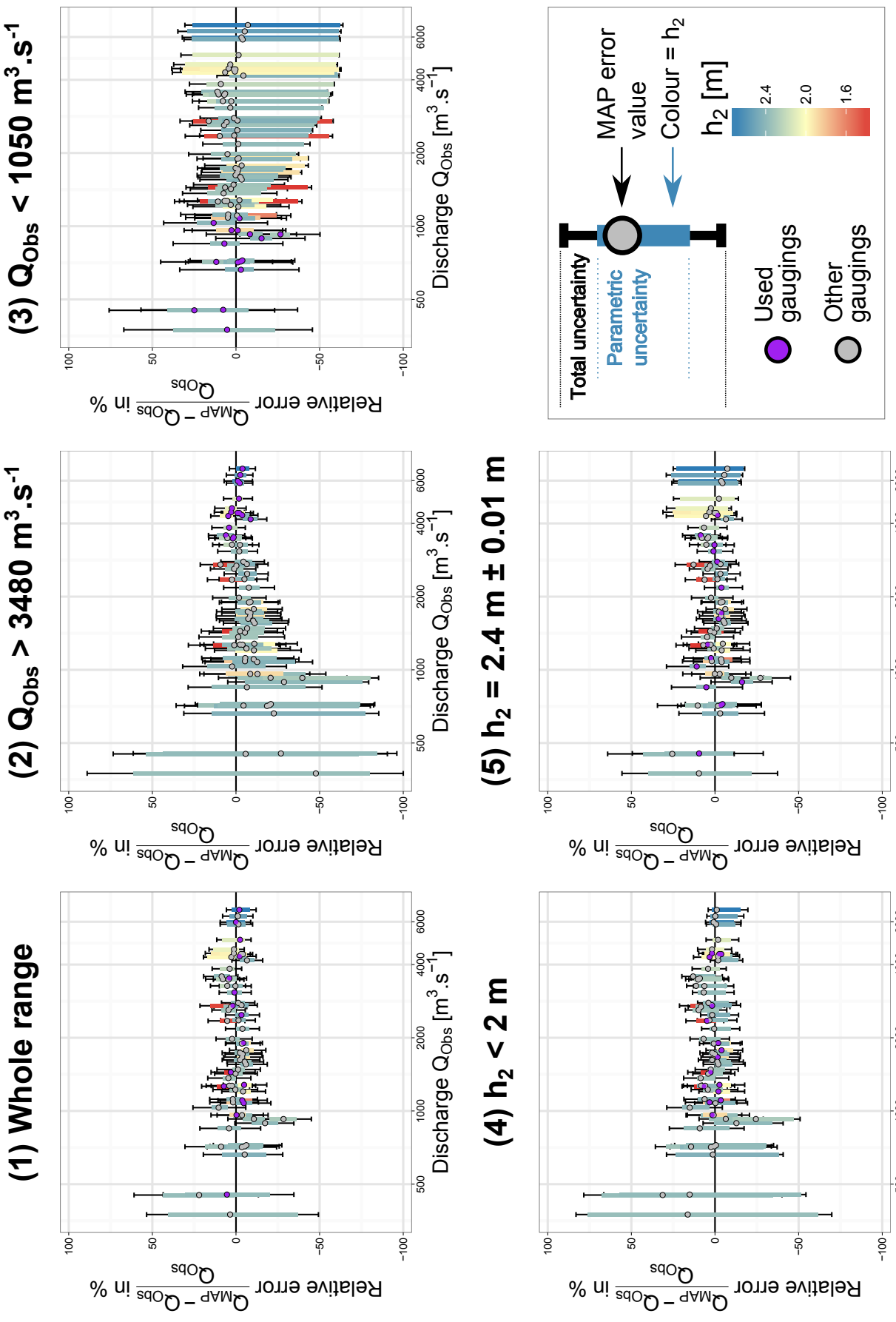

Figure 4.9 – Sensitivity analysis of the stage-fall-discharge model to gauging dataset applied to the Rhône River at Valence: relative errors of estimated discharges compared to discharge observations Q_{Obs}. Q_{Obs} values are represented using a logarithm scale.

4.5. Application to a challenging case

4.5.1. The Madeira River at Fazenda Vista Alegre

The Madeira River is one of the two largest tributaries of the Amazon (including the Solimoes) by mean discharge, the other one being the Rio Negro. Arguably, the Madeira River would rank between the 4th and 8th largest rivers by mean discharge in the world [e.g., Latrubesse, 2008].

The main hydrometric station is at Fazenda Vista Alegre (GPS locations: 4°53′44.0″S, 60°01′19.9″W), Brazil, approximatively 92 km upstream of the auxiliary station of Borba (GPS locations: 4°23′06.9″S, 59°35′39.3″W). The Fazenda station covers a basin area of 1324700 km^2 with a mean interannual discharge of 31 000 $m^3.s^{-1}$. It is located at the downstream part of the catchment and is strongly influenced by important variable backwater effect [Callède et al., 2001] correlated with the yearly flood regime of the Amazon hydrosystem [Callède et al., 2002].

The river bed is covered with large sand dunes. The dynamics and relative submergence of such bedforms induce flow resistance to vary with stage [e.g., Karim, 1995]. Flow resistance computed from the gaugings was indeed observed to increase with stage, towards an apparently asymptotic value (cf. figure 4.10). The flow resistance coefficients can be computed using hydraulic radii R_h from the gaugings bathymetry profiles by inverting the Manning-Strickler formula $K_S = A\sqrt{S_0}R_h^{2/3}/Q$. As a first-order approach, possible hysteresis effects due to dune-flat bed transitions [Shimizu et al., 2009] are ignored in this work.

As variable backwater effects are always present even during major floods, transition to an unaffected channel control is no longer needed. Equation (4.8) is modified for a single control rating curve as follows:

$$Q\left(h_1, h_2\right) = K_S\left(h_1\right) B \left(h_1 - h_0\right)^M \sqrt{\frac{h_1 - h_2 - \delta_h}{L}} \quad \text{(variable slope)} \tag{4.15}$$

where the Strickler coefficient K_S can be considered to be either constant ($K_S = K_{\text{channel}}$) or to vary with stage. We propose the following empirical relation for modelling this stage-roughness relation:

$$K_S\left(h_1\right) = \begin{cases} K_{\text{channel}} - \alpha(h_1 - h_{\text{channel}})^2 & \text{if } \; h_1 \leq h_{\text{channel}} \\ K_{\text{channel}} & \text{if } \; h_1 > h_{\text{channel}} \end{cases} \tag{4.16}$$

where α is a coefficient, h_{channel} and K_{channel} are related to the high-flow asymptotic roughness. In the Bayesian analysis, the three parameters will be estimated as additional parameters of the SFD model.

Priors may be set up from the following considerations. Parameter α is expected to be positive since the Strickler coefficient (inverse to Manning's n) is expected to increase with increasing submergence of the bedforms. Assuming that K_{channel} cannot exceed the extreme value of 100 $\text{m}^{\frac{1}{3}}.\text{s}^{-1}$, for a possible difference of 10 m between stage h_1 and h_{channel}, parameter α needs to be smaller than 1 (otherwise $K_S < 0$). Therefore, a uniform distribution $\mathcal{U}(0,1)$ is set up as prior on parameter α. From the site configuration, the average roughness of the bankful channel K_{channel} is assessed to be 35 $\text{m}^{\frac{1}{3}}.\text{s}^{-1} \pm$ 10 $\text{m}^{\frac{1}{3}}.\text{s}^{-1}$. The stage h_{channel} is set up to 19 m $\pm$ 4 m.

The section between both gauges is a fairly straight reach with a mean width of 1200 m which can vary ($\pm$ 200 m) due to the presence of few small islands and a bend upstream of the auxiliary gauge. Cross-sectional shape is modelled as a wide rectangle, hence parameter M, the hydraulic exponent, is set to 1.667 $\pm$ 0.05. The channel offset h_0 is set to -3 m $\pm$ 1 m from available cross-sectional profiles surveyed at the station. The official value of the datum difference δ_h is -1.57 m. This value comes from quite uncertain topography measurements, due to the long distances, the difficult maintenance of staff gauges in such mega-river sites, and departures between geographical reference systems and the gravity-based hydraulic heads. This value obviously leads to conflicts since it induces marked negative slope values at low flows whereas reverse flows were never gauged. Uncertainty of this parameter is accordingly imposed to $\pm$ 2 m, i.e. the imprecise prior $\mathcal{N}(-1.57, 1)$ is specified.

Prior distributions based on this information are detailed in table 4.3. Three single-segment rating curve models are applied: constant slope channel control (SD model), SFD model with constant roughness, and SFD model with variable roughness.

The SFD model with variable roughness is applied considering either an imprecise or a precise prior on parameter δ_h. Two comparisons are made: the impact of the roughness model and the impact of the parameter δ_h on the SFD model. The results are shown in figure 4.11 and in table 4.3. Figure 4.11 is the propagation of the estimated rating curves from those three models over the 2001-2004 period (3 hydrological years). Figure 4.11-a corresponds to the comparison between the two prior options on the δ_h parameter for the SFD model with variable roughness, figure 4.11-b is the comparison between the constant roughness and the variable roughness options in the SFD model. All the models illustrate the yearly flood cycles: 3 floods

over this period with, for each flood, approximatively 5 months of rising limb and 7 months of falling limb.

The stage-discharge (SD) model is not appropriate for capturing the variable backwater effects. The maximum posterior (MAP) curve markedly overestimates discharges (up to more than 100%) at low flows and underestimates them (down to −11%) at high flows (cf. figure 4.11). Related uncertainties are very large (up to more than ± 100% at low flows and never less than ± 40%).

4.5.2. Variable roughness and influence of datum difference δ_h

Both SFD models with or without variable roughness yield good results at high flows: MAP curves agree well with gaugings and uncertainties fluctuate around ±10% of the discharge. At low flows the constant roughness option is unable to keep up the better results of the variable roughness option (figure 4.11-b). For discharges lower than 20000 $m^3.s^{-1}$, uncertainties are larger (between ± 25% and ± 70%) than for the variable roughness option (less than ± 25%).

The constant roughness option implies a calibration of the roughness parameter on the whole range of flow. This calibration leads to an overestimation of the roughness value: the model adjusts parameters h_0 and M to compensate for this high value. This leads to unrealistic values for the two parameters. The exponent value (1.78, in table 4.3), though realistic, does not match with the hydraulic assumptions of a wide rectangular cross-section (prior value 1.67 ± 0.05). All these results clearly show that accounting for the measured variable slope may not be enough to accurately estimate low flows, when modelling a variable roughness is also required.

Different priors on δ_h appear not to affect high flow estimates (figure 4.11-a): MAP values and uncertainty envelopes are the same whether or not the prior on δ_h is imprecise. Indeed, for high flows, the parameter δ_h has less influence on the computation of the variable slope. The stage-roughness (Strickler coefficient) relation is moderately affected by the prior information on δ_h (cf. figure 4.10). The widths of the uncertainty envelopes are the same but the MAP curves for precise but inaccurate prior on δ_h is further away from the manually computed Strickler coefficient curve. A too precise but inaccurate prior on δ_h also involves higher uncertainties at low flows. Below 20000 $m^3.s^{-1}$, uncertainties on discharges fluctuate between ± 25% and more than ± 400% instead of less than ± 25% using a imprecise prior. The slope is sometimes estimated to be negative over periods where reverse flows were never gauged nor observed. Then

the result is discarded and no discharge is computed (cf. blank spaces in Figure 4.11-a in the beginning of years 2002 and 2003 for the BaRatin SFD model with variable roughness and precise prior on σ_h). Therefore, in such a case the datum difference δ_h is preferred to be estimated from gaugings, as a free parameter of the SFD model. The prior uncertainty on this parameter has to be set up according to each situation but can be kept reasonably wide since this parameter has little interaction with the other ones.

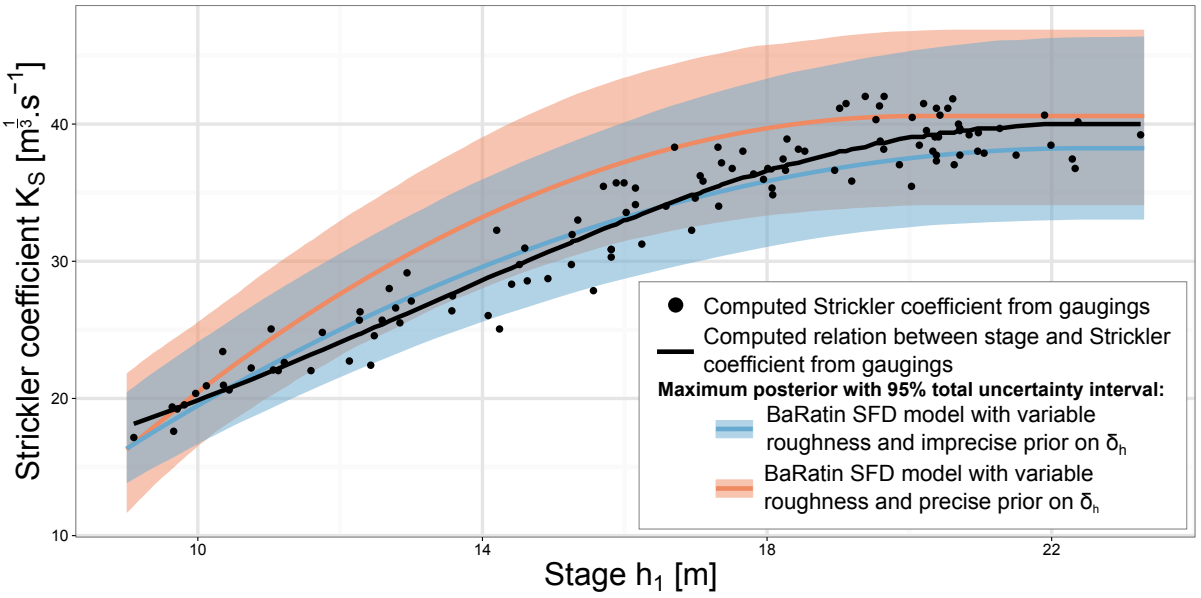

Figure 4.10 – Strickler flow resistance coefficient of the Madeira River at Fazenda, as a function of stage at main gauge: data derived from gaugings, and empirical functions calibrated either manually or automatically with Bayesian SFD models.

The BaRatin SFD model with variable roughness and imprecise prior on δ_h parameter yields good discharge estimations. Despite some very uncertain gaugings, MAP error values are always under 10% for the other gaugings (under 20% for all). Associated total uncertainty envelopes are also acceptable (less than ±25% for low flows and less than ± 10% for discharges $Q >$ 20000 $m^3.s^{-1}$). This case illustrates the limitations of the stage-fall-discharge approach: when flow resistance also varies as a function of flow depth, this has to be captured in the rating curve model in addition to the variable slope due to backwater effects. It also illustrates the importance of reflecting the real uncertainties of the prior information on the datum difference, δ_h, to accurately model low flow discharges.

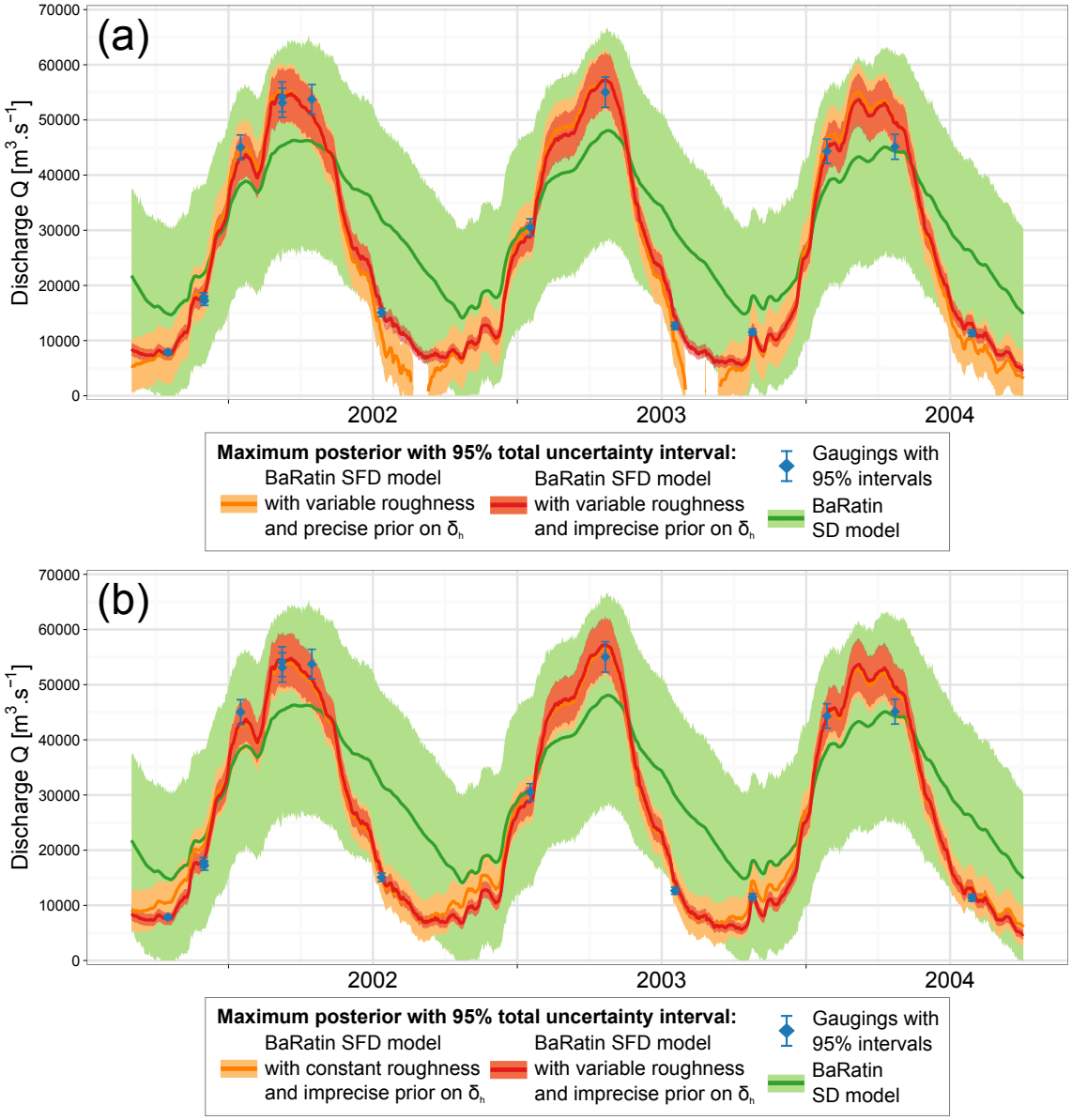

Figure 4.11 – The Madeira River at Fazenda over the 2001-2004 period: gaugings, MAP computed flow records and their 95% total uncertainties envelopes. (a) the SFD model with variable roughness is used for a comparison between two prior distributions on the datum difference δ_h: imprecise prior ($\pm$ 127% uncertainty) *vs.* precise prior ($\pm$ 1.27% uncertainty). (b) comparison of the variable and constant roughness options, both for a imprecise prior on δ_h. In both graphs, the results from the standard stage-discharge (SD) model are also plotted.

4.5.3. A flood-specific rating curve

For a better understanding of the BaRatin SFD model with variable roughness according to the yearly flood cycles, stage-discharge relations are represented in figure 4.12. MAP rating

curves and their total uncertainty envelopes over the 1980-2013 period are represented as well as for 5 contrasted hydrological years.

The rating curve of such phenomenon plots as a loop $h_1 - Q$ relation (cf. figure 4.12). The size and opening of the SFD rating curve of the Fazenda station depend on the magnitude of the Madeira flood and of the Amazon flood, respectively. The loops have the same direction as rating curves affected by hysteresis due to transient flows but differ by their characteristic bow-shapes: during the rising limb, the $h_1 - Q$ relation is more linear than during the falling limb, opposite to the usual shape of the hysteretic rating curves. The station is less influenced by the Amazon flows during the rising limb: the downstream and upstream stages increase in similar proportions. Conversely, during the falling limb the influence of the Amazon main stem increases. The energy slope decreases as the upstream stage h_1 decreases but the downstream stage decreases slowly, due to the slower dynamics of the Amazon flood. Energy slope values are then smaller than during the rising limb.

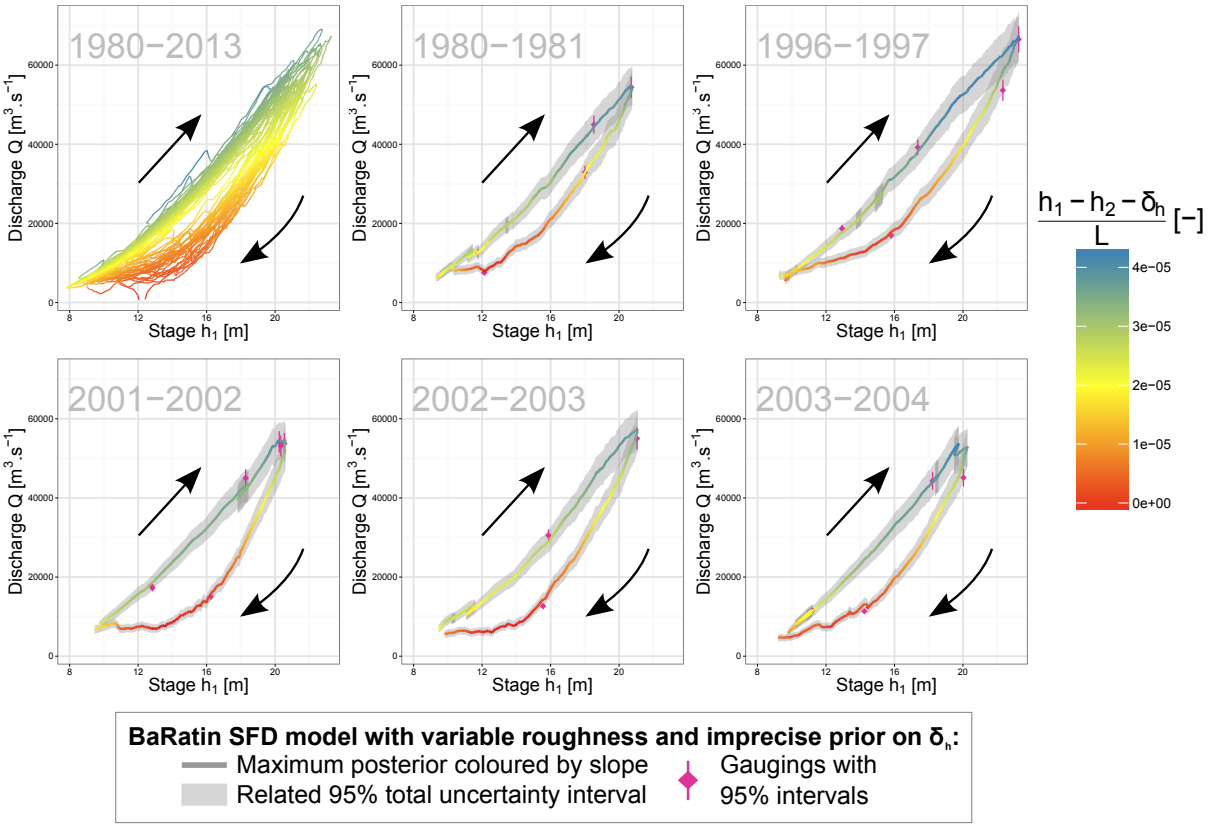

Figure 4.12 – The Madeira River at Fazenda: stage-discharge representation of the results from the SFD model with variable roughness and imprecise prior on datum difference δ_h. Maximum *a posteriori* (MAP) rating curves for the 1980-2013 period and five contrasted hydrological years are coloured according to the computed energy slope $(h_1 - h_2 - \delta_h)/L$.

Table 4.3 – Bayesian analysis of the stage-fall-discharge (SFD) rating curves of the Madeira River at Fazenda Vista Alegre: parameters, prior distributions and maximum *a posteriori* (MAP) results with 2.5% and 97.5% quantiles ($Q_{2.5}$ and $Q_{97.5}$).

BaRatin parameters	Physical parameters with units	Prior distributions	Results: MAP[$Q_{2.5}$; $Q_{97.5}$]			
			SD model	SFD model with constant K_S	SFD model with $K_S(h_1)$ variable	
					reasonable prior $\delta_h \sim \mathcal{N}(-1.57, 1)$	precise but inaccurate prior $\delta_h \sim \mathcal{N}(-1.57, 0.01)$
θ_1	B [m]	$\mathcal{N}(1200, 100)$	-	-	1245 [1061; 1404]	1296 [1096; 1436]
θ_1	$K_S B$ [$m^{\frac{1}{3}}.s^{-1}$]	$\mathcal{N}(42000, 3500)$	-	46896 [42593; 52864]	-	-
θ_1	$K_S B\sqrt{S_0}$ [$m^{\frac{1}{3}}.s^{-1}$]	$\mathcal{N}(1328, 350)$	240 [197; 287]	-	-	-
θ_2	h_0 [m]	$\mathcal{N}(-3, 0.5)$	−1.58 [−2.62; −0.56]	0.64 [−0.09, 2.40]	−2.90 [−3.72, −1.90]	−2.95 [−3.99; −2.11]
θ_3	$M = 5/3$ [−]	$\mathcal{N}(1.6667, 0.025)$	1.697 [1.644, 1.746]	1.780 [1.751, 1.828]	1.687 [1.644, 1.725]	1.674 [1.641; 1.725]
θ_4	L [m]	$\mathcal{N}(92000, 500)$	-	92021 [91017; 92951]	92038 [91030; 92993]	91749 [91038; 92906]
θ_5	h_{channel} [m]	$\mathcal{N}(19, 2)$	-	-	22.46 [21.00; 23.99]	20.13 [18.13; 21.43]
θ_6	α [$m^{-\frac{5}{3}}.s^{-1}$]	$\mathcal{U}(0, 1)$	-	-	0.121 [0.096; 0.161]	0.196 [0.136; 0.318]
θ_7	K_{channel} [$m^{\frac{1}{3}}.s^{-1}$]	$\mathcal{N}(35, 5)$	-	-	38.23 [33.04; 46.41]	40.59 [34.09; 46.88]
θ_8	δ_h [m]	$\mathcal{N}(-1.57, 1)$	-	−1.90 [−2.05; −1.83]	−1.98 [−2.03; −1.92]	−1.59 [−1.62, −1.58]
γ_1	- [$m^3.s^{-1}$]	$\mathcal{U}(0, 10^6)$	8596 [3189; 9324]	2060 [186; 2537]	126 [13; 598]	2472 [2063; 2874]
γ_2	- [−]	$\mathcal{U}(0, 10^6)$	0.00024 [0.0011; 0.19]	0.0022 [0.00047; 0.052]	0.041 [0.024; 0.054]	0.00015 [0.00011; 0.013]

4.6. Conclusions and perspectives

To avoid some assumptions made in the model proposed by Petersen-Øverleir and Reitan [2009a] for the Bayesian analysis of stage-fall-discharge rating curves, we introduced an alternative model accounting for transition between a backwater-affected control and a backwater-unaffected control. The main differences lie in the definition of distinct parameters for both controls and in solving transition between controls using continuity conditions only. The new model also acknowledges the uncertain nature of the difference in reference levels of the main and auxiliary gauges.

The robustness of this new model was investigated through sensitivity analyses to the prior information and to the gaugings dataset. When the stage-fall-discharge domain is well documented with gaugings, the performance of the new model appears to be acceptable for hydrometric applications. In particular, transition to backwater-unaffected flow was correctly simulated in the Rhône River at Valence station, discharge estimates are in good agreement with gaugings, and uncertainty bounds are usually acceptable. The example of a section control combined with a variable slope channel control (Guthusbekken) yielded acceptable though less convincing results, likely due to limitations in both hydraulic knowledge and gaugings available at that site.

A challenging channel-controlled case, the Madeira at Fazenda Vista Alegre, eventually showed the limitations of the stage-fall-discharge approach: in that large sand-bed river with large dune systems, flow resistance also varies as a function of flow depth, and this has to be captured in the rating curve model, in addition to variable slope due to backwater from the Amazon main stem. This difficult case also illustrates the interest of estimating the difference in staff gauge reference levels, when this parameter bears non negligible uncertainties.

With such improvements brought to the Bayesian approach initiated by Petersen-Øverleir and Reitan [2009a], the method now appears as a mature and credible solution to the issue of stage-fall-discharge rating curves, and as a substitution for the graphical and empirical techniques still proposed in hydrometry guidance and standards [e.g., ISO 9123:2001, 2001]. It has been operationally deployed by the Compagnie Nationale du Rhône (CNR) for developing SFD rating curves at their twin-gauge stations. The method provides rating curve results in both functional and table formats; uncertainty results come as probabilistic distributions from which any statistics can be derived. The uncertainty analysis is compliant with the concepts of the Guide for the expression of the Uncertainty in Measurement (GUM, e.g., JCGM 100:2008 [2008]) and could embed the propagation of stage record uncertainties.

Chapter 5

Rating changes due to bed evolution

This chapter is planned to be published soon.

Contents

5.1. Introduction

5.1.1. Rating changes

Various types of rating changes may occur temporally according to more or less complex processes (bed evolution, vegetation growth, debris/ice jams, dike break, etc.). The mechanisms behind these processes are not addressed in this chapter but comprehensive reviews can be found in the literature [e.g., Schumm, 1977, Schumm and Winkley, 1994, Knighton, 1998].

Rating changes lead to the modification of the elements controlling stage-discharge relation through changes in the channel geometry, its roughness or the type of control. These modifications imply changes in the rating curve parameters, and possibly in the equation itself. There are two types of rating changes due to bed evolution: a net change refers to the difference between two stable rating curves before and after the morphogenic event; a transient change is a continuous evolution of the stage-discharge relation during the morphogenic event (e.g. transient scour-fill) or even after the morphogenic event (gradual adjustments of the local topography). We do not address the issue of transient changes: only net changes between two rating curves are studied in this chapter.

Generally, the low-flow section control is more frequently affected by net changes than the high-flow channel control. This is because the section controls are sensitive to local fluctuations in the bed topography whereas the channel controls are not. Both section controls and channel controls are affected by changes in the whole channel controlling reach (such as degradation/aggradation or widening/narrowing of the channel reach). Hence, minor flood events may induce changes at low flows whereas greater flood events are required to induce changes at high flows.

The main issues related to rating changes include the detection of rating change times and the estimation of successive rating curves with their associated uncertainties. The former issue is not treated in this manuscript but should be addressed in further developments.

5.1.2. Rating changes in operational practices

Once the times of rating changes are identified, the common practice is to assess the stage-discharge relation by estimating steady rating curves for each period of validity defined by these

detected times [Rantz, 1982b, WMO No. 1044, 2010]. It is hence assumed that the hydraulic controls are stable over these periods . Several practices exist:

(1) a naive practice is to estimate each of these steady rating curves from scratch, using only gaugings performed during the period of validity of the stage-discharge relation. It is problematic because it is not always possible to re-gauge the SD relation over its whole range of variability. Indeed, at some stations, flood events frequently yield rating changes: the upper segments (high flows) are thus not always gauged. Therefore, the quality of the rating curve assessment is fully controlled by the available information, i.e. the number of gaugings performed between two rating changes;

(2) sometimes some gaugings are kept from older periods (especially high-flow gaugings) when they are assumed unaffected by the rating change. However, as with the previous practice, the rating curve is re-estimated from scratch without transferring the information from the previous periods. It therefore still takes many gaugings to properly assess the rating curve, which is not always possible. For instance, in France usually, the rating curve after a rating change is officially updated once a new set of gaugings is available to establish the new rating curve;

(3) another common practice is to use some measurements across periods but start with the information brought by a 'base' curve or by the rating curve of the previous period, as illustrated by Burkham and Dawdy [1970]. In this practice, rating curve parameters are often estimated or adjusted one at a time, verifying between each of these estimations the goodness-of-fit with discharge measurements. This practice is common in North America [e.g., Rantz, 1982b, WMO No. 1044, 2010, Environment Canada, 2016], but usually changes in offsets only are assessed (handled). These changes are deviations from a 'base' rating curve: a ratio describing the discrepancy between this base curve and observations is used to compute a correction (or 'shift') to apply to the base curve. For this practice, parameter changes need to be estimated with at least a few new discharge measurements.

Note that some practices impose a 'convergence' point to the successive rating curves [Rantz, 1982b, WMO No. 1044, 2010, Morlot et al., 2014]. All rating curves are assumed to converge at this particular point. Above this point it is sometimes assumed that a unique steady rating curve, or an upper 'convergence segment' applies. This is equivalent to using 'knee-bend' or 'truss' patterns for the rating shifts described in Environment Canada [2016]. Log scales used to plot SD relations may give the false impression that parallel rating curves converge at high

flows. However, the 'convergence' point or the 'base curve' methods should not be applied systematically, without a site- and event-specific expertise. Indeed, some stage-discharge relations changes up to the upper segment: the assumptions of a 'convergence' point or segment no longer apply and may bring misleading extrapolation results.

As highlighted by Reitan and Petersen-Øverleir [2011], these practices need discharge measurements which are not always available in sufficient quantity: the uncertainties of the resulting streamflow data may be very large when there are not many gaugings. Last, the correction ratio is sometimes computed using only the discharge measurement values, without taking into account their uncertainties. Therefore, a highly uncertain discharge measurement may be misinterpreted as the sign of a new rating change.

5.1.3. Rating changes in the research literature

Some proposed methods tackle the problem of changing rating curve by modelling the evolution of the cross-sectional shape as a change of roughness in the rating curve [e.g., Leonard et al., 2000]. Although this has shown acceptable results, some limitations can be pointed out as these methods are site-specific and cannot be applied to any station.

A few other methods account for rating changes through the rating curve assessment. McMillan et al. [2010] investigate the uncertainties in the stage-discharge relation induced by cross-sectional changes due to scour, transport and deposition of sediment. These uncertainties are quantified under epistemic error scenarios. For a given stage, a probability-density function of true discharge is computed and used in a likelihood function. Rating curve parameters are finally calibrated using a Markov Chain Monte Carlo (MCMC) method. Westerberg et al. [2011] also assessed uncertainties from cross-sectional changes but rating curve calibration is made with a fuzzy-regression approach. Reitan and Petersen-Øverleir [2011] propose a stage-time-discharge model with time-varying rating curve parameters implemented as an Ornstein-Uhlenbeck processes (continuous time stochastic processes). Ornstein-Uhlenbeck processes corresponds to the continuous-time analogue of autoregressive models of order one. Estimation of the parameters of their stage-time-discharge model is performed using a Bayesian framework and MCMC simulation techniques. The temporal variations of rating curve parameters can be hence determined by their method from the information available in the gaugings. Guerrero et al. [2012] also explore the temporal variability of rating curves and related uncertainties using the GLUE methodology.

Morlot et al. [2014] propose a dynamic method for assessing rating curves uncertainties. In their method, each gauging is seen as an individual realisation of the current rating curve. The

method leads to computing as many rating curves as there are gaugings at a hydrometric station. An uncertainty model is associated with each of these rating curves. It takes into account the stage record uncertainties, the discrepancy between rating curves and gaugings, uncertainties from gaugings and the 'aging' of the computed rating curves. This 'aging' is assessed using a variographic analysis proposed by Jalbert et al. [2011]. This dynamic method starts to be operationally implemented by Électricité De France (EDF), the first French power company but remains specific to their station management procedures: frequent gaugings are needed to ensure the acceptability of the rating curve results.

McMillan and Westerberg [2015] include both random and epistemic error components in a single likelihood function to assess rating curve uncertainty including the uncertainty induced by rating changes. This method does not require prior specification of the particular types and causes of epistemic error at the hydrometric station and therefore can be easily applied to a wide range of catchments.

All these methods are heavily based on gaugings and hence uncertainty results depend on the number and frequency of available discharge measurements. Since collecting many gaugings for a frequently-changing rating curve is challenging, it seems particularly relevant to also use information on the hydraulic configuration as efficiently as possible. It could be also a first step for real-time applications as the rating curve estimation can be performed with the hydraulic configuration only, before any new gauging is available.

5.1.4. Objectives

In this chapter, we will only focus on the issues of modelling the changing rating curve and assessing the associated uncertainties. The detection of the times of rating changes is left aside: we therefore work assuming the periods are known. This detection should be further investigated in future work, as a second step towards a fully operational method, applicable in real-time. Before that, we need to develop a robust method for estimating the rating curves and changes, based on physical priors and gaugings. Transient changes and continuous transitions of rating curves between periods such as 'phasing', 'merging' and 'blending' are also left aside in this chapter.

The proposed model in this chapter is a Bayesian analysis based on steady stage-discharge rating curves, with the knowledge of the period of validity of these rating curves. It incorporates information from hydraulic knowledge and stage-period-discharge observations (gauging data). Moreover, the proposed model avoids deciding whether or not a particular gauging is relevant

for several periods. Indeed, gaugings are always assigned to the period during which they were performed: it is the rating curve parameters that may or may not change across periods. Both changes in coefficients and offsets of the rating curves are considered by the model: the practitioner has to decide which parameters may change between periods. Information on changes is transferred across periods: if a change is precisely identified at a given period, it should help estimating the rating curve for nearby periods. Information on change is also transferred between controls: if a change is precisely identified for the main channel, it should help estimating the changes for the low-flow controls as changes in channel controls may affect changes in low-flow section controls. The obtained total uncertainty combines parametric uncertainty (estimation of the rating curve parameters) and structural uncertainty (imperfection of the rating curve model). This method provides the estimation of the rating change across periods.

The application of the proposed method is illustrated with two case studies:

(a) the Ardèche River at Meyras station, France. Rating changes are due to marked bed degradation after floods. This station has well-gauged stage-discharge rating curves for stable periods;

(b) the Wairau River at Barnett's Bank station, New Zealand. This is a complex site with frequent rating changes. Some periods have few or no gaugings, in spite of very frequent gauging operations.

Further exploration of the stage-period-discharge (SPD) rating curve estimation process is presented:

- the evaluation of the transfer of information between controls;
- the evaluation of the transfer of information between periods;
- the comparison with the naive strategy of re-estimating a steady stage-discharge model from scratch for each stable period, independently.

5.2. Vocabulary, notations and assumptions

In the remainder of this chapter, it is assumed that the stage-discharge relation is governed by N_c controls: a succession (activation or deactivation) of N_s section controls, then a channel control (riverbed) and finally a succession (activation only) of $N_c - N_s - 1$ floodways (channel controls). For example, the following describes a common situation: a succession of $N_s = 2$ section controls, then a channel control, then an additional floodway control ($N_c = 4$). The matrix of controls $\mathcal{M}$ (defined in section 2.2.4) can be written as follows:

$$\mathcal{M} = \begin{array}{c} 1 \\ N_s{=}2 \\ 3 \\ N_c{=}4 \end{array} \begin{bmatrix} 1 & 0 & 0 & 0 \\ 0 & 1 & 0 & 0 \\ 0 & 0 & 1 & 0 \\ 0 & 0 & 1 & 1 \end{bmatrix}$$

'Change' or 'rating change' refers to any modification of the stage-discharge relation. A 'stable period' is defined by any period of time between two consecutive changes. The 'reference period' is the period from which all deviations are computed. Generally, the reference period is chosen so as to maximise the available information.

Let N_{change} denote the number of changes. There are hence $N_{change} + 1$ periods. Periods are numbered in increasing order from the most recent period to the oldest. The reference period is numbered k_{ref}. Any period older than the reference period has an index greater than k_{ref}, $k_{ref} \in [\![1, N_{change} + 1]\!]$ (for instance $k_{ref} + 1$, $k_{ref} + 2$, etc.) and any period more recent has an index smaller than k_{ref} (for example $k_{ref} - 1$, $k_{ref} - 2$, etc.).

The rating curve model developed in this chapter makes the following restrictive assumptions:

- the dates of stable periods are known;
- the matrix of controls does not change, i.e. controls cannot be created or deleted;
- exponents c of the control equations $Q = a(h - b)^c$ do not change, i.e. the physical properties of a control may change but neither its type nor its geometrical shape (e.g. a rectangular cross-section control cannot become triangular).

The first assumption implies that we do not tackle the issue of *detecting* changes. Instead we solely focus on modelling rating curves subject to net changes at known dates. The model developed in this chapter is therefore called the stage-period-discharge (SPD) model, to make it clear that the period is a known input of the model.

5.3. The stage-period-discharge (SPD) model

5.3.1. Rating curve equation for several periods

Following the notations of section 5.2, the rating curve equation $Q^{(k)}(h)$ for the k-th period can be written as follows:

$$Q^{(k)}(h) = \sum_{i=1}^{N_{\text{seg}}} \left(\mathbf{1}_{\left[\kappa_{i-1}^{(k)};\kappa_i^{(k)}\right[}(h) \sum_{j=1}^{N_{\text{c}}} \mathcal{M}(i,j)\, a_j^{(k)} \left(h - b_j^{(k)}\right)^{c_j} \right) \tag{5.1}$$

where:

- h is the stage;
- Q is the discharge;
- N_{seg} is the number of segments. This yields $N_{\text{seg}}+1$ transition stages $\kappa_i^{(k)},\ i \in [\![0, N_{\text{seg}}]\!]$, with $\kappa_0^{(k)} = b_1^{(k)}$;
- $\mathcal{M}(i,j)$ is the matrix of controls (see section 2.2.4), taking 1 if the control is active, 0 otherwise. As creation or deletion of controls are not allowed (see assumptions in section 5.2), the matrix $\mathcal{M}$ does not change between periods;
- the function $\mathbf{1}_{\left[\kappa_{i-1}^{(k)};\kappa_i^{(k)}\right[}(h)$ is the indicator function of the interval $\left[\kappa_{i-1}^{(k)};\kappa_i^{(k)}\right[$ equal to 1 if h belongs to this interval and 0 otherwise;
- $a_j^{(k)}$, $b_j^{(k)}$ and c_j are the parameters of the rating curve equation for period k. $a_j^{(k)}$ is the coefficient related to the characteristics of the control j, $b_j^{(k)}$ is the offset and c_j is the exponent related to the type of control (which does not depend on k, see assumptions in section 5.2).

The transition stage $\kappa_i^{(k)}$ can be deduced from other parameters using a discharge continuity condition for $h = \kappa_i^{(k)}$ between the i-th control and the $(i+1)$-th control. If the $(i+1)$-th control adds to the i-th control, the transition stage $\kappa_i^{(k)}$ is equal to the offset $b_{i+1}^{(k)}$ of the $(i+1)$-th control. Conversely, if the $(i+1)$-th control replaces the i-th control, the discharge continuity condition leads to:

$$a_i^{(k)} \left(\kappa_i^{(k)} - b_i^{(k)}\right)^{c_i} - a_{i+1}^{(k)} \left(\kappa_i^{(k)} - b_{i+1}^{(k)}\right)^{c_{i+1}} = 0. \tag{5.2}$$

The Newton-Raphson algorithm is used to solve numerically equation (5.2) and find the transition stage $\kappa_i^{(k)}$.

Note that this is different from what is done in the current operational version of BaRatin, where parameters b, not κ, are deduced using a discharge continuity equation. To address stage-discharge changes due to bed evolution, it is more convenient to work with offsets rather than transition stages.

5.3.2. The matrix of changes

Changes of parameters between two successive periods are described by the matrix $\mathcal{MC}$ called the 'matrix of changes'. It is a $(N_{\text{change}}+1; 3N_{\text{c}})$ matrix defined by:

$$\mathcal{MC}(k,j) = \begin{cases} -1 & \text{if } k = k_{\text{ref}} \text{ (dummy value indicating the reference period)} \\ 1 & \text{if the } j^{\text{th}} \text{ parameter changes at the } k^{\text{th}} \text{ period} \\ 0 & \text{if the } j^{\text{th}} \text{ parameter does not change at the } k^{\text{th}} \text{ period} \end{cases} \tag{5.3}$$

The matrix $\mathcal{MC}$ just below is a general example of a matrix of changes assuming that only offsets $b_j^{(k)}$ may change between periods for all the controls (*wrt* stands for *with respect to*).

$\mathcal{MC}$

		Rating curve parameters									
		1st control			2nd control			...	N_{c}-th control		
	k	$a_1^{(k)}$	$b_1^{(k)}$	$c_1^{(k)}$	$a_2^{(k)}$	$b_2^{(k)}$	$c_2^{(k)}$	...	$a_{N_{\text{c}}}^{(k)}$	$b_{N_{\text{c}}}^{(k)}$	$c_{N_{\text{c}}}^{(k)}$
Recent	1	0	1	0	0	1	0	...	0	1	0
	2	0	1	0	0	1	0	...	0	1	0
	3	0	1	0	0	1	0	...	0	1	0
	⋮	⋮	⋮	⋮	⋮	⋮	⋮	...	⋮	⋮	⋮
	$k_{\text{ref}}-1$	0	1	0	0	1	0	...	0	1	0
Period	k_{ref}	−1	−1	−1	−1	−1	−1	...	−1	−1	−1
	$k_{\text{ref}}+1$	0	1	0	0	1	0	...	0	1	0
	⋮	⋮	⋮	⋮	⋮	⋮	⋮	...	⋮	⋮	⋮
	$N_{\text{change}}-1$	0	1	0	0	1	0	...	0	1	0
Old	N_{change}	0	1	0	0	1	0	...	0	1	0
	$N_{\text{change}}+1$	0	1	0	0	1	0	...	0	1	0

change *wrt* period 2+1

reference period

change *wrt* period $N_{\text{changes}}-1$

The row number k_{ref} indicates the reference period. It is filled with -1 which are just used as dummy values to identify the reference row. Other rows are interpreted depending on their position with respect to the reference row:

- if the row k has a greater index than the reference row (i.e. the period is older than the reference period), value 1 indicates that the parameter changes with respect to the period $k-1$ (and value 0 indicates no change);
- if the row k has a smaller index than the reference row (i.e. the period is more recent than the reference period), value 1 indicates that the parameter changes with respect to the period $k+1$.

Note that in the matrix $\mathcal{MC}$ presented just above, values of columns of exponent c_j are set to zero. Indeed, it corresponds to the assumption that the types of controls (weir, channel, etc.) do not change over periods.

Changes of parameters between the k-th period and the reference period are quantified by deviations parameters $\Delta a_j^{(k)}$ and $\Delta b_j^{(k)}$, $k \neq k_{\text{ref}}$. They are called *cumulated* changes (for coefficients and offsets, respectively). The parameters of each period can be written as functions of the cumulated changes:

$$
\forall k < k_{\text{ref}},\ \begin{cases} a_j^{(k)} = \begin{cases} a_j^{(k+1)} & \text{if } \mathcal{MC}\,(k, 3(j-1)+1) = 0 \quad \text{(no change);} \\ a_j^{(k_{\text{ref}})}\left(1 - \Delta a_j^{(k)}\right) & \text{if } \mathcal{MC}\,(k, 3(j-1)+1) = 1 \quad \text{(change);} \end{cases} \\ b_j^{(k)} = \begin{cases} b_j^{(k+1)} & \text{if } \mathcal{MC}\,(k, 3(j-1)+2) = 0 \quad \text{(no change);} \\ b_j^{(k_{\text{ref}})} - \Delta b_j^{(k)} & \text{if } \mathcal{MC}\,(k, 3(j-1)+2) = 1 \quad \text{(change);} \end{cases} \end{cases}
$$

$$
\forall k > k_{\text{ref}},\ \begin{cases} a_j^{(k)} = \begin{cases} a_j^{(k-1)} & \text{if } \mathcal{MC}\,(k, 3(j-1)+1) = 0 \quad \text{(no change);} \\ a_j^{(k_{\text{ref}})}\left(1 - \Delta a_j^{(k)}\right) & \text{if } \mathcal{MC}\,(k, 3(j-1)+1) = 1 \quad \text{(change);} \end{cases} \\ b_j^{(k)} = \begin{cases} b_j^{(k-1)} & \text{if } \mathcal{MC}\,(k, 3(j-1)+2) = 0 \quad \text{(no change);} \\ b_j^{(k_{\text{ref}})} - \Delta b_j^{(k)} & \text{if } \mathcal{MC}\,(k, 3(j-1)+2) = 1 \quad \text{(change);} \end{cases} \end{cases}
\tag{5.4}
$$

Note that changes of the reference coefficients $a_j^{(k_{\text{ref}})}$ are expressed multiplicatively because these parameters are factors of the stage h in the basic control equation $Q = a(h-b)^c$. Alternatively, changes of the reference offsets $b_j^{(k_{\text{ref}})}$ are expressed additively as they are linked with stage h by addition.

5.4. Bayesian inference

5.4.1. Parameterisation

Let $\boldsymbol{\theta} = (\boldsymbol{\theta_{RC}}, \boldsymbol{\gamma})$ denote the inferred parameters where parameters $\boldsymbol{\theta_{RC}}$ are the SPD rating curve parameters and parameters $\boldsymbol{\gamma} = (\gamma_1, \gamma_2)$ are the parameters of the error model. $\boldsymbol{\theta}$ takes the following form:

$$\boldsymbol{\theta} = \Big(\underbrace{\boldsymbol{\theta^{(k_{ref})}}}_{(k_{\text{ref}})\text{-th period}}, \underbrace{\boldsymbol{\theta^{(1)}}}_{1^{\text{st}}\text{ period}}, \ldots, \underbrace{\boldsymbol{\theta^{(k_{ref}-1)}}}_{(k_{\text{ref}}-1)\text{-th period}}, \underbrace{\boldsymbol{\theta^{(k_{ref}+1)}}}_{(k_{\text{ref}}+1)\text{-th period}}, \ldots, \underbrace{\boldsymbol{\theta^{(N_{change}+1)}}}_{(N_{\text{change}}+1)\text{-th period}}, \boldsymbol{\gamma} \Big) \tag{5.5}$$

where:

$$\boldsymbol{\theta^{(k_{ref})}} = \Big(\underbrace{\theta_1^{(k_{\text{ref}})}, \theta_2^{(k_{\text{ref}})}, \theta_3^{(k_{\text{ref}})}}_{1^{\text{st}}\text{ control}}, \ldots, \underbrace{\theta_{3N_c-2}^{(k_{\text{ref}})}, \theta_{3N_c-1}^{(k_{\text{ref}})}, \theta_{3N_c}^{(k_{\text{ref}})}}_{N_c\text{-th control}} \Big)$$

Note that parameters $\boldsymbol{\gamma}$ of the structural error model, defined in section 2.4.1, are not assigned to any period: they are assumed to remain constant across periods.

For all $k \neq k_{\text{ref}}$, vector $\boldsymbol{\theta^{(k)}}$ represents the couple of cumulated change parameters $\Delta a_j^{(k)}$ and $\Delta b_j^{(k)}$, filled in this order and sorted by the number of controls of the k-th period. In this vector, for each control, only cumulated change parameters for which rating curve parameters change are specified. In the example related to section 5.3.2, vectors $\boldsymbol{\theta^{(k)}}$ take the following form:

$$\forall k \in [\![1; N_{\text{change}}+1]\!], k \neq k_{\text{ref}},\ \boldsymbol{\theta^{(k)}} = \Big(\underbrace{\theta_1^{(k)}}_{\Delta b_1^{(k)}\ 1^{\text{st}}\text{ control}} \ldots \underbrace{\theta_{N_c}^{(k)}}_{\Delta b_{N_c}^{(k)}\ N_c\text{-th control}} \Big)$$

5.4.2. Likelihood computation

As described in section 2.4.1, gaugings $\left(\widetilde{h}_i, \widetilde{k}_i, \widetilde{Q}_i\right)_{i \in [\![1;N]\!]}$ are seen as the N estimates of the N real values $(h_i, k_i, Q_i)_{i \in [\![1;N]\!]}$ of stages, periods and associated discharges. As dates of changes are imposed known, we assume that $\forall i \in [\![1; N]\!],\ \widetilde{k}_i = k_i \in [\![1, N_{\text{changes}}+1]\!]$. Each gauging is,

therefore, associated to the stable period k_i during which it was performed. We also further assume that stage errors are negligible compared to discharge errors:

$$\begin{cases} \widetilde{h}_i = h_i \\ \widetilde{k}_i = k_i \\ \widetilde{Q}_i = Q_i + \epsilon_{Q,i} \quad \text{with} \quad \epsilon_{Q,i} \overset{\text{indep.}}{\sim} \mathcal{N}\left(0, u_{Q,i}\right) \end{cases} \tag{5.6}$$

where the standard deviations $u_{Q,i}$ (uncertainties of discharge measurements) are assumed to be known (see section 2.3).

The true discharge is then written as the discharge predicted by the rating curve plus a structural error:

$$Q_i = \underbrace{f\left(h_i, k_i \middle| \boldsymbol{\theta}_{\mathbf{RC}}^{(\boldsymbol{k_i})}\right)}_{\widehat{Q}_i} + \epsilon_{f,i} \quad \text{with} \quad \epsilon_{f,i} \overset{\text{indep.}}{\sim} \mathcal{N}\left(0, \sigma_{f,i} = \gamma_1 + \gamma_2 \widehat{Q}_i\right) \tag{5.7}$$

where $\boldsymbol{\theta}_{\mathbf{RC}}^{(\boldsymbol{k_i})} = \left(\boldsymbol{\theta}^{(\boldsymbol{k_{\text{ref}}})}, \boldsymbol{\theta}^{(\boldsymbol{k_i})}\right)$ are the rating curve parameters of the period k_i (for $k_i = k_{\text{ref}}$, $\boldsymbol{\theta}_{\mathbf{RC}}^{(\boldsymbol{k_i})} = \boldsymbol{\theta}^{(\boldsymbol{k_{\text{ref}}})}$), $\boldsymbol{\epsilon_f} = (\epsilon_{f,1}, \ldots, \epsilon_{f,N})$ are the structural errors, $(\sigma_{f,1}, \ldots, \sigma_{f,N})$ are the standard deviations of the structural errors $(\epsilon_{f,1}, \ldots, \epsilon_{f,N})$ and $\widehat{\boldsymbol{Q}} = \left(\widehat{Q}_1, \ldots, \widehat{Q}_N\right)$ are the discharge estimations related to the N gaugings (see section 2.4.1).

The linear function used for modelling the standard deviation $\sigma_{f,i}$ is the same as that described in section 2.4.1. We also assume that the structural errors $(\epsilon_{f,1}, \ldots, \epsilon_{f,N})$ and the discharge errors $(\epsilon_{Q,1}, \ldots, \epsilon_{Q,N})$ are independent.

Combining equations (5.6) and (5.7) yields the following stage-period-discharge relation between observed values:

$$\widetilde{Q}_i = f\left(\widetilde{h}_i, \widetilde{k}_i \middle| \boldsymbol{\theta}_{\mathbf{RC}}^{(\widetilde{\boldsymbol{k}}_{\boldsymbol{i}})}\right) + \epsilon_{Q,i} + \epsilon_{f,i} \quad \text{with} \quad \epsilon_{Q,i} + \epsilon_{f,i} \sim \mathcal{N}\left(0, \sqrt{\sigma_{f,i}^2 + u_{Q,i}^2}\right) \tag{5.8}$$

The likelihood L of observed discharge values $\widetilde{\boldsymbol{Q}}$ for the stage-period-discharge (SPD) model is given by:

$$L\left(\widetilde{\boldsymbol{Q}} \middle| \boldsymbol{\theta} = (\boldsymbol{\theta}_{\mathbf{RC}}, \boldsymbol{\gamma}), \widetilde{\boldsymbol{h}}, \widetilde{\boldsymbol{k}}\right) = \prod_{i=1}^{N} p_{\text{norm}}\left[\widetilde{Q}_i \middle| f\left(\widetilde{h}_i, \widetilde{k}_i \middle| \boldsymbol{\theta}_{\mathbf{RC}}^{(\widetilde{\boldsymbol{k}}_{\boldsymbol{i}})}\right), \sqrt{\sigma_{f,i}^2 + u_{Q,i}^2}\right] \tag{5.9}$$

where $\widetilde{\boldsymbol{Q}} = \left(\widetilde{Q}_1, \ldots, \widetilde{Q}_N\right)$ are the N gauged discharge, $\widetilde{\boldsymbol{h}} = \left(\widetilde{h}_1, \ldots, \widetilde{h}_N\right)$ are the N observed stage values, $\widetilde{\boldsymbol{k}} = \left(\widetilde{k}_1, \ldots, \widetilde{k}_N\right)$ are the related periods and $p_{\text{norm}}[z|m, s]$ denote the probability density function (pdf) of a Gaussian distribution with mean m and standard deviation s,

evaluated at some value z. Moreover, $\boldsymbol{\theta}_{\mathbf{RC}}^{(\boldsymbol{k})}$ denotes the corresponding rating curve parameters assigned to the period k.

As an aside, equation (5.9) implies that each gauging is assigned to one (and only one) specific period. This is to be contrasted with the standard practice of using some gaugings across several periods (typically high-flow gaugings), arguing that they remain representative of the stage-discharge relation despite the changes (that typically affect low flows). In the SPD model, it is the stable parameters that are used across periods.

Indeed, consider the simple example of a single-control rating curve changing only in offset between two stable periods (number 1 and 2) and that only 2 gaugings were performed for each of the two periods. Let $\widetilde{\boldsymbol{Q}} = \left(\widetilde{Q}_1, \widetilde{Q}_2, \widetilde{Q}_3, \widetilde{Q}_4\right)$ denotes these gaugings (ordered by periods in this example) and let $\widetilde{\boldsymbol{h}} = \left(\widetilde{h}_1, \widetilde{h}_2, \widetilde{h}_3, \widetilde{h}_4\right)$ and $\widetilde{\boldsymbol{k}} = \left(\widetilde{k}_1 = 1, \widetilde{k}_2 = 1, \widetilde{k}_3 = 2, \widetilde{k}_4 = 2\right)$ be their related stage and period values, respectively.

The rating curves for the two periods are given by:

$$\begin{cases} Q^{(1)}(h) & = a\left(h - b^{(1)}\right)^c \\ Q^{(2)}(h) & = a\left(h - b^{(2)}\right)^c \end{cases} \tag{5.10}$$

Therefore, the likelihood L takes the following form:

$$\begin{aligned} L\left(\widetilde{\boldsymbol{Q}} \middle| c, b^{(1)}, b^{(2)}, \boldsymbol{\gamma}, \tilde{\boldsymbol{h}}, \tilde{\boldsymbol{k}}\right) = \quad & p_{\text{norm}}\left[\widetilde{Q}_1 \middle| f(\tilde{h}_1, \widetilde{k}_1 = \mathbf{1} \middle| a, c, b^{(\mathbf{1})}), \sqrt{\sigma_{f,1}^2 + u_{Q,1}^2}\right] \\ & \times p_{\text{norm}}\left[\widetilde{Q}_2 \middle| f(\tilde{h}_2, \widetilde{k}_2 = \mathbf{1} \middle| a, c, b^{(\mathbf{1})}), \sqrt{\sigma_{f,2}^2 + u_{Q,2}^2}\right] \\ & \times p_{\text{norm}}\left[\widetilde{Q}_3 \middle| f(\tilde{h}_3, \widetilde{k}_3 = \mathbf{2} \middle| a, c, b^{(\mathbf{2})}), \sqrt{\sigma_{f,3}^2 + u_{Q,3}^2}\right] \\ & \times p_{\text{norm}}\left[\widetilde{Q}_4 \middle| f(\tilde{h}_4, \widetilde{k}_4 = \mathbf{2} \middle| a, c, b^{(\mathbf{2})}), \sqrt{\sigma_{f,4}^2 + u_{Q,4}^2}\right] \end{aligned} \tag{5.11}$$

Parameters a and c appear in all 4 terms of this quadruple product. Their estimation is hence informed by all available gaugings (4 gaugings). Conversely, each offset only appears in 2 terms of the quadruple product. Their estimation is hence only informed by gaugings of the related period (2 gaugings each).

This simple example highlights the difference with techniques based on the 'aging' of gaugings as such 'aging' is not needed in the SPD model because of information transfer between periods through the stable parameters (here, a and c).

5.4.3. Prior specification: introducing alternative parameterisations

Bayesian inference requires specifying a prior distribution for the vector of parameters $\boldsymbol{\theta}$ as described in section 5.4.2. However, the prior information that the practitioner may have is not always consistent with this parameterisation. Typically, he may prefer specifying a prior distribution for a change between two *successive* periods, as opposed to a change with respect to a reference period, as parameterised in section 5.4.2. In such a case, it is necessary to transform the prior distribution entered by the practitioner into the prior distribution in the final parameterisation. This section describes such transformations.

5.4.3.1. Cumulated changes vs. incremental changes

The information used to specify priors on rating change parameters can take different forms:

- bathymetry profiles may be available for all periods. In such a case it is possible to directly specify priors for the cumulated change parameters $\Delta a_j^{(k)}$ and $\Delta b_j^{(k)}$;
- an analysis of the sediment transport capacity may provide some information on the possible change after a morphogenic flood. However this information is necessarily expressed as a change between two successive periods.

We therefore introduce parameters $\delta a_j^{(k)}$ and $\delta b_j^{(k)}$, $k \neq k_{\text{ref}}$. They are called *incremental* changes (as opposed to *cumulated* changes). Incremental parameters $\delta a_j^{(k)}$ and $\delta b_j^{(k)}$ can be expressed as a function of cumulated parameters as follows:

$$\begin{aligned}
&\forall k < k_{\text{ref}} - 1, && \begin{cases} \delta a_j^{(k)} &= \Delta a_j^{(k)} - \Delta a_j^{(k+1)} \\ \delta b_j^{(k)} &= \Delta b_j^{(k)} - \Delta b_j^{(k+1)} \end{cases} \\
&\forall k \in \{k_{\text{ref}} - 1; k_{\text{ref}} + 1\}, && \begin{cases} \delta a_j^{(k)} &= \Delta a_j^{(k)} \\ \delta b_j^{(k)} &= \Delta b_j^{(k)} \end{cases} \\
&\forall k > k_{\text{ref}} + 1, && \begin{cases} \delta a_j^{(k)} &= \Delta a_j^{(k)} - \Delta a_j^{(k-1)} \\ \delta b_j^{(k)} &= \Delta b_j^{(k)} - \Delta b_j^{(k-1)} \end{cases}
\end{aligned} \tag{5.12}$$

Inversely, the cumulated parameters can be expressed as a sum of incremental parameters:

$$\forall k \neq k_{\text{ref}}, \begin{cases} \Delta a_j^{(k)} &= \sum_{m=min(k,k_{\text{ref}}+1)}^{max(k,k_{\text{ref}}-1)} \delta a_j^{(m)} \\ \Delta b_j^{(k)} &= \sum_{m=min(k,k_{\text{ref}}+1)}^{max(k,k_{\text{ref}}-1)} \delta b_j^{(m)} \end{cases} \tag{5.13}$$

Note the vocabulary convention we adopt here: a cumulated change is with respect to the reference period (symbol Δ) whereas an incremental change is between two successive periods (symbol δ).

5.4.3.2. Links between hydraulic controls

Irrespective of the type of prior information (cumulated change Δ or incremental change δ), and for any rating curve parameters (coefficients $a_j^{(k)}$ or offsets $b_j^{(k)}$), changes for a given period k can be linked between controls. Indeed, consider the example in figure 5.1 which illustrates the frequent case of a change due to the scouring of the channel over the whole reach (with no change in the channel width): only the offset of the channel control changes. However, because the riffle lies on the riverbed, the offset of the corresponding control should also be affected by a similar change (middle panel in figure 5.1). We therefore refer to such a change as a *global* change.

In addition, the riffle may move longitudinally and its crest elevation with respect to the riverbed may also slightly change. Consequently the offset of the corresponding control may also be affected by a *local* change, which adds to the global change (right panel in figure 5.1). This implies that the changes are linked between controls, in the sense that the global change affects both riffle and channel controls, whereas the local change only affects the riffle control.

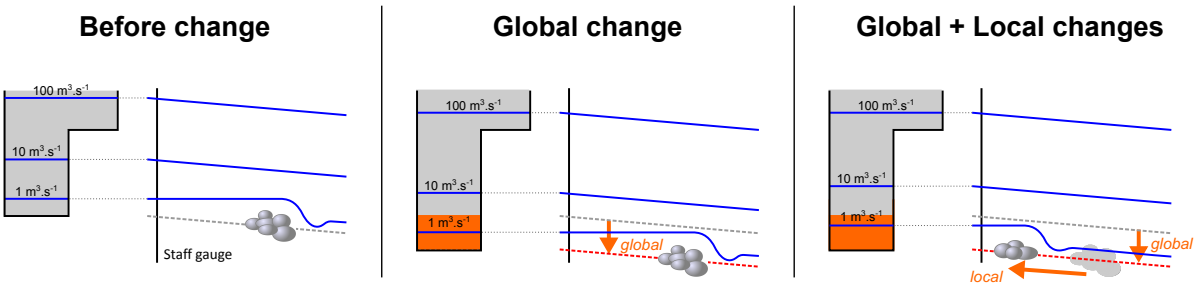

Figure 5.1 – Illustration of local and global riverbed changes. The cross-section is at the staff gauge.

It is therefore of interest to adopt a parameterisation that reflects the existence of global and local changes. This corresponds to the 'additive link' option shown in table 5.1: the change for the riffle is the sum of a global change parameter $\delta b_2^{(k)}$ and a local change parameter $\delta l_{b,1}^{(k)}$, while the change for the channel is equal to the global change parameter $\delta b_2^{(k)}$ only. By contrast, a naive parameterisation would be to use two unrelated parameters for the riffle and the channel, as shown in the 'no link' column of table 5.1.

Control	Change	Parameterisation options		
		No link	Additive link	Multiplicative link
Riffle	Global + Local	$\delta b_1^{(k)}$	$\delta b_2^{(k)} + \delta l_{b,1}^{(k)}$	$\delta b_1^{(k)}$
Channel	Global	$\delta b_2^{(k)}$	$\delta b_2^{(k)}$	$\lambda_{b,2}^{(k)} \times \delta b_1^{(k)}$
Floodway	None	0	0	0

Table 5.1 – Parameterisation options for the example shown in figure 5.1

It is also of interest to discuss these parameterisations in relation with the information that can be used to specify priors:

- channel bathymetry profiles for two periods can directly provide information on the global change parameter $\delta b_2^{(k)}$;
- an analysis of the sediment transport capacity may provide information on the possible channel change after a morphogenic flood: again this directly provides information on the global change parameter $\delta b_2^{(k)}$;
- the stage record also provides another useful source of information. Consider for instance the stage record in figure 5.2: changes can clearly be seen by focusing on the smallest stage values. However, such small stage values are related to the riffle control, and are hence informative for the combined global + local change. This is inconvenient because it provides information for a *sum* of two parameters, which cannot be decomposed for each parameter individually.

In order to allow using the latter source of prior information in a convenient way, a third parameterisation is proposed as shown in the 'multiplicative link' column in table 5.1: a single parameter $\delta b_1^{(k)}$ is now used to describe the combined global + local change affecting the riffle. The global change for the channel control is described with a multiplicative coefficient $\lambda_{b,2}^{(k)}$ of the combined change. It is expected that this coefficient should remain fairly close to 1.

The parameterisations proposed above for a simple three-control case can be generalised in several ways:

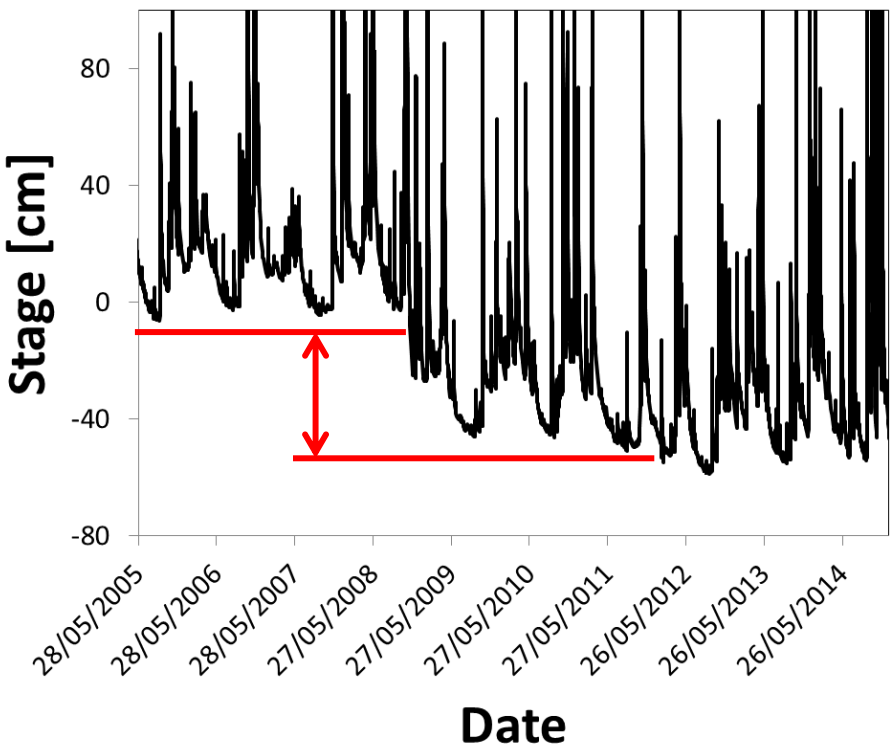

Figure 5.2 – Illustration of the use of a stage record to get information on the combined global + local change.

- an arbitrary number of controls can be considered as long as the assumptions made in section 5.2 are met (succession of section controls, then a main channel, then addition of floodways). This leads to table 5.2;
- changes can also affect the coefficients $a_j^{(k)}$: this would typically occur for a change in the channel width. This can simply be obtained by replacing b's by a's in table 5.2.

Note that the framework above is flexible enough to account for practices recommended in rating curve standards [e.g., ISO 1100-2:2010, 2010], described by Rantz [1982b], WMO No. 1044 [2010], Environment Canada [2016] or implemented in operational software (e.g. Aquarius software [Halmilton, 2015], used by the USGS, Environment Canada and many others). In particular, a shift of the rating curve (in the sense of a geometric translation parallel to the stage axis) is obtained by modifying all controls by the same change (as implemented in Aquarius software): it corresponds to setting local changes to 0 in the additive parameterisation ($\delta l_{b,1}^{(k)} = 0$ in table 5.1) or the multiplicative coefficient to 1 in the multiplicative parameterisation ($\lambda_{b,2}^{(k)} = 1$ in table 5.1). More complex changes (as those described by Rantz [1982b], WMO No. 1044 [2010]) can also be obtained with changing coefficient parameters $a_j^{(k)}$.

Number	Control	Change	Parameterisation options		
			No link	Additive link	Multiplicative link
1	Section	Global + local 1	$\delta b_1^{(k)}$	$\delta b_{N_s+1}^{(k)} + \delta l_{b,1}^{(k)}$	$\delta b_1^{(k)}$
$\vdots$	$\vdots$	$\vdots$	$\vdots$	$\vdots$	$\vdots$
$N_s - 1$	Section	Global + local $N_s - 1$	$\delta b_{N_s-1}^{(k)}$	$\delta b_{N_s+1}^{(k)} + \delta l_{b,N_s-1}^{(k)}$	$\delta b_{N_s-1}^{(k)}$
N_s	Last Section	Global + local N_s	$\delta b_{N_s}^{(k)}$	$\delta b_{N_s+1}^{(k)} + \delta l_{b,N_s}^{(k)}$	$\delta b_{N_s}^{(k)}$
$N_s + 1$	Main channel	Global	$\delta b_{N_s+1}^{(k)}$	$\delta b_{N_s+1}^{(k)}$	$\lambda_{b,N_s+1}^{(k)} \times \delta b_{N_s}^{(k)}$
$N_s + 2$	Floodway	Floodway 1	$\delta b_{N_s+2}^{(k)}$	$\delta b_{N_s+2}^{(k)}$	$\lambda_{b,N_s+2}^{(k)} \times \delta b_{N_s}^{(k)}$
$\vdots$	$\vdots$	$\vdots$	$\vdots$	$\vdots$	$\vdots$
N_c	Floodway	Floodway $N_c - N_s - 1$	$\delta b_{N_c}^{(k)}$	$\delta b_{N_c}^{(k)}$	$\lambda_{b,N_c}^{(k)} \times \delta b_{N_s}^{(k)}$

Table 5.2 – Parameterisation options for incremental changes in offsets $b_j^{(k)}$ for a given k period. A similar table ($b \leftrightarrow a$) can be made for incremental changes in coefficient parameters $a_j^{(k)}$, and for cumulated changes ($\delta \leftrightarrow \Delta$ and $\lambda \leftrightarrow \Lambda$).

5.4.3.3. Prior transformation formulas

While several parameterisations are possible for prior specification, the inference will always be made with the final parameterisation described in section 5.4.1. It is therefore necessary to transfer the prior information specified by the practitioner into this final parameterisation.

In the remainder of this current section 5.4.3.3, only offsets $b_j^{(k)}$ are considered. The reasoning applies to coefficients $a_j^{(k)}$ alike. Consider for instance the prior parameterisation corresponding to the additive link option, with incremental changes for the offsets. The final parameterisation can be obtained with the following formula (derived from equation (5.13)):

$$\forall k \neq k_{\text{ref}}, \begin{cases} \Delta b_j^{(k)} = \sum_{m=min(k,k_{\text{ref}}+1)}^{max(k,k_{\text{ref}}-1)} \left(\delta l_{b,j}^{(m)} + \delta b_{N_s+1}^{(m)} \right) & \text{if } j < N_s + 1 \quad \text{(section control)} \\ \Delta b_j^{(k)} = \sum_{m=min(k,k_{\text{ref}}+1)}^{max(k,k_{\text{ref}}-1)} \delta b_j^{(m)} & \text{if } j \geq N_s + 1 \quad \text{(channel control)} \end{cases} \tag{5.14}$$

Assuming that the practitioner always uses independent normal distributions to specify priors for all parameters $\delta b_j^{(k)}$ and $\delta l_{b,j}^{(k)}$, the joint prior distribution of cumulated changes $\Delta b_j^{(k)}$ (final parameterisation) follows a multivariate normal distribution, whose mean vector and covariance matrix can be deduced from the prior means and variances specified by the practitioner, as described in appendix B. Appendix B also describes the formulas for all other prior specification options (cumulated vs. incremental changes, no link vs. additive link vs. multiplicative link).

5.4.3.4. Interest of prior preprocessing

Prior preprocessing, explained in section 5.4.3.3, allows taking into account various sources of prior information. This information is transferred into the final parameterisation according to links between controls and between periods.

Figure 5.3 illustrates how this transfer of information is performed. Prior information given by the practitioner corresponds to the local and global incremental change parameters ($\delta l_{b,i}^{(k)}$ and $\delta b_j^{(k)}$, $i \in [\![1; N_s]\!]$, $j \in [\![N_s+1; N_c]\!]$ and $k \in [\![1; N_{changes}+1]\!]$, $k \neq k_{ref}$) for an additive link between controls. These parameters are assumed to be independent, correlations between each of them are hence zero (left panel in figure 5.3).

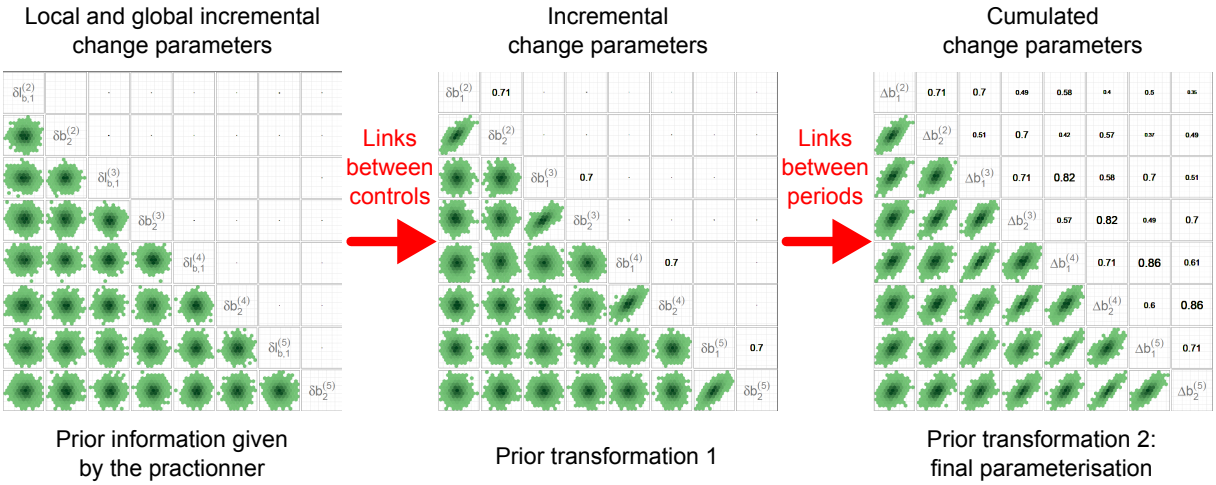

Figure 5.3 – Prior preprocessing: effect of links between controls and between periods for an additive link option. The upper triangular part of these matrix shows the correlation between parameters while the lower triangular part is the scatterplot of Monte-Carlo sampled values.

The first prior transformation takes into account links between controls for each period. Therefore, for a same period non-zero correlations appear between incremental change parameters $\delta b_j^{(k)}$. The second transformation takes into account links between periods: incremental changes are transformed into cumulated changes. Non-zero correlations appear also between periods, these correlations being larger for closer periods (see figure 5.3).

These correlations appearing in the final prior distribution are very important, because they will play a key role in the transfer of information between controls and between periods. As an illustration, figure 5.4 shows the joint prior distribution for cumulated change parameters of two successive periods (parameters $\Delta b_1^{(4)}$ and $\Delta b_1^{(5)}$ of the application at Meyras station, see section 5.5.1). As soon as one of these parameters is precisely identified (e.g. $\Delta b_1^{(4)} = -2$ or $\Delta b_1^{(4)} = 2$), the other one ($\Delta b_1^{(5)}$) becomes also more precisely identified according to the

strength of the correlation. Therefore, any information on change parameters from observations on a specific period and/or controls is propagated to other periods and controls through this final parameterisation.

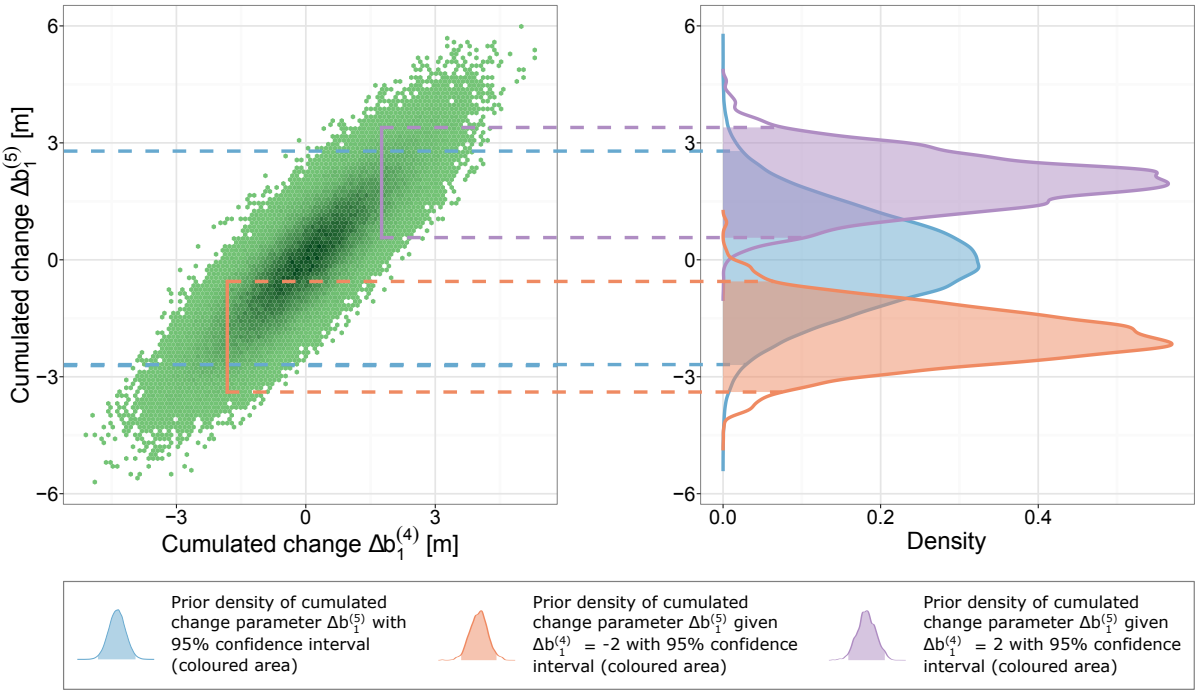

Figure 5.4 – Prior preprocessing: information transfer between two cumulated parameters. Data comes from the application at Meyras station for an additive link between controls.

5.5. Application to distinct cases

5.5.1. The Ardèche River at Meyras, France

5.5.1.1. Data and models

At Meyras station (see section 2.5) morphogenic events occur periodically and sometimes lead to marked net changes in the stage-discharge relation. Since 2001 until the major floods of Autumn 2014, four main flood peaks can be distinguished: 04/11/2011, 07/09/2010, 01/11/2008 and 17/11/2006. These four main floods correspond to official dates of rating changes. The periods delineated by these dates are summarised in table 5.3.

Period number	Start date	End date	Number of gaugings
1	04/11/2011 00:00	18/09/2014 00:00	(25,11,13,1)
2	07/09/2010 00:00	04/11/2011 00:00	(24,9,15,0)
3	01/11/2008 00:00	07/09/2010 00:00	(14,8,6,0)
4	17/11/2006 00:00	01/11/2008 00:00	(8,2,6,0)
5	20/10/2001 00:00	17/11/2006 00:00	(33,7,24,2)

Table 5.3 – The Ardèche River at Meyras: stable periods between 2001 and 2014 and related number of gaugings per segments (total, riffle, main channel, and main channel + floodway).

Figure 5.5 shows all the available discharge measurements (216) since year 1984. 104 gaugings were performed during the period of interest (2001-2014). Distributions of these gaugings through controls for the five stable periods are listed in table 5.3. The first two segments (riffle and main channel) were densely gauged whereas the third one (main channel + floodway) was almost never gauged.

The five sets of gaugings related to these periods appear to be well aligned and usually cover a wide range of stages (Figure 5.5), except for the third segment (main channel + floodway) for which only three gaugings were performed over these periods (see table 5.3). The shifts can be clearly seen in figure 5.5 except for the change after the 17/11/2006 (smaller flood) which is not obvious in the gaugings.

The most recent stable period (period number 1) is set up as the reference period. We use the same hydraulic configuration as in section 2.5. For this station, we assume that only the

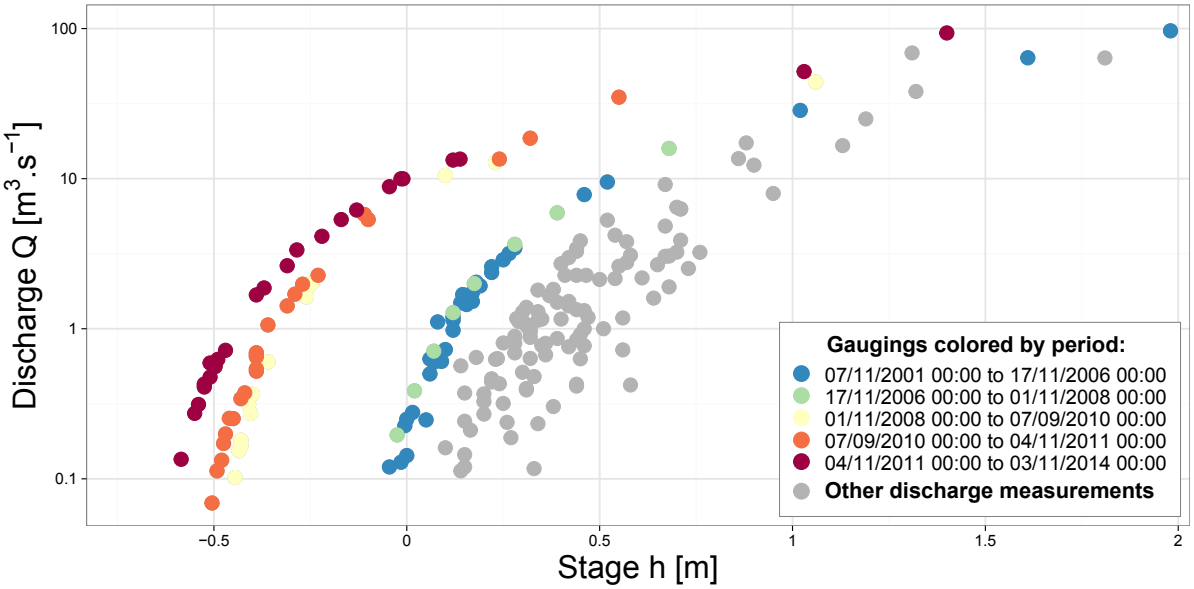

Figure 5.5 – Gaugings available at the Ardèche River at Meyras station.

offsets of the first two controls change between stable periods since the floodway and the banks of the main channel are quite stable (rock). The $\mathcal{MC}$ matrix of changes takes the following form:

$$\mathcal{MC} \quad \overleftrightarrow{\text{Rating curve parameters}}$$

k		$\overleftrightarrow{1^{\text{st}}\text{ control}}$			$\overleftrightarrow{2^{\text{nd}}\text{ control}}$			$\overleftrightarrow{3^{\text{rd}}\text{ control}}$		
		a_1	$b_1^{(k)}$	c_1	a_2	$b_2^{(k)}$	c_2	a_3	$b_3^{(k)}$	c_3
Recent ↑	$k_{\text{ref}} = 1$	−1	−1	−1	−1	−1	−1	−1	−1	−1
	2	0	1	0	0	1	0	0	0	0
Period	3	0	1	0	0	1	0	0	0	0
	4	0	1	0	0	1	0	0	0	0
Old ↓	5	0	1	0	0	1	0	0	0	0

change *wrt* previous period

Therefore, the rating curve equation for the k^{th} period, $k \in [\![1;5]\!]$ can be written as follows:

$$Q^{(k)}(h) = \begin{cases} a_1 \left(h - b_1^{(k)}\right)^{c_1} & \text{if } h < \kappa^{(k)} \quad \text{(first segment)} \\ a_2 \left(h - b_2^{(k)}\right)^{c_2} & \text{if } \kappa^{(k)} \leq h < b_3 \quad \text{(second segment)} \\ a_2 \left(h - b_2^{(k)}\right)^{c_2} + a_3 \left(h - b_3\right)^{c_3} & \text{if } h \geq b_3 \quad \text{(third segment)} \end{cases} \tag{5.15}$$

5.5.1.2. Prior specification

As the bathymetry is not available for all the periods, cumulated change parameters on offsets (parameters $\Delta b_1^{(k)}$ and $\Delta b_2^{(k)}$, $k \in [\![2;5]\!]$) cannot be specified: incremental change parameters are therefore preferred.

For the additive link option all local and global incremental change parameters ($\delta l_{b,1}^{(k)}$ and $\delta b_2^{(k)}$, $k \in [\![2;5]\!]$) are set to 0 m $\pm$ 1 m whereas for the multiplicative link option, the incremental change parameters for the first control ($\delta b_1^{(k)}$, $k \in [\![2;5]\!]$) are set to 0 m $\pm$ 1 m and the multiplicative coefficients ($\lambda_2^{(k)}$, $k \in [\![2;5]\!]$) are set to 1 ± 0.5.

5.5.1.3. Results

Figure 5.6 shows the estimated rating curves as stage-discharge representations with 95% uncertainty envelopes, for the five periods. Whatever the link option between controls (figure 5.6-a for an additive link; figure 5.6-b for a multiplicative link), posterior results are almost identical. This can also be seen in figure 5.7, which shows that estimated discharges are virtually identical with both options. Therefore, only the additive link option is used in the remaining of this case study.

The SPD model with an additive link between controls yields accurate rating curves that agree well with gaugings (figure 5.6). Moreover, these rating curves are precise, due to the high number of gaugings for all the periods.

Most parameters of the rating curve are precisely estimated (figure 5.8). Among stable parameters (figure 5.8-a), the third control parameters a_3 and b_3 are less precisely estimated due to the scarcity of high-flow gaugings (the posterior is similar to the vague prior). Changing offsets are very precisely estimated for all periods (figure 5.8-b). The rating change between periods 3 and 4 is very large (around 0.4 m) while changes between other periods are much smaller: this was already observable in gaugings (figure 5.5). The rating changes are almost entirely explained by global changes (figure 5.8-c) with the local changes being always precisely identified close to zero (figure 5.8-d). It matches with the knowledge we have at this station: scouring of the whole channel has indeed been observed.

Figure 5.9 shows the agreement between predicted and gauged discharges as relative errors. MAP rating curves estimated by the SPD model with additive link option agree well with gaugings: error values are acceptable (less than $\pm$20%), except for the fifth period which has a

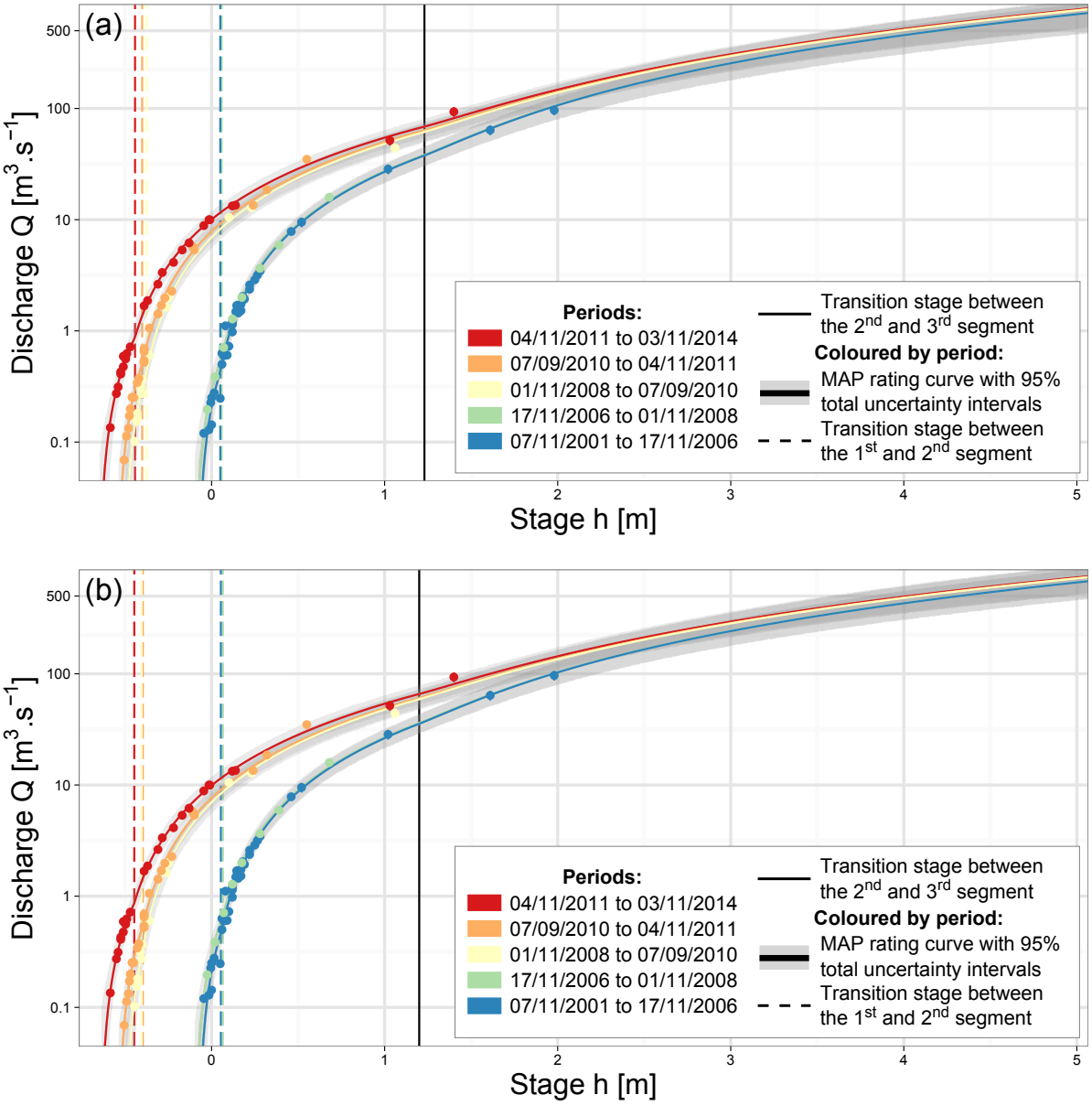

Figure 5.6 – The Ardèche River at Meyras: stage-discharge representation of the stage-period-discharge (SPD) model with discharges in logarithm scale: (a) for the additive link option; (b) for the multiplicative link option.

higher variability in low-flow gaugings (see figure 5.5). Total uncertainty envelopes are acceptable for every period (less than ±30% at high flows).

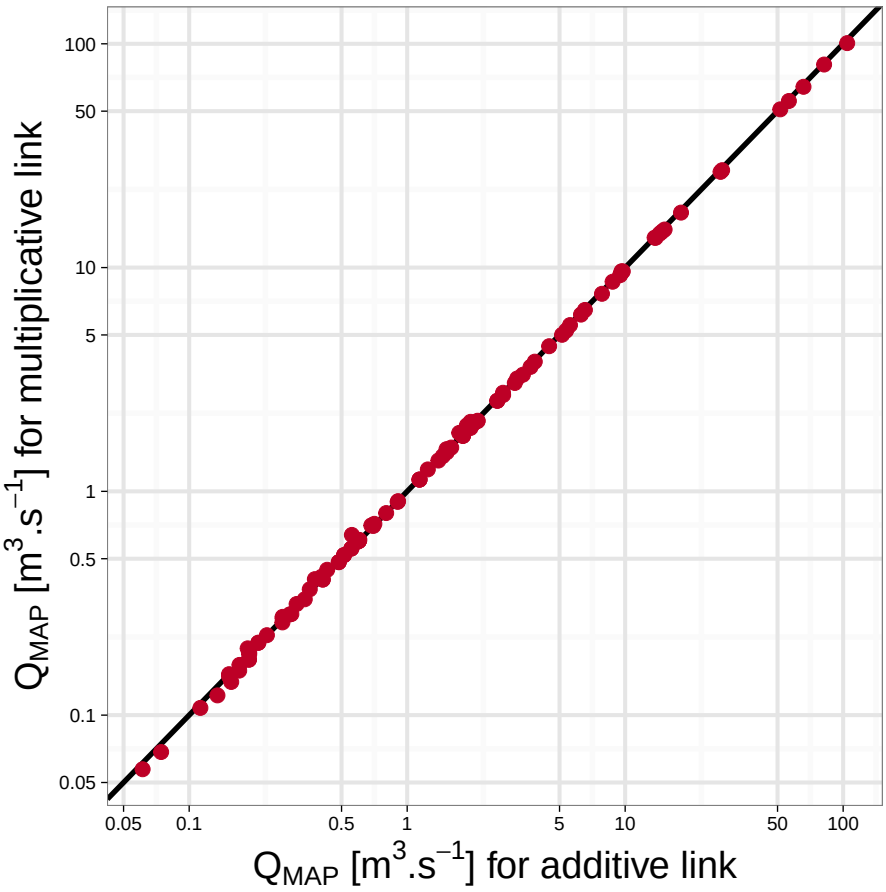

Figure 5.7 – Comparison of estimated discharges Q_{MAP} for the stage-period-discharge (SPD) model between additive and multiplicative link options for the Ardèche River at Meyras.

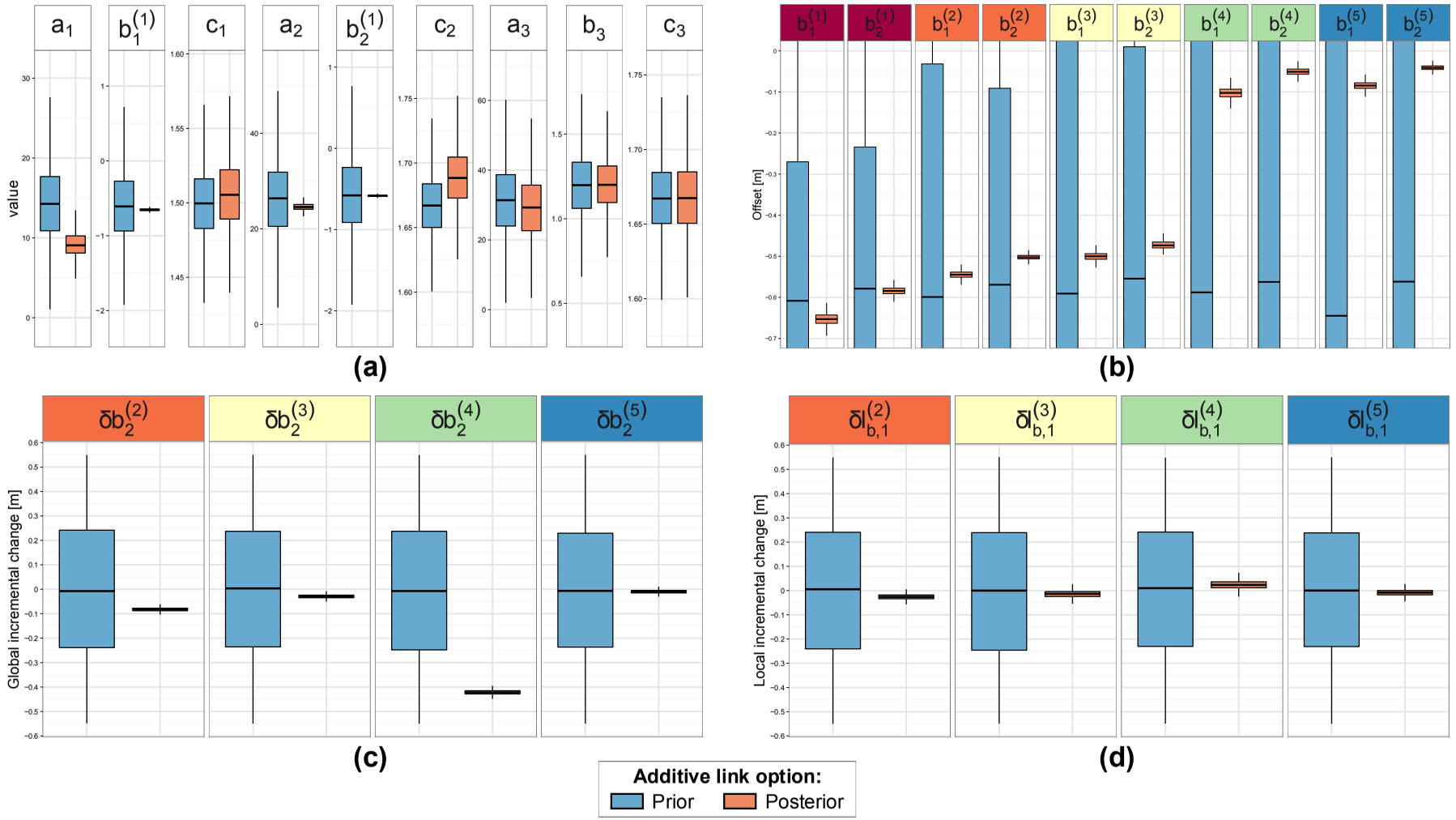

Figure 5.8 – Application of the stage-period-discharge (SPD) model to the Ardèche River at Meyras, boxplots of: (a) stable parameters; (b) offsets of the first two controls; (c) global incremental changes; (d) lobal incremental changes.

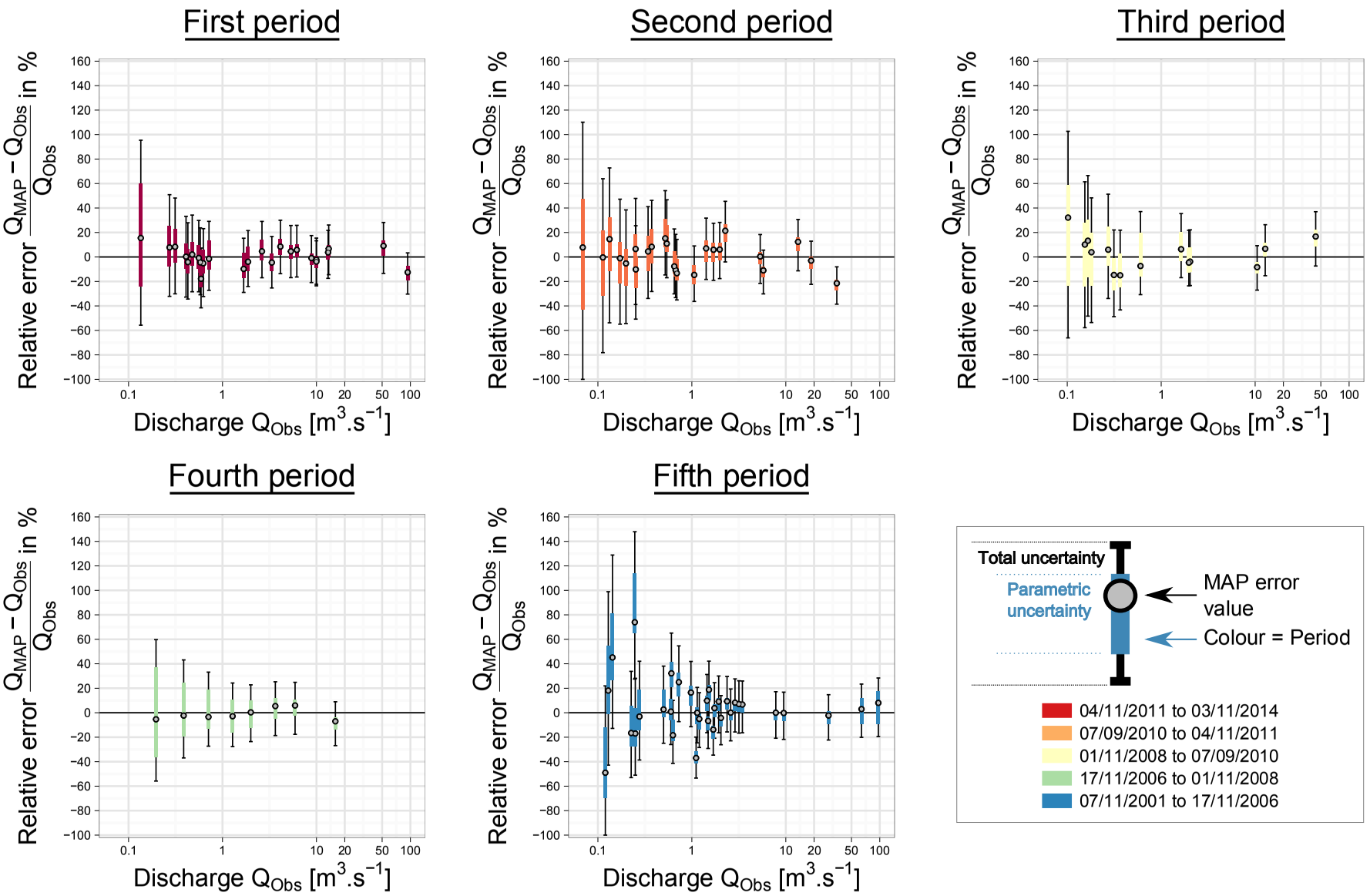

Figure 5.9 – Application to the stage-period-discharge (SPD) model to the Ardèche River at Meyras: relative errors between the maximum *a posteriori* discharges (Q_{MAP}) and the gaugings (Q_{Obs}) for the additive link option between controls. Error bars represent the parametric and total 95% uncertainty bounds of the discharge estimates, with period colour-coded.

5.5.2. The Wairau River at Barnett's Bank, New Zealand

5.5.2.1. Data and models

The Wairau River is located in the northern South Island of New Zealand (see figure 5.10-a) and drains a catchment area of 3825 km^2 [Clark et al., 2008]. It flows along 169 km from the Spenser Mountains, down into Cloudy Bay of Cook Strait. It is a braided river with highly mobile bed.

Barnett's Bank station, near the outlet of the Wairau basin, is a mobile gravel bed where the cross-section changes frequently with floods. The gauge at Barnett's Bank is located 500 metres upstream of a road bridge, 4 km upstream of the sea. Variable backwater effects from the sea are assumed negligible. Moreover, hysteresis effects are also neglected, outweighed by the river bed movement and the steep gradient [McMillan et al., 2010].

A shingle-made riffle controls the stage-discharge relation at low flows (see figure 5.10-b): it is approximated by a rectangular section control. As flow increases, a main channel takes over the riffle and then a floodway is added to this main channel for high flows. Both channel controls are assumed to have wide rectangular cross-sectional shapes. Overbank flows in the floodplain are not considered here.

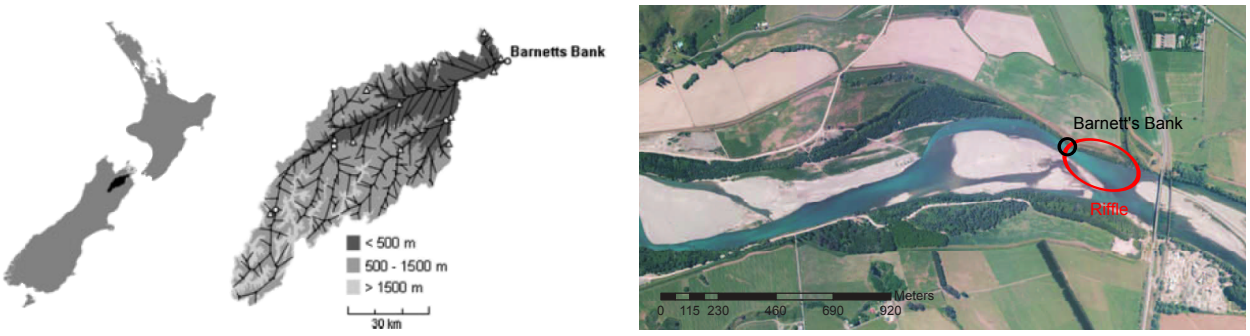

(a) (b)

Figure 5.10 – The Wairau River at Barnett's Bank: (a) the Wairau basin showing (left) location; (right) the basin with elevation, figure reproduced from Clark et al. [2008] and McMillan et al. [2010]; (b) view from above of the hydraulic controls at the Barnett's Bank station.

The Barnett's Bank station is the longest and most reliable record of the Wairau River [McMillan et al., 2010]. 270 gaugings were performed from 11/08/1999 to 07/04/2015 (see figure 5.11): it corresponds to a frequently gauged station with more than 17 gaugings per year on average.

However, low-flow changes are severe and frequent: the stage-discharge relation is scattered (see figure 5.11) over time. Overall, a marked scour occurred around 2004, then the channel

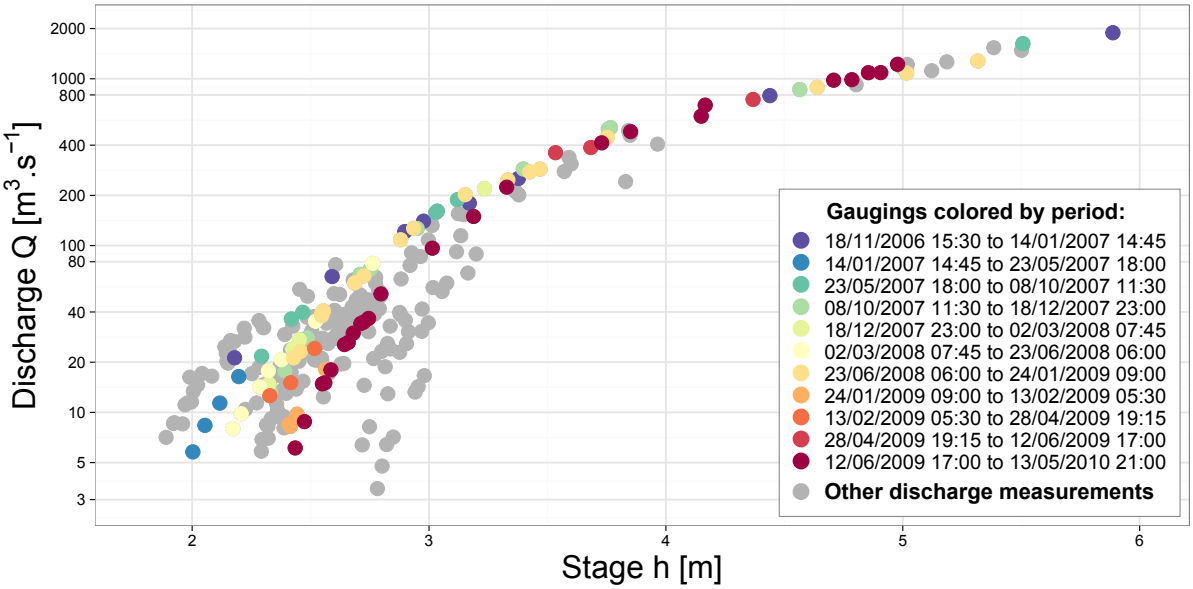

Figure 5.11 – Gaugings available at the Wairau River at Barnett's Bank station.

aggraded again and changes are of much less amplitude in the few recent years. 60 official rating changes were recorded during this 15-year period from 29/07/1999 14:45 to 06/03/2015 21:00, which means, on average, almost 3.8 new ratings per year and 4.4 gaugings per period. Thus, stable periods are seldom gauged on average despite the large number of gaugings.

In this chapter we focus on a more frequently gauged period, from 18/11/2006 15:30 to 13/05/2010 21:00. 10 changes were recorded for a total number of 91 gaugings (8.2 gaugings per period on average). This information is summarised in table 5.4.

Period number	Start date	End date	Number of gaugings
1	12/06/2009 17:00	13/05/2010 21:00	24
2	28/04/2009 19:15	12/06/2009 17:00	3
3	13/02/2009 05:30	28/04/2009 19:15	3
4	24/01/2009 09:00	13/02/2009 05:30	4
5	23/06/2008 17:00	24/01/2009 09:00	17
6	02/03/2008 07:45	23/06/2008 17:00	7
7	18/12/2007 23:00	02/03/2008 07:45	4
8	08/10/2007 11:30	18/12/2007 23:00	10
9	23/05/2007 18:00	08/10/2007 11:30	7
10	14/01/2007 14:45	23/05/2007 18:00	4
11	18/11/2006 15:30	14/01/2007 14:45	8

Table 5.4 – The Wairau River at Barnett's Bank: stable periods between 2001 and 2014 and related numbers of gaugings. Dates in grey are the official dates of net changes.

The most recent period is set up as the reference period. Only offsets of the first two controls are assumed to change between periods. The matrix of changes $\mathcal{MC}$ takes the following form:

$\mathcal{MC}$ — Rating curve parameters

	k	1st control a_1	1st control $b_1^{(k)}$	1st control c_1	2nd control a_2	2nd control $b_2^{(k)}$	2nd control c_2	3rd control a_3	3rd control $b_3^{(k)}$	3rd control c_3	
↑	$k_{\text{ref}} = 1$	−1	−1	−1	−1	−1	−1	−1	−1	−1	
Recent	2	0	1	0	0	1	0	0	0	0	change *wrt* previous period
	3	0	1	0	0	1	0	0	0	0	
	4	0	1	0	0	1	0	0	0	0	
	5	0	1	0	0	1	0	0	0	0	
Period	6	0	1	0	0	1	0	0	0	0	
	7	0	1	0	0	1	0	0	0	0	
	8	0	1	0	0	1	0	0	0	0	
	9	0	1	0	0	1	0	0	0	0	
Old	10	0	1	0	0	1	0	0	0	0	
↓	11	0	1	0	0	1	0	0	0	0	

Therefore, the rating curve equation for the k^{th} period, $k \in [\![1; 11]\!]$ can be written as follows:

$$Q^{(k)}(h) = \begin{cases} a_1\left(h - b_1^{(k)}\right)^{c_1} & \text{if } h < \kappa^{(k)} \quad \text{(first segment)} \\ a_2\left(h - b_2^{(k)}\right)^{c_2} & \text{if } \kappa^{(k)} \leq h < b_3 \quad \text{(second segment)} \\ a_2\left(h - b_2^{(k)}\right)^{c_2} + a_3\left(h - b_3\right)^{c_3} & \text{if } h \geq b_3 \quad \text{(third segment)} \end{cases} \tag{5.16}$$

5.5.2.2. *Prior specification*

Field visit and discussion with station manager (Mike Ede, Marlborough Region Council) allowed to specify the following prior information. Widths of the riffle, main channel and floodway controls are respectively set to 65 m ± 10 m, 25 m ± 5 m and 150 m ± 30 m. From existing hydraulic models, bed slopes of both channel controls are equally set to 0.00143 ± 0.0005. Strickler flow resistance coefficients of both channel controls are also equally set to 25 $\text{m}^{\frac{1}{3}}.\text{s}^{-1}$ ± 10 $\text{m}^{\frac{1}{3}}.\text{s}^{-1}$. For the most recent period (number 1), offsets of the first and second control (parameter $b_1^{(1)}$ and $b_2^{(1)}$), are set to 2 m ± 0.5 m. The offset $b_3^{(1)}$ corresponding to the overflow stage of the main channel into the floodway is set to 2.35 m ± 0.2 m. This transition stage is assumed stable between periods: only offsets of the first two controls are assumed to change between stable periods.

Bathymetry profiles are not available: consequently, incremental change parameters (parameters $\delta b_1^{(k)}$ and $\delta b_2^{(k)}$, $k \in [\![2;11]\!]$) are used. For the additive link option all local and global incremental changes ($\delta l_{b,1}^{(k)}$ and $\delta b_2^{(k)}$, $k \in [\![2;11]\!]$) are respectively set to 0 m $\pm$ 0.2 m and 0 m $\pm$ 0.4 m. We also use the multiplicative link option, and prior distributions are set in order to match with prior distributions of the additive link option. This can be done by applying property 2 in appendix B. As a result, incremental changes $\delta b_1^{(k)}$ of the first control are set to 0 m $\pm$ 0.4472 m and the multiplicative coefficients $\lambda_2^{(k)}$ are set to 0.8588 ± 0.5.

5.5.2.3. Results

Figure 5.12 shows the estimated rating curves as stage-discharge representations with 95% uncertainty envelopes for the eleven periods and for both additive and multiplicative link options (respectively figure 5.12-a and figure 5.12-b). Results are very similar for both options. This is further confirmed by figure 5.13 which shows that the estimated discharges are almost equal. Therefore, only the additive link option is used in the remainder of this case study.

Overall the rating curves agree with gaugings (figure 5.12-a), however uncertainty is much larger than in the Meyras case study, due to the smaller number of gaugings per period. There is a lot of variations in the MAP values of transition stages $\kappa^{(k)}$ between the first two controls (figure 5.12-a). For some periods (e.g. periods 7 and 8), the second segment seems to be neglected as these transition stages reached the overflow stage b_3. For these periods, the transition stages $\kappa^{(k)}$ have wide skewed distributions: they are not precisely identified in gaugings (see figure 5.14). In fact it goes a step further: most of the transition stages are identifiable (as posterior distributions differ from prior distributions) but still remain wide. This may be due to the low number of low-flow gaugings on the first two segments. It may also show some limitations of the assumptions on changes: the offset of the third control (floodway) may change across periods.

Stable parameters for the third control (a_3 and b_3) are well identified: parametric uncertainty envelopes are within 10% of the MAP value (figure 5.15-a). This is due to the numerous high-flow gaugings on the third segment. Conversely, the coefficient a_1 of the first control remains similar to its wide prior distribution. Noticeable changes can be seen for offsets of the first two controls (figure 5.15-b). The precision of the estimated offsets depends on the availability of low-flow gaugings. For instance, the offset for the lower control is very precisely estimated for periods 6 and 10 thanks to gaugings performed at very low flows. As for the Meyras case study, global changes (figure 5.15-c) appear much larger than local changes (figure 5.15-d).

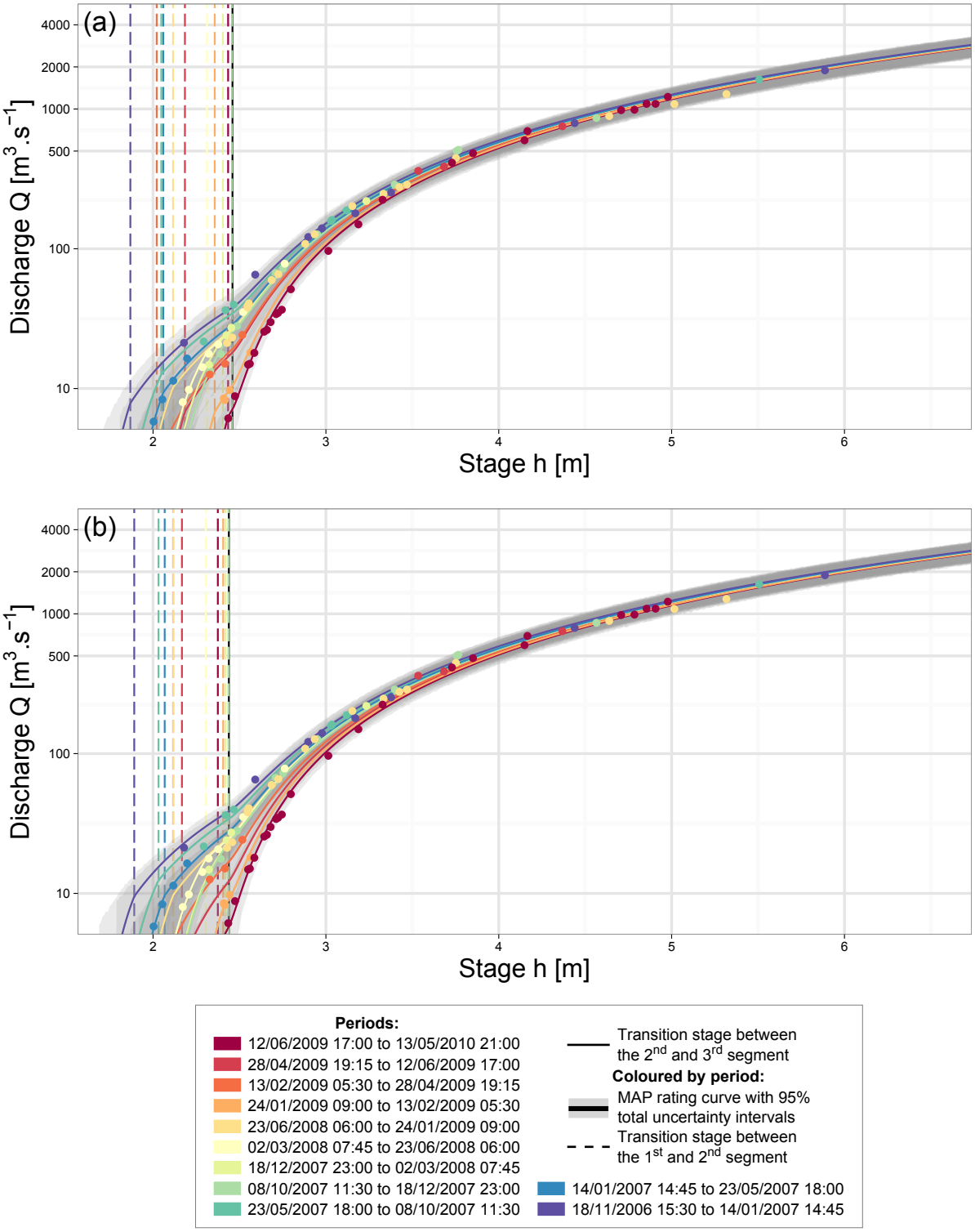

Figure 5.12 – The Wairau River at Barnett's Bank: stage-discharge representation of the stage-period-discharge (SPD) model with discharges in logarithm scale: (a) for the additive link option; (b) for the multiplicative link option.

The overflow stage is identified in gaugings (MAP value of 2.46 with 95% total uncertainty envelopes under ±5%, see b_3 in figure 5.15-a). Three quarters of the gaugings are assigned to

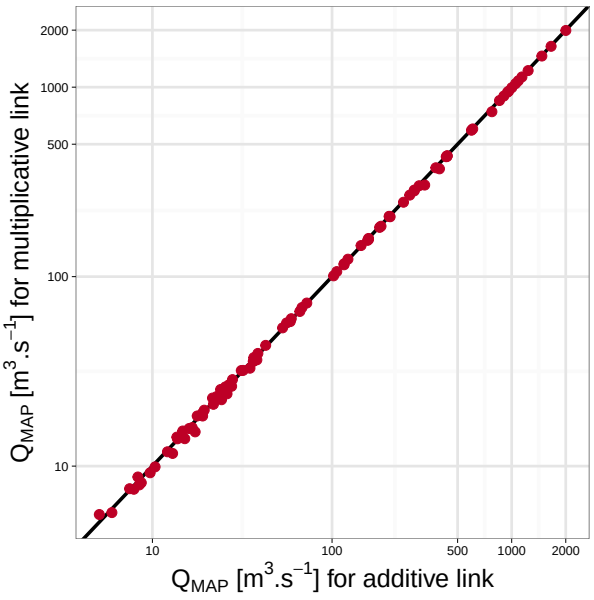

Figure 5.13 – Comparison of estimated discharges Q_{MAP} for the stage-period-discharge (SPD) model between additive and multiplicative link options for the Wairau River at Barnett's Bank.

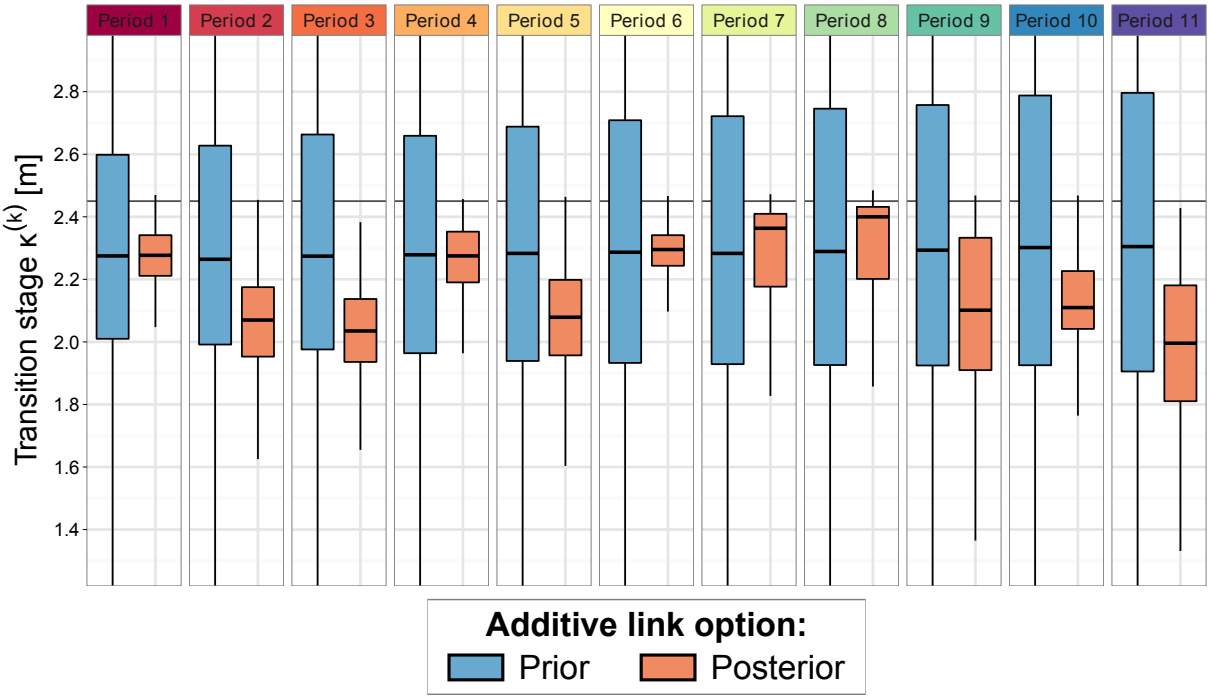

Figure 5.14 – Application of the stage-period-discharge (SPD) model to the Wairau River at Barnett's Bank: boxplots of the transition stages between the first two controls. The MAP value of the overflow stage b_3 is represented in black vertical line.

the third segment (see figure 5.12-a). There is hence not enough discharge observations (only

24 gaugings for 2 controls and 11 periods) for identifying the transition stages between the first two controls.

Figure 5.16 shows the agreement between predicted and gauged discharges as relative errors for the additive link option. MAP rating curves agree with gaugings: error values are within ±20%. Total uncertainty envelopes are acceptable at high flows (less than ±20% for $Q >$ 50 $m^3.s^{-1}$) for all the periods. Parameters a_3 and b_3 of the third control (floodway, high flows) are indeed well identified as discussed above. The second period, with only three high-flow gaugings, illustrates the performance of the model for high flows: all uncertainty envelopes and MAP errors are less than ±20%. Total uncertainty envelopes are higher at low flow (within ± 60%) especially for poorly-gauged periods (e.g. fourth and tenth periods).

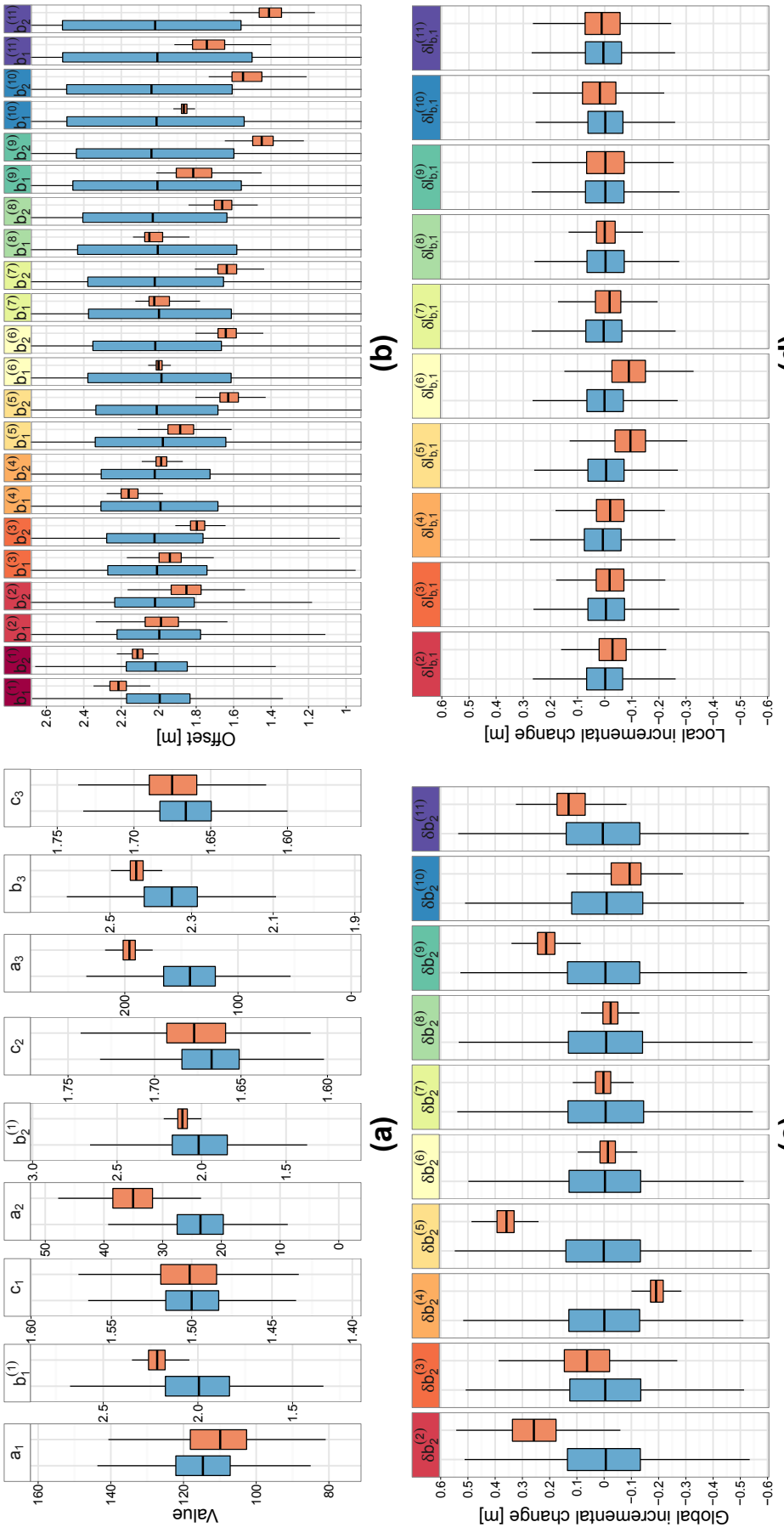

Figure 5.15 – Application of the stage-period-discharge (SPD) model to the Wairau River at Barnett's Bank, boxplots of: (a) stable parameters; (b) offsets of the first two controls; (c) global incremental changes; (d) local incremental changes.

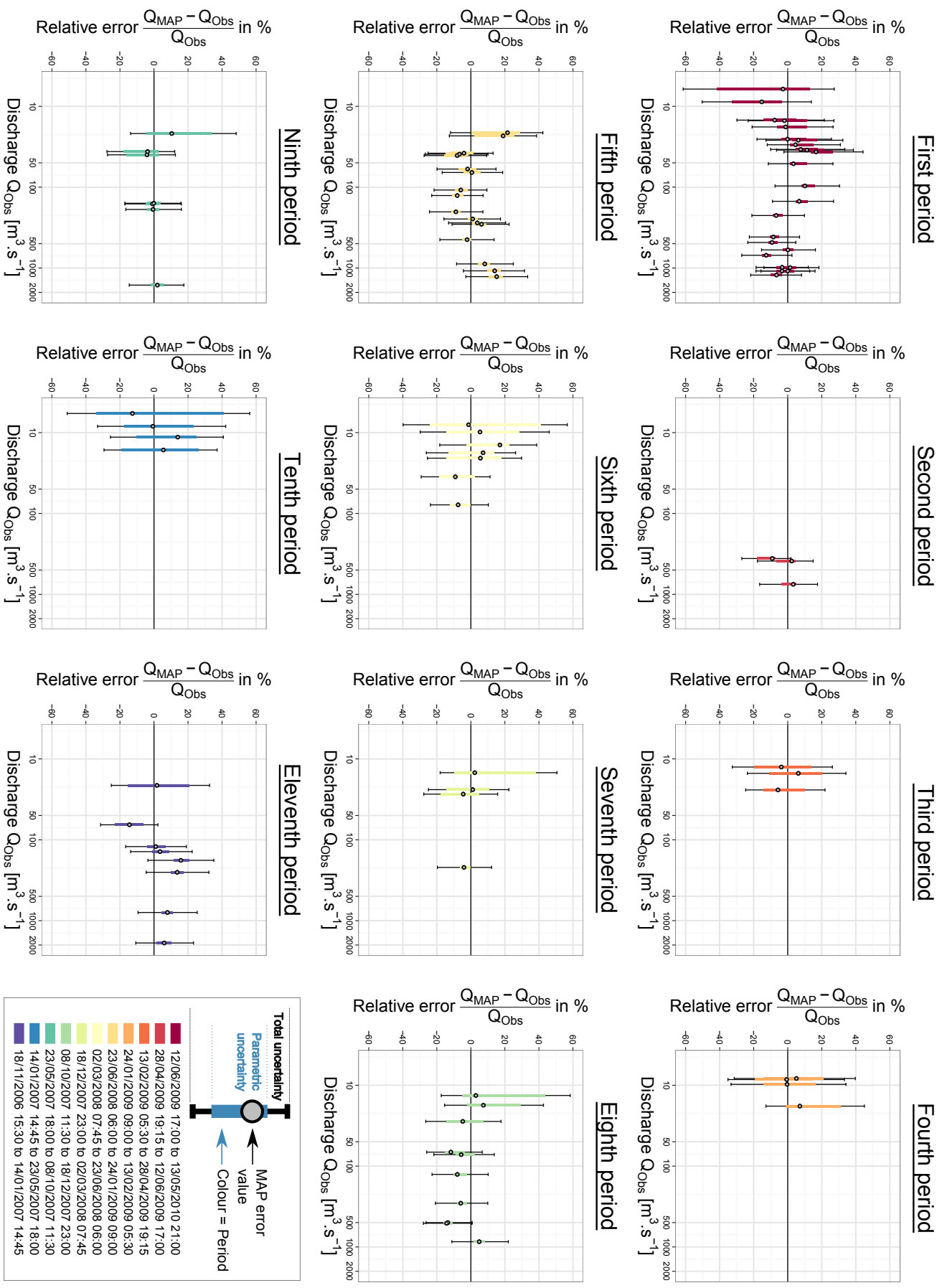

Figure 5.16 – Application to the stage-period-discharge (SPD) model to the Wairau River at Barnett's Bank: relative errors between the maximum *a posteriori* discharges (Q_{MAP}) and the gaugings (Q_{Obs}) for the additive link option between controls.

5.6. Evaluation of the stage-period-discharge (SPD) model

The objective of this section is to highlight the ability of the stage-period-discharge (SPD) model to transfer information between periods and between controls. Moreover, the SPD model is compared to a stage-discharge (SD) model applied separately to each stable period, which would correspond to the most naive practice. This evaluation is based on the Meyras case study.

5.6.1. Transfer of information between controls

The impact of the link between changes in the riffle control and changes in the main channel control is studied. The SPD models with 'no link' and 'additive link' options are calibrated using all the gaugings of the first period but only high flows gaugings of the second period. For the additive link option, incremental change parameters are set to 0 m ± 1 m (global change $\delta b2^{(k)}$) and to 0 m ± 0.01 m (local change $\delta l_{b,1}^{(k)}$). The same prior information is used for the 'no link' option.

Note that prior standard deviations of the local incremental changes $\delta l_{b,1}^{(k)}$ differ from those used in section 5.5.1: we impose low values to better highlight the transfer of information between controls.

The results are shown in figure 5.17 as the stage-discharge representations of the first two periods for the two link options. Densities of the offset $b_1^{(2)}$ of the first control (riffle) of the second period are also shown.

On the first period both options yield similar results: uncertainty intervals and transition stages are nearly identical. On the second period results differ at low flow: uncertainty intervals are much wider for the 'no link' option. As there is no gauging for the first control (riffle) during the second period, the posterior distribution of the incremental change parameter $\delta b_1^{(2)}$ is entirely based on the vague prior information. Therefore, the density of related offset $b_1^{(2)} = b_1^{(1)} - \delta b_1^{(2)}$ remains vague (figure 5.17-d). This illustrates that the 'no link' option cannot transfer information from the channel control, for which gaugings are available.

Conversely, for the 'additive link' option, the incremental change parameter $\delta b_1^{(2)} = \delta l_{b,1}^{(2)} + \delta b_2^{(2)}$ is identified much more precisely. This is because parameter $\delta b_2^{(2)}$, corresponding to the incremental change for the main channel, is identified in high-flow gaugings of the second period.

The resulting density of the offset $b_1^{(2)} = b_1^{(1)} - \delta l_{b,1}^{(2)} - \delta b_2^{(2)}$ is therefore more precise. In turn, uncertainty intervals for the rating curve is also much more precise, while remaining consistent with validation gaugings (figure 5.17-c, although gaugings are on the edge of the uncertainty interval).

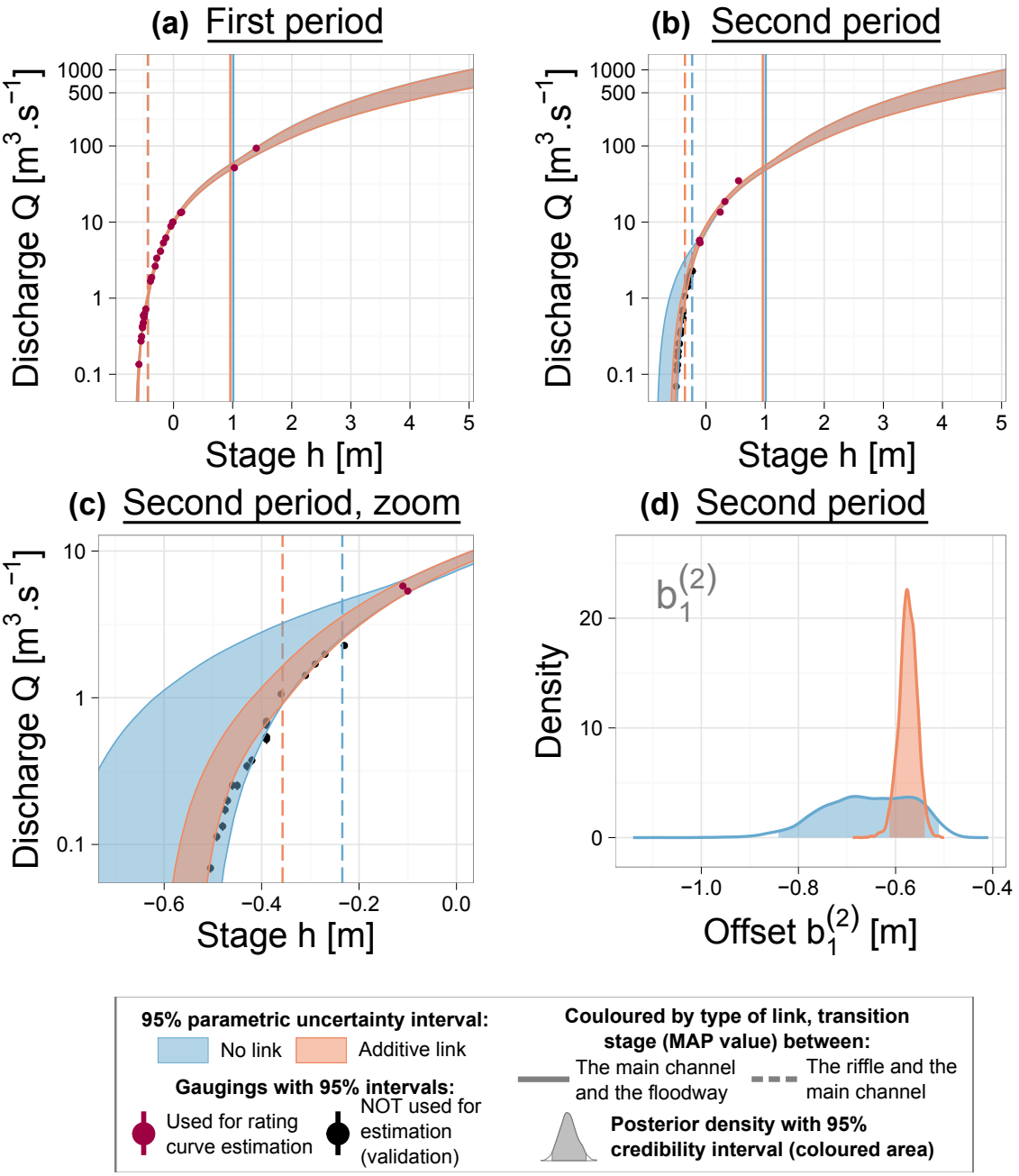

Figure 5.17 – The Ardèche River at Meyras over the 2001-2014 period: stage-discharge representation (a-b-c) and density of the offset $b_1^{(2)}$ (d) for the SPD model using all gaugings of the first period but only high-flow gaugings of the second period for calibration. Comparison between the SPD model with an additive link between controls and the SPD model with no link between controls.

Using a link between controls therefore allows transferring information from one control to another and thus compensating the lack of gaugings.

5.6.2. Transfer of information between periods

The SPD model with additive link option is calibrated using only gaugings of the first period. Posterior estimates are compared with prior ones to highlight the impact of the link between periods. The prior distributions for both incremental change parameters (global and local) are set to 0 m ± 0.5 m. These prior distribution differ from those used in section 5.5.1 in order to better highlight the transfer of information and its dynamics across periods.

The results are shown in figure 5.18 which shows the stage-discharge representations for all stable periods. The rating curve is precisely identified for the first period as the posterior interval is much smaller than the prior one (see first period in figure 5.18). This is not surprising given the high number of gaugings.

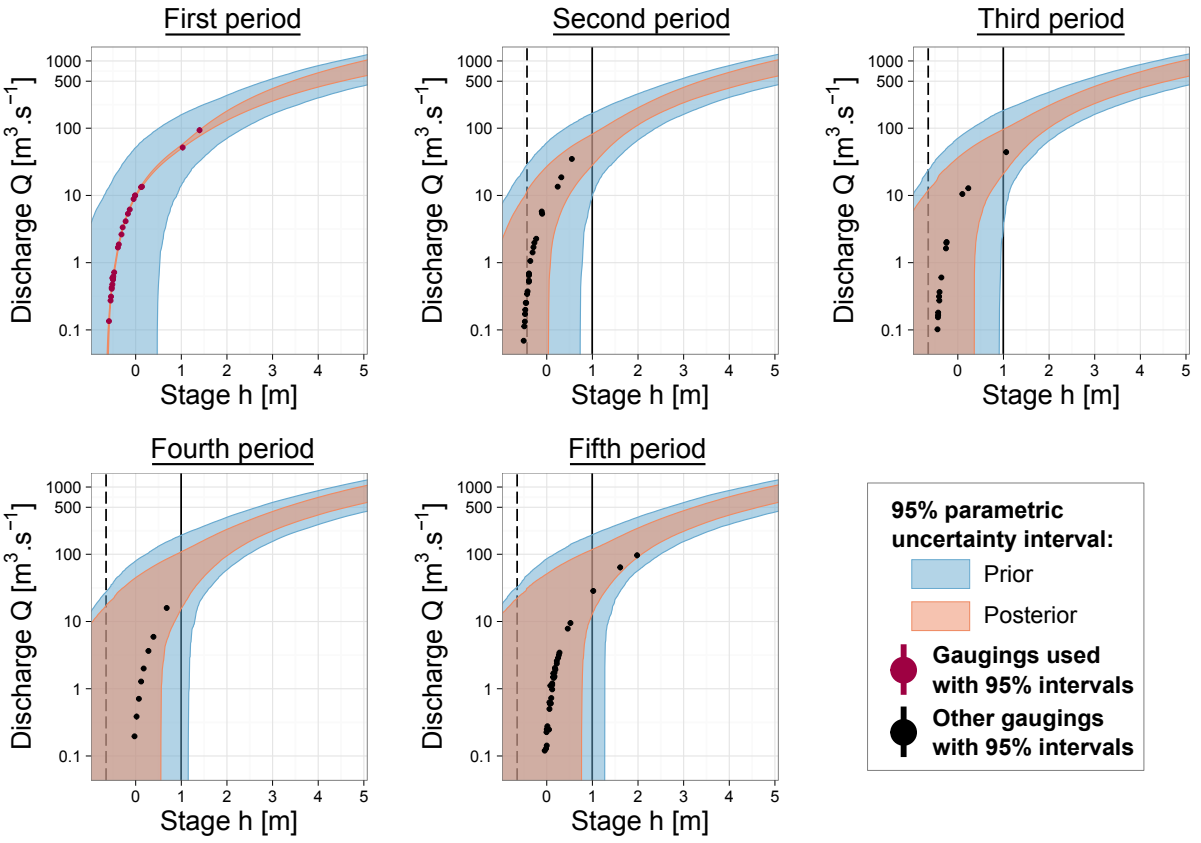

Figure 5.18 – The Ardèche River at Meyras over the 2001-2014 period: stage-discharge representation of the SPD model using only gaugings of the first period for calibration. Comparison between posterior and prior results.

The information identified on the first period is propagated to other periods: posterior intervals are smaller than prior ones (figure 5.18). This propagation tends to fade away as the period k is further away from the first period (reference period): for the fifth period the posterior interval is much closer to the prior one than for the second period.

This can be further explained by analysing posterior densities of the offset $b_1^{(k)}$ (figure 5.19). For the second period, the posterior density is more precise than the prior one. As soon as the period is too far from a gauged period, information no longer propagates: offset parameters becomes based on prior information (see the fifth period in figure 5.19).

Therefore, using links between periods allows transferring information from another period, this transfer being efficient for closer periods and fading away for more distant periods. The mechanism behind this propagation is explained in figure 5.4.

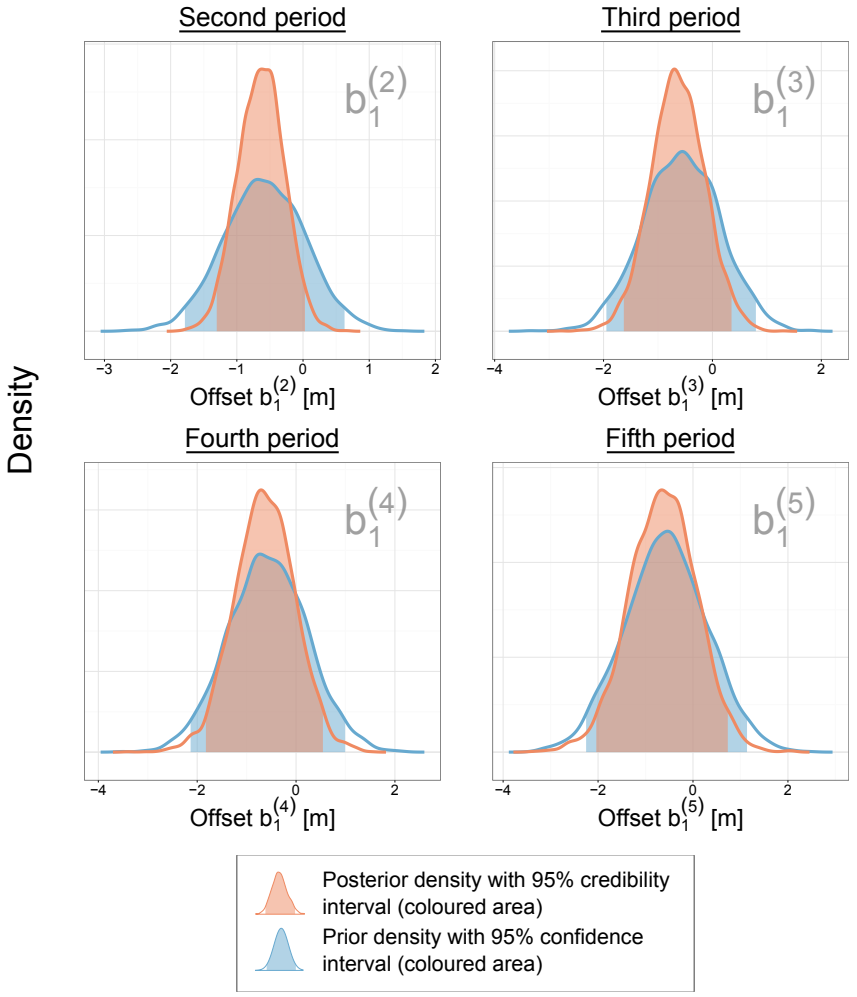

Figure 5.19 – The Ardèche River at Meyras over the 2001-2014 period: prior vs. posterior densities of offsets for the last four periods using only gaugings of the first period for calibration.

5.6.3. Comparison with stage-discharge (SD) model applied separately to each stable period

In this section, a comparison is made between the stage-period-discharge (SPD) model and a stage-discharge (SD) model separately applied to each stable period. Both SPD and SD models are applied to the Meyras case study, considering only 4 gaugings per period (scarcely gauged station, comparable to the Wairau station), 8 gaugings per period (reasonably gauged station), or all available gaugings (very well gauged station). The 4 and 8 gaugings are evenly split between the first two controls (e.g. 2 gaugings for the riffle control and 2 gaugings for the main channel control). For the SPD model we use the same priors as in section 5.5.1. For the SD model, prior specification is made as to ensure the equivalence with the prior information used by the SPD model.

Figure 5.20 shows the results for the stable parameters b_3, a_i and c_i, $i \in [\![1;3]\!]$. Irrespective of the number of gaugings, both SPD and SD models yield similar results for exponent parameters c_1, c_2 and c_3 because their respective prior distributions are precise (figure 5.20). Similar results are also found for parameters a_3 and b_3 of the third control: both posterior distributions are similar to the priors. There is indeed not enough high-flow gaugings (see table 5.3) to precisely identify these parameters.

When the station is scarcely gauged (4 gaugings per period), some differences between SPD and SD models can be seen for coefficients a_1 and a_2. Estimations made by the SPD model are more precise (figure 5.20) as these parameters are assumed constant across periods. Their estimation is therefore informed by all the gaugings of the five periods (20 gaugings) instead of only 4 gaugings for the SD model. The difference between SPD and SD models is more pronounced as the number of gaugings increases.

As an aside, figure 5.20 also supports the assumption made by the SPD model that these parameters are constant across periods. Indeed, for all stable parameters, posterior distributions obtained with the SD model are similar across periods. This is the case for rating curve parameters (b_3, a_i and c_i, $i \in [\![1;3]\!]$) as well as for parameters of the error model (γ_1 and γ_2). Moreover, the SPD model yields more precise estimations of the error model as its error parameters are estimated with more gaugings (5 times as many for this comparison) than for the 5 separate application of the SD model (especially with few gaugings on each periods)

Figure 5.21 shows the results for the offsets that change between periods. Overall posterior boxplots are similar for the SPD and SD models. This is not surprising as these parameters

are period-specific, and their estimation is therefore informed by the same number of gaugings. However, the SPD boxplots are always slightly more precise than the SD ones. This is likely due to the ability of the SPD model to transfer information between periods.

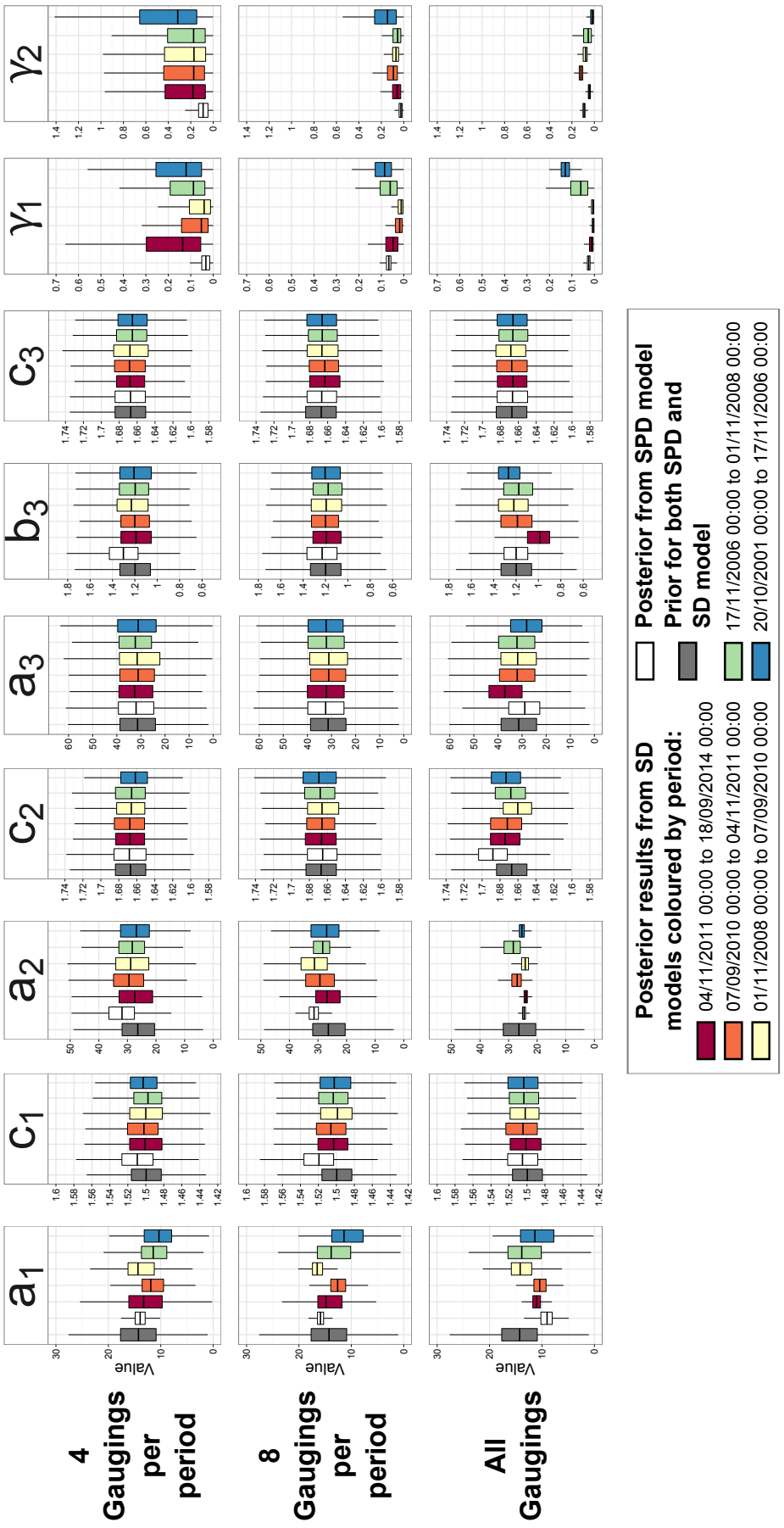

Figure 5.20 – The Ardèche River at Meyras over the 2001-2014 period: comparison between SPD and SD models for stable parameters, using only 4 gaugings per period, 8 gaugings per period and all available gaugings.

Figure 5.21 – The Ardèche River at Meyras over the 2001-2014 period: comparison between SPD and SD models for changing offset parameters, using only 4 gaugings per period, 8 gaugings per period and all available gaugings.

5.7. Conclusions and perspectives

5.7.1. Summary

This chapter proposes a stage-period-discharge (SPD) model to describe 'net' rating changes due to bed evolution. This SPD model is based on a segmentation of stable periods delimited by rating changes: dates of rating changes are assumed to be known. The SPD model needs two variables as inputs: the stage and the related period. The second input can be computed from the dates of rating changes and the date of the stage observation.

The proposed method uses Bayesian analysis. An expertise of the hydrometric station is needed to set up the prior distributions of the hydraulic variables. The method also requires information on the changing parameters: the practitioner indicates which specific parameter of the rating curve equation may change across periods, and provides prior information on the related changes.

Depending on the available hydraulic knowledge at the station, two types of prior information can be given on changes: a cumulated change indicates a change of parameter with respect to a reference period whereas an incremental change indicates a change between two successive periods. Changes on controls can be linked as well: an additive link connects the global change of the main channel with the change on lower flow controls whereas a multiplicative link connects the changes of the main channel control and upper flow controls with the change of the last section control of the riverbed. As results, it provides a rating curve with a total uncertainty envelope for every stable period. This total uncertainty can be split into parametric uncertainty (uncertainty of the rating curve parameters) and structural uncertainty (linked to the imperfection of the rating curve model). This method also provides a direct estimation of the physical parameters of the rating curve: results can therefore be criticised based on their physical meaning.

This SPD model does not need to assume that the gaugings 'age' contrary to other methods [Jalbert et al., 2011, Morlot et al., 2014] and does not replicate some discharge measurements for use across periods. The gaugings are assigned to the specific period during which they were performed and their uncertainty measurements remain constant. It seems more logical that the rating curve parameters may be allowed to remain stable across periods depending on an expertise given by the practitioner. Therefore, for scarcely gauged periods or even ungauged periods, rating curve parameters are still identified as soon as information on these parameters can be found in other periods. Indeed, information on these parameters is transferred between

periods as well as the information between controls. This latter transfer is useful for practice in the sense that it reproduces what is already done in some operational services (e.g., USGS and Environment Canada) through rating shifts and base curve.

The SPD model shows acceptable results at a well-gauged station with changes in offset only, enhancing the estimation of stable parameters. Change parameters are well-identified between periods and controls: precise values of the changes of offsets between two successive periods are identified. At a less-gauged station per stable period, the goodness-of-fit of rating curve remains acceptable but more uncertain. Stable parameters are still identified but change parameters estimations are less precise. As a result, transition stages are also uncertain but still match with the station knowledge.

Contrary to a naive practice which consists in separately estimating the rating curves for each period, the SPD model leads to better results on a scarcely gauged station as information is transferred between periods and controls.

5.7.2. Discussion

5.7.2.1. Assessing dates of the rating changes

The main issue of the SPD model is that it does not assess the dates of rating changes. As we choose to impose the period number as an input of the model, the dates of rating changes, cannot be assessed using the gaugings. Therefore, it is of primary importance to build a methodology for detecting the dates of rating changes.

Sediment transport analysis may help in achieving this assessment. It uses bedload capacity [Meyer-Peter and Müller, 1948] but one parameter, the critical shear for incipient motion of sediment, has to be calibrated using the Shields diagram [Soulsby and Whitehouse, 1997, Ribberink, 1998], which problematic as is is site-specific. However, once calibrated, the cumulated bedload at a station can detect significant incipient motion of sediment which suggests some dates for which the stage-discharge relation may have changed. It is only based on the stage record and hydraulic parameters which have to be assessed. Figure 5.22-a shows an example of such theory applied on the Meyras station (see section 5.5.1). For this example, 12 dates of changes are detected.

The use of sediment transport information raises several questions:

- how to calibrate the cumulated bedload parameters which are site-specific?

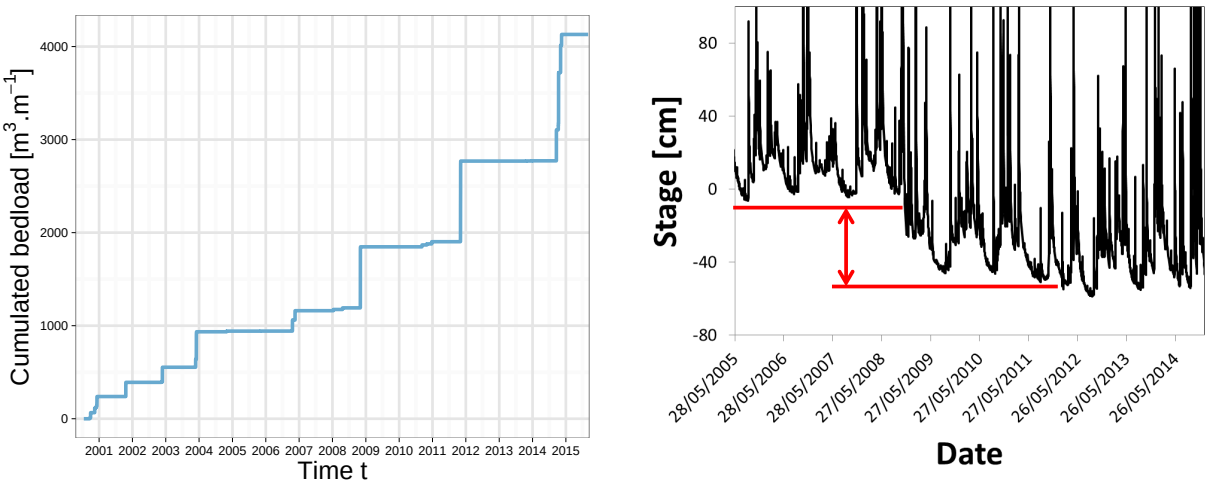

(a) (b)

Figure 5.22 – The Ardèche River at Meyras, assessing dates of changes using: (a) sediment transport theory through cumulated bedload; (b) analysis of lower stage records.

- does this method detect every relevant rating change or does it detect other insignificant flood events for which there was no change?
- how to assess whether a detected date matches with a real rating change?
- how to assess precisely the beginning and the end of the event ? This issue in particularly important as high-flow gaugings are often made during this kind of event, and hence affected by bedload transport. Determining the period they belong to is therefore important.

The analysis of lower stage records can also suggest the dates of rating changes (figure 5.22-b). It may also be useful to identify the value of the changes on offset for the lower control as it corresponds to the difference in low-water stages between two periods. The feasibility of using the shape of the recession to provide information on the dates of change and the changes in coefficient is also worth exploring.

Both sources of information could therefore be used both for detecting changes and for enhancing prior information of the SPD model.

5.7.2.2. Improving the SPD model

Only net changes were studied in this chapter: a further development is to investigate transient changes during a flood event and also between flood events.

The creation, the deletion and the substitution of controls during flood events are also worth further investigations. Note that creations or deletions of controls imply a change of matrix of controls whereas a substitution of controls only implies a change of exponent parameter c: the matrix of controls is unchanged.

A continuity condition on transition stages is used in the SPD model. This is not the case for the operational version of BaRatin for which the continuity condition is on the offset. A comparison of these two conditions could assess which one is more adapted. Some limitations on these conditions remain as the information on transition stage changes seems more difficult to specify.

The structural error model can also be improved. Currently, the error model is common to al the periods. This assumptions has been validated by comparing the SPD model with several independent applications of SD model on every period (see section 5.6.3). However, for other stations, it might be more relevant to use a specific error model for each stable period with distinct parameters. The feasibility of such highly parameterised model should be for both well-gauged and poorly-gauged stations per period.

Combining information on cumulated changes and incremental changes for assessing available information on a specific period may also enhance the SPD results as bathymetry can be available for some periods (but not alls). The current SPD model does not allow mixing information for cumulated changes and incremental changes.

5.7.2.3. Understanding of the model

In this chapter, only changes on offsets have been tested. The next step is to test the SPD model on stations for which coefficients change and on stations for which both coefficients and offsets change.

The impact of high-flows gaugings on the rating curve estimation of low-flow parameters could be investigated: do we need to keep gauging high-flow events for high-flow stable stations? Does the information brought by these high-flow gaugings enhance the understanding of low flows? Answering to these questions is of primary importance for operational services.

5.7.2.4. Going beyond retrospective analysis: real-time estimation of the rating curve

Operational issues (dam operation, flood forecasting, administrative decisions, etc.) sometimes require providing flow data and their uncertainties in real time. Dynamic management

of real-time rating curves is possible via a sequential Bayesian approach. This approach is currently been tested using the BaRatin software, following the idea that even when gaugings are lacking, changes in rating curves are guided by physical assumptions about the controls and the possibility and magnitude of changes. For instance, a possible change could be detected as soon as the stage goes above some critical value (to be determined). After such a possible change, the uncertainty in parameters subject to change can be inflated to reflect the fact that such parameters may have changed, and their current value is therefore poorly known. Consequently, after a possible rating change, the total uncertainty of the rating curve increases sharply, and several new gaugings will be needed to reduce it to an acceptable level. Such uncertainty analysis brings an answer to the recurring operational question: how many gaugings does it take to build an accurate rating curve after a change?

The SPD model could also be coupled to this sequential Bayesian approach in order to enhance the transfer of past information and the transfer of information between controls.

Chapter 6

Conclusions and perspectives

Contents

6.1. Summary

In this dissertation, three complex stage-discharge models are proposed. These models differ from simple stage-discharge (SD) models in their inputs and their parameterisation. A continuity with these simple SD models is made using the same Bayesian framework, the same structural error model and the same hydraulic analysis of the prior information. Taking into account both the hydraulic knowledge such as the geometry of controls or roughness estimates and stage-discharge observations leads to acceptable rating curve results even for poorly-gauged segments or poorly-documented sites.

Specific main results are related to each model:

- the stage-gradient-discharge (SGD) model allows accounting for hysteresis effect due to transient flow. As far as we are aware of, it is the first Bayesian model accounting for hysteresis event in the literature. This model needs the stage gradient as an additional input with the stage measurement. No additional measurement is required since stage records can be used to compute the stage gradient. However, fluctuations in the stage measurements may challenge the rating curve estimation as they are not related to the flood wave propagation. A suitable smoothing of the stage gradient is then required to solve the issue. Several hysteresis formulas, differing in their orders of expansion, were compared: the simpler Jones' formula shows the best results. The SGD model has valuable advantages: a SGD rating curve calibrated with a single flood event can be accurately applied to other events and the calibration can also be performed on several distinct flood events. A gauging strategy is proposed and shows better results than common ones. This strategy implies gauging near some remarkable points describing the loop curve (minimum and maximum of the stage, maximum of discharge, minimum and maximum of the stage gradient), and during the falling limb (to properly explore negative stage gradients) but not necessarily during the same event. To finish, the SGD method does not detect hysteresis when it is applied to well-known and well-identifiable unique stage-discharge relation.

- the stage-fall-discharge (SFD) model accounts for the influence in the stage-discharge relation of variable backwater effects due to unsteady downstream boundary conditions. This influence makes the energy slope variable when the control is backwater-affected. Two types of backwater-affected controls were studied, which has led to two variants of the SFD model: (SFD-s) a backwater-affected channel control which follows a section

control drowned by the downstream surge of the river; (SFD-c) a backwater-unaffected channel control which follows a backwater-affected channel control. The energy slope for modelling the friction effect of backwater-affected controls is directly computed using the stage records from two gauge stations. The interest of estimating the difference in staff gauge reference levels as an additional parameter was illustrated: this difference may bear non negligible errors, and hence need to be estimated, not fixed. The SFD model has been operationally deployed by the Compagnie Nationale du Rhône (CNR) and yields acceptable results [Horner et al., 2015, Le Coz et al., 2016b].

- the stage-period-discharge (SPD) model estimates net rating changes due to bed evolution. Rating changes between periods are modelled as net changes in parameters of the rating curve, assuming that dates of changes are known. This is an original method as gaugings are not used across periods and the model does not need to assume that gaugings 'age'. The gaugings are assigned to the period during which they were performed and their uncertainties remain unchanged over time. The information on assumed stable controls is transferred by assessing stable parameters which are used across periods. Moreover, the global changes on the main channel are also applied to lower controls. This transfer of information between periods and controls allows identifying rating curves on scarcely gauged controls and scarcely gauged periods. The SPD model also shows accurate and precise results when the station is well-documented with gaugings. Only changes in offsets were tested but the SPD model was also implemented for changes in coefficients. The detection of the dates of rating changes remains untreated in this thesis but several approaches can be further investigated.

All the methods proposed in this thesis have been implemented as executables in the most general way.

6.2. Perspectives

6.2.1. Modelling other causes of rating curve non-uniqueness

Getting back to the examples of causes of rating curve non-uniqueness shown in figure 1.1, this PhD addressed several physical processes: hysteresis due to transient flow (g), variable backwater effects due to unsteady boundary condition (e-f) and net changes due to bed evolution (b). However, several other causes remain to be studied.

Some of these other non-uniqueness relations may be similar to the ones studied in the thesis. For example, the external influences on the flow exerted by the wind (wind shear stress) or exerted by ice jams and the influence of log jams both modify the energy slope (table 2.1), and could therefore be treated in a similar way as hysteresis due to transient flow. The formula accounting for such non-uniqueness would of course be different and the input variables would also differ: for instance wind shear stress may need the wind velocity magnitude and direction instead of hydraulic gradient [Falconer et al., 1991]. Another example could be the hysteresis due to overbank flow in compound channel [Sellin, 1964, Smart, 1992, Ackers, 1993]. This stage-discharge relation shows non-uniqueness as discharge values in the upper segment (main channel + floodplain) differ at a given stage: discharges in the rising limb are smaller than discharges in the falling limb due to head losses (e.g., roughness difference between controls and flow turbulences).

Some physical processes may be more challenging, because the main covariate may be difficult to obtain. Typically rating changes due to aquatic vegetation may be more difficult to model: a quantitative covariate describing the development stage of vegetation is unlikely to be available at every gauging station. Two options may help solving this problem:

- a deterministic seasonal signal (pattern) combined to frequent summer gaugings may be used to identify more precisely the drift of the rating curve;
- the use of aquatic vegetation growth models. The existence of such models needs to be evaluated in the literature, but it may help accounting for the specificities of each year, in terms of climate for instance, or the specificities of the vegetation.

6.2.2. Combining several causes of rating curve non-uniqueness

In this dissertation, causes of non-uniqueness are separately treated, but could be combined. For instance, the rating curves of two dam flushes of the Ebro River at Ásco (see section 3.4.1) present a shift: a net rating change in offsets was observed by operating managers. Hysteresis due to transient flow and rating changes may hence be combined. Another example of such combination may be the backwater influence and net rating changes.

It is probably feasible in principle to combine several formulas as some of them do not have the same influence in the rating curve parameters. Note however that some combinations make little sense: for instance mixing a SFD and a SGD model is useless because directly measuring the fall makes the stage gradient irrelevant as it is already taken into account in the computed fall. It also raises questions on the identifiability of several causes from gaugings only: which effect would gaugings represent when two or more causes of non-uniqueness apply? The hydraulic expertise would probably have to play an important role.

The combination of several non-uniqueness causes raises an unsolved issue in this PhD: can all causes be studied within a unique framework? In principle, it can be implemented: we simply calibrate a model with potentially many covariates as inputs. However, in practice, it is more difficult, because we want to preserve the hydraulic consistency and interpretability of such a general model.

6.2.3. Improving the error models

Several of the error models used in this PhD could be improved. These improvements are of general interest, and are not specific to the particular complex rating curve models developed in this thesis:

- the assumption that errors in gauged discharges are independent and of mean zero can be criticised. It is problematic because there may be unknown biases between gaugings that are specific to each gauging method. For instance all surface velocity gaugings may be affected by the same bias induced by the surface velocity coefficient. A possible solution may be to include an unknown non-zero mean common to all gaugings made with the same method;

- the measurements errors of the inputs are neglected. For stage measurement, recent work by Horner et al. [2017] shows that the effect of stage errors in discharge prediction is not always negligible, especially if the errors encompass a systematic component. This approach could be generalised for other input variables such as stage gradient or fall. Note for instance that a systematic error on stage would cancel in the stage gradient.

- the structural error model raises a significant issue as this model should recognise a systematic component. It is probably the biggest challenge of the error model improvements. Currently, structural errors are indeed assumed independent which facilitates their expression. It may be problematic because independently-sampled errors tend to disappear for aggregated variables [Horner et al., 2017], so that for instance structural uncertainty is often negligible for monthly discharge. The current structural error model is clearly unsatisfying and disputable. However, the improvement of the structural error model remains unclear at this stage: we do not know how it could be done.

6.2.4. Real-time discharge estimation

This PhD only dealt with the retrospective analysis of rating curves: the final objective of such analysis, and hence the proposed models (SGD, SFS, SPD) is basically to predict discharge times series and their uncertainties, given all historical gaugings and hydraulic information.

The real-time context has a different objective: predicting the discharge and its uncertainties NOW, using all information that can be made available at the time of the prediction. In particular, the real-time prediction is only valuable at the time it was made: correcting it two months later for example is irrelevant in the real-time context (this is rather the purpose of a retrospective analysis).

The adaptation of the methods developed in this thesis to a real-time context is not trivial. Neglecting stage error measurements, the SGD and SFD models may be less difficult to adapt to real time context as all their inputs, which are both related to stage records, can therefore be assessed in real time. However, this is particularly less obvious with the SPD model as several issues on the detection of periods need to be solved first. Indeed, it needs to be able to detect a possible change before a new gauging is performed. The most promising approach seems to be using critical stage values that trigger a possible change, based on sediment transport capacity considerations (see section 5.7.2.1).

6.2.5. Exploring the impact of rating curve uncertainties in Hydrology

As explained in the introduction, discharge is the basic variable of Hydrology. Impact of rating curve uncertainties should therefore be ubiquitous. For example in the context of flood frequency analysis, it has been reasonably thoroughly studied [e.g., Kuczera, 1992, 1996, Petersen-Øverleir and Reitan, 2009b, Neppel et al., 2010, Lang et al., 2010, Di Baldassarre et al., 2012, Steinbakk et al., 2016]. However, it is much less studied for non-flood variables, which is problematic because e.g., low flows are also strongly impacted by rating curve uncertainties.

It should also be investigated in the context of hydrologic modelling: rating curve uncertainties impact the calibration of the hydrologic model. This has been studied [e.g., Thyer et al., 2009, McMillan et al., 2010, Sikorska et al., 2013], but the error models used in these studies may be too simplistic, especially for complex rating curves. Rating curve uncertainties also impact the evaluation of hydrologic models [e.g., Westerberg and McMillan, 2015].

6.2.6. Operational perspectives

Several achievements in this respect were already realised during the PhD:

- a documented executable piloted by text files is currently used by the CNR for establishing SFD rating curves at their twin-gauge stations;
- other models are ready in a similar form;
- practical gauging strategies were suggested in order to enhance the rating curve estimation.

A main strong objective is the integration of complex models in BaRatinAGE, the software currently released and used by some hydrometric services for permanent rating curves. The actual integration in BaRatinAGE was clearly not part of this PhD work. However, this was kept in mind by always trying to maintain the greatest generality and compatibility with existing concepts, in particular the matrix of controls, which is at the core of BaRatinAGE. For instance SGD models could be integrated by enabling its application for the main channel control only. Similarly, the SPD model is fairly general and compatible with the matrix of control. As a matter of fact, equation (5.1) directly shows this compatibility. The integration of the SFD model in BaRatinAGE is more challenging: the two models developed are actually specific to two particular hydraulic configurations, and it is unclear how this could be fully generalised.

Another objective is the Bayesian inference of the index velocity method. This method (see e.g., side-looking ADCP, Doppler flowmeters like the gauging flume A1 in section 3.4.2, permanent surface velocity radars), described in Levesque and Oberg [2012], consists of computing discharges using two calibrated rating curves: a stage-area rating curve and a index velocity-average velocity rating curve. This method, which can be seen as a complex rating curve, is more and more used at hydrometric stations, and may help modelling non-unique relations such as variable backwater influence or hysteresis due to transient flow.

Practical tools for detecting non-uniqueness in rating curves would also be valuable, not only based on gaugings:

- detecting hysteresis based on the properties of the gauging site and information extracted from the stage time series ($h(t)$ and dh/dt);
- detecting rating changes and estimating their magnitudes based on the stage time series:
  - analysis of lower stages and/or of stage recessions;
  - use of sediment transport capacity.

Acknowledgements

Many people have helped me during my PhD: here is a non-exhaustive list of those persons.

My PhD fellowship is funded by Irstea and the Compagnie nationale du Rhône (CNR), with the support of the French national hydrological services (SCHAPI).

I am very grateful to the Hydrology department of the *Confederación Hidográfica del Ebro* (CHE) and the researchers of the RIUS group of the University of Lleida who have share the Ascó data (Ebro River, Spain). Expertise given by Ramonón Sánchez and M^{a} Luisa Moreno (CHE) on the Ascó station was also helpful. I also thank François Birgand (Associate Professor, Biological & Agricultural Engineering, North Carolina State University) for sharing the gauging flume data (near Plymouth, USA).

The use of the data of the Madeira River at Fazenda was possible thanks to the Brazilian National Water Agency (ANA), the Brazil Geological Survey (CPRM) and the HyBAM observation service. These data are available online (`http://www.ore-hybam.org/index.php/eng`) from the HyBAM observation service following registration. Work realised on the Madeira River would never have been possible without Philippe Vauchel (IRD). Data for the Guthusbekken station were made available online by Trond Reitan (`http://folk.uio.no/trondr/hydrasub/ratingcurve.html`). Data for the Valence station were provided by CNR (special thanks to Gilles Pierrefeu, Raphaël Le Boursicaud and Karine Pobanz). These data are available from them upon request (`g.pierrefeu@cnr.tm.fr`).

During my New Zealand stay, exchanges with hydrologists, hydrometers and operational managers were very helpful in the SPD model development. I personally thank Mike EDE and his team, from Marlborough Regional Council. The field visit of the Barnett's Bank station (Wairau River, New Zealand) and the personal expertise of Mike EDE on this station helped me a lot. I also thank Martin Doyle and his team from Tasmin Regional Council as they provided thoughtful advices on my first (was it the fourth?) version of the SPD model. The kayak gauging was very interesting to see too. I would like to personally thank Martin and his wife for their

warm welcome in their house. During this New Zealand stay other people have also helped me: I thank Marty Flanagan from NIWA for the Rakaia data and his expertise, Andrew Willsman also from NIWA for the Shotover data and Kathy Walter from NIWA for the amazing help she provided on the New Zealand data. I also thank Brent Watson from Horizon Regional Council for the Pohangina data. And last but not least, I want to thank Graeme Smart (NIWA) and Hilary McMillan (ex NIWA, now Associate Professor at San Diego State University) for their help during my stay. These exchanges were possible thank to PHC Dumont D'Urville project 34185SH (2015-2016), financed by the French Ministry of Foreign and European Affairs and the French Ministry of Higher Education and Research, by an Irstea grant for both the 1-year scientific stay of Jérôme Le Coz at the NIWA in Christchurch, New Zealand. I also wish to acknowledge the research funding provided by the Région Rhône-Alpes (Explora'doc) for my 3-month stay, also at the NIWA in Christchurch, New Zealand. Other people have also helped me to finish this SPD model. I thank the Pôle HPC Grand-Delta and Guillaume Fourquet for data and informations on the station of the Ardèche River at Meyras-Barutel, France. This station have been studied by the ANR (Agence Nationale de la Recherche) project FloodScale (under contrat ANR 2011 BS56 027) which contributes to the HyMeX international program. I also thank people involved in this ANR project.

In this thesis, I have used the DMSL Fortran library developed by Dmitri Kavetski (University of Adelaide, Australia) and I thank him for it.

Annexes

Appendix A

Application of the SGD model to additional sites

Contents

A.1. The Ohio river at Wheeling, West Virginia, USA

This case study is presented in Petersen-Øverleir [2006]. In the end of March 1905, a hysteresis flood event occurred in the Ohio River at Wheeling near Pittsburgh in the USA. 13 stage-discharge measurements were performed during this hysteretic flood event. 4 stage-discharge measurements were also made at low flows around 10 days before the event.

Only one control is considered: the main channel, 340 m in width. The Strickler coefficient of this natural river is set to 30 $\mathrm{m}^{\frac{1}{3}}.\mathrm{s}^{-1} \pm 10\ \mathrm{m}^{\frac{1}{3}}.\mathrm{s}^{-1}$. It is a relatively flat channel (slope S_0 around 5×10^{-4}) with a wide rectangular cross-section. We use the SGD model using the Jones formula with variable celerity. The prior distributions are set up accordingly (see table A.1). We assigned a 10% uncertainty discharge to all the gaugings.

Two calibrations are made: one with only the 13 hysteretic gaugings, the other with all the gaugings, including the 4 gaugings made at low flows before the flood event.

Parameter	**Prior distribution**	**Posterior distribution**	
		All gaugings	**Only hysteretic gaugings**
K_S $[\mathrm{m}^{\frac{1}{3}}.\mathrm{s}^{-1}]$	$\mathcal{N}(30, 5)$	37.0 (4.13)	34.0 (4.91)
h_0 [m]	$\mathcal{N}(0, 1)$	−1.54 (0.207)	−1.84 (0.509)
exponent M [−]	$\mathcal{N}(1.6667, 0.05)$	1.684 (0.0414)	1.676 (0.0459)
B [m]	$\mathcal{N}(340, 20)$	344.9 (18.91)	353.8 (19.32)
S_0 [−]	$\mathcal{N}(0.0005, 0.001)$	8.19×10^{-5} $\left(3.27 \times 10^{-5}\right)$	8.85×10^{-5} $\left(5.08 \times 10^{-5}\right)$
γ_1 $[\mathrm{m}^3.\mathrm{s}^{-1}]$	$\mathcal{U}\left(-10^6, 10^6\right)$	0.141 (28.8)	1.09 (114)
γ_2 [−]	$\mathcal{U}\left(-10^6, 10^6\right)$	0.00935 (0.00757)	0.00407 (0.0136)

Table A.1 – Distribution of the hydraulic variables for the event of March 1905 at Wheeling. The symbol $\mathcal{N}(\mu, \sigma)$ corresponds to the normal distribution with mean μ and standard deviation σ. The symbol $\mathcal{U}(a, b)$ corresponds to the uniform distribution on the interval $[a, b]$. For posterior distributions, the given values correspond to the MAP (Maximum a posteriori) estimator and the standard deviation in brackets.

A first observation of rating curves shows that both calibrations detect hysteresis. As we can see on figure A.1, the rating curve of the calibration with all the gaugings is a loop and fits well the discharge measurements. The hysteresis effect cannot be considered to be negligible because differences in discharge between rising and falling limbs can be as high as 20%. The structural uncertainty interval is very small: the model is suitable for this kind of event.

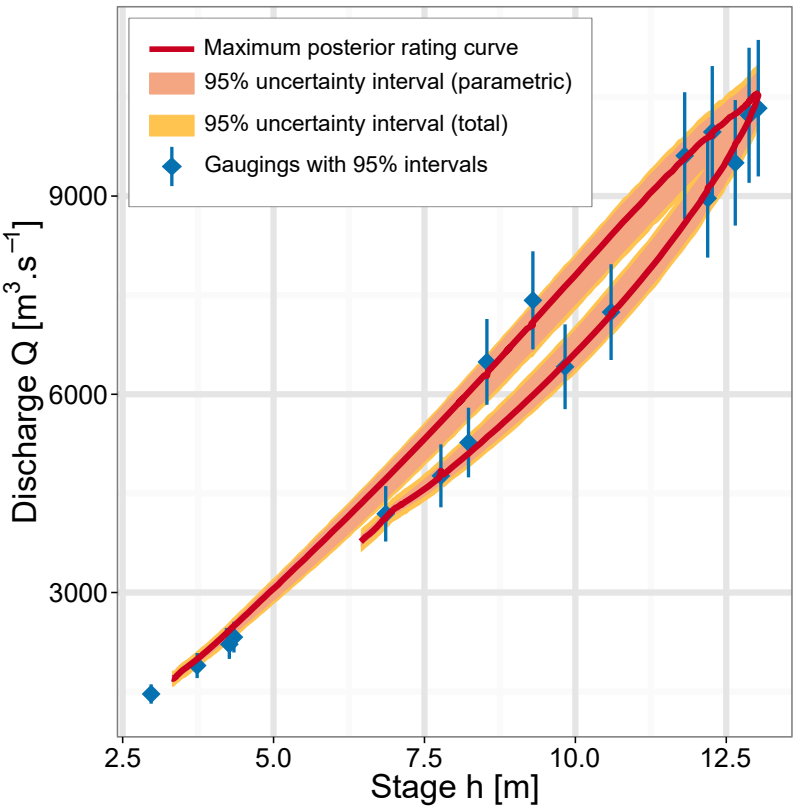

Figure A.1 – The Ohio River at Wheeling: maximum posterior rating curve of the SGD model using the Jones formula with variable celerity c. The rating curve is calibrated using all the gaugings (the 13 gaugings made during the flood) plus the 4 gaugings made before the flood.

Discharge time series computed with both calibrations (see figure A.2) follow the dynamics of the flood. There is less than 5% of errors between MAP rating curves and gaugings for both calibrations. This event differs from the two dam flushing events in the Ebro River (see section 3.4.1) by the severity of the flood: it is not a quick and strong rising limb as it lasted more than 3 days. The stage gradients in the rising limb have the same order of magnitude than those in the falling limb.

Maximum posterior rating curves are quite similar for both calibrations. However, including a few low-flow discharge measurements in the calibration of the rating curve brings better results. Indeed, lengths of uncertainty intervals (see figure A.3) are significantly reduced. For low flows, it is because the bottom h_0 of the riverbed is better identified (see associated posterior density in figure A.4). The estimation of error parameter γ_1 (dominant term in the structural error model for low discharges) is also more precise (figure A.4).

The improvement of γ_2 estimation is less pronounced.

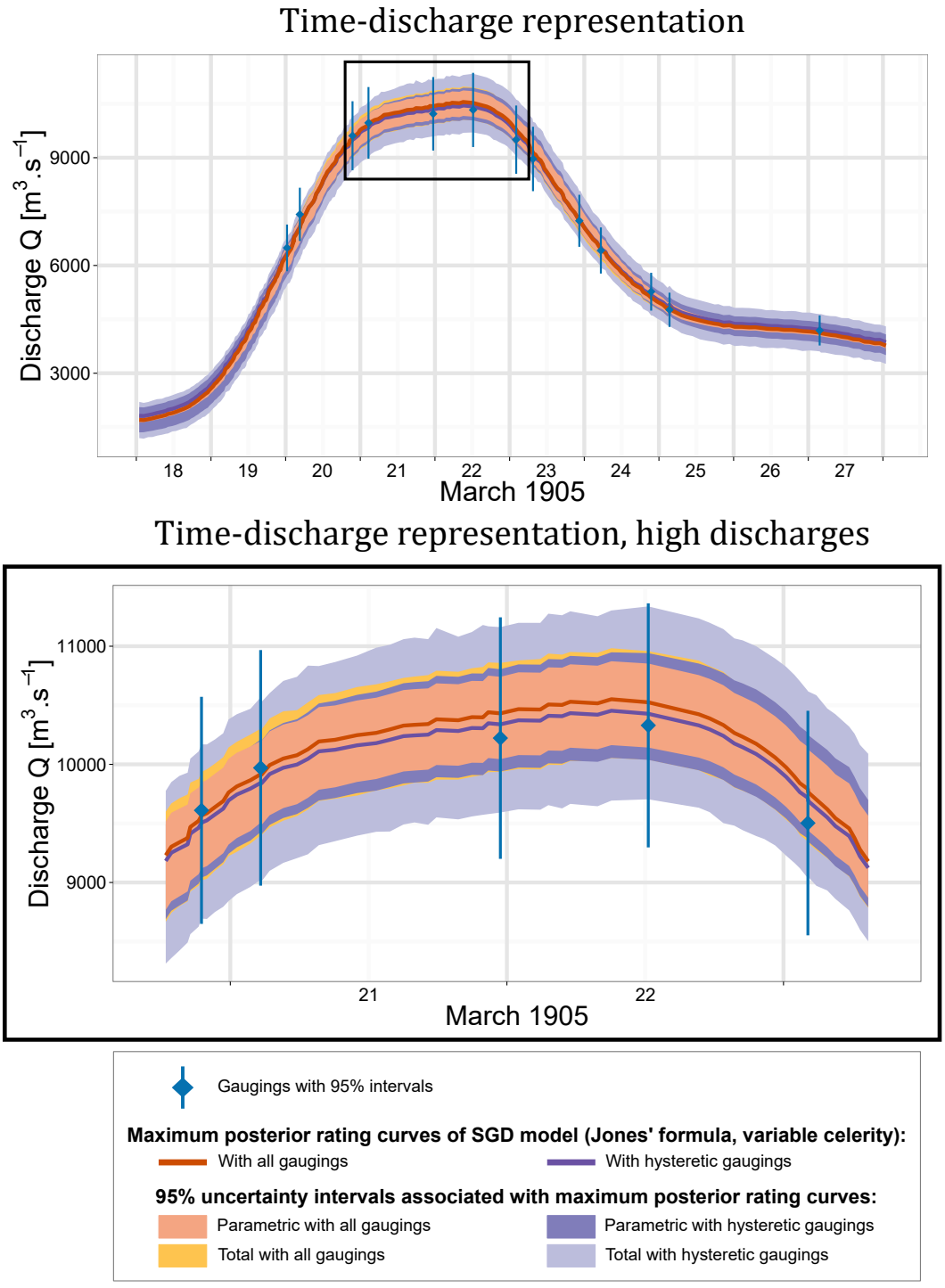

Figure A.2 – Ohio river at Wheeling: time-discharge representation. Use of the SGD model using the Jones formula with variable celerity c. Comparison between a calibration made with all the gaugings and a calibration made with hysteretic gaugings only.

Thus, adding some steady discharge measurements to hysteretic gaugings in the calibration of the rating curve lead to more precise parameter estimates. In turn, this reduce uncertainties both both low flows and at the peak flow.

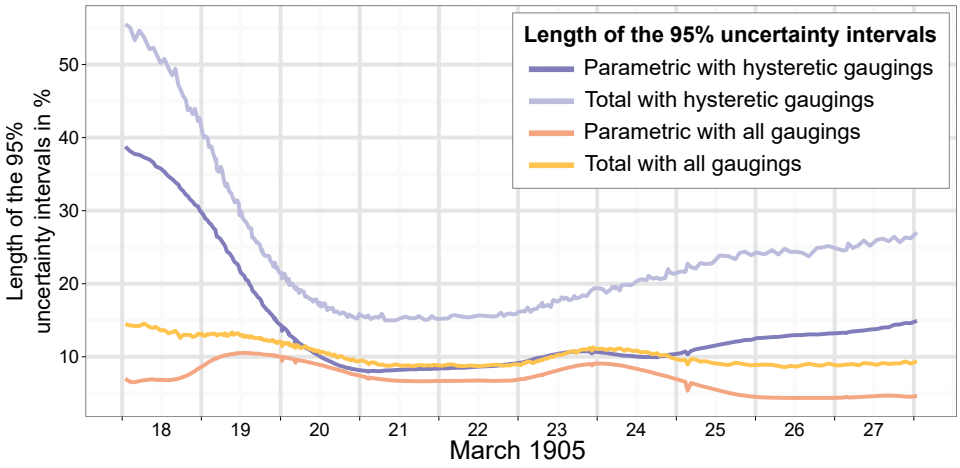

Figure A.3 – The Ohio River at Wheeling: length in percentage of the 95% uncertainty intervals of the SGD model using the Jones formula with variable celerity c. Comparison between a calibration made with all gaugings and a calibration made with only hysteretic gaugings.

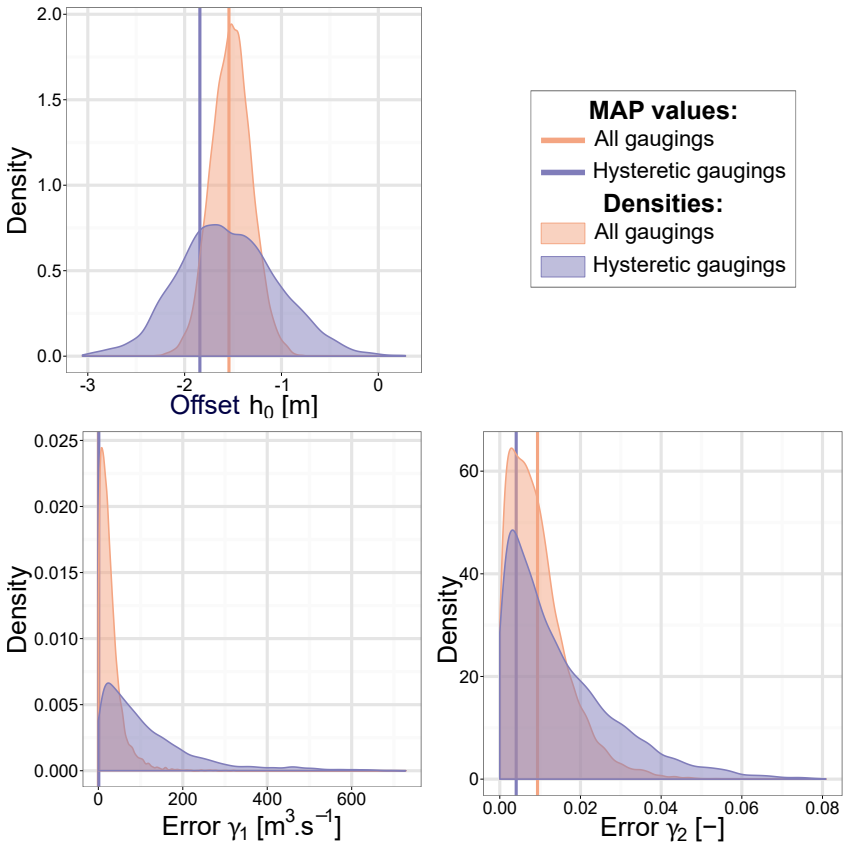

Figure A.4 – Ohio river at Wheeling: densities of posterior distributions and maximum posterior (MAP) values of the offset h_0, the error γ_1 and the error γ_2. Use of the SGD model using the Jones formula with variable celerity. Comparison between a calibration made with all gaugings and a calibration made with only hysteretic gaugings.

A.2. The Ardèche River at Sauze, France: negligible hysteresis

Already presented by Le Coz et al. [2014], the Sauze station in Saint-Martin-d'Ardèche is a straight channel carved in an inerodible limestone bedrock. Flows are governed by two controls (see figure A.5): a riffle at low flows and the main channel. Due to the instability of the riffle, changes of the low-flow control happen. However, we only focus on the second control, and hence on a very stable stage-discharge relation because hysteresis only affects the energy slope of channel controls.

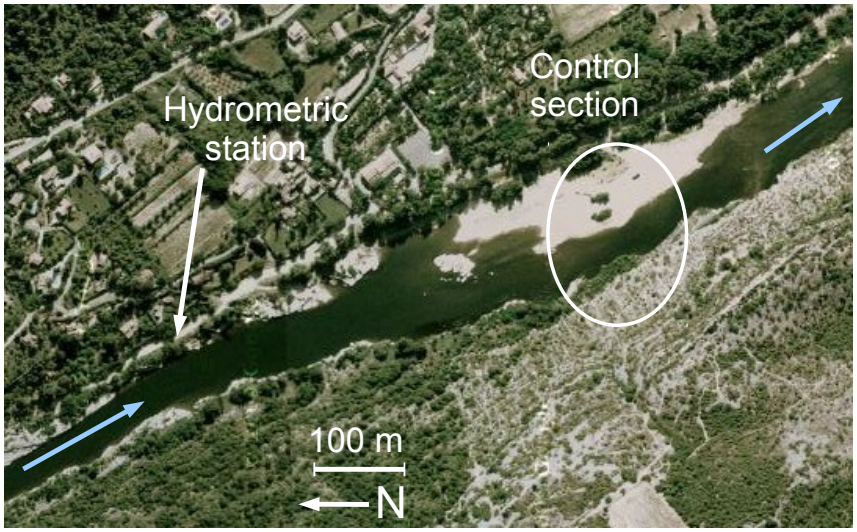

Figure A.5 – The Ardèche River at Sauze: view of the hydraulic controls [Le Coz et al., 2014].

We want to know if the main channel control can be prone to hysteresis effects, which seems unlikely given the high slope.

Two models are used: a stage-discharge (SD) model and the stage-gradient-discharge (SGD) model using the Jones formula with variable celerity. Both models are calibrated with 107 gaugings and with strictly the same prior information on rating curve parameters. We will denote by B_1 the width of the riffle, g the gravity and C a discharge coefficient. Both models are recalled below:

- SD model:

$$Q(h) = \begin{cases} CB_1\sqrt{2g}\,(h-h_0)^M & \text{if } h < \kappa \\ K_S B\sqrt{S_0}\left(h-h_0^{'}\right)^{M^{'}} & \text{if } h \geq \kappa \end{cases}$$

where $h_0^{'} = \kappa - \left[\frac{CB_1\sqrt{2g}}{K_S B\sqrt{S_0}}(\kappa - h_0)^M\right]^{\frac{1}{M'}}$ is computed by continuity in $h = \kappa$;

- the SGD model using the Jones formula with variable celerity for two controls:

$$Q\left(h, \frac{\partial h}{\partial t}\right) = \begin{cases} CB_1\sqrt{2g}\,(h - h_0)^M & \text{if } h < \kappa \\ K_S B\left(h - h_0^{'}\right)^{M'}\sqrt{S_0 + \dfrac{1}{M' K_S\sqrt{S_0}\left(h - h_0^{'}\right)^{M'-1}}\dfrac{\partial h}{\partial t}} & \text{if } h \geq \kappa \end{cases} \quad \text{(A.1)}$$

where $h_0^{'} = \kappa - \left[\frac{CB_1\sqrt{2g}}{K_S B\sqrt{S_0}}(\kappa - h_0)^M\right]^{\frac{1}{M'}}$ is also computed by continuity in $h = \kappa$ and $\frac{\partial h}{\partial t} = 0$;

Physical parameters with units	**Prior distributions**	**Posterior distributions**	
		SGD model using the Jones formula with variable celerity	**SD model**
$CB_1\sqrt{2g}$ [$m^{\frac{3}{2}}.s^{-1}$]	$\mathcal{N}(50, 100)$	48.3 (2.01)	47.2 (2.01)
h_0 [m]	$\mathcal{N}(-0.5, 1)$	−0.358 (0.0244)	−0.367 (0.0244)
exponent M [−]	$\mathcal{N}(1.5, 0.05)$	1.54 (0.0434)	1.53 (0.0434)
κ [m]	$\mathcal{N}(1, 1)$	1.08 (0.0381)	1.06 (0.0381)
$K_S B\sqrt{S_0}$ [$m^{\frac{4}{3}}.s^{-1}$]	$\mathcal{N}(145, 40)$	122.5 (9.33)	118.9 (9.37)
K_S [$m^{\frac{1}{3}}.s^{-1}$]	$\mathcal{N}(33, 5)$	31.4 (4.27)	-
B [m]	$\mathcal{N}(80, 10)$	77.8 (9.03)	-
S_0 [−]	$\mathcal{N}(0.003, 0.001)$	2.52×10^{-3} $\left(7.72 \times 10^{-4}\right)$	-
$h_0^{'}$ [m]	Computed by continuity	0.284 (0.0515)	0.263 (0.0515)
exponent $M^{'}$ [−]	$\mathcal{N}(1.6667, 0.05)$	1.65 (0.0395)	1.67 (0.0396)
γ_1 [$m^3.s^{-1}$]	$\mathcal{U}\left(-10^6, 10^6\right)$	2.66 (0.624)	2.41 (0.628)
γ_2 [−]	$\mathcal{U}\left(-10^6, 10^6\right)$	0.0523 (0.0109)	0.0572 (0.0109)

Table A.2 – Prior and posterior results of the parameters of SGD and SD models applied to the Ardèche River at Sauze. The symbol $\mathcal{N}(\mu, \sigma)$ corresponds to the normal distribution with mean μ and standard deviation σ. The symbol $\mathcal{U}(a, b)$ corresponds to the uniform distribution on the interval $[a, b]$. For posterior distributions, the given values correspond to the MAP (Maximum a posteriori) estimator and the standard deviation in brackets. Gray values corresponds to a computation from others variables.

We use the same parameterisation as in table 3.3 (section 3.3.1). Thus the SD model has 8 parameters only (6 for hydraulic variables and 2 for the error model) whereas the SGD model has 10 parameters. Prior distributions (table A.2) are set up according to hydraulic knowledge (see Le Coz et al. [2014] for more information).

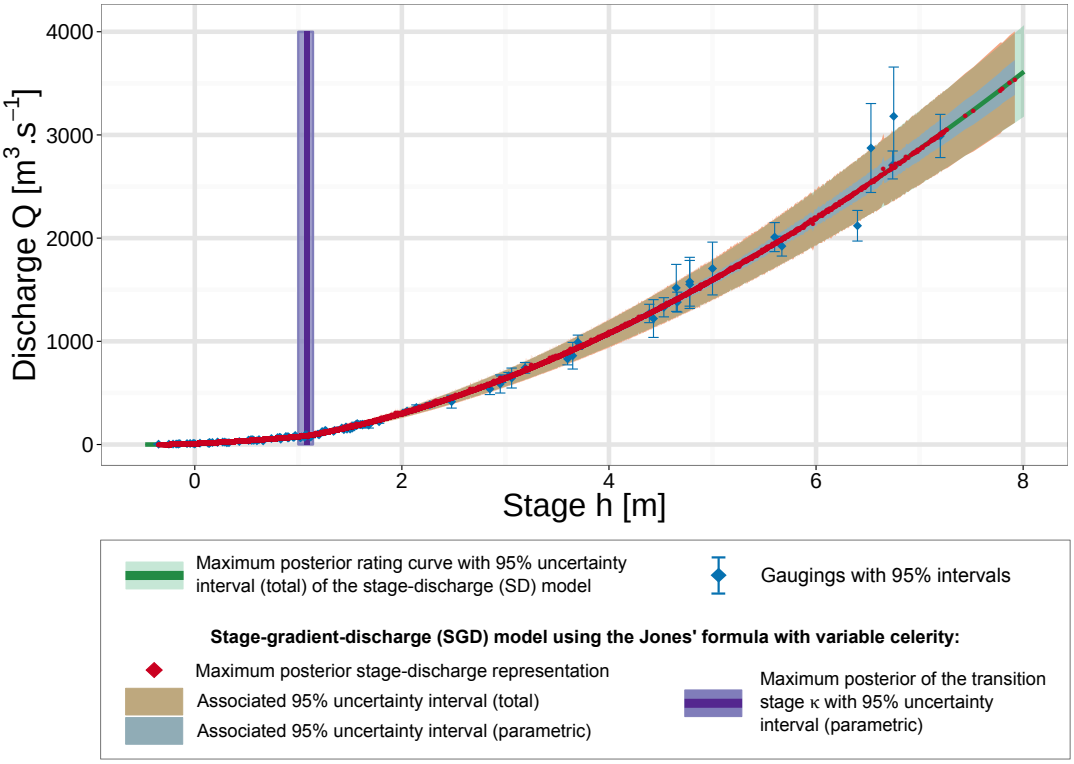

Figure A.6 – The Ardèche River at Sauze: stage-discharge representations.

There is no difference between both models: total and parametric uncertainties are exactly the same. If we look into values from the posterior distribution (MAP and standard deviation values in table A.2), we also notice that all values are very similar between models.

The Jones formula with variable celerity c (equation (A.2)) can be rewritten as a correction of the rated discharge $Q_0 = K_S A \sqrt{S_0} R_h^{2/3}$ at steady flows as follows:

$$Q = K_S A \sqrt{S_0} R_h^{2/3} \times \sqrt{1 + \frac{1}{S_0\, c\,(h)} \frac{\partial h}{\partial t}} = Q_0 \times \sqrt{1 + \frac{J_0}{S_0}} = Q_0 \times J\left(h, \frac{\partial h}{\partial t}\right) \tag{A.2}$$

where $J\left(h, \frac{\partial h}{\partial t}\right) = \sqrt{1 + \frac{J_0}{S_0}}$ is the correction of Jones, $J_0 = \frac{1}{c\,(h)} \frac{\partial h}{\partial t}$ is the correction of the slope of the riverbed S_0 and $c\,(h) = \frac{1}{B} \frac{\partial Q_0}{\partial h}\,(h)$ is the variable kinematic wave celerity. Therefore, the use of a hysteresis model becomes relevant as soon as the correction $J\left(h, \frac{\partial h}{\partial t}\right)$ is far from 1, or the slope correction J_0 is far from 0.

The temporal representation during the 35-years time period of the correction J_0 of the slope reveals 6 flood events (circled in black in figure A.7) which could be affected by the hysteresis. Indeed, whereas for all the other events this correction is of the order of 5.0×10^6, these 6 flood events have a correction which ranges up to 5.0×10^4.

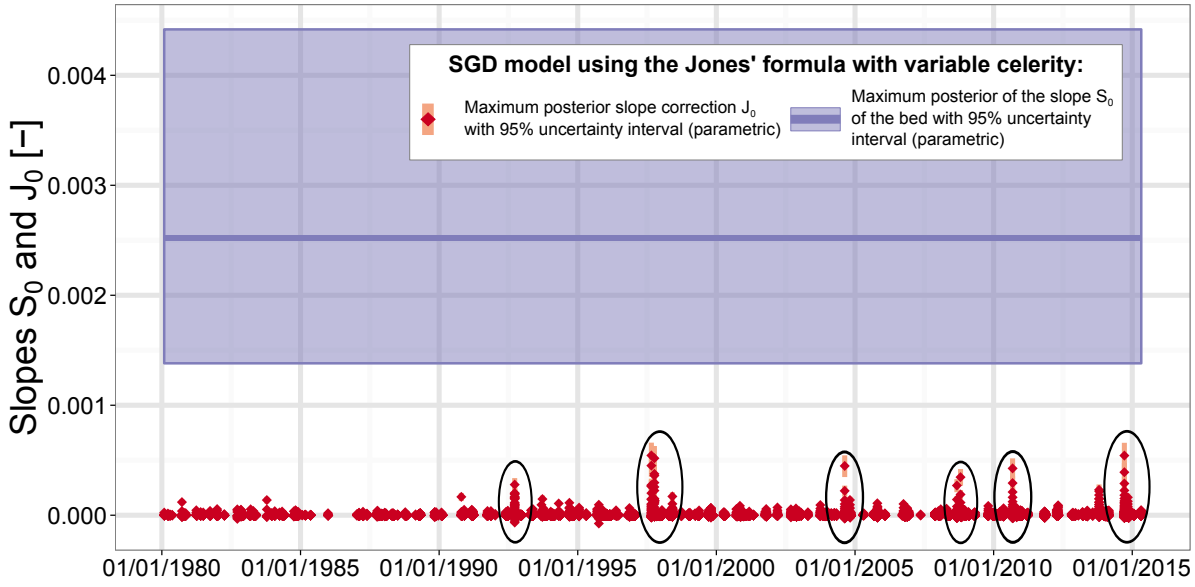

Figure A.7 – The Ardèche River at Sauze: temporal evolution of the slope correction J_0. Comparison with the posterior distribution of the slope S_0 of the bed. The events with the greatest correction J_0 are circled in black.

We also find these six events in the representation of the correction of Jones $J\left(h, \frac{\partial h}{\partial t}\right)$ of the rated discharge Q_0 at steady flow. This correction may vary up to 10% with the unique relation (see figure A.8) but only for very few events (less than 0.2% of the points corresponding to the high-flow channel control).

The frequency of the correction of Jones $J\left(h, \frac{\partial h}{\partial t}\right)$ during the last 35 years reveals that a correction of 5% exists in less than 0.002% of the cases.

An in-depth study of the events associated with these cases shows that there is no hysteresis effect: the rating curve for each event does not present a loop (see figure A.9). Moreover the stage measurements associated with the biggest corrections of Jones are always near the transition between the two controls. This phenomenon is observed as soon as the riffled is drowned, and not just for these 6 events. This is due to higher stage gradients during this transition which leads to isolated errors.

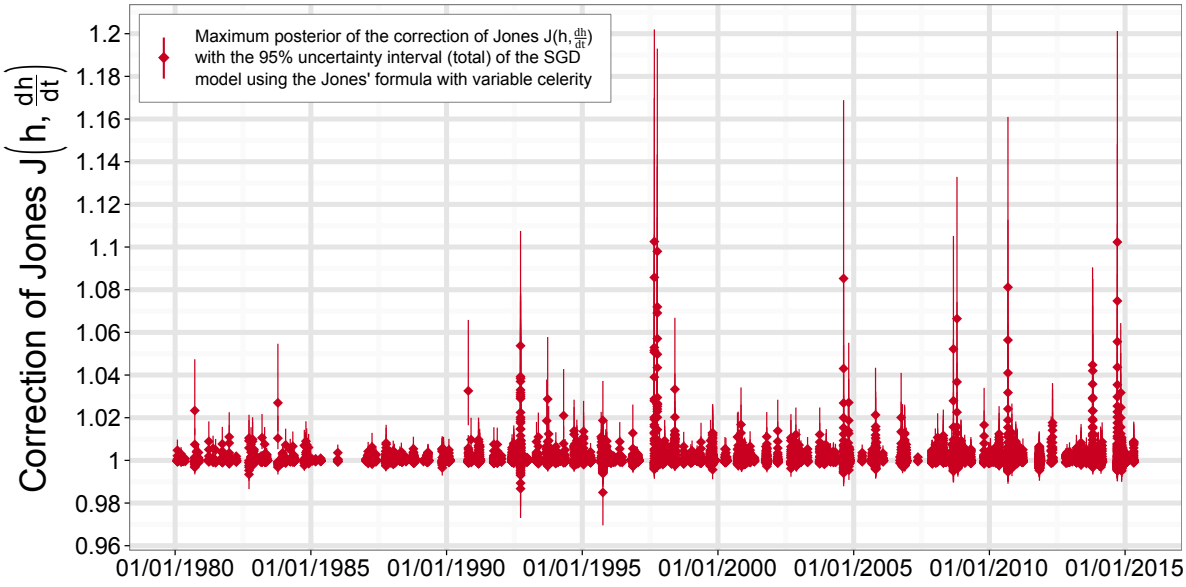

Figure A.8 – The Ardèche River at Sauze: representation of the correction of Jones. Use of the Jones model with variable celerity c.

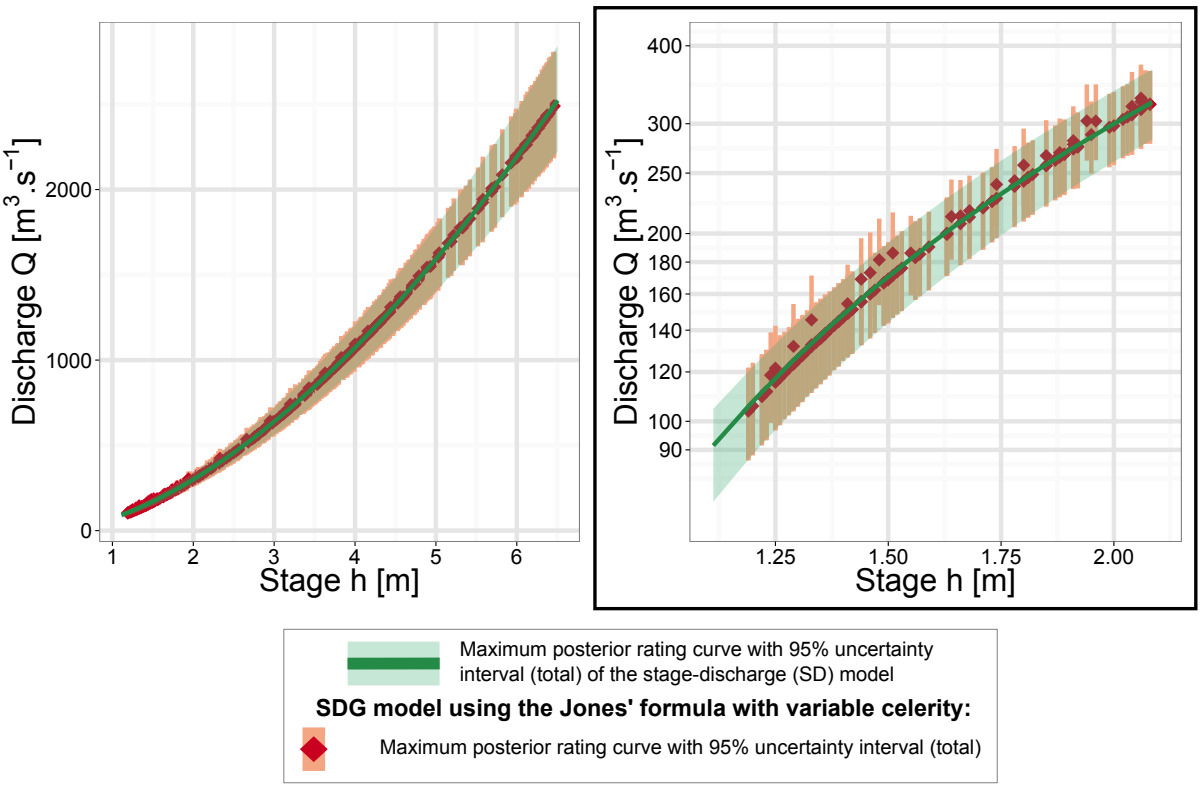

Figure A.9 – The Ardèche River at Sauze: stage-discharge representation of the events with the greatest values of correction J_0 of the slope. Comparison with SD model (on the left). Log representation of discharges for low stages (on the right).

A.3. Conclusions

Application of the stage-gradient-discharge (SGD) model to the classic event of the Ohio River at Wheeling station confirms the efficiency of the method to capture hysteresis. It also confirms that the best gauging strategy is to combine low-flow gaugings and gaugings all around the hysteresis loop.

Application to the Ardèche River at Sauze shows that the SGD model yields results identical to the SD model at sites where hysteresis is negligible. Isolated errors may occur due to higher stage gradients during transition between the low-flow section control and the channel control.

Appendix B

Multivariate distribution for offset change parameters

Contents

B.1. Properties

This section is the summary of definitions, properties, theorems and relations used in this annexe. We let the reader refer to the literature for a better understanding.

B.1.1. Expectation and Covariance

Property 1 (Product of independent random variables) *Let $(X_1, \ldots, X_n)$ be n independent random variables. Then, for all measurable functions φ_i, we have:*

$$\mathbb{E}\left[\prod_{i=1}^{n} \varphi_i\left(X_i\right)\right] = \prod_{i=1}^{n} \mathbb{E}\left[\varphi_i\left(X_i\right)\right]$$

Definition 1 (Covariance) *Let X and Y be two jointly distributed random variables with finite second moments. The covariance $Cov(X, Y)$ between X and Y is defined as:*

$$Cov(X, Y) = \mathbb{E}\left[\left(X - \mathbb{E}\left[X\right]\right)\left(Y - \mathbb{E}\left[Y\right]\right)\right]$$

Theorem 1 (König-Huygens) *If X is a real random variable, then:*

$$\mathbb{V}ar[X] = \mathbb{E}\left[X^2\right] - \left(\mathbb{E}\left[X\right]\right)^2$$

Combining definition 1 and theorem 1 gives the following relation:

$$\mathrm{Cov}\left(X, Y\right) = \mathbb{E}\left[XY\right] - \mathbb{E}\left[X\right]\mathbb{E}\left[Y\right] \tag{B.1}$$

Therefore, if X and Y are independent, using property 1 in equation gives:

$$\mathrm{Cov}\left(X, Y\right) = 0 \tag{B.2}$$

Let X, Y and Z be 3 independent real random variables. Then:

$$\begin{aligned}
\mathrm{Cov}\left(XZ, YZ\right) = &\ \mathbb{E}\left[XYZ^2\right] - \mathbb{E}\left[XZ\right]\mathbb{E}\left[YZ\right] \ \text{(cf. equation B.1)} \\
= &\ \mathbb{E}\left[X\right]\mathbb{E}\left[Y\right]\mathbb{E}\left[Z^2\right] - \mathbb{E}\left[X\right]\mathbb{E}\left[Y\right]\left(\mathbb{E}\left[Z\right]\right)^2 \ \text{(cf. property 1)} \\
= &\ \mathbb{E}\left[X\right]\mathbb{E}\left[Y\right]\left(\mathbb{E}\left[Z^2\right] - \left(\mathbb{E}\left[Z\right]\right)^2\right) \\
= &\ \mathbb{E}\left[X\right]\mathbb{E}\left[Y\right]\mathbb{V}\mathrm{ar}\left[Z\right] \ \text{(cf. theorem 1)}
\end{aligned} \tag{B.3}$$

In the particular case of $X = Y$, equation B.3 no longer applies. Therefore, we use the following property:

Property 2 (Variance of the product of independent variables) *Let X and Z be 2 independent real random variables. Then, the variance of the product XZ is can be written as follows:*

$$\mathbb{V}ar\left[XZ\right] = \left(\mathbb{E}\left[X\right]\right)^2\mathbb{V}ar\left[Z\right] + \left(\mathbb{E}\left[Z\right]\right)^2\mathbb{V}ar\left[X\right] + \mathbb{V}ar\left[X\right]\mathbb{V}ar\left[Z\right]$$

Let W, X, Y and Z be 4 independent real random variables. Then:

$$\begin{aligned}
\mathrm{Cov}\left(X, YZ\right) &= \mathbb{E}\left[XYZ\right] - \mathbb{E}\left[X\right]\mathbb{E}\left[YZ\right] \ \text{(cf. equation B.1)} \\
&= \mathbb{E}\left[X\right]\mathbb{E}\left[Y\right]\mathbb{E}\left[Z\right] \\
&\quad - \mathbb{E}\left[X\right]\mathbb{E}\left[Y\right]\mathbb{E}\left[Z\right] \ \text{(independence, cf. property 1)} \\
&= 0
\end{aligned} \tag{B.4}$$

$$\begin{aligned}
\mathrm{Cov}\left(X, YX\right) &= \mathbb{E}\left[YX^2\right] - \mathbb{E}\left[X\right]\mathbb{E}\left[YX\right] \ \text{(cf. equation B.1)} \\
&= \mathbb{E}\left[Y\right]\mathbb{E}\left[X^2\right] - \mathbb{E}\left[Y\right]\left(\mathbb{E}\left[X\right]\right)^2 \ \text{(independence, cf. property 1)} \\
&= \mathbb{E}\left[Y\right]\left(\mathbb{E}\left[X^2\right] - \left(\mathbb{E}\left[X\right]\right)^2\right) \\
&= \mathbb{E}\left[Y\right]\mathbb{V}\mathrm{ar}\left[X\right] \ \text{(cf. theorem 1)}
\end{aligned} \tag{B.5}$$

$$\begin{aligned}\mathrm{Cov}\left(WX, YZ\right) &= \mathbb{E}\left[WXYZ\right] - \mathbb{E}\left[WX\right]\mathbb{E}\left[YZ\right] \text{ (cf. equation B.1)} \\ &= \mathbb{E}\left[W\right]\mathbb{E}\left[X\right]\mathbb{E}\left[Y\right]\mathbb{E}\left[Z\right] \\ &\quad - \mathbb{E}\left[W\right]\mathbb{E}\left[X\right]\mathbb{E}\left[Y\right]\mathbb{E}\left[Z\right] \text{ (independence, cf. property 1)} \\ &= 0\end{aligned} \tag{B.6}$$

Property 3 (Linearity of expectation) *Let $(X_1, \ldots, X_n)$ be n random variables. Therefore:*

$$\mathbb{E}\left[\sum_{i=1}^{n} X_i\right] = \sum_{i=1}^{n} \mathbb{E}\left[X_i\right]$$

Property 4 (Bilinearity of covariance) *Let $(X_1, \ldots, X_n)$ and $(Y_1, \ldots, Y_n)$ be $2n$ random variables. Therefore:*

$$Cov\left(\sum_{i=1}^{n} X_i, \sum_{j=1}^{n} Y_j\right) = \sum_{i=1}^{n}\sum_{j=1}^{n} Cov\left(X_i, Y_j\right)$$

B.1.2. Normal distributions

Property 5 (Sum of normal distributions) *Let $(X_1, \ldots, X_n)$ be n independent random variables following, respectively, n normal distributions $\mathcal{N}\left(\mu_1, \sigma_1\right), \ldots, \mathcal{N}\left(\mu_n, \sigma_n\right)$. Then, $\sum_{i=1}^{n} X_i$ is normally distributed as follows:*

$$\sum_{i=1}^{n} X_i \sim \mathcal{N}\left(\mu = \sum_{i=1}^{n} \mu_i; \sigma = \sqrt{\sum_{i=1}^{n} \left(\sigma_i\right)^2}\right)$$

B.2. Cumulated change option

B.2.1. No link option

There is no need of processing prior. Distributions given by the practitioner correspond exactly to the inferred parameters (cumulated change parameters).

B.2.2. Additive link

B.2.2.1. Assumptions

$\forall k \in [\![1; N_{\text{shift}}+1]\!], k \neq k_{\text{ref}}$, let $\forall j \in [\![1; N_{\text{cs}}]\!]$, $\Delta l_{b,j}^{(k)}$ and $\forall j \in [\![N_{\text{cs}}+1; N_{\text{c}}]\!]$, $\Delta b_j^{(k)}$ be $N_{\text{c}} \times N_{\text{shift}}$ independent and random variables distributed as follows:

$$\forall k \in [\![1; N_{\text{shift}}]\!], k \neq k_{\text{ref}}, \begin{cases} \Delta l_{b,j}^{(k)} \sim \mathcal{N}\left(\mu_{\Delta l_b,j}^{(k)}; \sigma_{\Delta l_b,j}^{(k)}\right), & \forall j \in [\![1; N_{\text{cs}}]\!] \quad \text{(local)} \\ \Delta b_j^{(k)} \sim \mathcal{N}\left(\mu_{\Delta b,j}^{(k)}; \sigma_{\Delta b,j}^{(k)}\right), & \forall j \in [\![N_{\text{cs}}+1; N_{\text{c}}]\!] \quad \text{(global)} \end{cases} \tag{B.7}$$

B.2.2.2. Cumulated change distribution

Links between controls can be found in table 5.2. As only addition is used in these links and all the prior distributions entered by the practitioner are normal distributions, the inferred parameters corresponding to the cumulated changes follow exactly a multivariate normal distribution. Parameters (mean and covariance matrix) of this distribution are computed as follows:

Mean $\forall k \in [\![1; N_{\text{shift}}+1]\!], k \neq k_{\text{ref}}, \ \forall j \in [\![1; N_{\text{c}}]\!]$,

$$\begin{aligned} \mathbb{E}\left[\Delta b_j^{(k)}\right] &= \begin{cases} \mathbb{E}\left[\Delta l_{b,j}^{(k)} + \Delta b_{N_{\text{cs}}+1}^{(k)}\right] & \text{if } j \leq N_{\text{cs}} \\ \mathbb{E}\left[\Delta b_j^{(k)}\right] & \text{if } j > N_{\text{cs}} \end{cases} \\ &= \begin{cases} \mathbb{E}\left[\Delta l_{b,j}^{(k)}\right] + \mathbb{E}\left[\Delta b_{N_{\text{cs}}+1}^{(k)}\right] & \text{if } j \leq N_{\text{cs}} \quad \text{(cf. property 3)} \\ \mathbb{E}\left[\Delta b_j^{(k)}\right] & \text{if } j > N_{\text{cs}} \end{cases} \\ &= \begin{cases} \mu_{\Delta l_b,j}^{(k)} + \mu_{\Delta b,N_{\text{cs}}+1}^{(k)} & \text{if } j \leq N_{\text{cs}} \quad \text{(cross-section control)} \\ \mu_{\Delta b,j}^{(k)} & \text{if } j > N_{\text{cs}} \quad \text{(channel control)} \end{cases} \end{aligned} \tag{B.8}$$

Covariance

- $\forall k \in [\![1; N_{\text{shift}}+1]\!]$, $\forall l \in [\![1; N_{\text{shift}}+1]\!]$, $k \neq l$,

– $\forall i \in [\![1; N_{\text{cs}}]\!]$, $\forall j \in [\![1; N_{\text{cs}}]\!]$,

$$\begin{aligned}
&\text{Cov}\left(\Delta b_i^{(k)}, \Delta b_j^{(l)}\right) \\
&= \text{Cov}\left(\Delta l_{b,i}^{(k)} + \Delta b_{N_{\text{cs}}+1}^{(k)}, \Delta l_{b,j}^{(l)} + \Delta b_{N_{\text{cs}}+1}^{(l)}\right) \\
&= \text{Cov}\left(\Delta l_{b,i}^{(k)}, \Delta l_{b,j}^{(l)}\right) + \text{Cov}\left(\Delta l_{b,i}^{(k)}, \Delta b_{N_{\text{cs}}+1}^{(l)}\right) + \text{Cov}\left(\Delta b_{N_{\text{cs}}+1}^{(k)}, \Delta l_{b,j}^{(l)}\right) \\
&\quad + \text{Cov}\left(\Delta b_{N_{\text{cs}}+1}^{(k)}, \Delta b_{N_{\text{cs}}+1}^{(l)}\right) \text{ (cf. property 4)} \\
&= 0 \text{ (independence, cf. equation B.2)}
\end{aligned} \tag{B.9}$$

– $\forall i \in [\![N_{\text{cs}} + 1; N_{\text{c}}]\!]$, $\forall j \in [\![N_{\text{cs}} + 1; N_{\text{c}}]\!]$,

$$\text{Cov}\left(\Delta b_i^{(k)}, \Delta b_j^{(l)}\right) = 0 \text{ (independence, cf equation B.2)} \tag{B.10}$$

– $\forall i \in [\![1; N_{\text{cs}}]\!]$, $\forall j \in [\![N_{\text{cs}} + 1; N_{\text{c}}]\!]$,

$$\begin{aligned}
&\text{Cov}\left(\Delta b_i^{(k)}, \Delta b_j^{(l)}\right) \\
&= \text{Cov}\left(\Delta l_{b,i}^{(k)} + \Delta b_{N_{\text{cs}}+1}^{(k)}, \Delta b_j^{(l)}\right) \\
&= \text{Cov}\left(\Delta l_{b,i}^{(k)}, \Delta b_j^{(l)}\right) + \text{Cov}\left(\Delta b_{N_{\text{cs}}+1}^{(k)}, \Delta b_j^{(l)}\right) \text{ (cf. property 4)} \\
&= 0 \text{ (independence, cf. equation B.2)}
\end{aligned} \tag{B.11}$$

- $\forall k \in [\![1; N_{\text{shift}} + 1]\!]$,

– $\forall i \in [\![1; N_{\text{cs}}]\!]$, $\forall j \in [\![1; N_{\text{cs}}]\!]$,

$$\begin{aligned}
&\text{Cov}\left(\Delta b_i^{(k)}, \Delta b_j^{(k)}\right) \\
&= \text{Cov}\left(\Delta l_{b,i}^{(k)} + \Delta b_{N_{\text{cs}}+1}^{(k)}, \Delta l_{b,j}^{(k)} + \Delta b_{N_{\text{cs}}+1}^{(k)}\right) \\
&= \text{Cov}\left(\Delta l_{b,i}^{(k)}, \Delta l_{b,j}^{(k)}\right) + \text{Cov}\left(\Delta l_{b,i}^{(k)}, \Delta b_{N_{\text{cs}}+1}^{(k)}\right) + \text{Cov}\left(\Delta b_{N_{\text{cs}}+1}^{(k)}, \Delta l_{b,j}^{(k)}\right) \\
&\quad + \text{Cov}\left(\Delta b_{N_{\text{cs}}+1}^{(k)}, \Delta b_{N_{\text{cs}}+1}^{(k)}\right) \text{ (cf. property 4)} \\
&= \text{Cov}\left(\Delta l_{b,i}^{(k)}, \Delta l_{b,j}^{(k)}\right) + \mathbb{V}\text{ar}\left[\Delta b_{N_{\text{cs}}+1}^{(k)}\right] \text{ (cf. equation B.2)} \\
&= \begin{cases} \mathbb{V}\text{ar}\left[\Delta l_{b,j}^{(k)}\right] + \mathbb{V}\text{ar}\left[\Delta b_{N_{\text{cs}}+1}^{(k)}\right] & \text{if } i = j \\ \mathbb{V}\text{ar}\left[\Delta b_{N_{\text{cs}}+1}^{(k)}\right] & \text{if } i \neq j \end{cases} \\
&= \begin{cases} \left(\sigma_{\Delta l_b,j}^{(k)}\right)^2 + \left(\sigma_{\Delta b,N_{\text{cs}}+1}^{(k)}\right)^2 & \text{if } i = j \\ \left(\sigma_{\Delta b,N_{\text{cs}}+1}^{(k)}\right)^2 & \text{if } i \neq j \end{cases}
\end{aligned} \tag{B.12}$$

– $\forall i \in [\![N_{\text{cs}}+1; N_{\text{c}}]\!]$, $\forall j \in [\![N_{\text{cs}}+1; N_{\text{c}}]\!]$,

$$\begin{aligned}\text{Cov}\left(\Delta b_i^{(k)}, \Delta b_j^{(k)}\right) &= \begin{cases} \mathbb{V}\text{ar}\left[\Delta b_j^{(k)}\right] & \text{if } i = j \\ 0 & \text{if } i \neq j \text{ (independence, cf equation B.2)} \end{cases} \\ &= \begin{cases} \left(\sigma_{\Delta b,j}^{(k)}\right)^2 & \text{if } i = j \\ 0 & \text{if } i \neq j \end{cases}\end{aligned} \tag{B.13}$$

– $\forall i \in [\![1; N_{\text{cs}}]\!]$, $\forall j \in [\![N_{\text{cs}}+1; N_{\text{c}}]\!]$,

$$\begin{aligned}&\text{Cov}\left(\Delta b_i^{(k)}, \Delta b_j^{(k)}\right) \\ &= \text{Cov}\left(\Delta l_{b,i}^{(k)} + \Delta b_{N_{\text{cs}}+1}^{(k)}, \Delta b_j^{(k)}\right) \\ &= \text{Cov}\left(\Delta l_{b,i}^{(k)}, \Delta b_j^{(k)}\right) + \text{Cov}\left(\Delta b_{N_{\text{cs}}+1}^{(k)}, \Delta b_j^{(k)}\right) \text{ (cf. property 4)} \\ &= \mathbb{V}\text{ar}\left[\Delta b_{N_{\text{cs}}+1}^{(k)}\right] \mathbb{1}_{\{N_{\text{cs}}+1\}}(j) \text{ (independence, cf. equation B.2)} \\ &= \begin{cases} \left(\sigma_{\Delta b,N_{\text{cs}}+1}^{(k)}\right)^2 & \text{if } j = N_{\text{cs}}+1 \\ 0 & \text{if } j \neq N_{\text{cs}}+1 \end{cases}\end{aligned} \tag{B.14}$$

B.2.3. Multiplicative link

B.2.3.1. Assumptions

$\forall k \in [\![1; N_{\text{shift}}+1]\!], k \neq k_{\text{ref}}$, let $\forall j \in [\![1; N_{\text{cs}}]\!]$, $\Delta b_j^{(k)}$ and $\forall j \in [\![N_{\text{cs}}+1; N_{\text{c}}]\!]$, $\Lambda_{b,j}^{(k)}$ be $N_{\text{c}} \times N_{\text{shift}}$ independent and random variables distributed as follows:

$$\forall k \in [\![1; N_{\text{shift}}+1]\!], k \neq k_{\text{ref}}, \begin{cases} \Delta b_j^{(k)} \sim \mathcal{N}\left(\mu_{\Delta b,j}^{(k)}; \sigma_{\Delta b,j}^{(k)}\right), & \forall j \in [\![1; N_{\text{cs}}]\!] \quad \text{(local)} \\ \Lambda_{b,j}^{(k)} \sim \mathcal{N}\left(\mu_{\Lambda_b,j}^{(k)}; \sigma_{\Lambda_b,j}^{(k)}\right), & \forall j \in [\![N_{\text{cs}}+1; N_{\text{c}}]\!] \quad \text{(global)} \end{cases} \tag{B.15}$$

B.2.3.2. Cumulated change distribution

Relations between controls for the multiplicative link option and cumulated change parameters are expressed by table 5.2. As addition and multiplication are used in these relations, the multivariate distribution of the inferred parameters corresponding to the cumulated changes for each controls can be approximated by a multivariate normal distribution. This approximation have been compared with and validated by results from Monte-Carlo propagation. The follow-

ing paragraph in this subsection are the theoretical calculations of the parameters (mean and covariance matrix) of this approximated multivariate distribution.

Mean $\forall k \in [\![1; N_{\text{shift}}+1]\!], k \neq k_{\text{ref}},\ \forall j \in [\![1; N_{\text{c}}]\!]$,

$$\begin{aligned}
\mathbb{E}\left[\Delta b_j^{(k)}\right] &= \begin{cases} \mathbb{E}\left[\Delta b_j^{(k)}\right] & \text{if } j \leq N_{\text{cs}} \quad \text{(section control)} \\ \mathbb{E}\left[\Lambda_{b,j}^{(k)} \times \Delta b_{N_{\text{cs}}}^{(k)}\right] & \text{if } j > N_{\text{cs}} \quad \text{(channel control)} \end{cases} \\
&= \begin{cases} \mathbb{E}\left[\Delta b_j^{(k)}\right] & \text{if } j \leq N_{\text{cs}} \\ \mathbb{E}\left[\Lambda_{b,j}^{(k)}\right] \mathbb{E}\left[\Delta b_{N_{\text{cs}}}^{(k)}\right] & \text{if } j > N_{\text{cs}} \quad \text{(independence, cf. property 1)} \end{cases} \\
&= \begin{cases} \mu_{\Delta b,j}^{(k)} & \text{if } j \leq N_{\text{cs}} \\ \mu_{\Lambda_b,j}^{(k)} \times \mu_{\Delta b,N_{\text{cs}}}^{(k)} & \text{if } j > N_{\text{cs}} \end{cases}
\end{aligned} \tag{B.16}$$

Covariance

- $\forall k \in [\![1; N_{\text{shift}}+1]\!],\ k \neq k_{\text{ref}},\ \forall l \in [\![1; N_{\text{shift}}+1]\!],\ l \neq k_{\text{ref}},\ k \neq l$,

  - $\forall i \in [\![1; N_{\text{cs}}]\!],\ \forall j \in [\![1; N_{\text{cs}}]\!]$,

$$\text{Cov}\left(\Delta b_i^{(k)}, \Delta b_j^{(l)}\right) = \ 0 \text{ (independence, cf equation B.2)} \tag{B.17}$$

  - $\forall i \in [\![N_{\text{cs}}+1; N_{\text{c}}]\!],\ \forall j \in [\![N_{\text{cs}}+1; N_{\text{c}}]\!]$,

$$\begin{aligned}
\text{Cov}\left(\Delta b_i^{(k)}, \Delta b_j^{(l)}\right) &= \text{Cov}\left(\Lambda_{b,i}^{(k)} \Delta b_{N_{\text{cs}}}^{(k)}, \Lambda_{b,j}^{(l)} \Delta b_{N_{\text{cs}}}^{(l)}\right) \\
&= \mathbb{E}\left[\Lambda_{b,i}^{(k)} \Delta b_{N_{\text{cs}}}^{(k)} \Lambda_{b,j}^{(l)} \Delta b_{N_{\text{cs}}}^{(l)}\right] - \mathbb{E}\left[\Lambda_{b,i}^{(k)} \Delta b_{N_{\text{cs}}}^{(k)}\right] \mathbb{E}\left[\Lambda_{b,j}^{(l)} \Delta b_{N_{\text{cs}}}^{(l)}\right] \\
&= \mathbb{E}\left[\Lambda_{b,i}^{(k)}\right] \mathbb{E}\left[\Delta b_{N_{\text{cs}}}^{(k)}\right] \mathbb{E}\left[\Lambda_{b,j}^{(l)}\right] \mathbb{E}\left[\Delta b_{N_{\text{cs}}}^{(l)}\right] \\
&\quad - \mathbb{E}\left[\Lambda_{b,i}^{(k)}\right] \mathbb{E}\left[\Delta b_{N_{\text{cs}}}^{(k)}\right] \mathbb{E}\left[\Lambda_{b,j}^{(l)}\right] \mathbb{E}\left[\Delta b_{N_{\text{cs}}}^{(l)}\right] \\
&\quad \text{(independence, cf. property 2)} \\
&= 0
\end{aligned} \tag{B.18}$$

  - $\forall i \in [\![1; N_{\text{cs}}]\!],\ \forall j \in [\![N_{\text{cs}}+1; N_{\text{c}}]\!]$,

$$\begin{aligned}
\text{Cov}\left(\Delta b_i^{(k)}, \Delta b_j^{(l)}\right) &= \text{Cov}\left(\Delta b_i^{(k)}, \Lambda_{b,j}^{(l)} \Delta b_{N_{\text{cs}}}^{(l)}\right) \\
&= 0 \text{ (cf. equation B.4)}
\end{aligned} \tag{B.19}$$

- $\forall k \in [\![1; N_{\text{shift}}+1]\!],\ k \neq k_{\text{ref}}$,

– $\forall i \in [\![1; N_{\text{cs}}]\!],\ \forall j \in [\![1; N_{\text{cs}}]\!]$,

$$\begin{aligned}\text{Cov}\left(\Delta b_i^{(k)}, \Delta b_j^{(k)}\right) &= \begin{cases} \mathbb{V}\text{ar}\left[\Delta b_j^{(k)}\right] & \text{if } i = j \\ 0 & \text{if } i \neq j \text{ (independence, cf equation B.2)} \end{cases} \\ &= \begin{cases} \left(\sigma_{\Delta b,j}^{(k)}\right)^2 & \text{if } i = j \\ 0 & \text{if } i \neq j \end{cases}\end{aligned} \tag{B.20}$$

– $\forall i \in [\![N_{\text{cs}}+1; N_{\text{c}}]\!],\ \forall j \in [\![N_{\text{cs}}+1; N_{\text{c}}]\!]$,

$$\begin{aligned}&\text{Cov}\left(\Delta b_i^{(k)}, \Delta b_j^{(k)}\right) \\ &\quad= \text{Cov}\left(\Lambda_{b,i}^{(k)} \Delta b_{N_{\text{cs}}}^{(k)}, \Lambda_{b,j}^{(k)} \Delta b_{N_{\text{cs}}}^{(k)}\right) \\ &\text{if } i = j \\ &\quad= \mathbb{V}\text{ar}\left[\Lambda_{b,j}^{(k)} \Delta b_{N_{\text{cs}}}^{(k)}\right] \\ &\quad= \mathbb{V}\text{ar}\left[\Lambda_{b,j}^{(k)}\right] \mathbb{V}\text{ar}\left[\Delta b_{N_{\text{cs}}}^{(k)}\right] + \mathbb{V}\text{ar}\left[\Lambda_{b,j}^{(k)}\right] \left(\mathbb{E}\left[\Delta b_{N_{\text{cs}}}^{(k)}\right]\right)^2 \\ &\qquad + \mathbb{V}\text{ar}\left[\Delta b_{N_{\text{cs}}}^{(k)}\right] \left(\mathbb{E}\left[\Lambda_{b,j}^{(k)}\right]\right)^2 \text{ (independence, cf. property 2)} \\ &\quad= \left(\sigma_{\Lambda_b,j}^{(k)}\right)^2 \left(\sigma_{b,N_{\text{cs}}}^{(k)}\right)^2 + \left(\sigma_{\Lambda_b,j}^{(k)}\right)^2 \left(\mu_{b,N_{\text{cs}}}^{(k)}\right)^2 + \left(\sigma_{b,N_{\text{cs}}}^{(k)}\right)^2 \left(\mu_{\Lambda_b,j}^{(k)}\right)^2 \\ &\text{if } i \neq j \\ &\quad= \mathbb{E}\left[\Lambda_{b,i}^{(k)}\right] \mathbb{E}\left[\Lambda_{b,j}^{(k)}\right] \mathbb{V}\text{ar}\left[\Delta b_{N_{\text{cs}}}^{(k)}\right] \text{ (independence, cf. equation B.3)} \\ &\quad= \mu_{\Lambda_b,i}^{(k)} \mu_{\Lambda_b,j}^{(k)} \left(\sigma_{\Delta b,N_{\text{cs}}}^{(k)}\right)^2\end{aligned} \tag{B.21}$$

– $\forall i \in [\![1; N_{\text{cs}}]\!]$, $\forall j \in [\![N_{\text{cs}}+1; N_{\text{c}}]\!]$,

$$\begin{aligned}\text{Cov}\left(\Delta b_i^{(k)}, \Delta b_j^{(k)}\right) &= \text{Cov}\left(\Delta b_i^{(k)}, \Lambda_{b,j}^{(k)} \Delta b_{N_{\text{cs}}}^{(k)}\right) \\ &= \begin{cases} \mathbb{E}\left[\Lambda_{b,j}^{(k)}\right] \mathbb{V}\text{ar}\left[\Delta b_{N_{\text{cs}}}^{(k)}\right] & \text{if } i = N_{\text{cs}} \quad \text{(cf. equation B.5)} \\ 0 & \text{if } i \neq N_{\text{cs}} \quad \text{(cf. equation B.4)} \end{cases} \\ &= \begin{cases} \mu_{\Lambda_b,j}^{(k)} \left(\sigma_{\Delta b,N_{\text{cs}}}^{(k)}\right)^2 & \text{if } i = N_{\text{cs}} \\ 0 & \text{if } i \neq N_{\text{cs}} \end{cases}\end{aligned} \tag{B.22}$$

B.3. Incremental change option

Distributions given by the practitioner correspond to the incremental change parameters (change between two successive periods). Link between cumulated and incremental change parameters:

$$\begin{aligned} \forall k < k_{\text{ref}}, \quad \Delta b_j^{(k)} &= \sum_{m=k}^{k_{\text{ref}}-1} \delta b_j^{(m)} \\ \forall k > k_{\text{ref}}, \quad \Delta b_j^{(k)} &= \sum_{m=k_{\text{ref}}+1}^{k} \delta b_j^{(m)} \end{aligned} \tag{B.23}$$

B.3.1. No link option

B.3.1.1. Assumptions

$\forall k \in [\![1; N_{\text{shift}}+1]\!], k \neq k_{\text{ref}}$, let $\forall j \in [\![1; N_{\text{c}}]\!],\ \delta b_j^{(k)}$ be $N_{\text{c}} \times N_{\text{shift}}$ independent and random variables distributed as follows:

$$\forall k \in [\![1; N_{\text{shift}}+1]\!], k \neq k_{\text{ref}},\ \forall j \in [\![1; N_{\text{c}}]\!],\ \delta b_j^{(k)} \sim \mathcal{N}\left(\mu_{\delta b,j}^{(k)}; \sigma_{\delta b,j}^{(k)}\right), \tag{B.24}$$

B.3.1.2. Cumulated change distribution

Mean $\forall k \in [\![1; N_{\text{shift}}]\!],\ k \neq k_{\text{ref}},\ \forall j \in [\![1; N_{\text{c}}]\!]$,

$$\begin{aligned} \mathbb{E}\left[\Delta b_j^{(k)}\right] &= \mathbb{E}\left[\sum_m \delta b_j^{(m)}\right] \\ &= \sum_m \mathbb{E}\left[\delta b_j^{(m)}\right] \text{ (cf. property 3)} \\ &= \begin{cases} \sum_{m=k}^{k_{\text{ref}}-1} \mu_{\delta b,j}^{(k)} & \text{if } k < k_{\text{ref}} \\ \sum_{m=k_{\text{ref}}+1}^{k} \mu_{\delta b,j}^{(k)} & \text{if } k > k_{\text{ref}} \end{cases} \end{aligned} \tag{B.25}$$

Covariance $\forall i \in [\![1; N_{\text{c}}]\!],\ \forall j \in [\![1; N_{\text{c}}]\!]$,

- $\forall k \in [\![1; k_{\text{ref}}-1]\!],\ \forall l \in [\![1; k_{\text{ref}}-1]\!]$,

$$\begin{aligned} \text{Cov}\left(\Delta b_i^{(k)}, \Delta b_j^{(l)}\right) &= \text{Cov}\left(\sum_{m=k}^{k_{\text{ref}}-1} \delta b_i^{(m)}, \sum_{p=l}^{k_{\text{ref}}-1} \delta b_j^{(p)}\right) \\ &= \sum_{m=k}^{k_{\text{ref}}-1} \sum_{p=l}^{k_{\text{ref}}-1} \text{Cov}\left(\delta b_i^{(m)}, \delta b_j^{(p)}\right) \text{ (cf. property 4)} \\ &= \sum_{m=k}^{k_{\text{ref}}-1} \sum_{\substack{p=l \\ p\neq m}}^{k_{\text{ref}}-1} \text{Cov}\left(\delta b_i^{(m)}, \delta b_j^{(p)}\right) + \sum_{m=\max(k,l)}^{k_{\text{ref}}-1} \text{Cov}\left(\delta b_i^{(m)}, \delta b_j^{(m)}\right) \\ &= \sum_{m=\max(k,l)}^{k_{\text{ref}}-1} \text{Cov}\left(\delta b_i^{(m)}, \delta b_j^{(m)}\right) \text{ (independence, cf. equation B.2)} \end{aligned} \tag{B.26}$$

– $k \leq l$,

$$\begin{aligned}
&\mathrm{Cov}\left(\Delta b_i^{(k)}, \Delta b_j^{(l)}\right) \\
&= \sum_{m=k}^{k_{\mathrm{ref}}-1} \mathrm{Cov}\left(\delta b_i^{(m)}, \delta b_j^{(m)}\right) \\
&= \begin{cases} \sum_{m=k}^{k_{\mathrm{ref}}-1} \mathbb{V}\mathrm{ar}\left[\delta b_j^{(m)}\right] & \text{if } i = j \\ 0 & \text{if } i \neq j \text{ (independence, cf. equation B.2)} \end{cases} \\
&= \begin{cases} \sum_{m=k}^{k_{\mathrm{ref}}-1} \left(\sigma_{\delta b,j}^{(m)}\right)^2 & \text{if } i = j \\ 0 & \text{if } i \neq j \end{cases}
\end{aligned} \tag{B.27}$$

– $k > l$,

$$\begin{aligned}
&\mathrm{Cov}\left(\Delta b_i^{(k)}, \Delta b_j^{(l)}\right) \\
&= \sum_{m=l}^{k_{\mathrm{ref}}-1} \mathrm{Cov}\left(\delta b_i^{(m)}, \delta b_j^{(m)}\right) \\
&= \begin{cases} \sum_{m=l}^{k_{\mathrm{ref}}-1} \mathbb{V}\mathrm{ar}\left[\delta b_j^{(m)}\right] & \text{if } i = j \\ 0 & \text{if } i \neq j \text{ (independence, cf. equation B.2)} \end{cases} \\
&= \begin{cases} \sum_{m=l}^{k_{\mathrm{ref}}-1} \left(\sigma_{\delta b,j}^{(m)}\right)^2 & \text{if } i = j \\ 0 & \text{if } i \neq j \end{cases}
\end{aligned} \tag{B.28}$$

- $\forall k \in [\![k_{\mathrm{ref}}+1; N_{\mathrm{shift}}+1]\!],\ \forall l \in [\![k_{\mathrm{ref}}+1; N_{\mathrm{shift}}+1]\!]$,

$$\begin{aligned}
\mathrm{Cov}\left(\Delta b_i^{(k)}, \Delta b_j^{(l)}\right) &= \mathrm{Cov}\left(\sum_{m=k_{\mathrm{ref}}+1}^{k} \delta b_i^{(m)}, \sum_{p=k_{\mathrm{ref}}+1}^{l} \delta b_j^{(p)}\right) \\
&= \sum_{m=k_{\mathrm{ref}}+1}^{k} \sum_{p=k_{\mathrm{ref}}+1}^{l} \mathrm{Cov}\left(\delta b_i^{(m)}, \delta b_j^{(p)}\right) \text{ (cf. property 4)} \\
&= \sum_{m=k_{\mathrm{ref}}+1}^{k} \sum_{\substack{p=k_{\mathrm{ref}}+1 \\ p\neq m}}^{l} \mathrm{Cov}\left(\delta b_i^{(m)}, \delta b_j^{(p)}\right) + \sum_{m=k_{\mathrm{ref}}+1}^{\min(k,l)} \mathrm{Cov}\left(\delta b_i^{(m)}, \delta b_j^{(m)}\right) \\
&= \sum_{m=k_{\mathrm{ref}}+1}^{\min(k,l)} \mathrm{Cov}\left(\delta b_i^{(m)}, \delta b_j^{(m)}\right) \text{ (independence, cf. equation B.2)}
\end{aligned} \tag{B.29}$$

– $k \leq l$,

$$\begin{aligned}
&\mathrm{Cov}\left(\Delta b_i^{(k)}, \Delta b_j^{(l)}\right) \\
&= \sum_{m=k_{\mathrm{ref}}+1}^{k} \mathrm{Cov}\left(\delta b_i^{(m)}, \delta b_j^{(m)}\right) \\
&= \begin{cases} \sum_{m=k_{\mathrm{ref}}+1}^{k} \mathbb{V}\mathrm{ar}\left[\delta b_j^{(m)}\right] & \text{if } i = j \\ 0 & \text{if } i \neq j \text{ (independence, cf. equation B.2)} \end{cases} \\
&= \begin{cases} \sum_{m=k_{\mathrm{ref}}+1}^{k} \left(\sigma_{\delta b,j}^{(m)}\right)^2 & \text{if } i = j \\ 0 & \text{if } i \neq j \end{cases}
\end{aligned} \tag{B.30}$$

– $k > l$,

$$\begin{aligned}
&\mathrm{Cov}\left(\Delta b_i^{(k)}, \Delta b_j^{(l)}\right) \\
&= \sum_{m=k_{\mathrm{ref}}+1}^{l} \mathrm{Cov}\left(\delta b_i^{(m)}, \delta b_j^{(m)}\right) \\
&= \begin{cases} \sum_{m=k_{\mathrm{ref}}+1}^{l} \mathbb{V}\mathrm{ar}\left[\delta b_j^{(m)}\right] & \text{if } i = j \\ 0 & \text{if } i \neq j \text{ (independence, cf. equation B.2)} \end{cases} \\
&= \begin{cases} \sum_{m=k_{\mathrm{ref}}+1}^{l} \left(\sigma_{\delta b,j}^{(m)}\right)^2 & \text{if } i = j \\ 0 & \text{if } i \neq j \end{cases}
\end{aligned} \tag{B.31}$$

- $\forall k \in [\![k_{\mathrm{ref}}+1, N_{\mathrm{shift}}+1]\!], \forall l \in [\![1; k_{\mathrm{ref}}-1]\!]$,

$$\begin{aligned}
\mathrm{Cov}\left(\Delta b_i^{(k)}, \Delta b_j^{(l)}\right) &= \mathrm{Cov}\left(\sum_{m=k_{\mathrm{ref}}+1}^{k} \delta b_i^{(m)}, \sum_{p=l}^{k_{\mathrm{ref}}-1} \delta b_j^{(p)}\right) \\
&= \sum_{m=k_{\mathrm{ref}}+1}^{k} \sum_{p=l}^{k_{\mathrm{ref}}-1} \mathrm{Cov}\left(\delta b_i^{(m)}, \delta b_j^{(p)}\right) \text{ (cf. property 4)} \\
&= 0 \text{ (independence, cf. equation B.2)}
\end{aligned} \tag{B.32}$$

B.3.2. Additive link

B.3.2.1. Assumptions

$\forall k \in [\![1; N_{\mathrm{shift}}+1]\!], k \neq k_{\mathrm{ref}}$, let $\forall j \in [\![1; N_{\mathrm{cs}}]\!],\ \delta l_{b,j}^{(k)}$ and $\forall j \in [\![N_{\mathrm{cs}}+1; N_{\mathrm{c}}]\!],\ \delta b_j^{(k)}$ be $N_{\mathrm{c}} \times N_{\mathrm{shift}}$ independent and random variables distributed as follows:

$$\forall k \in [\![1; N_{\text{shift}}]\!], k \neq k_{\text{ref}}, \begin{cases} \delta l_{b,j}^{(k)} \sim \mathcal{N}\left(\mu_{\delta l_b,j}^{(k)}; \sigma_{l_b,j}^{(k)}\right), & \forall j \in [\![1; N_{\text{cs}}]\!] \quad \text{(local)} \\ \delta b_j^{(k)} \sim \mathcal{N}\left(\mu_{\delta b,j}^{(k)}; \sigma_{\delta b,j}^{(k)}\right), & \forall j \in [\![N_{\text{cs}}+1; N_{\text{c}}]\!] \quad \text{(global)} \end{cases} \tag{B.33}$$

B.3.2.2. Cumulated change distribution

Relations between cumulated changes and incremental changes for the additive link option are expressed by equation (5.14). As only addition is used in these relations and all the prior distributions entered by the practitioner are normal distributions, the inferred parameters corresponding to the cumulated changes follow exactly a multivariate normal distribution. Parameters (mean and covariance matrix) of this distribution are computed as follows:

Mean $\forall k \in [\![1; N_{\text{shift}}]\!], k \neq k_{\text{ref}},\ \forall j \in [\![1; N_{\text{c}}]\!]$

$$\begin{aligned} \mathbb{E}\left[\Delta b_j^{(k)}\right] &= \begin{cases} \mathbb{E}\left[\sum_m \left(\delta l_{b,j}^{(m)} + \delta b_{N_{\text{cs}}+1}^{(m)}\right)\right] & \text{if } j < N_{\text{cs}}+1 \\ \mathbb{E}\left[\sum_m \delta b_j^{(m)}\right] & \text{if } j \geq N_{\text{cs}}+1 \end{cases} \\ &= \begin{cases} \sum_m \left(\mathbb{E}\left[\delta l_{b,j}^{(m)}\right] + \mathbb{E}\left[\delta b_{N_{\text{cs}}+1}^{(m)}\right]\right) & \text{if } j < N_{\text{cs}}+1 \\ \sum_m \mathbb{E}\left[\delta b_j^{(m)}\right] & \text{if } j \geq N_{\text{cs}}+1 \end{cases} \quad \text{(cf. property 3)} \\ &= \begin{cases} \sum_{m=k}^{k_{\text{ref}}-1} \left(\mu_{\delta l_b,j}^{(m)} + \mu_{\delta b,N_{\text{cs}}+1}^{(m)}\right) & \text{if } j < N_{\text{cs}}+1 \text{ and } k < k_{\text{ref}} \\ \sum_{m=k_{\text{ref}}+1}^{k} \left(\mu_{\delta l_b,j}^{(m)} + \mu_{\delta b,N_{\text{cs}}+1}^{(m)}\right) & \text{if } j < N_{\text{cs}}+1 \text{ and } k > k_{\text{ref}} \\ \sum_{m=k}^{k_{\text{ref}}-1} \mu_{\delta b,j}^{(k)} & \text{if } j \geq N_{\text{cs}}+1 \text{ and } k < k_{\text{ref}} \\ \sum_{m=k_{\text{ref}}+1}^{k} \mu_{\delta b,j}^{(k)} & \text{if } j \geq N_{\text{cs}}+1 \text{ and } k > k_{\text{ref}} \end{cases} \end{aligned} \tag{B.34}$$

Covariance

- $\forall i \in [\![N_{\text{cs}}+1, N_{\text{c}}]\!], j \in [\![N_{\text{cs}}+1, N_{\text{c}}]\!]$,

– $\forall k \in [\![k_{\text{ref}}+1; N_{\text{shift}}+1]\!]$, $\forall l \in [\![k_{\text{ref}}+1; N_{\text{shift}}+1]\!]$,

$$\begin{aligned}
&\text{Cov}\left(\Delta b_i^{(k)}, \Delta b_j^{(l)}\right) \\
&= \text{Cov}\left(\sum_{m=k_{\text{ref}}+1}^{k} \delta b_i^{(m)}, \sum_{p=k_{\text{ref}}+1}^{l} \delta b_j^{(p)}\right) \\
&= \sum_{m=k_{\text{ref}}+1}^{k} \sum_{p=k_{\text{ref}}+1}^{l} \text{Cov}\left(\delta b_i^{(m)}, \delta b_j^{(p)}\right) \text{ (cf. property 4)} \\
&= \sum_{m=k_{\text{ref}}+1}^{k} \sum_{\substack{p=k_{\text{ref}}+1 \\ p\neq m}}^{l} \text{Cov}\left(\delta b_i^{(m)}, \delta b_j^{(p)}\right) + \sum_{m=k_{\text{ref}}+1}^{\min(k,l)} \text{Cov}\left(\delta b_i^{(m)}, \delta b_j^{(m)}\right) \\
&= \sum_{m=k_{\text{ref}}+1}^{\min(k,l)} \text{Cov}\left(\delta b_i^{(m)}, \delta b_j^{(m)}\right) \text{ (independence, cf. equation B.2)}
\end{aligned} \tag{B.35}$$

$$\begin{aligned}
&\text{Cov}\left(\Delta b_i^{(k)}, \Delta b_j^{(l)}\right) \\
&= \begin{cases}
0 & \text{if } k \leq l \text{ and } i \neq j \text{ (independence, cf. equation B.2)} \\
\sum_{m=k_{\text{ref}}+1}^{k} \mathbb{V}\text{ar}\left[\delta b_j^{(m)}\right] & \text{if } k \leq l \text{ and } i = j \\
0 & \text{if } k > l \text{ and } i \neq j \text{ (independence, cf. equation B.2)} \\
\sum_{m=k_{\text{ref}}+1}^{l} \mathbb{V}\text{ar}\left[\delta b_j^{(m)}\right] & \text{if } k > l \text{ and } i = j
\end{cases}
\end{aligned} \tag{B.36}$$

– $\forall k \in [\![1; k_{\text{ref}} - 1]\!]$, $\forall l \in [\![1; k_{\text{ref}} - 1]\!]$,

$$
\begin{aligned}
&\text{Cov}\left(\Delta b_i^{(k)}, \Delta b_j^{(l)}\right) \\
&= \text{Cov}\left(\sum_{m=k}^{k_{\text{ref}}-1} \delta b_i^{(m)}, \sum_{p=l}^{k_{\text{ref}}-1} \delta b_j^{(p)}\right) \\
&= \sum_{m=k}^{k_{\text{ref}}-1} \sum_{p=l}^{k_{\text{ref}}-1} \text{Cov}\left(\delta b_i^{(m)}, \delta b_j^{(p)}\right) \text{ (cf. property 4)} \\
&= \sum_{m=k}^{k_{\text{ref}}-1} \sum_{\substack{p=l \\ p\neq m}}^{k_{\text{ref}}-1} \text{Cov}\left(\delta b_i^{(m)}, \delta b_j^{(p)}\right) + \sum_{m=\max(k,l)}^{k_{\text{ref}}-1} \text{Cov}\left(\delta b_i^{(m)}, \delta b_j^{(m)}\right) \\
&= \sum_{m=\max(k,l)}^{k_{\text{ref}}-1} \text{Cov}\left(\delta b_i^{(m)}, \delta b_j^{(m)}\right) \text{ (independence, cf. equation B.2)} \\
&= \begin{cases}
0 & \text{if } k \leq l \text{ and } i \neq j \text{ (independence, cf. equation B.2)} \\
\sum_{m=l}^{k_{\text{ref}}-1} \mathbb{V}\text{ar}\left[\delta b_j^{(m)}\right] & \text{if } k \leq l \text{ and } i = j \\
0 & \text{if } k > l \text{ and } i \neq j \text{ (independence, cf. equation B.2)} \\
\sum_{m=k}^{k_{\text{ref}}-1} \mathbb{V}\text{ar}\left[\delta b_j^{(m)}\right] & \text{if } k > l \text{ and } i = j
\end{cases}
\end{aligned}
\tag{B.37}
$$

– $\forall k \in [\![1; k_{\text{ref}} - 1]\!]$, $\forall l \in [\![k_{\text{ref}} + 1; N_{\text{shift}} + 1]\!]$,

$$
\begin{aligned}
\text{Cov}\left(\Delta b_i^{(k)}, \Delta b_j^{(l)}\right) &= \text{Cov}\left(\sum_{m=k}^{k_{\text{ref}}-1} \delta b_i^{(m)}, \sum_{p=k_{\text{ref}}+1}^{l} \delta b_j^{(p)}\right) \\
&= \sum_{m=k}^{k_{\text{ref}}-1} \sum_{p=k_{\text{ref}}+1}^{l} \text{Cov}\left(\delta b_i^{(m)}, \delta b_j^{(p)}\right) \text{ (cf. property 4)} \\
&= 0 \text{ (independence, cf. equation B.2)}
\end{aligned}
\tag{B.38}
$$

- $\forall i \in [\![1; N_{\text{cs}}]\!]$, $\forall j \in [\![1; N_{\text{cs}}]\!]$,

– $\forall k \in [\![k_{\text{ref}}+1; N_{\text{shift}}+1]\!]$, $\forall l \in [\![k_{\text{ref}}+1; N_{\text{shift}}+1]\!]$,

$$
\begin{aligned}
&\text{Cov}\left(\Delta b_i^{(k)}, \Delta b_j^{(l)}\right) \\
&= \text{Cov}\left(\sum_{m=k_{\text{ref}}+1}^{k}\left(\delta l_{b,i}^{(m)} + \delta b_{N_{\text{cs}}+1}^{(m)}\right), \sum_{p=k_{\text{ref}}+1}^{l}\left(\delta l_{b,j}^{(p)} + \delta b_{N_{\text{cs}}+1}^{(p)}\right)\right) \\
&= \sum_{m=k_{\text{ref}}+1}^{k}\sum_{p=k_{\text{ref}}+1}^{l}\Big(\text{Cov}\left(\delta l_{b,i}^{(m)}, \delta l_{b,j}^{(p)}\right) + \text{Cov}\left(\delta l_{b,i}^{(m)}, \delta b_{N_{\text{cs}}+1}^{(p)}\right) \\
&\quad + \text{Cov}\left(\delta b_{N_{\text{cs}}+1}^{(m)}, \delta l_{b,j}^{(p)}\right) + \text{Cov}\left(\delta b_{N_{\text{cs}}+1}^{(m)}, \delta b_{N_{\text{cs}}+1}^{(p)}\right)\Big) \quad \begin{matrix}\text{(bilinearity,}\\ \text{cf. property 4)}\end{matrix} \\
&= \sum_{m=k_{\text{ref}}+1}^{k}\sum_{\substack{p=k_{\text{ref}}+1 \\ p\neq m}}^{l}\Big(\text{Cov}\left(\delta l_{b,i}^{(m)}, \delta l_{b,j}^{(p)}\right) + \text{Cov}\left(\delta l_{b,i}^{(m)}, \delta b_{N_{\text{cs}}+1}^{(p)}\right) \\
&\quad + \text{Cov}\left(\delta b_{N_{\text{cs}}+1}^{(m)}, \delta l_{b,j}^{(p)}\right) + \text{Cov}\left(\delta b_{N_{\text{cs}}+1}^{(m)}, \delta b_{N_{\text{cs}}+1}^{(p)}\right)\Big) \\
&\quad + \sum_{m=k_{\text{ref}}+1}^{\min(k,l)}\Big(\text{Cov}\left(\delta l_{b,i}^{(m)}, \delta l_{b,j}^{(m)}\right) + \text{Cov}\left(\delta l_{b,i}^{(m)}, \delta b_{N_{\text{cs}}+1}^{(m)}\right) \\
&\quad + \text{Cov}\left(\delta b_{N_{\text{cs}}+1}^{(m)}, \delta l_{b,j}^{(m)}\right) + \text{Cov}\left(\delta b_{N_{\text{cs}}+1}^{(m)}, \delta b_{N_{\text{cs}}+1}^{(m)}\right)\Big) \qquad \text{(B.39)} \\
&= \sum_{m=k_{\text{ref}}+1}^{\min(k,l)}\left(\mathbb{V}\text{ar}\left[\delta l_{b,j}^{(m)}\right]\mathbb{1}_{\{j\}}(i) + \mathbb{V}\text{ar}\left[\delta b_{N_{\text{cs}}+1}^{(m)}\right]\right) \quad \begin{matrix}\text{(independence,}\\ \text{cf. equation B.2)}\end{matrix} \\
&= \begin{cases}
\displaystyle\sum_{m=k_{\text{ref}}+1}^{k}\left(\left(\sigma_{\delta l_b,j}^{(m)}\right)^2 + \left(\sigma_{\delta b,N_{\text{cs}}+1}^{(m)}\right)^2\right) & \text{if } i=j \text{ and } k \leq l \\
\displaystyle\sum_{m=k_{\text{ref}}+1}^{l}\left(\left(\sigma_{\delta l_b,j}^{(m)}\right)^2 + \left(\sigma_{\delta b,N_{\text{cs}}+1}^{(m)}\right)^2\right) & \text{if } i=j \text{ and } k > l \\
\displaystyle\sum_{m=k_{\text{ref}}+1}^{k}\left(\sigma_{\delta b,N_{\text{cs}}+1}^{(m)}\right)^2 & \text{if } i\neq j \text{ and } k \leq l \\
\displaystyle\sum_{m=k_{\text{ref}}+1}^{l}\left(\sigma_{\delta b,N_{\text{cs}}+1}^{(m)}\right)^2 & \text{if } i\neq j \text{ and } k > l
\end{cases}
\end{aligned}
$$

– $\forall k \in [\![1; k_{\text{ref}} - 1]\!]$, $\forall l \in [\![1; k_{\text{ref}} - 1]\!]$,

$$
\begin{aligned}
&\text{Cov}\left(\Delta b_i^{(k)}, \Delta b_j^{(l)}\right) \\
&= \text{Cov}\left(\sum_{m=k}^{k_{\text{ref}}-1}\left(\delta l_{b,i}^{(m)} + \delta b_{N_{\text{cs}}+1}^{(m)}\right), \sum_{p=l}^{k_{\text{ref}}-1}\left(\delta l_{b,j}^{(p)} + \delta b_{N_{\text{cs}}+1}^{(p)}\right)\right) \\
&= \sum_{m=k}^{k_{\text{ref}}-1}\sum_{p=l}^{k_{\text{ref}}-1}\left(\text{Cov}\left(\delta l_{b,i}^{(m)}, \delta l_{b,j}^{(p)}\right) + \text{Cov}\left(\delta l_{b,i}^{(m)}, \delta b_{N_{\text{cs}}+1}^{(p)}\right)\right. \\
&\quad \left. + \text{Cov}\left(\delta b_{N_{\text{cs}}+1}^{(m)}, \delta l_{b,j}^{(p)}\right) + \text{Cov}\left(\delta b_{N_{\text{cs}}+1}^{(m)}, \delta b_{N_{\text{cs}}+1}^{(p)}\right)\right) \quad \begin{array}{l}\text{(bilinearity,} \\ \text{cf. property 4)}\end{array} \\
&= \sum_{m=k}^{k_{\text{ref}}-1}\sum_{\substack{p=l \\ p\neq m}}^{k_{\text{ref}}-1}\left(\text{Cov}\left(\delta l_{b,i}^{(m)}, \delta l_{b,j}^{(p)}\right) + \text{Cov}\left(\delta l_{b,i}^{(m)}, \delta b_{N_{\text{cs}}+1}^{(p)}\right)\right. \\
&\quad \left. + \text{Cov}\left(\delta b_{N_{\text{cs}}+1}^{(m)}, \delta l_{b,j}^{(p)}\right) + \text{Cov}\left(\delta b_{N_{\text{cs}}+1}^{(m)}, \delta b_{N_{\text{cs}}+1}^{(p)}\right)\right) \\
&\quad + \sum_{m=\max(k,l)}^{k_{\text{ref}}-1}\left(\text{Cov}\left(\delta l_{b,i}^{(m)}, \delta l_{b,j}^{(m)}\right) + \text{Cov}\left(\delta l_{b,i}^{(m)}, \delta b_{N_{\text{cs}}+1}^{(m)}\right)\right. \\
&\quad \left. + \text{Cov}\left(\delta b_{N_{\text{cs}}+1}^{(m)}, \delta l_{b,j}^{(m)}\right) + \text{Cov}\left(\delta b_{N_{\text{cs}}+1}^{(m)}, \delta b_{N_{\text{cs}}+1}^{(m)}\right)\right) \qquad \text{(B.40)} \\
&= \sum_{m=\max(k,l)}^{k_{\text{ref}}-1}\left(\mathbb{V}\text{ar}\left[\delta l_{b,j}^{(m)}\right]\mathbb{1}_{\{j\}}(i) + \mathbb{V}\text{ar}\left[\delta b_{N_{\text{cs}}+1}^{(m)}\right]\right) \quad \begin{array}{l}\text{(independence,} \\ \text{cf. equation B.2)}\end{array} \\
&= \begin{cases}
\sum_{m=l}^{k_{\text{ref}}-1}\left(\left(\sigma_{\delta l_b,j}^{(m)}\right)^2 + \left(\sigma_{\delta b,N_{\text{cs}}+1}^{(m)}\right)^2\right) & \text{if } i = j \text{ and } k \leq l \\
\sum_{m=k}^{k_{\text{ref}}-1}\left(\left(\sigma_{\delta l_b,j}^{(m)}\right)^2 + \left(\sigma_{\delta b,N_{\text{cs}}+1}^{(m)}\right)^2\right) & \text{if } i = j \text{ and } k > l \\
\sum_{m=l}^{k_{\text{ref}}-1}\left(\sigma_{\delta b,N_{\text{cs}}+1}^{(m)}\right)^2 & \text{if } i \neq j \text{ and } k \leq l \\
\sum_{m=k}^{k_{\text{ref}}-1}\left(\sigma_{\delta b,N_{\text{cs}}+1}^{(m)}\right)^2 & \text{if } i \neq j \text{ and } k > l
\end{cases}
\end{aligned}
$$

– $\forall k \in [\![1; k_{\text{ref}} - 1]\!]$, $\forall l \in [\![k_{\text{ref}} + 1; N_{\text{shift}} + 1]\!]$,

$$
\begin{aligned}
&\text{Cov}\left(\Delta b_i^{(k)}, \Delta b_j^{(l)}\right) \\
&= \text{Cov}\left(\sum_{m=k}^{k_{\text{ref}}-1}\left(\delta l_{b,i}^{(m)} + \delta b_{N_{\text{cs}}+1}^{(m)}\right), \sum_{p=k_{\text{ref}}+1}^{l}\left(\delta l_{b,j}^{(p)} + \delta b_{N_{\text{cs}}+1}^{(p)}\right)\right) \\
&= \sum_{m=k}^{k_{\text{ref}}-1}\sum_{p=k_{\text{ref}}+1}^{l}\left(\text{Cov}\left(\delta l_{b,i}^{(m)}, \delta l_{b,j}^{(p)}\right) + \text{Cov}\left(\delta l_{b,i}^{(m)}, \delta b_{N_{\text{cs}}+1}^{(p)}\right)\right. \qquad \text{(B.41)} \\
&\quad \left. + \text{Cov}\left(\delta b_{N_{\text{cs}}+1}^{(m)}, \delta l_{b,j}^{(p)}\right) + \text{Cov}\left(\delta b_{N_{\text{cs}}+1}^{(m)}, \delta b_{N_{\text{cs}}+1}^{(p)}\right)\right) \quad \begin{array}{l}\text{(bilinearity,} \\ \text{cf. property 4)}\end{array} \\
&= 0 \text{ (independence, cf. equation B.2)}
\end{aligned}
$$

- $\forall i \in [\![1; N_{\text{cs}}]\!]$, $\forall j \in [\![N_{\text{cs}}+1; N_{\text{c}}]\!]$,

  - $\forall k \in [\![k_{\text{ref}}+1; N_{\text{shift}}+1]\!]$, $\forall l \in [\![k_{\text{ref}}+1; N_{\text{shift}}+1]\!]$,

$$
\begin{aligned}
&\text{Cov}\left(\Delta b_i^{(k)}, \Delta b_j^{(l)}\right) \\
&= \text{Cov}\left(\sum_{m=k_{\text{ref}}+1}^{k}\left(\delta l_{b,i}^{(m)} + \delta b_{N_{\text{cs}}+1}^{(m)}\right), \sum_{p=k_{\text{ref}}+1}^{l}\delta b_j^{(p)}\right) \\
&= \sum_{m=k_{\text{ref}}+1}^{k}\sum_{p=k_{\text{ref}}+1}^{l}\Big(\text{Cov}\left(\delta l_{b,i}^{(m)}, \delta b_j^{(p)}\right) \\
&\quad +\text{Cov}\left(\delta b_{N_{\text{cs}}+1}^{(m)}, \delta b_j^{(p)}\right)\Big) \text{ (bilinearity, cf. property 4)} \\
&= \sum_{m=k_{\text{ref}}+1}^{k}\sum_{\substack{p=k_{\text{ref}}+1 \\ p\neq m}}^{l}\left(\text{Cov}\left(\delta l_{b,i}^{(m)}, \delta b_j^{(p)}\right) + \text{Cov}\left(\delta b_{N_{\text{cs}}+1}^{(m)}, \delta b_j^{(p)}\right)\right) \\
&\quad + \sum_{m=k_{\text{ref}}+1}^{\min(k,l)}\left(\text{Cov}\left(\delta l_{b,i}^{(m)}, \delta b_j^{(m)}\right) + \text{Cov}\left(\delta b_{N_{\text{cs}}+1}^{(m)}, \delta b_j^{(m)}\right)\right) \qquad \text{(B.42)} \\
&= \sum_{m=k_{\text{ref}}+1}^{\min(k,l)}\text{Cov}\left(\delta b_{N_{\text{cs}}+1}^{(m)}, \delta b_j^{(m)}\right) \text{ (independence, cf. equation B.2)} \\
&= \sum_{m=k_{\text{ref}}+1}^{\min(k,l)}\mathbb{V}\text{ar}\left[\delta b_{N_{\text{cs}}+1}^{(m)}\right]\mathbb{1}_{\{N_{\text{cs}}+1\}}(j) \\
&= \begin{cases}
\displaystyle\sum_{m=k_{\text{ref}}+1}^{k}\left(\sigma_{\delta b, N_{\text{cs}}+1}^{(m)}\right)^2 & \text{if } j = N_{\text{cs}}+1 \text{ and } k \leq l \\
\displaystyle\sum_{m=k_{\text{ref}}+1}^{l}\left(\sigma_{\delta b, N_{\text{cs}}+1}^{(m)}\right)^2 & \text{if } j = N_{\text{cs}}+1 \text{ and } k > l \\
0 & \text{if } j \neq N_{\text{cs}}+1
\end{cases}
\end{aligned}
$$

– $\forall k \in [\![1; k_{\text{ref}} - 1]\!]$, $\forall l \in [\![1; k_{\text{ref}} - 1]\!]$,

$$
\begin{aligned}
&\text{Cov}\left(\Delta b_i^{(k)}, \Delta b_j^{(l)}\right) \\
&= \text{Cov}\left(\sum_{m=k}^{k_{\text{ref}}-1}\left(\delta l_{b,i}^{(m)} + \delta b_{N_{\text{cs}}+1}^{(m)}\right), \sum_{p=l}^{k_{\text{ref}}-1}\delta b_j^{(p)}\right) \\
&= \sum_{m=k}^{k_{\text{ref}}-1}\sum_{p=l}^{k_{\text{ref}}-1}\Big(\text{Cov}\left(\delta l_{b,i}^{(m)}, \delta b_j^{(p)}\right) \\
&\quad + \text{Cov}\left(\delta b_{N_{\text{cs}}+1}^{(m)}, \delta b_j^{(p)}\right)\Big) \text{ (bilinearity, cf. property 4)} \\
&= \sum_{m=k}^{k_{\text{ref}}-1}\sum_{\substack{p=l \\ p\neq m}}^{k_{\text{ref}}-1}\left(\text{Cov}\left(\delta l_{b,i}^{(m)}, \delta b_j^{(p)}\right) + \text{Cov}\left(\delta b_{N_{\text{cs}}+1}^{(m)}, \delta b_j^{(p)}\right)\right) \\
&\quad + \sum_{m=\max(k,l)}^{k_{\text{ref}}-1}\left(\text{Cov}\left(\delta l_{b,i}^{(m)}, \delta b_j^{(m)}\right) + \text{Cov}\left(\delta b_{N_{\text{cs}}+1}^{(m)}, \delta b_j^{(m)}\right)\right) \\
&= \sum_{m=\max(k,l)}^{k_{\text{ref}}-1}\text{Cov}\left(\delta b_{N_{\text{cs}}+1}^{(m)}, \delta b_j^{(m)}\right) \text{ (independence, cf. equation B.2)} \\
&= \sum_{m=\max(k,l)}^{k_{\text{ref}}-1}\mathbb{V}\text{ar}\left[\delta b_{N_{\text{cs}}+1}^{(m)}\right]\mathbb{1}_{\{N_{\text{cs}}+1\}}(j) \\
&= \begin{cases}
\displaystyle\sum_{m=\max(k,l)}^{k_{\text{ref}}-1}\left(\sigma_{\delta b,N_{\text{cs}}+1}^{(m)}\right)^2 & \text{if } j = N_{\text{cs}}+1 \text{ and } k \leq l \\
\displaystyle\sum_{m=\max(k,l)}^{k_{\text{ref}}-1}\left(\sigma_{\delta b,N_{\text{cs}}+1}^{(m)}\right)^2 & \text{if } j = N_{\text{cs}}+1 \text{ and } k > l \\
0 & \text{if } j \neq N_{\text{cs}}+1
\end{cases}
\end{aligned}
\tag{B.43}
$$

– $\forall k \in [\![1; k_{\text{ref}} - 1]\!]$, $\forall l \in [\![k_{\text{ref}} + 1; N_{\text{shift}} + 1]\!]$,

$$
\begin{aligned}
\text{Cov}\left(\Delta b_i^{(k)}, \Delta b_j^{(l)}\right) &= \text{Cov}\left(\sum_{m=k}^{k_{\text{ref}}-1}\left(\delta l_{b,i}^{(m)} + \delta b_{N_{\text{cs}}+1}^{(m)}\right), \sum_{p=k_{\text{ref}}+1}^{l}\delta b_j^{(p)}\right) \\
&= \sum_{m=k}^{k_{\text{ref}}-1}\sum_{p=k_{\text{ref}}+1}^{l}\Big(\text{Cov}\left(\delta l_{b,i}^{(m)}, \delta b_j^{(p)}\right) \\
&\quad + \text{Cov}\left(\delta b_{N_{\text{cs}}+1}^{(m)}, \delta b_j^{(p)}\right)\Big) \text{ (bilinearity, cf. property 4)} \\
&= 0 \text{ (independence, cf. equation B.2)}
\end{aligned}
\tag{B.44}
$$

B.3.3. Multiplicative link

B.3.3.1. Assumptions

$\forall k \in [\![1; N_{\text{shift}} + 1]\!], k \neq k_{\text{ref}}$, let $\forall j \in [\![1; N_{\text{cs}}]\!]$, $\delta b_j^{(k)}$ and $\forall j \in [\![N_{\text{cs}} + 1; N_{\text{c}}]\!]$, $\lambda_{b,j}^{(k)}$ be $N_{\text{c}} \times N_{\text{shift}}$ independent and random variables distributed as follows:

$$\forall k \in [\![1; N_{\text{shift}}]\!], k \neq k_{\text{ref}}, \begin{cases} \delta b_j^{(k)} \sim \mathcal{N}\left(\mu_{\delta b,j}^{(k)}; \sigma_{\delta b,j}^{(k)}\right), & \forall j \in [\![1; N_{\text{cs}}]\!] \quad \text{(local)} \\ \lambda_{b,j}^{(k)} \sim \mathcal{N}\left(\mu_{\lambda_b,j}^{(k)}; \sigma_{\lambda_b,j}^{(k)}\right), & \forall j \in [\![N_{\text{cs}}+1; N_{\text{c}}]\!] \quad \text{(global)} \end{cases} \tag{B.45}$$

B.3.3.2. Cumulated change distribution

Relations between cumulated changes and incremental changes for the multiplicative link option are expressed by equation (5.13) using table 5.2. As addition and multiplication are used in these relations, the multivariate distribution of the inferred parameters corresponding to the cumulated changes can be approximated by a multivariate normal distribution. This approximation have been compared with and validated by results from Monte-Carlo propagation.The following paragraph in this subsection are the theoretical calculations of the parameters (mean and covariance matrix) of this approximated multivariate distribution.

Mean $\forall k \in [\![1; N_{\text{shift}}]\!], k \neq k_{\text{ref}},$

$$\begin{aligned}
\mathbb{E}\left[\Delta b_j^{(k)}\right] &= \begin{cases} \mathbb{E}\left[\sum_m \delta b_j^{(m)}\right] & \text{if } j \leq N_{\text{cs}} \quad \text{(section control)} \\ \mathbb{E}\left[\sum_m \lambda_{b,j}^{(m)} \delta b_{N_{\text{cs}}}^{(m)}\right] & \text{if } j > N_{\text{cs}} \quad \text{(channel control)} \end{cases} \\
&= \begin{cases} \sum_m \mathbb{E}\left[\delta b_j^{(m)}\right] & \text{if } j \leq N_{\text{cs}} \\ \sum_m \mathbb{E}\left[\lambda_{b,j}^{(m)} \delta b_{N_{\text{cs}}}^{(m)}\right] & \text{if } j > N_{\text{cs}} \end{cases} \quad \text{(cf. property 3)} \\
&= \begin{cases} \sum_m \mathbb{E}\left[\delta b_j^{(m)}\right] & \text{if } j \leq N_{\text{cs}} \\ \sum_m \mathbb{E}\left[\lambda_{b,j}^{(m)}\right] \mathbb{E}\left[\delta b_{N_{\text{cs}}}^{(m)}\right] & \text{if } j > N_{\text{cs}} \text{ (independence, cf. property 1)} \end{cases} \\
&= \begin{cases} \sum_{m=k}^{k_{\text{ref}}-1} \mu_{\delta b,j}^{(m)} & \text{if } j \leq N_{\text{cs}} \text{ and } k < k_{\text{ref}} \\ \sum_{m=k_{\text{ref}}+1}^{k} \mu_{\delta b,j}^{(m)} & \text{if } j \leq N_{\text{cs}} \text{ and } k > k_{\text{ref}} \\ \sum_{m=k}^{k_{\text{ref}}-1} \mu_{\lambda_b,j}^{(m)} \mu_{\delta b,j}^{(m)} & \text{if } j > N_{\text{cs}} \text{ and } k < k_{\text{ref}} \\ \sum_{m=k_{\text{ref}}+1}^{k} \mu_{\lambda_b,j}^{(m)} \mu_{\delta b,j}^{(m)} & \text{if } j > N_{\text{cs}} \text{ and } k > k_{\text{ref}} \end{cases}
\end{aligned} \tag{B.46}$$

Covariance

- $\forall i \in [\![1; N_{\text{cs}}]\!],\ \forall j \in [\![1; N_{\text{cs}}]\!],$

– $\forall k \in [\![1; k_{\text{ref}} - 1]\!],\ \forall l \in [\![1; k_{\text{ref}} - 1]\!]$,

$$
\begin{aligned}
&\text{Cov}\left(\Delta b_i^{(k)}, \Delta b_j^{(l)}\right) \\
&= \text{Cov}\left(\sum_{m=k}^{k_{\text{ref}}-1} \delta b_i^{(m)}, \sum_{p=l}^{k_{\text{ref}}-1} \delta b_j^{(p)}\right) \\
&= \sum_{m=k}^{k_{\text{ref}}-1} \sum_{p=l}^{k_{\text{ref}}-1} \text{Cov}\left(\delta b_i^{(m)}, \delta b_j^{(p)}\right) \text{ (bilinearity, cf. property 4)} \\
&= \sum_{m=k}^{k_{\text{ref}}-1} \sum_{\substack{p=l \\ p\neq m}}^{k_{\text{ref}}-1} \text{Cov}\left(\delta b_i^{(m)}, \delta b_j^{(p)}\right) + \sum_{m=\max(k,l)}^{k_{\text{ref}}-1} \text{Cov}\left(\delta b_i^{(m)}, \delta b_j^{(m)}\right) \\
&= \sum_{m=\max(k,l)}^{k_{\text{ref}}-1} \mathbb{V}\text{ar}\left[\delta b_j^{(m)}\right] \mathbb{1}_{\{j\}}(i) \text{ (independence, cf. equation B.2)} \\
&= \begin{cases} \displaystyle\sum_{m=l}^{k_{\text{ref}}-1} \left(\sigma_{\delta b,j}^{(m)}\right)^2 & \text{if } i = j \text{ and } k \leq l \\ \displaystyle\sum_{m=k}^{k_{\text{ref}}-1} \left(\sigma_{\delta b,j}^{(m)}\right)^2 & \text{if } i = j \text{ and } k > l \\ 0 & \text{if } i \neq j \end{cases}
\end{aligned}
\tag{B.47}
$$

– $\forall k \in [\![k_{\text{ref}} + 1; N_{\text{shift}} + 1]\!],\ \forall l \in [\![k_{\text{ref}} + 1; N_{\text{shift}} + 1]\!]$,

$$
\begin{aligned}
&\text{Cov}\left(\Delta b_i^{(k)}, \Delta b_j^{(l)}\right) \\
&= \text{Cov}\left(\sum_{m=k_{\text{ref}}+1}^{k} \delta b_i^{(m)}, \sum_{p=k_{\text{ref}}+1}^{l} \delta b_j^{(p)}\right) \\
&= \sum_{m=k_{\text{ref}}+1}^{k} \sum_{p=k_{\text{ref}}+1}^{l} \text{Cov}\left(\delta b_i^{(m)}, \delta b_j^{(p)}\right) \text{ (bilinearity, cf. property 4)} \\
&= \sum_{m=k_{\text{ref}}+1}^{k} \sum_{\substack{p=k_{\text{ref}}+1 \\ p\neq m}}^{l} \text{Cov}\left(\delta b_i^{(m)}, \delta b_j^{(p)}\right) + \sum_{m=k_{\text{ref}}+1}^{\min(k,l)} \text{Cov}\left(\delta b_i^{(m)}, \delta b_j^{(m)}\right) \\
&= \sum_{m=k_{\text{ref}}+1}^{\min(k,l)} \mathbb{V}\text{ar}\left[\delta b_j^{(m)}\right] \mathbb{1}_{\{j\}}(i) \text{ (independence, cf. equation B.2)} \\
&= \begin{cases} \displaystyle\sum_{m=k_{\text{ref}}+1}^{k} \left(\sigma_{\delta b,j}^{(m)}\right)^2 & \text{if } i = j \text{ and } k \leq l \\ \displaystyle\sum_{m=k_{\text{ref}}+1}^{l} \left(\sigma_{\delta b,j}^{(m)}\right)^2 & \text{if } i = j \text{ and } k > l \\ 0 & \text{if } i \neq j \end{cases}
\end{aligned}
\tag{B.48}
$$

– $\forall k \in [\![1; k_{\text{ref}} - 1]\!],\ \forall l \in [\![k_{\text{ref}} + 1; N_{\text{shift}} + 1]\!]$,

$$\begin{aligned}
\text{Cov}\left(\Delta b_i^{(k)}, \Delta b_j^{(l)}\right) &= \text{Cov}\left(\sum_{m=k}^{k_{\text{ref}}-1} \delta b_i^{(m)}, \sum_{p=k_{\text{ref}}+1}^{l} \delta b_j^{(p)}\right) \\
&= \sum_{m=k}^{k_{\text{ref}}-1} \sum_{p=k_{\text{ref}}+1}^{l} \text{Cov}\left(\delta b_i^{(m)}, \delta b_j^{(p)}\right) \text{ (bilinearity, cf. property 4)} \\
&= 0 \text{ (independence, cf. equation B.2)}
\end{aligned} \tag{B.49}$$

- $\forall i \in [\![N_{\text{cs}} + 1; N_{\text{c}}]\!],\ \forall j \in [\![N_{\text{cs}} + 1; N_{\text{c}}]\!]$,

– $\forall k \in [\![1; k_{\text{ref}} - 1]\!],\ \forall l \in [\![1; k_{\text{ref}} - 1]\!]$,

$$
\begin{aligned}
&\operatorname{Cov}\left(\Delta b_i^{(k)}, \Delta b_j^{(l)}\right) \\
&= \operatorname{Cov}\left(\sum_{m=k}^{k_{\text{ref}}-1} \lambda_{b,i}^{(m)} \delta b_{N_{\text{cs}}}^{(m)}, \sum_{p=l}^{k_{\text{ref}}-1} \lambda_{b,j}^{(p)} \delta b_{N_{\text{cs}}}^{(p)}\right) \\
&= \sum_{m=k}^{k_{\text{ref}}-1} \sum_{p=l}^{k_{\text{ref}}-1} \operatorname{Cov}\left(\lambda_{b,i}^{(m)} \delta b_{N_{\text{cs}}}^{(m)}, \lambda_{b,j}^{(p)} \delta b_{N_{\text{cs}}}^{(p)}\right) \text{ (bilinearity, cf. property 4)} \\
&= \sum_{m=k}^{k_{\text{ref}}-1} \sum_{\substack{p=l \\ p\neq m}}^{k_{\text{ref}}-1} \operatorname{Cov}\left(\lambda_{b,i}^{(m)} \delta b_{N_{\text{cs}}}^{(m)}, \lambda_{b,j}^{(p)} \delta b_{N_{\text{cs}}}^{(p)}\right) \\
&\quad + \sum_{m=\max(k,l)}^{k_{\text{ref}}-1} \operatorname{Cov}\left(\lambda_{b,i}^{(m)} \delta b_{N_{\text{cs}}}^{(m)}, \lambda_{b,j}^{(m)} \delta b_{N_{\text{cs}}}^{(m)}\right) \\
&= \sum_{m=\max(k,l)}^{k_{\text{ref}}-1} \operatorname{Cov}\left(\lambda_{b,i}^{(m)} \delta b_{N_{\text{cs}}}^{(m)}, \lambda_{b,j}^{(m)} \delta b_{N_{\text{cs}}}^{(m)}\right) \text{ (cf. equation B.6)} \\
&= \sum_{m=\max(k,l)}^{k_{\text{ref}}-1} \mathbb{V}\text{ar}\left[\lambda_{b,j}^{(m)} \delta b_{N_{\text{cs}}}^{(m)}\right] \mathbb{1}_{\{j\}}(i) \text{ (cf. equation B.6)} \\
&= \sum_{m=\max(k,l)}^{k_{\text{ref}}-1} \left[\left(\mathbb{E}\left[\lambda_{b,i}^{(m)}\right] \mathbb{E}\left[\lambda_{b,j}^{(m)}\right] \mathbb{V}\text{ar}\left[\delta b_{N_{\text{cs}}}^{(m)}\right]\right) \mathbb{1}_{\{i\neq j\}}(i,j)\right. \\
&\quad + \left(\left(\mathbb{E}\left[\lambda_{b,j}^{(m)}\right]\right)^2 \mathbb{V}\text{ar}\left[\delta b_{N_{\text{cs}}}^{(m)}\right] + \left(\mathbb{E}\left[\delta b_{N_{\text{cs}}}^{(m)}\right]\right)^2 \mathbb{V}\text{ar}\left[\lambda_{b,j}^{(m)}\right]\right. \\
&\quad \left.\left. + \mathbb{V}\text{ar}\left[\lambda_{b,j}^{(m)}\right] \mathbb{V}\text{ar}\left[\delta b_{N_{\text{cs}}}^{(m)}\right]\right) \mathbb{1}_{\{j\}}(i)\right] \text{ (cf. equation B.3 and property 2)} \\
&= \begin{cases}
\displaystyle\sum_{m=l}^{k_{\text{ref}}-1} \left(\left(\mu_{\lambda_b,j}^{(m)}\right)^2 \left(\sigma_{\delta b,N_{\text{cs}}}^{(m)}\right)^2 + \left(\mu_{\delta b,N_{\text{cs}}}^{(m)}\right)^2 \left(\sigma_{\lambda_b,j}^{(m)}\right)^2 \right. & \text{if } i = j \text{ and } k \leq l \\
\qquad \left. + \left(\sigma_{\lambda_b,j}^{(m)}\right)^2 \left(\sigma_{\delta b,N_{\text{cs}}}^{(m)}\right)^2\right) & \\
\displaystyle\sum_{m=k}^{k_{\text{ref}}-1} \left(\left(\mu_{\lambda_b,j}^{(m)}\right)^2 \left(\sigma_{\delta b,N_{\text{cs}}}^{(m)}\right)^2 + \left(\mu_{\delta b,N_{\text{cs}}}^{(m)}\right)^2 \left(\sigma_{\lambda_b,j}^{(m)}\right)^2 \right. & \text{if } i = j \text{ and } k > l \\
\qquad \left. + \left(\sigma_{\lambda_b,j}^{(m)}\right)^2 \left(\sigma_{\delta b,N_{\text{cs}}}^{(m)}\right)^2\right) & \\
\displaystyle\sum_{m=l}^{k_{\text{ref}}-1} \mu_{\lambda_b,j}^{(m)} \mu_{\lambda_b,j}^{(m)} \left(\sigma_{\delta b,N_{\text{cs}}}^{(m)}\right)^2 & \text{if } i \neq j \text{ and } k \leq l \\
\displaystyle\sum_{m=k}^{k_{\text{ref}}-1} \mu_{\lambda_b,j}^{(m)} \mu_{\lambda_b,j}^{(m)} \left(\sigma_{\delta b,N_{\text{cs}}}^{(m)}\right)^2 & \text{if } i \neq j \text{ and } k > l
\end{cases}
\end{aligned}
\tag{B.50}
$$

– $\forall k \in [\![k_{\text{ref}}+1; N_{\text{shift}}+1]\!],\ \forall l \in [\![k_{\text{ref}}+1; N_{\text{shift}}+1]\!]$,

$$
\begin{aligned}
&\operatorname{Cov}\left(\Delta b_i^{(k)}, \Delta b_j^{(l)}\right) \\
&= \operatorname{Cov}\left(\sum_{m=k_{\text{ref}}+1}^{k} \lambda_{b,i}^{(m)} \delta b_{N_{\text{cs}}}^{(m)}, \sum_{p=k_{\text{ref}}+1}^{l} \lambda_{b,j}^{(p)} \delta b_{N_{\text{cs}}}^{(p)}\right) \\
&= \sum_{m=k_{\text{ref}}+1}^{k} \sum_{p=k_{\text{ref}}+1}^{l} \operatorname{Cov}\left(\lambda_{b,i}^{(m)} \delta b_{N_{\text{cs}}}^{(m)}, \lambda_{b,j}^{(p)} \delta b_{N_{\text{cs}}}^{(p)}\right) \text{ (bilinearity, cf. property 4)} \\
&= \sum_{m=k_{\text{ref}}+1}^{k} \sum_{\substack{p=k_{\text{ref}}+1 \\ p\neq m}}^{l} \operatorname{Cov}\left(\lambda_{b,i}^{(m)} \delta b_{N_{\text{cs}}}^{(m)}, \lambda_{b,j}^{(p)} \delta b_{N_{\text{cs}}}^{(p)}\right) \\
&\quad + \sum_{m=k_{\text{ref}}+1}^{\min(k,l)} \operatorname{Cov}\left(\lambda_{b,i}^{(m)} \delta b_{N_{\text{cs}}}^{(m)}, \lambda_{b,j}^{(m)} \delta b_{N_{\text{cs}}}^{(m)}\right) \\
&= \sum_{m=k_{\text{ref}}+1}^{\min(k,l)} \operatorname{Cov}\left(\lambda_{b,i}^{(m)} \delta b_{N_{\text{cs}}}^{(m)}, \lambda_{b,j}^{(m)} \delta b_{N_{\text{cs}}}^{(m)}\right) \text{ (cf. equation B.6)} \\
&= \sum_{m=k_{\text{ref}}+1}^{\min(k,l)} \mathbb{V}\text{ar}\left[\lambda_{b,j}^{(m)} \delta b_{N_{\text{cs}}}^{(m)}\right] \mathbb{1}_{\{j\}}(i) \text{ (cf. equation B.6)} \\
&= \sum_{m=k_{\text{ref}}+1}^{\min(k,l)} \Big[\left(\mathbb{E}\left[\lambda_{b,i}^{(m)}\right] \mathbb{E}\left[\lambda_{b,j}^{(m)}\right] \mathbb{V}\text{ar}\left[\delta b_{N_{\text{cs}}}^{(m)}\right]\right) \mathbb{1}_{\{i\neq j\}}(i,j) \\
&\quad + \Big(\left(\mathbb{E}\left[\lambda_{b,j}^{(m)}\right]\right)^2 \mathbb{V}\text{ar}\left[\delta b_{N_{\text{cs}}}^{(m)}\right] + \left(\mathbb{E}\left[\delta b_{N_{\text{cs}}}^{(m)}\right]\right)^2 \mathbb{V}\text{ar}\left[\lambda_{b,j}^{(m)}\right] \\
&\quad + \mathbb{V}\text{ar}\left[\lambda_{b,j}^{(m)}\right] \mathbb{V}\text{ar}\left[\delta b_{N_{\text{cs}}}^{(m)}\right]\Big) \mathbb{1}_{\{j\}}(i)\Big] \text{ (cf. equation B.3 and property 2)} \\
&= \begin{cases}
\displaystyle\sum_{m=k_{\text{ref}}+1}^{k} \Big(\left(\mu_{\lambda_b,j}^{(m)}\right)^2 \left(\sigma_{\delta b,N_{\text{cs}}}^{(m)}\right)^2 + \left(\mu_{\delta b,N_{\text{cs}}}^{(m)}\right)^2 \left(\sigma_{\lambda_b,j}^{(m)}\right)^2 & \text{if } i=j \text{ and } k\leq l \\
\qquad + \left(\sigma_{\lambda_b,j}^{(m)}\right)^2 \left(\sigma_{\delta b,N_{\text{cs}}}^{(m)}\right)^2\Big) & \\
\displaystyle\sum_{m=k_{\text{ref}}+1}^{l} \Big(\left(\mu_{\lambda_b,j}^{(m)}\right)^2 \left(\sigma_{\delta b,N_{\text{cs}}}^{(m)}\right)^2 + \left(\mu_{\delta b,N_{\text{cs}}}^{(m)}\right)^2 \left(\sigma_{\lambda_b,j}^{(m)}\right)^2 & \text{if } i=j \text{ and } k>l \\
\qquad + \left(\sigma_{\lambda_b,j}^{(m)}\right)^2 \left(\sigma_{\delta b,N_{\text{cs}}}^{(m)}\right)^2\Big) & \\
\displaystyle\sum_{m=k_{\text{ref}}+1}^{k} \mu_{\lambda_b,j}^{(m)} \mu_{\lambda_b,j}^{(m)} \left(\sigma_{\delta b,N_{\text{cs}}}^{(m)}\right)^2 & \text{if } i\neq j \text{ and } k\leq l \\
\displaystyle\sum_{m=k_{\text{ref}}+1}^{l} \mu_{\lambda_b,j}^{(m)} \mu_{\lambda_b,j}^{(m)} \left(\sigma_{\delta b,N_{\text{cs}}}^{(m)}\right)^2 & \text{if } i\neq j \text{ and } k>l
\end{cases}
\end{aligned}
\tag{B.51}
$$

– $\forall k \in [\![1; k_{\text{ref}} - 1]\!],\ \forall l \in [\![k_{\text{ref}} + 1; N_{\text{shift}} + 1]\!]$,

$$\begin{aligned}
&\text{Cov}\left(\Delta b_i^{(k)}, \Delta b_j^{(l)}\right) \\
&= \text{Cov}\left(\sum_{m=k}^{k_{\text{ref}}-1} \lambda_{b,i}^{(m)} \delta b_{N_{\text{cs}}}^{(m)}, \sum_{p=k_{\text{ref}}+1}^{l} \lambda_{b,j}^{(p)} \delta b_{N_{\text{cs}}}^{(p)}\right) \\
&= \sum_{m=k}^{k_{\text{ref}}-1} \sum_{p=k_{\text{ref}}+1}^{l} \text{Cov}\left(\lambda_{b,i}^{(m)} \delta b_{N_{\text{cs}}}^{(m)}, \lambda_{b,j}^{(p)} \delta b_{N_{\text{cs}}}^{(p)}\right) \text{ (bilinearity, cf. property 4)} \\
&= 0 \text{ (independence, cf. equation B.6)}
\end{aligned} \tag{B.52}$$

- $\forall i \in [\![N_{\text{cs}} + 1; N_{\text{c}}]\!],\ \forall j \in [\![1; N_{\text{cs}}]\!]$,

  – $\forall k \in [\![1; k_{\text{ref}} - 1]\!],\ \forall l \in [\![1; k_{\text{ref}} - 1]\!]$,

$$\begin{aligned}
&\text{Cov}\left(\Delta b_i^{(k)}, \Delta b_j^{(l)}\right) \\
&= \text{Cov}\left(\sum_{m=k}^{k_{\text{ref}}-1} \lambda_{b,i}^{(m)} \delta b_{N_{\text{cs}}}^{(m)}, \sum_{p=l}^{k_{\text{ref}}-1} \delta b_j^{(p)}\right) \\
&= \sum_{m=k}^{k_{\text{ref}}-1} \sum_{p=l}^{k_{\text{ref}}-1} \text{Cov}\left(\lambda_{b,i}^{(m)} \delta b_{N_{\text{cs}}}^{(m)}, \delta b_j^{(p)}\right) \text{ (bilinearity, cf. property 4)} \\
&= \sum_{m=k}^{k_{\text{ref}}-1} \sum_{\substack{p=l \\ p\neq m}}^{k_{\text{ref}}-1} \text{Cov}\left(\lambda_{b,i}^{(m)} \delta b_{N_{\text{cs}}}^{(m)}, \delta b_j^{(p)}\right) \\
&\quad + \sum_{m=\max(k,l)}^{k_{\text{ref}}-1} \text{Cov}\left(\lambda_{b,i}^{(m)} \delta b_{N_{\text{cs}}}^{(m)}, \delta b_j^{(m)}\right) \\
&= \sum_{m=\max(k,l)}^{k_{\text{ref}}-1} \text{Cov}\left(\lambda_{b,i}^{(m)} \delta b_{N_{\text{cs}}}^{(m)}, \delta b_j^{(m)}\right) \text{ (cf. equation B.4)} \\
&= \sum_{m=\max(k,l)}^{k_{\text{ref}}-1} \left(\text{Cov}\left(\lambda_{b,i}^{(m)} \delta b_{N_{\text{cs}}}^{(m)}, \delta b_j^{(m)}\right) \mathbb{1}_{\{j\neq N_{\text{cs}}\}}(j)\right. \\
&\quad \left. + \text{Cov}\left(\lambda_{b,j}^{(m)} \delta b_{N_{\text{cs}}}^{(m)}, \delta b_{N_{\text{cs}}}^{(m)}\right) \mathbb{1}_{\{N_{\text{cs}}\}}(j)\right) \\
&= \sum_{m=\max(k,l)}^{k_{\text{ref}}-1} \mathbb{E}\left[\lambda_{b,j}^{(m)}\right] \mathbb{V}\text{ar}\left[\delta b_{N_{\text{cs}}}^{(m)}\right] \mathbb{1}_{\{N_{\text{cs}}\}}(j) \text{ (cf. equations (B.4) and (B.6))} \\
&= \begin{cases}
0 & \text{if } j \neq N_{\text{cs}} \\
\sum_{m=l}^{k_{\text{ref}}-1} \mu_{\lambda_b, N_{\text{cs}}}^{(m)} \left(\sigma_{\delta b, N_{\text{cs}}}^{(m)}\right)^2 & \text{if } j = N_{\text{cs}} \text{ and } k \leq l \\
\sum_{m=k}^{k_{\text{ref}}-1} \mu_{\lambda_b, N_{\text{cs}}}^{(m)} \left(\sigma_{\delta b, N_{\text{cs}}}^{(m)}\right)^2 & \text{if } j = N_{\text{cs}} \text{ and } k > l
\end{cases}
\end{aligned} \tag{B.53}$$

– $\forall k \in [\![k_{\text{ref}}+1; N_{\text{shift}}+1]\!],\ \forall l \in [\![k_{\text{ref}}+1; N_{\text{shift}}+1]\!]$,

$$
\begin{aligned}
&\text{Cov}\left(\Delta b_i^{(k)}, \Delta b_j^{(l)}\right) \\
&= \text{Cov}\left(\sum_{m=k_{\text{ref}}+1}^{k} \lambda_{b,i}^{(m)} \delta b_{N_{\text{cs}}}^{(m)}, \sum_{p=k_{\text{ref}}+1}^{l} \delta b_j^{(p)}\right) \\
&= \sum_{m=k_{\text{ref}}+1}^{k} \sum_{p=k_{\text{ref}}+1}^{l} \text{Cov}\left(\lambda_{b,i}^{(m)} \delta b_{N_{\text{cs}}}^{(m)}, \delta b_j^{(p)}\right) \text{ (bilinearity, cf. property 4)} \\
&= \sum_{m=k_{\text{ref}}+1}^{k} \sum_{\substack{p=k_{\text{ref}}+1 \\ p\neq m}}^{l} \text{Cov}\left(\lambda_{b,i}^{(m)} \delta b_{N_{\text{cs}}}^{(m)}, \delta b_j^{(p)}\right) \\
&\quad + \sum_{m=k_{\text{ref}}+1}^{\min(k,l)} \text{Cov}\left(\lambda_{b,i}^{(m)} \delta b_{N_{\text{cs}}}^{(m)}, \delta b_j^{(m)}\right) \\
&= \sum_{m=k_{\text{ref}}+1}^{\min(k,l)} \text{Cov}\left(\lambda_{b,i}^{(m)} \delta b_{N_{\text{cs}}}^{(m)}, \delta b_j^{(m)}\right) \text{ (cf. equation B.4)} \\
&= \sum_{m=k_{\text{ref}}+1}^{\min(k,l)} \left(\text{Cov}\left(\lambda_{b,i}^{(m)} \delta b_{N_{\text{cs}}}^{(m)}, \delta b_j^{(m)}\right) \mathbb{1}_{\{j\neq N_{\text{cs}}\}}(j)\right. \\
&\quad \left. + \text{Cov}\left(\lambda_{b,j}^{(m)} \delta b_{N_{\text{cs}}}^{(m)}, \delta b_{N_{\text{cs}}}^{(m)}\right) \mathbb{1}_{\{N_{\text{cs}}\}}(j)\right) \\
&= \sum_{m=k_{\text{ref}}+1}^{\min(k,l)} \mathbb{E}\left[\lambda_{b,j}^{(m)}\right] \mathbb{V}\text{ar}\left[\delta b_{N_{\text{cs}}}^{(m)}\right] \mathbb{1}_{\{N_{\text{cs}}\}}(j) \text{ (cf. equations (B.4) and (B.6))} \\
&= \begin{cases} 0 & \text{if } j \neq N_{\text{cs}} \\ \displaystyle\sum_{m=k_{\text{ref}}+1}^{k} \mu_{\lambda_b, N_{\text{cs}}}^{(m)} \left(\sigma_{\delta b, N_{\text{cs}}}^{(m)}\right)^2 & \text{if } j = N_{\text{cs}} \text{ and } k \leq l \\ \displaystyle\sum_{m=k_{\text{ref}}+1}^{l} \mu_{\lambda_b, N_{\text{cs}}}^{(m)} \left(\sigma_{\delta b, N_{\text{cs}}}^{(m)}\right)^2 & \text{if } j = N_{\text{cs}} \text{ and } k > l \end{cases}
\end{aligned}
\tag{B.54}
$$

– $\forall k \in [\![1; k_{\text{ref}}-1]\!],\ \forall l \in [\![k_{\text{ref}}+1; N_{\text{shift}}+1]\!]$,

$$
\begin{aligned}
&\text{Cov}\left(\Delta b_i^{(k)}, \Delta b_j^{(l)}\right) \\
&= \text{Cov}\left(\sum_{m=k}^{k_{\text{ref}}-1} \lambda_{b,i}^{(m)} \delta b_{N_{\text{cs}}}^{(m)}, \sum_{p=k_{\text{ref}}+1}^{l} \delta b_j^{(p)}\right) \\
&= \sum_{m=k}^{k_{\text{ref}}-1} \sum_{p=k_{\text{ref}}+1}^{l} \text{Cov}\left(\lambda_{b,i}^{(m)} \delta b_{N_{\text{cs}}}^{(m)}, \delta b_j^{(p)}\right) \text{ (bilinearity, cf. property 4)} \\
&= 0 \text{ (independence, cf. equation B.4)}
\end{aligned}
\tag{B.55}
$$

Bibliography

P. Ackers. Flow formulae for straight two-stage channels. *Journal of Hydraulic Research*, 31 (4):509–531, 1993. doi: 10.1080/00221689309498874. URL http://dx.doi.org/10.1080/00221689309498874.

M. Adamovic, I. Braud, F. Branger, and J. W. Kirchner. Assessing the simple dynamical systems approach in a Mediterranean context: application to the ardéche catchment (France). *Hydrology and Earth System Sciences*, 19:2427–2449, 2015. doi: 10.5194/hess-19-2427-2015. URL http://www.hydrol-earth-syst-sci.net/19/2427/2015/.

B. Bhattacharya and D.P. Solomatine. Neural networks and m5 model trees in modelling water level-discharge relationship. *Neurocomputing*, 63(0):381–396, 2005. ISSN 0925-2312. doi: 10.1016/j.neucom.2004.04.016. URL http://www.sciencedirect.com/science/article/pii/S0925231204003315.

F. Birgand, G. Lellouche, and T. W. Appelboom. Measuring flow in non-ideal conditions for short-term projects: Uncertainties associated with the use of stage-discharge rating curves. *Journal of Hydrology*, 503(0):186–195, 2013. doi: 10.1016/j.jhydrol.2013.09.007. URL http://dx.doi.org/10.1016/j.jhydrol.2013.09.007.

M.C. Boyer. *Analysis of Methods of Adjusting Stage and Discharge for Measurements During Changing Stage*. Water Resources Bulletin, unpublished manuscript of the Water-Resources Branch of the U.S. Geological Survey, 192-200, 1937.

I. Braud, P.-A. Ayral, C. Bouvier, F. Branger, G. Delrieu, J. Le Coz, G. Nord, J.-P. Vandervaere, S. Anquetin, M. Adamovic, J. Andrieu, C. Batiot, B. Boudevillain, P. Brunet, J. Carreau, A. Confoland, J.-F. Didon-Lescot, J.-M. Domergue, J. Douvinet, G. Dramais, R. Freydier, S. Gérard, J. Huza, E. Leblois, O. Le Bourgeois, R. Le Boursicaud, P. Marchand, P. Martin, L. Nottale, N. Patris, B. Renard, J.-L. Seidel, J.-D. Taupin, O. Vannier, B. Vincendon,

and A. Wijbrans. Multi-scale hydrometeorological observation and modelling for flash flood understanding. *Hydrology and Earth System Sciences*, 18(9):3733–3761, 2014. doi: 10.5194/hess-18-3733-2014. URL `http://www.hydrol-earth-syst-sci.net/18/3733/2014/`.

D. E. Burkham and D. R. Dawdy. Error analysis of streamflow data for an alluvial stream. Technical report, 1970. URL `http://pubs.er.usgs.gov/publication/pp655C`. Report.

J. Callède, P. Kosuth, and E. De Oliveira. Établissement de la relation hauteur-débit de l'Amazone à óbidos: méthode de la dénivelée normale à "géométrie variable" [Establishment of the stage-discharge relationship of the River Amazon at óbidos: "normal difference in level" method using "variable geometry"]. *Hydrological Sciences-Journal-des Sciences Hydrologiques*, 46(3):451–463, 2001. doi: 10.1080/02626660109492838. URL `http://dx.doi.org/10.1080/02626660109492838`. (in French).

J. Callède, J. L. Guyot, J. Ronchail, M. Molinier, and E. De Oliveira. L'Amazone á òbidos (Brésil) : Étude statistique des débits et bilan hydrologique [The River Amazon at óbidos (Brazil): Statistical studies of the discharges and water balance]. *Hydrological Sciences-Journal-des Sciences Hydrologiques*, 47(2):321–333, 2002. doi: 10.1080/02626660209492933. URL `http://dx.doi.org/10.1080/02626660209492933`. (in French).

V. T. Chow. Open channel hydraulics. 1959.

V. T. Chow, D. R. Maidment, L. W. Mays, et al. *Applied hydrology*. 1988.

M. P. Clark, D. E. Rupp, R. A. Woods, X. Zheng, R. P. Ibbitt, A. G. Slater, J. Schmidt, and M. J. Uddstrom. Hydrological data assimilation with the ensemble Kalman filter: Use of streamflow observations to update states in a distributed hydrological model. *Advances in Water Resources*, 31(10):1309–1324, October 2008. doi: 10.1016/j.advwatres.2008.06.005. URL `http://dx.doi.org/10.1016/j.advwatres.2008.06.005`.

R. T. Clarke, E. M. Mendiondo, and L. C. Brusa. Uncertainties in mean discharges from two large South American rivers due to rating curve variability / l'incertitude concernant les modules de deux grands fleuves d'Amérique du Sud qui résulte de la diversité des méthodes d'ajustement de la courbe de tarage. *Hydrological Sciences-Journal-des Sciences Hydrologiques*, 45(2):221–236, December 2000. doi: 10.1080/02626660009492321. URL `http://dx.doi.org/10.1080/02626660009492321`.

R.T. Clarke. Uncertainty in the estimation of mean annual flood due to rating-curve indefinition. *Journal of Hydrology*, 222(1-4):185–190, September 1999. doi: 10.1016/S0022-1694(99)00097-9. URL `http://dx.doi.org/10.1016/S0022-1694(99)00097-9`.

G. Coxon, J. Freer, I. K. Westerberg, T. Wagener, R. Woods, and P. J. Smith. A novel framework for discharge uncertainty quantification applied to 500 uk gauging stations. *Water Resources Research*, 51(7):5531–5546, 2015. ISSN 1944-7973. doi: 10.1002/2014WR016532. URL `http://dx.doi.org/10.1002/2014WR016532`.

G. Degoutte. *Diagnostic, aménagement et gestion des rivières: hydraulique et morphologie fluviales appliquées*. Éditions Tec & Doc, 2006. (in French).

A. Despax, C. Perret, R. Garçon, A. Hauet, A. Belleville, J. Le Coz, and A.-C. Favre. Considering sampling strategy and cross-section complexity for estimating the uncertainty of discharge measurements using the velocity-area method. *Journal of Hydrology*, 533:128–140, 2016. doi: 10.1016/j.jhydrol.2015.11.048. URL `http://www.sciencedirect.com/science/article/pii/S002216941500935X`.

G. Di Baldassarre and A. Montanari. Uncertainty in river discharge observations: a quantitative analysis. *Hydrology and Earth System Sciences*, 13(6):913–921, 2009. doi: 10.5194/hess-13-913-2009. URL `http://www.hydrol-earth-syst-sci.net/13/913/2009/`.

G. Di Baldassarre, F. Laio, and A. Montanari. Effect of observation errors on the uncertainty of design floods. *Physics and Chemistry of the Earth, Parts A/B/C*, 42-44:85–90, 2012. ISSN 1474-7065. doi: http://dx.doi.org/10.1016/j.pce.2011.05.001. URL `http://www.sciencedirect.com/science/article/pii/S1474706511000787`.

G. Di Silvio. Flood wave modifications along prismatic channels. *J. Hydraul. Div. ASCE*, 95(5):1589–1614, 1969.

F. Dottori, M. L. V. Martina, and E. Todini. A dynamic rating curve approach to indirect discharge measurement. *Hydrology and Earth System Sciences*, 13(6):847–863, 2009. URL `www.hydrol-earth-syst-sci.net/13/847/2009/`.

G. Dramais, J. Le Coz, B. Camenen, and A. Hauet. Advantages of a mobile LSPIV method for measuring flood discharges and improving stage-discharge curves. *Journal of Hydro-environment Research*, 5(4):301 – 312, 2011. ISSN 1570-6443. doi: http://dx.doi.org/

10.1016/j.jher.2010.12.005. URL http://www.sciencedirect.com/science/article/pii/S1570644311000049.

J. R. Dymond and R. Christian. Accuracy of discharge determined from a rating curve. *Hydrological Sciences-Journal-des Sciences Hydrologiques*, 27(4):493–504, 1982. doi: 10.1080/02626668209491128. URL http://dx.doi.org/10.1080/02626668209491128.

Environment Canada. *qSOP-NA049-01-2016 Hydrometric Manual - Data Computation, Stage-Discharge Model, Development and Maintenance*. Ottawa, Canada, 2016.

R. A. Falconer, D. G. George, and P. Hall. Three-dimensional numerical modelling of wind-driven circulation in a shallow homogeneous lake. *Journal of Hydrology*, 124(1):59–79, 1991. ISSN 0022-1694. doi: http://dx.doi.org/10.1016/0022-1694(91)90006-4. URL http://www.sciencedirect.com/science/article/pii/0022169491900064.

R. E. Faye and R. N. Cherry. *Channel and dynamic flow characteristics of the Chattahoochee River, Buford Dam to Georgia Highway 141*. US Government Printing Office, 1980.

J. D. Fenton. Calculating hydrographs from stage records. In *Proc. 28th IAHR Congress, Graz, Austria*, 1999. URL http://johndfenton.com/Papers/Calculating-flow-over-rectangular-sharp-edged-weirs.pdf.

J. D. Fenton. Rating curves: Part 1-Correction for surface slope. In *6th Conference on Hydraulics in Civil Engineering: The State of Hydraulics; Proceedings*, pages 309–317. Institution of Engineers, Australia, November 2001. URL http://johndfenton.com/Papers/Fenton01Hobart1-Rating-curves-1-Correction-for-surface-slope.pdf.

J. D. Fenton and R. J. Keller. The calculation of streamflow from measurements of stage. Technical report, September 2001. URL http://johndfenton.com/Papers/Calculation-of-streamflow-from-measurements-of-stage.pdf.

M. G. Ferrick, J. Bilmes, and S. E. Long. Modeling rapidly varied flow in tailwaters. *Water Resources Research*, 20(2):271–289, 1984.

D. L. Fread. Computation of stage-discharge relationships affected by unsteady flow. *Water Resources Bulletin, JAWRA Journal of The American Water Resources Association*, 11(2): 213–228, April 1975.

A. Gelman and D. B. Rubin. Inference from Iterative Simulation Using Multiple Sequences. *Statistical Science*, 7(4):457–472, November 1992. URL `http://www.jstor.org/stable/2246093`.

W. H. Graf. *Fluvial hydraulics: Flow and transport processes in channels of simple geometry. In collaboration with M. S. Altinakar.* Number 551.483 G7. John Wiley and Sons, England, 1998.

J.-L. Guerrero, I. K. Westerberg, S. Halldin, C.-Y. Xu, and Lundin L.-C. Temporal variability in stage-discharge relationships. *Journal of Hydrology*, 446-447:90–102, 2012. doi: 10.1016/j.jhydrol.2012.04.031. URL `http://dx.doi.org/10.1016/j.jhydrol.2012.04.031`.

M. R. Hall, W. E. Hall, and C. H. Pierce. Daily Discharge Of River Of Variable Slope. *Water-Supply Paper*, 345:53–66, 1914. URL `http://pubs.usgs.gov/wsp/0345e/report.pdf`.

S. Halmilton. 5 best practices for building better stage-discharge rating curves. *Whitepaper, personal communication*, 2015.

F. M. Henderson. Open channel flow, 1966.

R. W. Herschy. *Streamflow Measurement.* E & FN Spon, London, 1995.

R. W. Herschy. *Hydrometry, Principles and Practices.* Wiley, 1999.

H. Hidayat, B. Vermeulen, M. G. Sassi, P. J. J. F. Torfs, and A. J. F. Hoitink. Discharge estimation in a backwater affected meandering river. *Hydrology and Earth System Sciences*, 15(8):2717–2728, 2011. doi: 10.5194/hess-15-2717-2011. URL `http://www.hydrol-earth-syst-sci.net/15/2717/2011/`.

A. J. F. Hoitink, F. A. Buschman, and B. Vermeulen. Continuous measurements of discharge from a horizontal acoustic Doppler current profiler in a tidal river. *Water Resources Research*, 45(11):n/a–n/a, 2009. ISSN 1944-7973. doi: 10.1029/2009WR007791. URL `http://dx.doi.org/10.1029/2009WR007791`. W11406.

R. R. Holmes. River rating complexity. In Garcia & Hanes (Eds) Constantinescu, editor, *River Flow 2016. July 10-14*, pages 679–686, 2016.

I. Horner, J. Le Coz, B. Renard, V. Mansanarez, G. Pierrefeu, R. Le Boursicaud, K. Pobanz, and T. Berthet. BaRatin : propagation des incertitudes aux chroniques de débit. Technical report, Collaboration CNR-IRSTEA, 2015. (in French).

I. Horner, B. Renard, J. Le Coz, F. Branger, H. K. McMillan, and G. Pierrefeu. How much are streamflow uncertainties increased by stage measurement errors? (submitted), 2017.

ISO 1088:2007. Hydrometry - Velocity-area methods using current-meters - Collection and processing of data for determination of uncertainties in flow measurement. International Organization for Standardization, 2007.

ISO 1100-2:2010. Hydrometry - Measurement of liquid flow in open channels - Part 2: Determination of the stage-discharge relationship. page 48 p, Geneva, Switzerland, 2010. International Organization for Standardization. URL `http://www.iso.org/iso/catalogue_detail.htm?csnumber=42894`.

ISO 748:2007. Hydrometry - Measurement of liquid flow in open channels using current-meters or floats. International Organization for Standardization, 2007.

ISO 772:2011. Hydrometry - Vocabulary and symbols. International Organization for Standardization, 2011.

ISO 9123:2001. Measurement of liquid ow in open channels - Stage-fall-discharge relationships. page 14 p, Geneva, Switzerland, 2001. International Organization for Standardization. URL `http://www.iso.org/iso/catalogue_detail.htm?csnumber=42894`.

ISO/TS 25377:2007. Hydrometric Uncertainty Guidance (HUG). page 51 p, Geneva, Switzerland, 2007. International Organization for Standardization. URL `http://www.iso.org/iso/catalogue_detail.htm?csnumber=42894`.

S. K. Jain and D. Chalisgaonkar. Setting up stage-discharge relations using ann. *Journal of Hydrologic Engineering*, 5(4):428–433, 2000.

J. Jalbert, T. Mathevet, and A.-C. Favre. Temporal uncertainty estimation of discharges from rating curves using a variographic analysis. *Journal of Hydrology*, 397(1-2):83–92, 2011. ISSN 0022-1694. doi: http://dx.doi.org/10.1016/j.jhydrol.2010.11.031. URL `http://www.sciencedirect.com/science/article/pii/S0022169410007274`.

JCGM 100:2008. Evaluation of measurement data - Guide to the expression of Uncertainty in Measurement (GUM). Number 120 p. JCGM member organizations (BIPM, IEC, IFCC, ILAC, ISO, IUPAC, IUPAP and OIML), 2008. URL `http://www.iso.org/iso/catalogue_detail.htm?csnumber=42894`.

B. E. Jones. A Method of Correcting River Discharge for a Changing Stage. *U. S. Geological Survey, Water-Supply Paper*, (375-E):117–130, 1915.

J. Juston, P.-E. Jansson, and D. Gustafsson. Rating curve uncertainty and change detection in discharge time series: case study with 44-year historic data from the nyangores river, kenya. *Hydrological Processes*, 28(4):2509–2523, 2014. ISSN 1099-1085. doi: 10.1002/hyp.9786. URL `http://dx.doi.org/10.1002/hyp.9786`.

F. Karim. Bed Configuration and Hydraulic Resistance in Alluvial-Channel Flows. *Journal of Hydraulic Engineering*, 121(1):15–25, 1995. doi: 10.1061/(ASCE)0733-9429(1995)121:1(15). URL `http://dx.doi.org/10.1061/(ASCE)0733-9429(1995)121:1(15)`.

A. D. Knighton. *Fluvial Forms and Processes: A New Perspective*. London, 1998.

G. Kuczera. Uncorrelated measurement error in flood frequency inference. *Water Resources Research*, 28(1):183–188, 1992. ISSN 1944-7973. doi: 10.1029/91WR02269. URL `http://dx.doi.org/10.1029/91WR02269`.

G. Kuczera. Correlated rating curve error in flood frequency inference. *Water Resources Research*, 32(7):2119–2127, 1996. doi: 10.1029/96WR00804. URL `http://dx.doi.org/10.1029/96WR00804`.

P. Lamberti and S. Pilati. Quasi-kinematic flood wave propagation. *Meccanica*, 25(2):107–114, 1990. ISSN 00256455.

M. Lang, R. Naulet, A. Recking, D. Coeur, and C. Gigon. Étude de cas : l'analyse des pluies et crues extrêmes observées depuis 200 ans dans un bassin cévenol, l'Ardèche [A case study on the Ardeche river: flood frequency analysis of historical events within the two last centuries]. *La Houille Blanche*, (6-7):131–138, 2002. doi: 10.1051/lhb/2002097. URL `http://dx.doi.org/10.1051/lhb/2002097`. (in French).

M. Lang, K. Pobanz, B. Renard, E. Renouf, and E. Sauquet. Extrapolation of rating curves by hydraulic modelling, with application to flood frequency analysis. *Hydrological Sciences Journal-Journal Des Sciences Hydrologiques*, 55(6):883–898, 2010. doi: 10.1080/02626667.2010.504186.

E. M. Latrubesse. Patterns of anabranching channels: The ultimate end-member adjustment of mega rivers. *Geomorphology*, 101(1-2):130–145, 2008. ISSN 0169-555X. doi:

http://dx.doi.org/10.1016/j.geomorph.2008.05.035. URL http://www.sciencedirect.com/science/article/pii/S0169555X08002389. The 39th Annual Binghamton Geomorphology Symposium: Fluvial Deposits and Environmental History: Geoarchaeology, Paleohydrology, and Adjustment to Environmental Change.

J. Le Coz, G. Pierrefeu, and A. Paquier. Evaluation of river discharges monitored by a fixed side-looking Doppler profiler. *Water Resources Research*, 44(4):n/a–n/a, 2008. ISSN 1944-7973. doi: 10.1029/2008WR006967. URL http://dx.doi.org/10.1029/2008WR006967. W00D09.

J. Le Coz, B. Camenen, G. Dramais, M. Ferry, J.L. Rosique, and J. Ribot-Bruno. *Contrôle des débits réglementaires. Application de l'article L. 214-18 du Code de l'environnement [Inspection of statutory discharges. Application of the L. 21418 article of the Environment Code]*. 2011. (in French).

J. Le Coz, B. Renard, L. Bonnifait, F. Branger, and R. Le Boursicaud. Combining hydraulic knowledge and uncertain gaugings in the estimation of hydrometric rating curves: A bayesian approach. *Journal of Hydrology*, 509:573–587, 2014. doi: 10.1016/j.jhydrol.2013.11.016. URL http://dx.doi.org/10.1016/j.jhydrol.2013.11.016.

J. Le Coz, B. Blanquart, K. Pobanz, G. Dramais, G. Pierrefeu, A. Hauet, and A. Despax. Estimating the uncertainty of streamgauging techniques using in situ collaborative interlaboratory experiments. *Journal of Hydraulic Engineering*, 142(7):04016011, 2016a. doi: 10.1061/(ASCE)HY.1943-7900.0001109. URL http://dx.doi.org/10.1061/(ASCE)HY.1943-7900.0001109.

J. Le Coz, V. Mansanarez, B. Renard, M. Lang, G. Pierrefeu, K. Pobanz, and R. Le Boursicaud. Bayesian analysis of rating curves at twin gauge stations. In Garcia & Hanes Constantinescu, editor, *River Flow 2016. July 10-14*, pages 664–670, 2016b.

K. Lee. *Evaluation of methodologies for continuous discharge monitoring in unsteady open-channel flows*. PhD thesis, 2013. URL http://ir.uiowa.edu/etd/5012/.

J. Leonard, M. Mietton, H. Najib, and P. Gourbesville. Rating curve modelling with manning's equation to manage instability and improve extrapolation. *Hydrological Sciences Journal/Journal des Sciences Hydrologiques*, 45(5):739–750, 2000. doi: 10.1080/02626660009492374. URL http://dx.doi.org/10.1080/02626660009492374.

V.A. Levesque and K.A. Oberg. *Computing discharge using the index velocity method*, volume 3-A23. U.S. Geological Survey Techniques and Methods, 2012. URL `http://pubs.usgs.gov/tm/3a23/`.

D. D. Lewis. Practical methods of determining discharge for gaging stations on streams where the slope is affected by variable discharge. *Water Resources Bulletin, unpublished manuscript of the Water-Resources Branch of the U.S. Geological Survey*, pages 487–489, 1939.

M. J. Lighthill and G. B. Whitham. On kinematic waves. I. Flood Movement in Long Rivers. *Proceedings of the Royal Society of London. Series A. Mathematical and Physical Sciences*, 229(1178):281–316, 1955. doi: 10.1098/rspa.1955.0088. URL `http://rspa.royalsocietypublishing.org/content/229/1178/281`.

V. Mansanarez, J. Le Coz, B. Renard, M. Lang, and F. Birgand. Bayesian analysis of stage-discharge relationships affected by hysteresis and quantification of the associated uncertainties. volume 17. EGU General Assembly 2016, Vienna, 2015.

V. Mansanarez, J. Le Coz, B. Renard, M. Lang, G. Pierrefeu, R. Le Boursicaud, and K. Pobanz. Bayesian analysis of stage-fall-discharge rating curves and their uncertainties. volume 18. EGU General Assembly 2016, Vienna, 2016a.

V. Mansanarez, J. Le Coz, B. Renard, M. Lang, G. Pierrefeu, and P. Vauchel. Bayesian analysis of stage-fall-discharge rating curves and their uncertainties. *Water Resources Research*, 52 (9):7424–7443, 2016b. doi: 10.1002/2016WR018916. URL `http://dx.doi.org/10.1002/2016WR018916`.

E. Marchi. La Propagazione delle onde di piena. *Atti Accademia Nazionale Lincei*, 64:594–602, 1976. (in Italian).

H. McMillan, J. Freer, F. Pappenberger, T. Krueger, and M. Clark. Impacts of uncertain river flow data on rainfall-runoff model calibration and discharge predictions. *Hydrological Processes*, 24(10):1270–1284, 2010. ISSN 1099-1085. doi: 10.1002/hyp.7587. URL `http://dx.doi.org/10.1002/hyp.7587`.

H. K. McMillan and I. K. Westerberg. Rating curve estimation under epistemic uncertainty. *Hydrological Processes*, 29(7):1873–1882, 2015. ISSN 1099-1085. doi: 10.1002/hyp.10419. URL `http://dx.doi.org/10.1002/hyp.10419`. HYP-14-0779.R1.

E. Meyer-Peter and R. Müller. Formulas for bed-load transport. In *Hydraulic Engineering Reports*, IAHSR 2nd meeting, Stockholm, appendix 2. IAHR, 1948.

T. Morlot. *La gestion dynamique des relations hauteur-débit des stations d'hydrométrie et le calcul des incertitudes associées : un indicateur de gestion, de qualité et de suivi des points de mesure*. PhD thesis, Terre, Univers, Environnement. Université de Grenoble, 2014. URL `https://tel.archives-ouvertes.fr/tel-01146918`. (in French).

T. Morlot, C. Perret, A.-C. Favre, and J. Jalbert. Dynamic rating curve assessment for hydrometric stations and computation of the associated uncertainties: Quality and station management indicators. *Journal of Hydrology*, 517:173–186, September 2014. ISSN 0022-1694. doi: 10.1016/j.jhydrol.2014.05.007. URL `http://dx.doi.org/10.1016/j.jhydrol.2014.05.007`.

R. A. Moyeed and R. T. Clarke. The use of bayesian methods for fitting rating curves, with case studies. *Advances in Water Resources*, 28(8):807–818, 2005. doi: 10.1016/j.advwatres.2005.02.005. URL `http://dx.doi.org/10.1016/j.advwatres.2005.02.005`.

M. Muste, H. C. Ho, and D. Kim. Considerations on direct stream flow measurements using video imagery: Outlook and research needs. *Journal of Hydro-Environment Research*, 5(4):289–300, 2011. doi: 10.1016/j.jher.2010.11.002. URL `http://dx.doi.org/10.1016/j.jher.2010.11.002`.

R. Naulet, M. Lang, T. B. M. J. Ouarda, D. Coeur, B. Bobée, A. Recking, and D. Moussay. Flood frequency analysis on the Ardéche river using French documentary sources from the last two centuries. *Journal of Hydrology*, 313(1-2):58–78, 2005. ISSN 0022-1694. doi: 10.1016/j.jhydrol.2005.02.011. URL `http://www.sciencedirect.com/science/article/pii/S0022169405000296`.

L. Neppel, B. Renard, M. Lang, P.-A. Ayral, D. Coeur, E. Gaume, N. Jacob, O. Payrastre, K. Pobanz, and F. Vinet. Flood frequency analysis using historical data: accounting for random and systematic errors. *Hydrological Sciences-Journal-des Sciences Hydrologiques*, 55(2):192–208, 2010. doi: 10.1080/02626660903546092. URL `http://dx.doi.org/10.1080/02626660903546092`.

Y. Nihei and A. Kimizu. A new monitoring system for river discharge with horizontal acoustic doppler current profiler measurements and river flow simulation. *Water Resources Research*,

44(4):n/a–n/a, 2008. ISSN 1944-7973. doi: 10.1029/2008WR006970. URL `http://dx.doi.org/10.1029/2008WR006970`. W00D20.

M. Perumal, K. B. Shrestha, and U. C. Chaube. Reproduction of hysteresis in rating curves. *Journal of Hydraulic Engineering-Asce*, 130(9):870–878, 2004. doi: 10.1016/j.jhydrol.2003.12.024. URL `http://dx.doi.org/10.1016/j.jhydrol.2003.12.024`.

A. Petersen-Øverleir. Accounting for heteroscedasticity in rating curve estimates. *Journal of Hydrology*, 292(1-4):173–181, 2004. doi: 10.1016/j.jhydrol.2003.12.024. URL `http://dx.doi.org/10.1016/j.jhydrol.2003.12.024`.

A. Petersen-Øverleir. Modelling stage-discharge relationships affected by hysteresis using the jones formula and nonlinear regression / modélisation des relations hauteur-débit affectées par de l'hystérésis en utilisant la formule de jones et la régression non-linéaire. *Hydrological Sciences-Journal-des Sciences Hydrologiques*, 51(3):365–388, 2006. doi: 10.1623/hysj.51.3.365. URL `http://dx.doi.org/10.1623/hysj.51.3.365`.

A. Petersen-Øverleir. Fitting depth-discharge relationships in rivers with floodplains. *Hydrology Research*, 39(5-6):369–384, 2008. doi: 10.2166/nh.2008.303. URL `http://hr.iwaponline.com/content/39/5-6/369`.

A. Petersen-Øverleir and T. Reitan. Objective segmentation in compound rating curves. *Journal of Hydrology*, 311(1-4):188–201, 2005. ISSN 0022-1694. doi: 10.1016/j.jhydrol.2005.01.016. URL `http://dx.doi.org/10.1016/j.jhydrol.2005.01.016`.

A. Petersen-Øverleir and T. Reitan. Bayesian analysis of stage-fall-discharge models for gauging stations affected by variable backwater. *Hydrological Processes*, 23(21):3057–3074, 2009a. doi: 10.1002/hyp.7417. URL `http://dx.doi.org/10.1002/hyp.7417`.

A. Petersen-Øverleir and T. Reitan. Accounting for rating curve imprecision in flood frequency analysis using likelihood-based methods. *Journal of Hydrology*, 366(1-4):89–100, 2009b. doi: 10.1016/j.jhydrol.2008.12.014.

S. E. Rantz. Measurement and computation of streamflow. volume 1: Measurement of stage and discharge. *Water-Supply Paper*, 2175:631, 1982a.

S. E. Rantz. Measurement and computation of streamflow. volume 2: Computation of discharge. *Water-Supply Paper*, 2175:631, 1982b.

T. Reitan and A. Petersen-Øverleir. Bayesian power-law regression with a location parameter, with applications for construction of discharge rating curves. *Stochastic Environmental Research and Risk Assessment*, 22(3):351–365, 2008. ISSN 1436-3259. doi: 10.1007/s00477-007-0119-0. URL `http://dx.doi.org/10.1007/s00477-007-0119-0`.

T. Reitan and A. Petersen-Øverleir. Dynamic rating curve assessment in unstable rivers using ornstein-uhlenbeck processes. *Water Resources Research*, 47(2):n/a–n/a, 2011. ISSN 1944-7973. doi: 10.1029/2010WR009504. URL `http://dx.doi.org/10.1029/2010WR009504`. W02524.

G. Réméniéras. Annuaire hydrologique de la france de 1949. Annuaire, Société Hydrotechnique de France, 1949.

B. Renard, V. Garreta, and M. Lang. An application of bayesian analysis and markov chain monte carlo methods to the estimation of a regional trend in annual maxima. *Water Resources Research*, 42(12):n/a–n/a, 2006. ISSN 1944-7973. doi: 10.1029/2005WR004591. URL `http://dx.doi.org/10.1029/2005WR004591`. W12422.

J. S. Ribberink. Bed-load transport for steady flows and unsteady oscillatory flows. *Coastal Engineering*, 34(1-2):59–82, 1998. ISSN 0378-3839. doi: http://dx.doi.org/10.1016/S0378-3839(98)00013-1. URL `http://www.sciencedirect.com/science/article/pii/S0378383998000131`.

R. Sanchez, M. L. Moreno, and C. Ferrer. L'influence de l'hystérésis dans le développement des relations niveau-débit [the influence of hysteresis in the development of stage-discharge relationships]. *Houille Blanche-Revue Internationale de L'Eau*, (6):48–52, 2013. doi: 10.1051/lhb/2013050.

A.R. Schmidt. *Analysis of stage-discharge relations for open-channel flows and their associated uncertainties*. PhD thesis, University of Illinois, Urbana-Champaign, 2002.

S. A. Schumm. *The Fluvial System*. New York, 1977. doi: 10.1017/CBO9781139165440. URL `http://dx.doi.org/10.1017/CBO9781139165440`.

S. A. Schumm and B. R. Winkley. *The Variability of Large Alluvial Rivers*. ASCE Press, New York, 1994.

R. H. J. Sellin. A laboratory investigation into the interaction between the flow in the channel of a river and that over its flood plain. *La Houille Blanche*, (7):793–802, 1964. doi: 10.1051/lhb/1964044. URL http://dx.doi.org/10.1051/lhb/1964044.

Y. Shimizu, S. Giri, S. Yamaguchi, and J. Nelson. Numerical simulation of dune-flat bed transition and stage-discharge relationship with hysteresis effect. *Water Resources Research*, 45(4), 2009. ISSN 1944-7973. doi: 10.1029/2008WR006830. URL http://dx.doi.org/10.1029/2008WR006830. W04429.

R. R. Shrestha, A. Bárdossy, and F. Nestmann. Analysis and propagation of uncertainties due to the stage-discharge relationship: a fuzzy set approach. *Hydrological Sciences Journal*, 52 (4):595–610, 2007. doi: 10.1623/hysj.52.4.595. URL http://dx.doi.org/10.1623/hysj.52.4.595.

A. E. Sikorska, A. Scheidegger, K. Banasik, and J. Rieckermann. Considering rating curve uncertainty in water level predictions. *Hydrology and Earth System Sciences*, 17(11):4415–4427, 2013. doi: 10.5194/hess-17-4415-2013. URL http://www.hydrol-earth-syst-sci.net/17/4415/2013/.

G. M. Smart. Stage-discharge discontinuity in composite flood channels. *Journal of Hydraulic Research*, 30(6):817–833, 1992. doi: 10.1080/00221689209498912. URL http://dx.doi.org/10.1080/00221689209498912.

R. L. Soulsby and R. J. S. Whitehouse. Threshold of sediment motion in coastal environments [online]. *Pacific Coasts and Ports '97: Proceedings of the 13th Australasian Coastal and Ocean Engineering Conference and the 6th Australasian Port and Harbour Conference*, 1:147–150, 1997. URL http://search.informit.com.au/documentSummary;dn=929741720399033;res=IELENG. Christchurch, N.Z.: Centre for Advanced Engineering, University of Canterbury.

G. H. Steinbakk, T. L. Thorarinsdottir, T. Reitan, L. Schlichting, S. Hølleland, and K. Engeland. Propagation of rating curve uncertainty in design flood estimatifon. *Water Resources Research*, 2016. ISSN 1944-7973. doi: 10.1002/2015WR018516. URL http://dx.doi.org/10.1002/2015WR018516.

K. P. Sudheer and S. K. Jain. Radial basis function neural network for modeling rating curves. *Journal of Hydrologic Engineering*, 8(3):161–164, 2003. doi: 10.1061/(ASCE)1084-0699(2003)8:3(161).

X. Sun. *Regional frequency analysis of precipitation accounting for climate variability and change*. PhD thesis, Terre, Univers, Environnement. Université de Grenoble, October 2013.

M. Tawfik, A. Ibrahim, and H. Fahmy. Hysteresis sensitive neural network for modeling rating curves. *Journal of Computing in Civil Engineering*, 11(3):206–211, 1997. doi: 10.1061/(ASCE)0887-3801(1997)11:3(206).

M. Thyer, B. Renard, D. Kavetski, G. Kuczera, S. W. Franks, and S. Srikanthan. Critical evaluation of parameter consistency and predictive uncertainty in hydrological modeling: A case study using Bayesian total error analysis. *Water Resources Research*, 45(12), 2009. ISSN 1944-7973. doi: 10.1029/2008WR006825. URL `http://dx.doi.org/10.1029/2008WR006825`. W00B14.

C. Venetis. A note on the estimation of the parameters in logarithmic stage-discharge relationships with estimate of their error. *International Association of Scientific Hydrology. Bulletin*, 15(2):105–111, 1970. doi: 10.1080/02626667009493957. URL `http://dx.doi.org/10.1080/02626667009493957`.

P. E. Weinmann and E. M. Laurenson. Approximate flood routing methods: a review. *Journal of the Hydraulics Division*, 105(12):1521–1536, 1979.

I. K. Westerberg and H. K. McMillan. Uncertainty in hydrological signatures. *Hydrology and Earth System Sciences*, 19(9):3951–3968, 2015. doi: 10.5194/hess-19-3951-2015. URL `http://www.hydrol-earth-syst-sci.net/19/3951/2015/`.

I. K. Westerberg, J.-L. Guerrero, J. Seibert, Beven K. J., and S. Halldin. Stage-discharge uncertainty derived with a non-stationary rating curve in the Choluteca River, Honduras. *Hydrological Processes*, 25(4):603–613, September 2011. doi: 10.1002/hyp.7848. URL `http://dx.doi.org/10.1002/hyp.7848`.

W. C. Wiggins. Correcting Discharge Measurements for Changing Stage. *Water Resources Branch, Circular No. 479, unpublished manuscript of the Water-Resources Branch of the U.S. Geological Survey*, 10(285), 1925.

WMO No. 1044. World Meteorological Organization (2010), Manual on Stream Gauging. Volume II - Computation of discharge. Number 1044, 195 p. World Meteorological Organization (WMO), 2010. URL http://www.iso.org/iso/catalogue_detail.htm?csnumber=42894.

WMO No. 385. World Meteorological Organization (2012), International Glossary of Hydrology. Number 385. World Meteorological Organization (WMO), 2012. URL http://www.wmo.int/pages/prog/hwrp/publications/international_glossary/385_IGH_2012.pdf.

Relations hauteur-débit non univoques: analyse bayésienne des courbes de tarage complexes et de leurs incertitudes

Les courbes de tarage complexes, qui prennent en entrée la hauteur d'eau et des variables supplémentaires, sont nécessaires pour établir les chroniques de débit des cours d'eau là où la relation hauteur-débit n'est pas univoque. Dans le même cadre bayésien, des méthodes à base hydraulique sont proposées et testées pour construire les courbes de tarage complexes et estimer leurs incertitudes : des modèles hauteur-gradient-débit (SGD) pour résoudre l'hystérésis due aux écoulements transitoires, des modèles hauteur-dénivelée-pente (SFD) pour résoudre le remous variable aux stations à double échelle, le modèle hauteur-période-débit (SPD) pour résoudre les détarages nets dus aux évolutions du lit. Chaque modèle a été appliqué à des stations hydrométriques variées et évalué grâce à des analyses de sensibilité. Pour chacune des trois sources de non-univocité de la relation hauteur-débit, les méthodes bayésiennes proposées fournissent non seulement une analyse d'incertitude quantitative mais aussi des solutions efficaces à des problèmes récurrents que posent les procédures traditionnelles pour les courbes de tarage complexes.

Mots clés : BaRatin, inférence bayésienne, contrôles hydrauliques, courbes de tarage complexes, Hydrométrie, hystérésis, MCMC, non univocité, détarages morphodynamiques, relations hauteur-débit, débit des cours d'eau, incertitudes, influence aval variable.

Non-unique stage-discharge relations: Bayesian analysis of complex rating curves and their uncertainties

Complex rating curves, with stage and additional variables as inputs are necessary to establish streamflow records at sites where the stage-discharge relation is non-unique. Within the same Bayesian framework, hydraulically-based methods are introduced and tested to develop complex rating curves and estimate their uncertainties: stage-gradient-discharge (SGD) models to address hysteresis due to transient flow, stage-fall-discharge (SFD) models to address variable backwater at twin gauge stations, stage-period-discharge (SPD) model to address net rating changes due to bed evolution. Each model was applied to contrasting hydrometric stations and evaluated through sensitivity analyses. For each of the three sources of non-uniqueness in the stage-discharge relation, the proposed Bayesian methods provide not only quantitative uncertainty analysis but also efficient solutions to recurrent problems with the traditional procedures for complex ratings.

Key words: BaRatin, Bayesian inference, controls, complex rating curves, Hydrometry, hysteresis, MCMC, non-uniqueness, rating changes, stage-discharge relation, streamflow, uncertainties, variable backwater influence.